Advanced Electrohydrodynamic Atomisation Engineered Microneedle Coatings

RADEYAH ALI

DEC 2020

A Thesis submitted in partial fulfilment of the requirements for

PhD in biomaterial engineering

Awarded by

De Montfort University

DE MONTFORT UNIVERSITY LEICESTER

Abstract

Transdermal drug delivery (TDD) is an emerging field in the pharmaceutical remit compared to conventional methods (oral and parenteral). Microneedle (MN) based devices have gained significant interest as a strategy to overcome the skins formidable barrier; the *stratum corneum* and enhance drug delivery. The research presented here shows the successful coating of MNs with polymeric dye composites using Electrohydrodynamic atomisation (EHDA). Initially the rheological behaviours of polymeric solutions and morphological characterisation was carried out. This was followed by Quality by Design (QBD) implementation for the optimisation of the key process parameters in EHDA. Here, the electrosprayed nanoparticles and electrospun nano/micro fibres consisted of a polymeric matrix and dye. Eight formulations were assessed consisting of 5% w/v of polycaprolactone (PCL) in dichloromethane (DCM) and 5% w/v polyvinylpyrrolidone (PVP) in ethanol. A full factorial Design of Experiments (DoE) was used to assess the various parameters (applied voltage, deposition distance and flow rate). Further particle and fibre analysis using Scanning Electron Microscopy (SEM), Differential Scanning Calorimetry (DSC), Fourier Transform Infrared Spectroscopy (FTIR), particle/fibre size distribution. In addition to this *in vitro* release studies were carried out using fluorescein (FL) and rhodamine B (RhB) as model dyes and *in vitro* permeation studies were applied. From optimising EHDA more than 52% of particles were under 500 nm and fibres were in the micron range. *In vitro* drug release studies showed 100% drug release after 7 days for PCL particles and fibres. It also showed 100% drug release within 120 min for PVP particles and 300 minutes for PVP fibres. The release kinetics and the permeation study showed that the MN successfully pierced the membrane and the Es and Esp MN coatings released a large amount of the loaded drug within 6 hours for all formulations. This study has demonstrated the capability of these robust MNs to encapsulate a diverse range of drugs within a polymeric matrix giving rise to the potential of developing personalised medical devices.

Declaration

I declare that all the work presented in this thesis is entirely my own and has not been submitted in whole or in part of any previous professional qualification; except where stated by reference or acknowledgment.

Signature: Radeyah Ali

Date: 11/12/20

Acknowledgements

بِسْمِ اللهِ الرَّحْمَنِ الرَّحِيمِ

"In the name of Allah, the most gracious, the most merciful"

I would like to dedicate this thesis to my nana and parents, without their continuous support, love, prayers and encouragement I wouldn't have made it this far. I would like to thank my mum the most for always encouraging me to seek knowledge and to pursue this PhD. I am grateful for all the sacrifices she has made and for giving me the drive to stay determined and carry out this PhD. I would also like to thank my siblings Safa, Safwaan and Ridhwaan as well as my sister in laws Naomi and Sabreen who have all helped keep me motivated and sane throughout this journey.

I am extremely fortunate and grateful for my supervisor Zeeshan. I am thankful to have had someone who always believed in me, kept me motivated and inspired me to pursue my dreams. I am very appreciative for the continuous support I've received during this PhD both academically and personally. Thank you to the technical team at DMU with special thanks to Rachel Armitage who was always available to help.

Finally, I would like to thank all my friends who have all helped in so many ways. I am thankful for all the students in the lab who are like my EHDA family you have always been available to help and listen. I am thankful for Anisa who has been supporting me from the very beginning keeping me on track, always listening and being the voice of reason. Sundas and Amar I would like to thank you for helping me stay focussed and for listening to my rants you have kept me sane throughout this. Aishah and Khalid I truly appreciate your constant reminder of faith, your prayers, guidance and encouragement throughout this PhD and helping me not to "fall at the last hurdle". It means a lot that you've all supported me throughout this journey and how proud you all are.

"All praise to Allah"

Conferences

- ESPRC EHDA Network. International PharmTech Conference. Leicester, UK. 4th November 2016 – POSTER PRESENTATION.

- 5th Quality by Design Symposium. Leicester, UK. 29th March 2017 – POSTER PRESENTATION.

- University College London 2nd International Pharmaceutical Conference. London, UK. July 2017 – POSTER PRESENTATION.

- UKPharmsci Science of Medicines APS conference. University of Hertfordshire, UK. 5-7th September 2017 – POSTER PRESENTATION.

- 6th Quality by Design Symposium. Leicester, UK. 14th March 2018 – POSTER PRESENTATION.

- 19th World Congress on Materials Science and Engineering). Barcelona, Spain. 11-13th June- 2018 - POSTER PRESENTATION.

- 7th Quality by Design Symposium. Leicester, UK. 26th March 2019 – POSTER PRESENTATION.

Publications

- Ali, R., Mehta, P., Arshad, M., Kucuk, I., Chang, M. and Ahmad, Z., 2019. Transdermal Microneedles—A Materials Perspective. *AAPS PharmSciTech*, 21(1).

- Ali, R., Mehta, P., Kyriaki Monou, P., Arshad, M., Panteris, E., Rasekh, M., Singh, N., Qutachi, O., Wilson, P., Tzetzis, D., Chang, M., Fatouros, D. and Ahmad, Z., 2020. Electrospinning/electrospraying coatings for metal microneedles: A design of experiments (DOE) and quality by design (QbD) approach. *European Journal of Pharmaceutics and Biopharmaceutics*, 156, pp.20-39.

Contents

List of Figures

List of Tables

Abbreviations

AFM Atomic force microscopy

AP Applied voltage

API Active pharmaceutical ingredient

Au Gold

CMNs Coated Microneedles

CMAs Critical Material Attributes

CMC Carboxymethyl cellulose

CQA Critical Quality Attributes

DAB Droplet Air Born

DCM Dichloromethane

DOE Design of experiments

DSC – Differential Scanning Calorimetry

DMNs Dissolved Microneedles

EHDA Electrohydrodynamic Atomisation

Es Electrospraying

Esp Electrospinning

FDA Food and Drug

FTIR Fourier-transform infrared spectroscopy

FR Flow rate

GMNs Glass Microneedles

HA Hyaluronic Acid

HFMNs Hydrogel Forming Microneedles

HMW High molecular weight

HMNs Hollow Microneedle

IF Interstitial Fluid

ISG Inorganic silica glass

LMW Low molecular weight

MSN Mesoporous Silica Nanoparticles

MNS Metal Microneedles

Mwt Molecular Weight

Np Nanoparticle

N-UNCD Nitrogen incorporated Ultra-nanocrystalline diamond

ODD Oral Drug Delivery

PCL Polycaprolactone

Pd Palladium

PDMS Polydimethylsiloxane

PLA Polylactic Acid)

PLGA Poly-lactic glycolic acid

PMMA Poly(methyl methacrylate)

PS Polystyrene

PVA Polyvinyl Alcohol

PVP Polyvinylpyrrolidone

QBD Quality by design

QTPP Quality Target Product Profile

RA Risk Assessment

SC Stratum Corneum

SEM Scanning electron microscope

SMNs Solid Microneedles

TDD Transdermal Drug Delivery

Ti Titanium

TP Transdermal Patches

UV-vis Ultraviolet-visible spectroscopy

WD Working distance

ZMNs Zeolite Microneedles

Chapter 1 Introduction

1.1 Fundamentals

The formation of complex nano/micron sized drug delivery systems, with multifunctional properties and favourable release kinetics has been of great interest within the pharmaceutical industry. Although many advancements have been made, with regards to current drug delivery systems they are still met with reservations.

Transdermal drug delivery (TDD) approach provides an attractive non-invasive systemic alternative to conventional routes (parenteral, oral), avoiding first pass metabolism and providing drug therapy in a minimally invasive and relatively painless manner. This route improves bioavailability of drugs and their ability to provide systemic and local treatment. The primary barrier for drug delivery to the skin is the outermost layer, the *stratum corneum* (SC) which can be difficult to overcome as a result of its structure.

To date, current methods which have been employed have had limited success in improving transdermal flux. Such methods include chemical permeation enhancers, laser/thermal ablation, iontophoresis and physical enhancement techniques. Thus, the development of microneedle (MN) systems to overcome the SC hence providing a more efficient device to deliver drugs through the layers of skin. MNs have the potential to deliver peptides, proteins, vaccines, oligonucleotides, insulin, ovalbumin, plasmid DNA, siRNA, human growth hormone in a less invasive and painless way compared to hypodermic needles. In recent years, MNs have been utilised for more novel applications including fluid sampling, biosensors, microanalysis and electrochemical biosensing.

Polymeric MNs have gained much interest in recent years. However, there are some drawbacks of this application such as potential polymer discharge into the skin upon insertion making it unfavourable with polymeric MNs. Recently,

biodegradable polymers such as poly-lactic glycolic acid (PLGA), have been incorporated into MNs: following insertion into the skin, these devices can degrade safely. Depending on material choice, it is also possible to alter and modify the release profile of the active ingredient. For example, polyvinylpyrrolidone (PVP) has been used to provide a rapid release whilst PLGA and poly-caprolactone (PCL) have been shown to provide more sustained release of tenofovir, a small hydrophilic drug.

Electrohydrodynamic atomisation (EHDA) is a promising technique for the engineering of nano-micron sized structures. It has the ability to atomise a liquid droplet into more fine mono disperse particles or spun into fibrous structures (electrospraying (Es) and electrospinning (Esp)). The process parameters can be manipulated using various modes (dripping, cone-jet, spindle, multi-jet). This one step versatile engineering method can be optimised for structures with controlled size and shape which can be utilised for a plethora of applications.

1.2 Aims and objectives

The main focus of this research was to assess and characterise the capability of EHDA using QBD as a viable method for the coating of MNs. It was vital to demonstrate the EHDA process as well as current applications of this technique in terms of drug loading and delivery and how it could be applied in my area of research.

The research presented aims to outline the fundamental process parameters of EHDA and its use in the fabrication of optimised MN coating structures using a polymeric carrier and model dye behaving as a drug. This work also intends to carefully select a polymer to enhance drug delivery and permeation of dyes with *in vitro* and *ex vivo* assessment.

In order to achieve this the following sequence of studies were conducted:

- Physically characterising polymeric formulations (concentration, molecular weight) and their behaviour.
- Optimising the EHDA process with the application of QBD
- Synthesis of polymeric nano/micron sized structured coatings using single needle EHDA
- Further validation studies for the production of optimised MN coatings
- Characterisation and assessment of nano-micro sized structured MN coatings.

1.3 Structure of thesis

Chapter 1 briefly summarises the key concepts of transdermal drug delivery, MNs and the EHDA process. This chapter provides an insight into the current challenges faced with transdermal drug delivery methods, materials and devices with a concise overview of the EHDA principles, requirements and application. Chapter 2 intends to provide more in-depth knowledge on the topics in chapter 1. A comprehensive literature review will analyse the current transdermal drug delivery approach and the existing systems, the principles and application of EHDA and the advancement of MNs and the utilisation of MNs in TDD systems. Chapter 3 includes the materials and methods used in this study and chapters 4-6 will include the experimental procedures carried out for the selected thesis subject. Chapter 4 involves pre-formulation data. This chapter involves physically characterising various polymeric formulations with different concentrations and observes how they behave during the EHDA process. The morphology of these structures is also assessed. This would act as a precursor to chapter 5. Chapter 5 involves the application of quality by design (QBD) principles to the different process parameters of the EHDA technique. This in turn would lead to the optimisation of the process by distinguishing the optimal parameters to work at (flow rate, voltage, deposition distance) using polymers (carrier matrix) and dye acting as a model drug resulting in nano/micron sized particular/fibrous

structures. These structures were then assessed morphologically, thermally and with spectroscopic techniques to determine the most promising formulation possessing the best characteristics for MN coatings. Chapter 6 demonstrates the effect of the inclusion of dye (behaving as model drug) as MN coatings with dye release from the electrosprayed and Electrospun structures. It also includes *in vitro* release studies as well as permeation. Chapter 7 concludes the thesis summarising the findings and suggestions for future work in this innovative, evolving area of research in pharmaceutics.

Chapter 2 Literature Review

2.1 The Skin

2.1.1 Introduction

Skin tissue accounts for 16% of the body weight, averaging 2 m^2 in surface with a thickness of 1.5-4 mm in the human body. It's considered one of the most important tissues, being made up of several layers. The subtypes of skin include glabrous (located in palms and soles), hairy (most of the human body) and mucocutaneous (orifices) (Ahmed Saeed AL-Japairai, Mahmood et al. 2020). As well as acting as a barrier that protects the body from physical, chemical and biological threats it also maintains homeostasis and other sensory and metabolic functions (Abdo, Sopko et al. 2020).

2.1.2 Anatomy of the skin

Skin is the largest multidimensional organ in the human body measuring approximately 2 m^2. The primary functions of this multi-layered organ include protection from the external environment which can be chemicals, UV radiation or microbial invasion. Figure 1 displays this dynamic biological structure which also provides sensation, regulation and undergoes continuous skin renewal (Ahmed Saeed AL-Japairai, Mahmood et al. 2020). From a histological perspective skin is comprised of three main layers epidermis (outermost layer), dermis (connective tissue below epidermis) and the subcutis (lowermost layer) (Planz, Lehr et al. 2016)
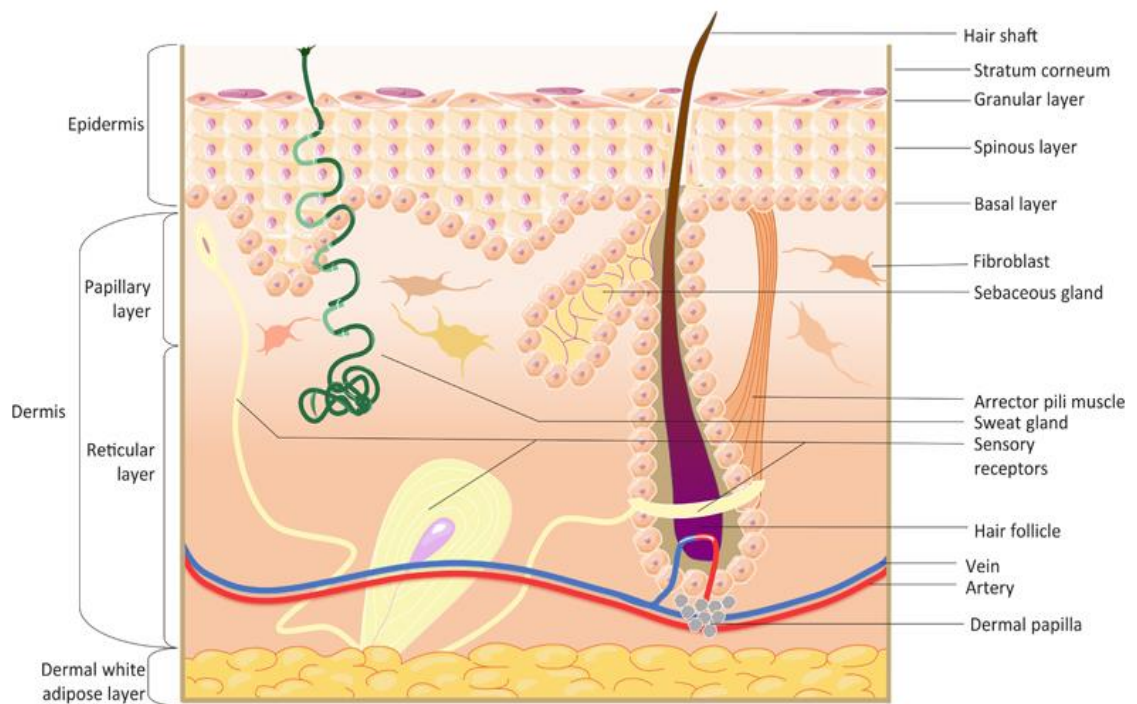
Figure 1 Schematic representation of Human skin (Belokhvostova, Berzanskyte et al. 2018)

2.1.2.1 Epidermis

The epidermis is the outer layer of the skin with a thickness of about 0.05 mm (eyelids) to 0.8-1.5 mm (thicker in palms and soles), It is mainly composed of keratinocytes (present in skin, hair and nails) and melanocytes, merkel cells and Langerhans which form the brick and mortar structure which aids the barrier function of skin (Sebastia-Saez, Burbidge et al. 2020, Alexander, Dwivedi et al. 2012). The epidermis consists of many sublayers including the following: strata corneum, lucidium, granulosum, spinosum/squamous and basale or germinativum as shown in Figure 1 and 2.

2.1.2.1.1 Stratum Basale

The stratum basale contains basal germinating cells which help with regeneration. They also contain melanocytes which produce melanin. Melanin is responsible for giving skin colour and protecting from exposure to the sun (Yousef, Alhajj et al. 2019).

2.1.2.1.2 Stratum Spinosum

The stratum spinosum contains a large number of keratinocytes. They are joined by desmosomes which. Dendritic Langerhans also reside here which can bind to antigens when the skin becomes damaged alerting the immune system (Cárcamo-Martínez, Mallon et al. 2021)

2.1.2.1.3 Stratum Granulosum

The granulosum layer contains around 3-5 cell sub-layers. This layer has diamond shaped cells, keratohyalin granules and lamellar granules. The keratohyalin has lipid packages and filaggrin proteins which bind to cytoskeletal filaments together function as glue keeping the cells adhered (Ahmed Saeed AL-Japairai, Mahmood et al. 2020).

2.1.2.1.4 Stratum Lucidum

The lucidum layers has around 2-3 cell sublayers. It is more present in palms and soles with much more keratinocytes. The mature keratinocytes located in these regions secrete lamellar bodies of lipids and proteins to the extracellular space resulting in a hydrophobic lipid envelope. Its primary function is to act as the mechanical barrier to skin (Yousef, Alhajj et al. 2019).

2.1.2.1.5 Stratum Corneum

The SC also known as the "horny layer" forms the uppermost layer made up of 20-30 layers. Due to the composition of SC it is considered heterogeneous in nature, as it is comprised of keratin (dead keratinocytes also known as anucleate squamous cells). Literature has reported that corneocytes are permeable and contribute largely to the permeability barrier. Due to the anisotropic nature of the lipid layers their permeability depends on the direction and so this heavily dictates the diffusion in skin (Barbero, Frasch 2017). The SC prevents desiccation by providing a permeability barrier which counteracts the water loss from skin and hydrophilic substances. The movement of water from the SC into the atmosphere is referred to as transepidermal water loss (TEWL). TEWL measurements can provide a useful insight into the damage caused to skin by chemicals or physical attacks. Generally, an increase in TEWL is due to damaged skin as a result of impairment in barrier skin function (loss of water from SC thus allowing excess moisture to evaporate from skin into the atmosphere) (Baroni, Buommino et al. 2012).

This layer's thickness can vary tremendously depending on the state of skin (callused). The dead keratinocytes in this layer can secrete defensins which are the layers first line of defence. The SC provides physical, chemical, biochemical (antimicrobial) immunological barriers. The cytoskeletal proteins located in the lower layers have cell to cell junctions which act as the physical barrier. The SC contains lipids, acids, enzymes, macrophages and antimicrobial peptides which aid its chemical and biochemical barrier function. (Sebastia-Saez, Burbidge et al. 2020).

The skins acidic surface serves as an important barrier function in preventing infection. The pH of skin has a sharp gradient across the SC which controls enzymatic activities and the renewal of skin. Its endogenous factors such as sweat, skin moisture, genetic predisposition, detergents, cosmetic products, dressings, topical drugs and antibiotics heavily influence the skins pH. Changes in the skin's pH give rise to various skin issues including dermatitis and eczema.

The drug coefficient of molecules within the SC is significantly smaller (500-10,000 times) than viable skin. The SC is known as the rate limiting step in TDD thus posing an issue with diffusion of high molecular weight (HMW) drugs which in turn makes them ineffective as they cannot enter the bloodstream (Davidson, Al-Qallaf et al. 2008).

The skin has a high level of enzymatic activity primarily due to large amount of biotransformation activity which is a third of that of the liver. Biotransformation usually occurs by enzymes located in the viable epidermis and dermis. It operates by increasing water solubility of foreign substances resulting in a higher excretion and elimination rate. This skin enzymes act as a second biochemical barrier which could explain why certain drugs show limited effect following penetration. Thus, many factors need to be considered as skin enzyme activity varies depending on age (dosage may need to be altered according to patient's metabolism) and anatomical site. The viable epidermis shows the greatest amount of enzymatic activity therefore dermal prodrugs and dermal soft drugs have been suggested as they will be either activated or inactivated prior to entering the dermis, therefore before systemic uptake (Pyo, Maibach 2019).
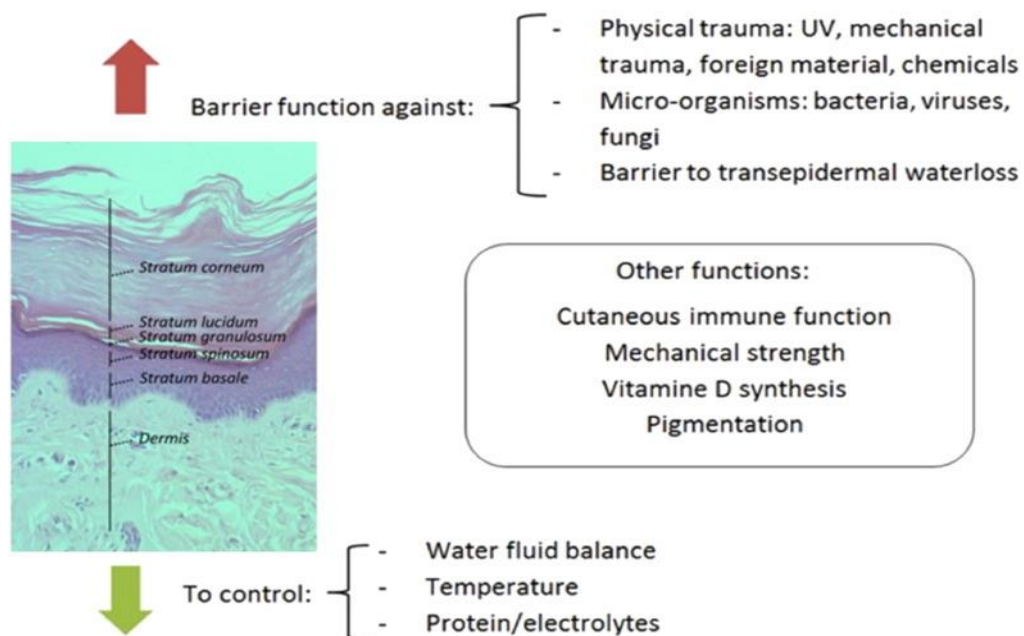
Figure 2 Anatomy of the viable epidermis and function (Ter Horst, Chouhan et al. 2018)

2.1.2.2 Dermis

The dermis lies between the epidermis and the hypodermis. It is highly vascularised. It has been referred to as a homogenous material with respect to the method of mass transport (diffusivity and permeability) (Sebastia-Saez, Burbidge et al. 2020, Donnelly, Ryan, Douroumis 2015). It hosts sweat glands, hair follicles, sensory neurones, muscles and blood vessels. It also contains many fibroblasts and macrophages. Fibroblasts control the renewal and synthesis of the extracellular matrix whilst macrophages work on the elimination of pathogen and foreign material and damaged tissue (Baroni, Buommino et al. 2012, Abdo, Sopko et al. 2020).

2.1.2.3 Hypodermis Subcutaneous layer

The hypodermis (subcutaneous layer) contains adipose lobules, hair follicles, sensory neurones and blood vessels providing mechanical protection, regulating the body temperature as well as aiding metabolism and storage (Pyo, Maibach 2019).

2.1.3 Drug Transport through the skin

TDD approach is a non-invasive systemic alternative to conventional routes (oral and parenteral), avoiding first pass metabolism and providing drug therapy in a minimally invasive and relatively painless manner (Pyo, Maibach 2019). The TDD route improves bioavailability of drugs and their ability to provide systemic and local treatment. The SC is the main barrier for drug delivery due to its composition which can be difficult to overcome as a result of its structure (Takeuchi, Shimamura et al. 2019).

The SC forms a barrier against exogenous substances. Therefore, limiting the delivery of therapeutic agents via this route and their efficiency (Miller, Yu et al. 2017). In order to penetrate through the intact SC, molecules need to meet a range of criteria such as good solubility, being lower than 600 Da, having a log P value between 1 and 3 and they need a high SC partition coefficient (Nurunnabi, Revuri et al. 2017). The SC serves as the primary barrier for drug permeation. However, there are different methods for transfer of natural compounds across skin which include intercellular, intercellular and follicular pathway (shown in Figure 3).
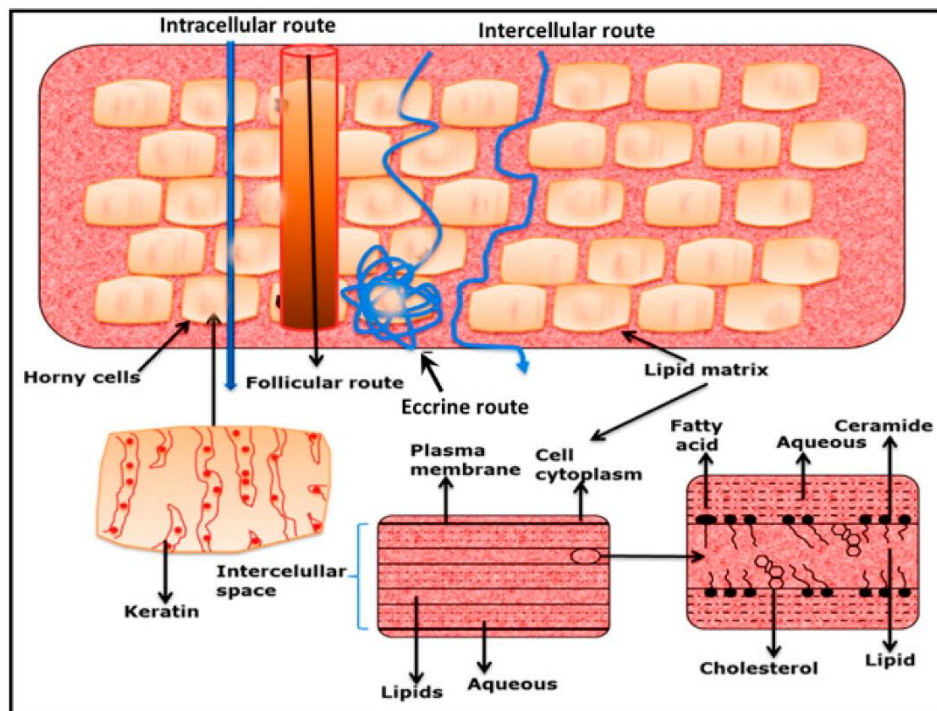
Figure 3 Drug permeation routes across human skin (Shahzad, Louw et al. 2015)

2.1.3.1 Intercellular Lipid Route

The intercellular (paracellular) pathway is the preferred route for delivery of hydrophilic drug substances. Drug molecules move through corneocytes located in SC. Lipophilic drug molecules have followed this route, but it has proved problematic due to the thickness of the SC (Shukla, Upmanyu et al. 2018).

2.1.3.2 Intracellular Transport

The intracellular (transcellular) route facilitates the permeation of lipophilic drug substances as this route has a much more complex environment of a highly cross-linked cellular envelope, keratin filled cell interior and a lipid layer at the surface of corneocytes. This route is lengthier due to the hydrophilic and hydrophobic domains hence this route is not preferred. Volz et al demonstrated the transportation of an amphiphilic molecule (ATTO-Oxa 12) using fluorescence microscopy the route of transport was through the lipid region of the stratum corneum close to the corneocytes showing successful intracellular transport (Qindeel, Ullah et al. 2020).

2.1.3.3 Follicular Penetration

The follicular and transappendegeal path provide rapid and direct transfer of contents into the infundibulum region. This route utilised the shunt route via hair follicles (follicular) and sweat ducts (eccrine). Hair follicles occupy a very small area of skin which is why this route hadn't received much attention (Shahzad, Louw et al. 2015). Recent studies however show that the assumption is only applicable to the forearm whereby most experimental procedures take place. Hair follicles however vary with different body regions the quantity of hair follicles, follicular size, diameter of hair shafts and volume and surface of infundibula. Therefore, hair follicles have been deemed a promising approach for

transcutaneous drug delivery in particular gene therapy and vaccination (Qindeel, Ullah et al. 2020).

2.1.4 Approaches in Transdermal Drug Delivery

There are various technologies and strategies to overcome the SC which can be divided into passive and active methods as outlined in Figure 4. Passive methods aim to optimise the formulation and focus on drug and vehicle interactions in order to overcome the SC. Passive methods include chemical enhancers. They are relatively simple, and they can used in transdermal patches. However, there are many limitations with passive methods primarily having a lag time with drug release which in turn has a negative effect on rapid onset drugs like insulin (Donnelly, Ryan, Douroumis 2015). For enhanced drug permeation it is recommended to use a carrier system to improve therapeutic efficacy.
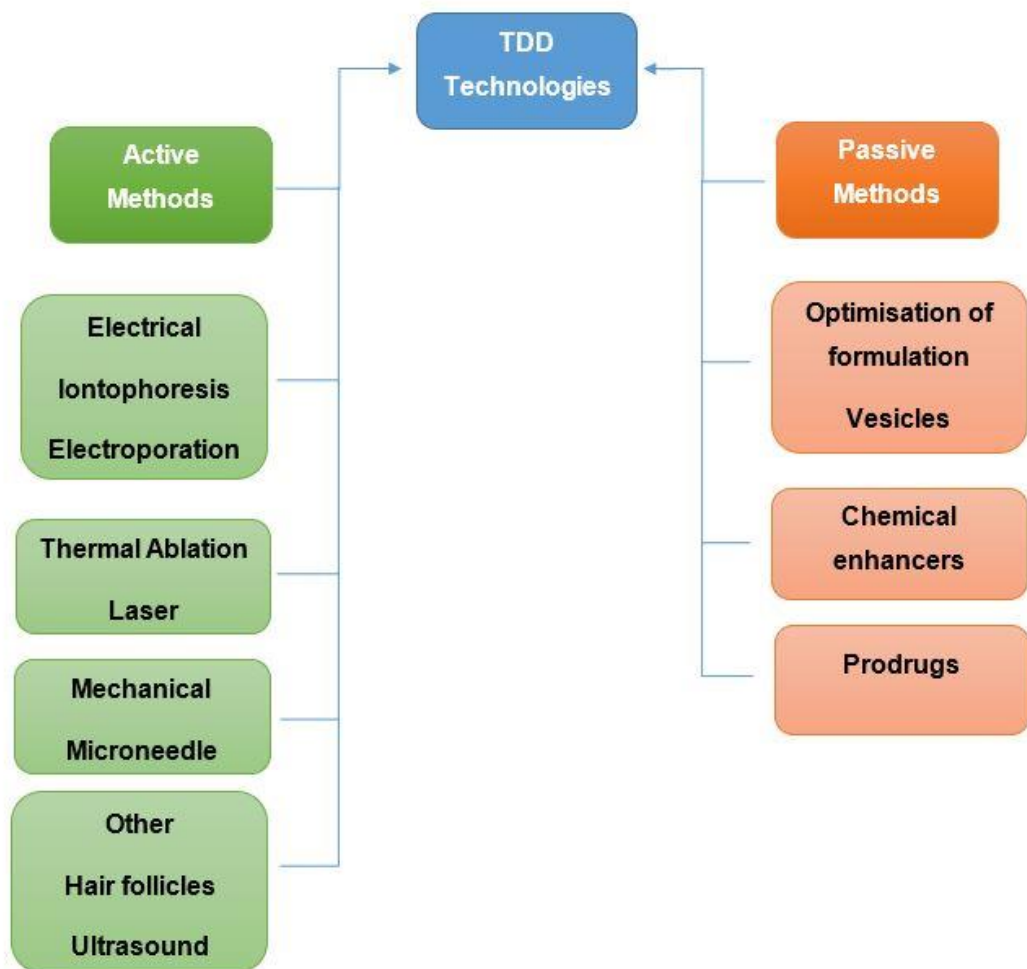
Figure 4: Approaches to enhance transdermal drug delivery

2.1.4.1 Passive permeation enhancement techniques

The most common approach to enhancing permeation through skin for TDD includes chemical permeation enhancers. Extensive research has been conducted in the use of chemical permeation enhancers as a means improve the delivery of molecules through skin. To date, many chemicals have shown enhanced skin delivery which include sulphoxides, terpenes, pyrrolidones, fatty acids, alcohol, glycol, surfactants and urea (Chen, Y., Quan et al. 2014).

Balazs et al reported a synergistic effect with transcutol and sucrose fatty acid esters into the deeper layers of skin (Balázs, Vizserálek et al. 2016). These

enhancers create nano-sized pores which improve permeability to a degree but restrict passage of larger molecules.

Chemical permeation enhancers have had no significant success in improving the transdermal flux of hydrophilic and hydrophobic compounds (Chen, Y., Wang et al. 2013). Therefore, there has been very few incorporated into transdermal formulations and restricted to the cosmetic market due to their incompatibility and skin irritation issues (Chen, Y., Quan et al. 2014).

The prodrug approach focusses primarily on modification of chemical properties of a drug to manipulate its pharmaceutical and pharmokinetic properties resulting in enhanced drug delivery. Diester prodrugs showed greatly enhanced skin permeation compared to the parent drug when it was formulated as an emulsion (Liu, K., Sung et al. 2011).

2.1.4.2 Topical transdermal drug delivery

The most common topical dosage forms include gels, ointments, cutaneous solutions and patches. Topical application has shown to be therapeutically valuable for many applications including acne, seborrhoea, allergic dermatisis growth disorders (Benson, Grice et al. 2019). One of the earliest forms of TDD includes transdermal patches. The ease of administration, control of drug release, ease of termination (system toxicity) and it being user friendly has made it an attractive form of TDD (Alexander, Dwivedi et al. 2012). Scolopamine, was the first transdermal patch commercialised which showed a significant effect against a placebo as well as less side effects. Nitroglycerin has been difficult to administer in an appropriate concentration therefore the Alza Corporation studied three nitroglycerin systems with varying dosage and structures. It proved to be efficacious administered as a patch. Clonidine patches were also produced for hypertension treatment (Pastore, Kalia et al. 2015).

2.1.4.3 Physical Permeation Enhancement Techniques

The main focus with TDD has been on improving delivery of hydrophilic and hydrophobic drug compounds, as well as macromolecules including proteins and peptides derived from biotechnology, which until recently were administered via the parenteral route (Takeuchi, Shimamura et al. 2019). Many physical permeation enhancement techniques have been developed and have successfully demonstrated an improvement in TDD.

2.1.4.3.1 Iontophoresis

Iontophoresis involves using an electric current to drive drug molecules through sweat glands and hair follicles. Hydrophilic drug molecules have been successfully delivered through skin using this technique (Malinovskaja-Gomez, Espuelas et al. 2017). Direct current iontophoresis allows drugs to be delivered directly proportional to the current passed across the skin. Although this method is highly efficient it's limited by the long-term effect which include skin polarisation (due to the continuous applied electrical field which alters the current across skin and so inhibits efficient drug delivery. Alternatively, a pulsed current being applied in a periodic way can depolarise the skin (during the "off intervals") which ensures no residual charge remains in skin before the next pulse. These modes are limited further by the accumulation of small ions on the electrodes which can result in electrochemical burns with prolonged application or with a poorly designed electrode. The pulsed current can bypass the potential of causing electrochemical burns by providing the same electrochemical environment of the solution surrounding the electrodes (Malinovskaja-Gomez, Labouta et al. 2016).

Iontophoresis uses electric currents and sweat glands and hair follicles for TDD whereas, permeation enhancement techniques such as laser and thermal ablation (Lee, Jeong Woo, Gadiraju et al. 2011, Ouyang, Feng et al. 2019), electroporation (Anirudhan, Nair 2019), sonopheresis, cavitational ultrasound and suction function by creating aqueous pores in the SC (Ahmed Saeed AL-Japairai, Mahmood et al. 2020).

2.1.4.3.2 Thermal Ablation

Thermal ablation in TDD involves heating the skin surface to remove SC locally. Research in this area includes a variety of methods, electrical heating elements, radiofrequency and lasers. Jeong Woo Lee et al have demonstrated 1000-fold increase in skin permeability of sulforhodamine B and bovine serum albumin using thermal ablation. This supports the conclusion that thermal ablation can selectively remove SC thus enhancing skin permeability for TDD (Lee, Jeong Woo, Gadiraju et al. 2011). Whilst laser ablation can heat the skin in milliseconds the bulky auxiliary equipment (laser, potentiostat and oscillators) greatly hinders TDD as there is limited sustainability and therapeutic environment as well as reducing patient compliance (Ouyang, Feng et al. 2019).

2.1.4.3.3 Electroporation

Skin electroporation uses high voltage pulses to temporarily disrupt the lipid bilayers. Thus, providing an aqueous pathway across lipid bilayers improving drug diffusion. Gold has been used with electroporation and has synergistically operated to successfully enhance skin permeability and facilitate the transport of diclofenac sodium (Anirudhan, Nair 2019).

2.1.4.3.4 Hair follicles

Hair follicles have been considered as a shortcut for the delivery of xenobiotics (chemicals that are extrinsic to the usual metabolism of that organism which could be unintentional like pollutants or cleaning products or intentional including cosmetics or medical drugs) to the dermis (highly vascularised) in particular for lipophilic and large molecules. Hair follicles are capable of reaching deep into the dermis they provide a larger penetration area as well as high vascularisation rendering them a viable option for transdermal drug delivery (Sebastia-Saez, Burbidge et al. 2020).

2.2 Nanotechnology

There has been an increasing demand to nano-micro sized particles which are highly functional and having complex release profiles which has led to the evolution of fabrication processes for composites. Nanotechnology in the pharma industry has contributed significantly towards formulation development in specialised medicines with enhanced therapeutic efficacy. There has been an exponential grown in nanotherapeutics.

Nanofibres have gained immense interest, with its large range of potential applications. With the ability to act as a nano carrier the diameter of a nanofibre is usually around 100 nm. Ultrafine nanofibres (diameters of less than 100 nm) can be fabricated via electrospinning. This intrinsic characteristic of nanofibres makes them favourable for applications requiring a high surface area (Kamble, P., Sadarani et al. 2017). Cross-linking of fibres has been shown to prevent burst release of biological molecules. Several methods can be utilised including UV irradiation and chemical treatment (Sedghi, Shaabani et al. 2017).

Nanoparticles cannot cross pores if their size is smaller than their own diameter. They can also coalesce when exposed to dry conditions. The first uses of nanoparticles date back several decades ago when they were incorporated into sun blockers. Dendrimers are nano sized macromolecules which could prove advantageous in transdermal drug applications as a skin penetration enhancer. Lower generation cationic dendrimers have shown to enhance skin permeability compared to larger dendrimers (Cevc, Vierl 2010). These nano structures have the ability to provide targeted drug delivery.

2.3 Microneedles

MNs based approach has proven to bypass the SC and provide a more efficient drug delivery device to deliver therapeutics through skin. MNs have the potential to deliver peptides (Zhao, X., Coulman et al. 2017), proteins (Yin, Kuang et al. 2018), vaccines (Chen, F., Yan et al. 2017), oligonucleotides, insulin (Larrañeta, Lutton et al. 2016, Donnelly, Ryan F., Singh et al. 2012), ovalbumin, (Ma, Wu 2017) plasmid DNA (Fernando, Zhang et al. 2016), siRNA (Tu, Du et al. 2017), human growth hormone (Yu, W., Jiang, Liu, Li, Chen et al. 2017) in a less invasive and painless way compared to hypodermic needles. In recent years, MNs have been utilised for more novel applications including fluid sampling, biosensors, microanalysis and electrochemical biosensing (Skoog, Miller et al. 2015). MNs generally are composed of arrays of sharp protrusions (25-2000 μm in length) (Ma, Wu 2017) which are able to penetrate into the SC but short enough to avoid stimulation of pain receptors (Ita 2015). MNs can be composed of various materials such as plastics (Luangveera, Jiruedee et al. 2015), silicon (Lee, Hyunjoo J., Son et al. 2015), metals, biodegradable polymers (Zhu, Wang et al. 2016), sugars, glass and other inorganic materials. These MN patches are able to perforate the SC, creating microscopic aqueous pores allowing drug to pass through via micro-channels to the target tissue (Yu, W., Jiang, Liu, Li, Chen et al. 2017, Larrañeta, Lutton et al. 2016).

Successful MN penetration is crucially influenced by various factors including the MN length (typically 900 μm), density, tip and base diameter and most importantly, the materials they are composed of (Loizidou, Inoue et al. 2016). Gill et al reported that by decreasing MN length it had significantly reduced the pain, between 5 to 40% more than when using hypodermic (26 gauge) needles. MN width, thickness and tip angle had no significant effects (Gill, Denson et al. 2008).

A synergistic approach amalgamating both hollow MNs and low frequency sonopheresis has been utilised to improve the rate of drug delivery. However, this method requires further study in terms of optimisation to improve efficacy (Chen, B., Wei et al. 2010). More recently, iontophoresis has been used with a MN has

been used for ocular drug delivery delivering nanoparticles (Jung, Chiang et al. 2018). MNs have also been integrated with electroporation to facilitate drug delivery of nucleic acids into cells but this adds to the complexity of them and costs (Zakrewsky, Kumar et al. 2015).

2.4 MN Design and Delivery Approach

2.4.1 MN Design

Microneedles have gained considerable interest as a viable system for TDD. The fact they are able to bypass the SC and deliver drugs efficaciously in a relatively painless manner have rendered them advantageous for this route. MNs possess the ability to deliver a range of compounds as well as act as biochemical sensors. Depending on the type of drug being delivered careful consideration must be given towards the design. There are many types of MNs which include solid, hollow, dissolving, coated and hydrogel forming MNs (shown in Figure 6).

2.4.1.1 Solid MNs

Solid MNs (SMNs) operate in a 'poke and patch' (Van der Maaden, Jiskoot et al. 2012) fashion whereby transitory aqueous micro-scale channels are created in the SC following insertion into the skin (Prausnitz 2004). A drug-loaded patch acting as an external drug reservoir is applied following the removal of SMNs allowing the active formulation to diffuse through the channels to reach the targeted tissue via passive diffusion. SMNs are simple to fabricate and can be composed of a range of materials including ceramic, metals, glass, silicone (Table 2) and non-degradable polymers (Ma, Wu 2017) with the ability to sufficiently enhance efficiency of drug delivery (Prausnitz 2004). The limiting

factor here is the pore characteristics (size and shape and density) which affect drug delivery efficiency (Kim, Yeu-Chun, Park et al. 2012).

2.4.1.2 Dissolving and Degradable Polymer MNs

Dissolving MNs (DMNs) upon insertion dissolve into the skin releasing the drug. They are composed of biocompatible material such as rapidly dissolving sugars (e.g. trehalose and raffinose) and biodegradable polymers (PVP and polyvinyl alcohol (PVA) (McGrath, Vucen et al. 2014). Sugars have been used in many applications due to their biocompatibility and controlled release profile (Lee, Jeong W., Park et al. 2008). However, the hygroscopic nature of sugars limits their applicability in DMNs as it can lead to physical and chemical degradation of DMNs. Coating the DMNs could provide a strategy to prevent the loss of active and improve DMNs storage and handling stability throughout its life cycle (McGrath, Vucen et al. 2014). Tranexamic acid and the bio-degradable PVP MN has been formulated with 34% local drug release with the remaining successfully permeating through skin with no dermal toxicity (Machekposhti, Soltani et al. 2017).

2.4.1.3 Hollow MNs

Hollow MNs (HMNs) operating similarly to hypodermic needles whereby upon insertion a liquid flow into the skin. Drug flow rates can be controlled via machine manipulation (syringe and infusion pump) (Martanto, Moore et al. 2006). The most noteworthy advantage of using such MNs is the direct targeted delivery of liquid formulations compared to SMNs (Roxhed, Griss et al. 2008) leading to protection of the formulation and reducing the loss of active. HMNs can be utilised for signal monitoring, blood and tissue sampling applications which have a significant influence within the healthcare remit (Ma, Wu 2017, Vinayakumar, Hegde et al. 2014). These HMNs can be made up of silicone (Vinayakumar,

Hegde et al. 2014), metal (Roxhed, Griss et al. 2008), polymers (Lhernould, Deleers et al. 2015), glass (Wang, Ping M., Cornwell et al. 2006) and ceramic materials (Ovsianikov, Chichkov et al. 2007). Drawbacks of such MNs include blockage of needle openings upon HMNs insertion into the skin and flow resistance (thickness of dermal tissue against the HMNs tips upon insertion).

2.4.1.4 Coated MNs

Coated MNs (CMNs) which adopt the 'coat and poke' principle. Once inserted into skin the drug coating dissolves into skin once removed. In recent years CMNs have received much attention for effective TDD into skin as well as other tissues. Various materials coated onto MNs have been investigated which include APIs, proteins, peptides, deoxyribonucleic acids and viruses. Matriano et al demonstrated that coated MNs compared to intramuscular administration of ovalbumin in guinea pigs, there was a 50-fold increase in the immune response for ovalbumin coated SMNs (Matriano, Cormier et al. 2002).

A range of coating methods have been developed. There are variations amongst the methods including the areas of the MNs which are coated. Selective coating of the shafts is the most desirable as there is better drug delivery efficiency and less drug wastage (some methods coat the base array as well as shafts) (Ingrole, Gill 2019).

Coating methods (shown in Figure 5) include dip-coating (a rapid and versatile process) (Chen, Y., Chen et al. 2017), spray coating (McGrath, Vrdoljak et al. 2011), gas jet drying (Fernando, Zhang et al. 2016), piezoelectric inkjet printing (O'Mahony, Hilliard et al. 2017) and electrohydrodynamic atomisation (EHDA) based processes (Haj-Ahmad, Khan et al. 2015).

Dip coating is a relatively rapid and simple method. This method involves dipping MNs in a coating liquid, which upon removal should leave an intact film. However, there are some issues associated with uncontrolled deposition of material on

substrate as well as uneven layers on the surface, variations in weight with the coated arrays, waste and reduced drug loading.

To improve and overcome the limitations of dip coating piezoelectric inkjet printing has been employed. The piezoelectric inkjet printing method (Figure 5E) of coating MNs, operates by ejecting small droplets of the coating material directly on the surface of MNs using piezoelectric nozzles (Uddin, Scoutaris et al. 2015). Ross et al demonstrated rapid solid-state insulin delivery (within 20 minutes) using franz diffusion cells from MNs inserted into porcine skin from metal MNs coated via inkjet printing with insulin polymeric (gelatin and poly(2-ethyl-2-oxazosaline) (Ross, Scoutaris et al. 2015).

Gas jet drying is another approach for assisted drying coting. This speeds up the drying process, allowing the dissolved solids to be coated onto MNs. The main issue with this method is that although MNs can be coated it cannot avoid the base substrate being coated too (Ingrole, Gill 2019).

Spray coating utilises fluid pressure to form droplets which are used to coat MNs. To ensure conformal coatings with this method coalescence of drops is preferred as well as smaller droplets. The size of droplets can be done so by achieving a balance between viscosity and surface tension. Studies have shown limited success with spray coatings as Vrdoljak et al's findings showed that coatings localised at the base of silicon MNs when spray coated (Vrdoljak, McGrath et al. 2012). Thus, the rapidly emerging EHDA process has been considered a better coating method. This process can provide more control over the thickness of the nano/micro-structure coatings and coating uniformity (Rai, Gautam et al. 2017, Hapgood, Litster et al. 2015). This involves Es or Esp a formulation and the resultant particles and fibres reach the MNs.

Polymers are commonly used in this process due to the ability to control release kinetics. For example, PVP provides rapid release profile whilst PLGA and PCL provide sustained release profiles. These can be utilised as encapsulating matrices for active drugs, providing further control over the drug release profile and allowing for personalised drug delivery (Chou, Woodrow 2017).
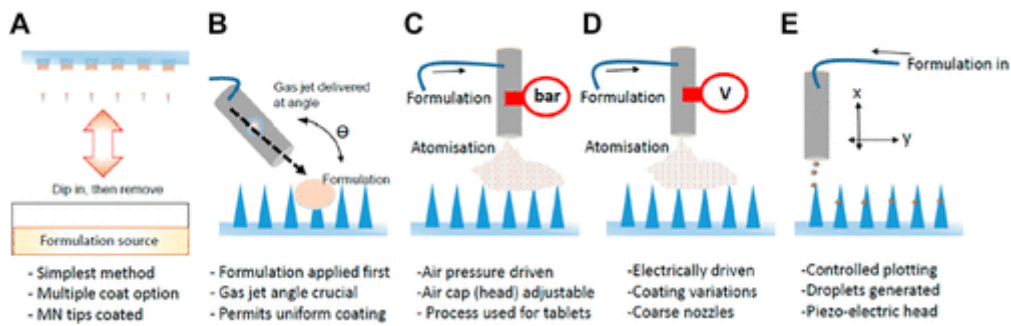
Figure 5: Coating methods for microneedles (A) Dip coating; (B) Gas-jet drying; (C) Spray drying; (D) EHDA processes; (E) Ink-jet printing (Haj-Ahmad, Khan et al. 2015)

1.4.1.5 Hydrogel forming MNs

Hydrogel forming MNs (HFMNs) operate similarly to SMNs 'poke and patch' principle; but the 2-step sequence is eliminated (Migdadi, Courtenay et al. 2018). Upon administration, HFMNs start to swell by taking up interstitial fluid (IF) without leaving polymeric residue following removal from the skin. As the needle tips swell, conduits are produced providing a drug diffusion reservoir to the dermal circulation thus enabling controlled drug release to skin (Donnelly, Ryan F., Singh et al. 2012). Migdadi et al study showed successful transdermal delivery of metformin hydrochloride with hydrogel forming MNs showing promise for other high dose drugs using this method (Migdadi, Courtenay et al. 2018).
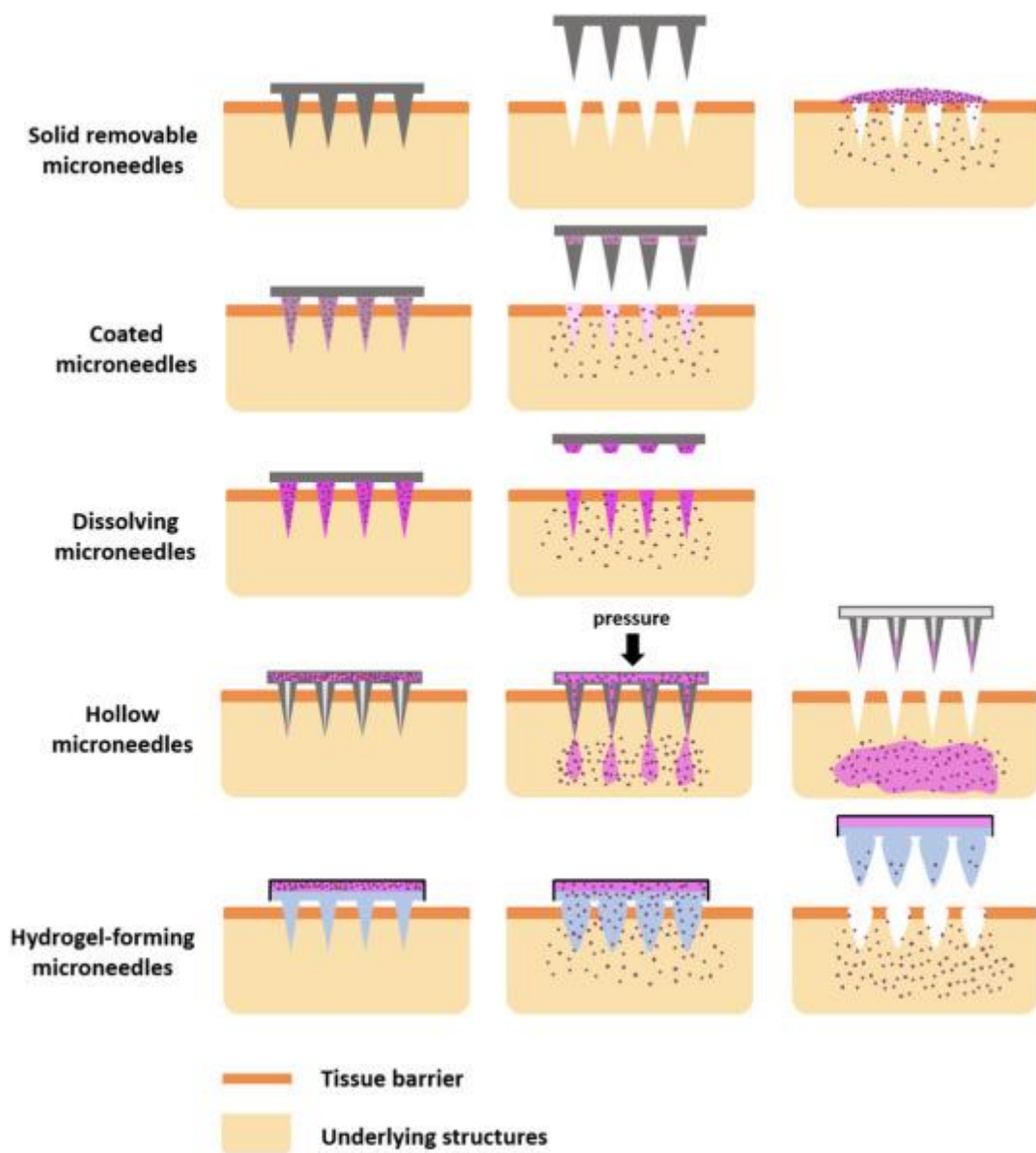
Figure 6: Microneedle design (Rzhevskiy, Singh et al. 2018)

2.4.2 Microneedle material composition

2.4.2.1 Metals

Metals are commonly used in MN fabrication due to their precise insertion capabilities and ability to provide rapid and efficacious drug delivery. An example of a coated metal MN is shown in Figure 7 A and B. Metal MNs are economically preferable with respect to high patient compliance due to their self-administering ability for a large range of drug molecules (Ross, Scoutaris et al. 2015).

Stainless steel is the most commonly used metal for metal MNs production Other metals include titanium (Ti) (Thakur, Fallows et al. 2014), alloys (Khandan, Kahook et al. 2016), palladium (Pd) (McConville, Davis 2016), nickel, copper (Kim, Yeu-Chun, Park et al. 2012), gold (Au) (Mukaibo, Johnson et al. 2015) and tungsten (Sergi, Jensen et al. 2016). Metals such as Ti, stainless steel and Au are more preferable for implantable medical devices. Current fabrication methods include laser ablation, micromachining, photochemical etching and laser cutting. Long-term stability of metal MNs can be greatly improved by coating them (Haj-Ahmad, Khan et al. 2015).

Metal MNs have already shown their potential in the delivery of various active molecules. For instance, vaccine coated stainless steel MNs have been developed. Inactivated influenza virus coated MNs prompted strong humoral and cellular immune responses providing protection against virus challenge as comparable as intramuscular immunization utilising a new highly effective immunization method (Koutsonanos, del Pilar Martin et al. 2009). Gold MNs have also been used for gene delivery into the microalgae *C. reinhardtii* (a unicellular plant organism) using nano-micro-needle arrays. The gene has been successfully delivered and expressed by the *C. reinhardtii* cells (Table 1) (Mukaibo, Johnson et al. 2015).

Titanium (Ti) has been extensively used in implantable and other medical devices (Skoog, Miller et al. 2015). More recently, Ti alloy MNs have been developed for monitoring blood glucose levels, which can be advantageous for patients suffering from diabetes. Ti MNs comprises an inner MN (100 µm) and an outer MN (200 µm) (Waghule, Singhvi et al. 2019). It is vital to consider the biological safety requirements ensuring the elimination of toxic elements for it to be considered for medical use. Accordingly, Ti alloy MNs (Tsuchiya, Jinnin et al. 2010) and Palladium (Pd) incorporated MNs (McConville, Davis 2016) can be safely used. Iron, nickel and vanadium metals should be excluded from such alloys due to their toxicity effects (Tsuchiya, Jinnin et al. 2010). There has been considerable interest in other application for MNs including sensor technology (e.g. Pd) (McConville, Davis 2016). Ti alloy MNs have also been utilised for electrochemical sensing. These MNs were coated with nitrogen incorporated ultra-nanocrystalline diamond (N-UNCD). The purpose of this device is for electrochemical detection of dopamine and uric acid. This coating enhanced MNs mechanical strength, biocompatibility, and hardness and provided an electrochemically stable surface (Skoog, Miller et al. 2015). Metal MN fabrication process include micromachining, electroplating, laser cutting. However, these methods have been reported to have reduced efficiency, costly and unsuitable for scaling up for mass production (Chen, Z., Ren et al. 2018).
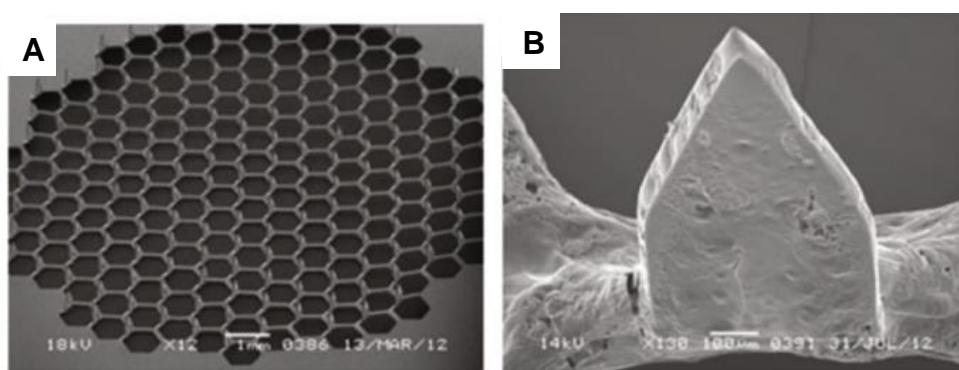
Figure 7 SEM of Polymer and metal MN arrays. a Low magnification of PVP dip-coated solid stainless steel (Khan, Mehta et al. 2014)

2.4.2.2 Polymers

Polymers are amongst the most versatile class of materials utilised in drug delivery (shown in Figure 8A and B). Ideally, polymers should be biocompatible and biodegradable. Dissolving polymers are considered the most effective materials in the composition of MNs and have many applications (Dangol, Yang et al. 2016). The choice of polymer utilised, is attributed to exceptional biocompatibility and biodegradability capabilities, reduced toxicity, sufficient toughness (more tough than glass and ceramics) and economic status.

A range of macromolecular compounds have been utilised efficiently for MNs fabrication. These include water-soluble sugars (sucrose, mannitol, xylitol, trehalose and galactose) and biodegradable polymers (including PVP, PLGA, PCL, PVA (Amodwala, Kumar et al. 2017), polylactic acid (PLA) (Zhu, Chen et al. 2017), carboxymethlcellulose (McGrath, Vucen et al. 2014), poly(methyl methacrylate) (PMMA) (Choi, S., Kim et al. 2010), polystyrene (PS) (Hegarty, McConville et al. 2019, Luangveera, Jiruedee et al. 2015), Gantrez®640 AN-139 (Caffarel-Salvador, Tuan-Mahmood et al. 2015), silk fibroin (Yin, Kuang et al. 2018), f 3-aminophenylboronic acid-modified alginate (Alg-APBA and Hyaluronic acid (HA) (Yu, W., Jiang, Liu, Li, Chen et al. 2017)).

Polymers are frequently used in DMNs and HFMNs and less commonly in coated, solid and hollow MNs. This is accredited to their soft nature, but they are highly likely to undergo buckling (structural) failure during insertion. Therefore, Park et al's studies indicate that MNs exhibiting an aspect ratio of length to equivalent diameter below 12:1 and Youngs modulus value above 3 GPa would greatly reduce buckling and lead to better skin insertion (Park, Prausnitz 2010).

Natural polymers such as silk fibroin protein have been used to create unique MN devices using reverse PDMS fabrication mould, showing great potential of this fibroin MN with controllable drug release. These materials are able to swell to aid drug release and possess enhanced biocompatibility (FDA approved) and strength (Yin, Kuang et al. 2018). Research with modified alginate and HA based MNs fabricated using micromolds has been used for transdermal delivery of

insulin for Type 1 diabetes. This MN demonstrated good mechanical strength and degradability (Yu, W., Jiang, Zhang et al. 2017). Many therapeutic biomolecules such as proteins (Monkare, Nejadnik et al. 2015), chemotherapeutic (doxorubicin) drug(Yang, J., Liu et al. 2019, Chen, M., Lin et al. 2016) have been incorporated into HA MNs. A HA and PVP DMN device has been used to deliver capsaicin as a robust TDD system to improve lipophilic drug delivery. This approach has shown promise in effective rheumatic arthritis treatment on model mice. This advanced polymeric system based DMNs represent an innovative approach for lipophilic drug delivery (Dangol, Yang et al. 2016).

HFMNs fabricated using such polymers can successfully penetrate into the skin whilst mechanically resisting fracture once dried. The addition of a pore-forming agent (e.g., NaH_2CO_3) can modify the swelling ability of HFMNs (Donnelly, Ryan F., Singh et al. 2012). Polyanhydride polymers are commonly used for HFMNs as well as PVA, CMC and polysaccharides (dextran and gelatin) (Hong, Wu et al. 2014). Drug loading is vastly improved in HFMN's compared to other polymeric DMNs as they are not limited by the composition of the formulation being loaded (Larrañeta, Lutton et al. 2016, Hong, Wu et al. 2014). Recent studies have found these MNs applicable for lithium monitoring (Eltayib, Brady et al. 2016), paediatric drug delivery (Caffarel-Salvador, Tuan-Mahmood et al. 2015) as well as electromodulated hydrogel MN array for chronic pain (Indermun, Choonara et al. 2017) and for therapeutic drug monitoring (Caffarel-Salvador, Tuan-Mahmood et al. 2015).

Polymeric MNs based-enzymatic electrodes have the ability to act as electrochemical biosensors. Calio et al developed a device which was manufactured by photolithography of poly (ethylene glycol) diacrylate (PEGDA) covered with glucose oxidase (GOx) and lactose oxidase (LOx) enzyme in addition to redox mediator (vinylferrocene) and photoinitiator (Darocur©). The electrochemical biosensor could detect lactic acid and glucose in phosphate buffer saline solution. This wearable patch was patented due to its ability to constantly observe the level of glucose in diabetes patient's blood and/or detecting acid lactic levels in athletes (Table 1) (Caliò, Dardano et al. 2016).

The most frequently utilised sugar for MN arrays is maltose. Unfortunately, carbohydrate based MNs have been reported to have instability issues during handling, processing and storage (Donnelly, Ryan F., Morrow et al. 2009). Manufacturing of such types of MNs requires thermal treatment thus limiting the type of drug to be utilised with such MNs. Drug delivery can also be adversely affected by partially dissolving sugar molecules which can block the MNs holes, limiting drug delivery. Moreover, various problems are associated with sugar MNs storage. For instance, subjecting these MNs to high temperature and humidity makes them more brittle and prone to liquefying (Luangveera, Jiruedee et al. 2015).
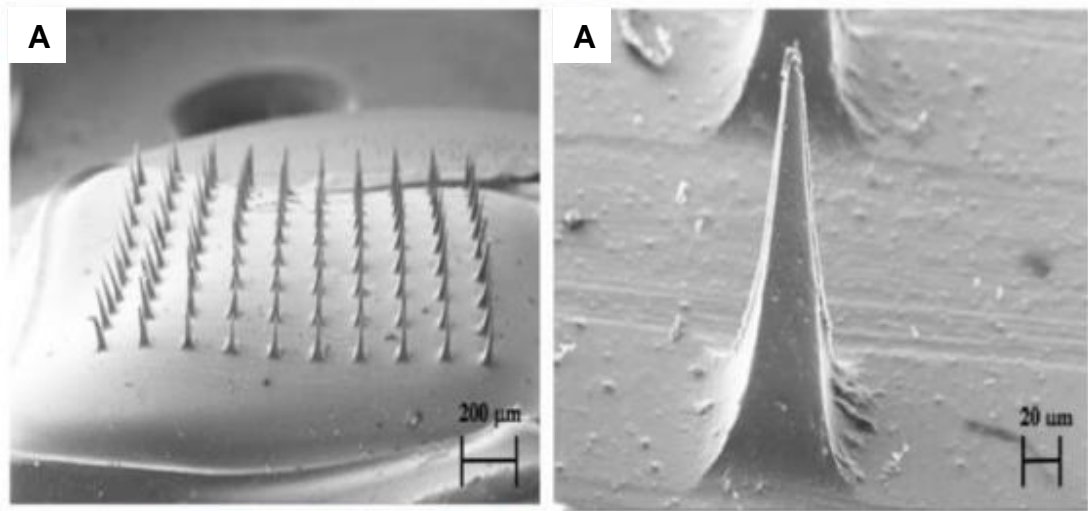
Figure 8 SEM (A) 10×10 Polymer MN array (B) Higher magnification of polymer MN (Khan, Mehta et al. 2014)

2.4.2.3 Inorganic material

Many inorganic materials have been utilised for MN fabrication. For instance, inorganic silica glass (ISG) has been used for MN devices. ISG is a brittle material that can be manufactured with a range of geometries for experimental use with nano-scale dimensions. Glass MNs (GMNs) are physiologically inert hollow MNs (shown in Figure 9 A and B) which allow the visualisation of the flowing fluid (Larrañeta, Lutton et al. 2016)**.**). An example of ISG is borosilicate glass (Pyrex®), an elastic material (Table 1) with an elastic modulus of 64 GPa (Bouras, Madjoubi et al. 2009). This system is still not commercially available for use in drug delivery, and they are restricted for experimental purposes only (Wang, Ping M., Cornwell et al. 2006). This is due to processing difficulties and the integrity of GMNs is an issue, with silica glass being a brittle material as the tips can break upon insertion and fabrication time-consuming (being handmade by drawn-glass micropipette techniques). However, glass HMNs can be inserted into the skin multiple times without compromising the needle structure demonstrating its mechanical stability. These MNs have successfully been used for insulin treatment.

Glucose monitoring is possible using GMNs, providing a more patient friendly method by withdrawing IF (1–10 µL) using multiple glass needles (tip radii of 15-40 µm) rather than conventional lancets which are considered painful causing the current lack of compliance. GMNs are economic and simple to use hence why they are widely used in patch-clamping, microperfusion, embryo handling systems and microinjection. GMNs and polydimethylsiloxane (PDMS)-based microsystems were merged together into GMNs and PDMS-based microfluidic valve to extract the advantages of both systems (Lee, S., Jeong et al. 2003). This microinjection system has various applications in biotechnology. It is very simple to fabricate, cheap, require less driving pressure and does not require highly skilled workers (Wang, Ping M., Cornwell et al. 2006).

Bioceramic composite MNs consisting of the organic polymer gelatine and the inorganic polymer (hydroxyapatite) were fabricated via a template method. The biocompatible (low cytotoxicity) system demonstrated sufficient mechanical

properties using a mouse model. These MNs can provide a more sustained release of insulin with pronounced and effective hyperglycaemic effect as compared to the subcutaneous injection (Yu, W., Jiang, Liu, Li, Tong et al. 2017). A similar composite MNs system for insulin TDD was fabricated from calcium sulfate (inorganic polymer) in combination with gelatin. There was better hypoglycaemic effect compared to subcutaneous injection of insulin (Yu, W., Jiang, Liu, Li, Chen et al. 2017).

The use of mesoporous silica nanoparticles (MSN) as drug delivery vehicles has gained favourable interest due to its controlled size, efficient *in-vivo* biocompatibility, large surface area and pore volume allowing for effective drug loading (small active molecules or proteins) (Narayan, Nayak et al. 2018, Mahony, Cavallaro et al. 2013). A novel intradermal antigen delivery system has been developed which involves the amalgamation of MSN and MNs. This system has synergistically provided vaccine delivery by coating pH-sensitive pyridine-modified silicon MNs loaded with Ovalbumin (model antigen) and lipid bilayer (LB). These MSNs were refined exposing larger pores (AEOP-MSNs) resulting in more efficient loading of AEP-MSNs. This conferred stability, targeting and multicomponent delivery and the ability to encapsulate any low molecular weight (LMW) compounds (RNA, DNA and proteins) in MSNs (Tu, Du et al. 2017).

Zeolite is an inorganic material, and their structure can be mesoporous, microporous or microporous. They can be modified for a range of controlled and targeted drug delivery systems including MNs. Their microscopic size dimensions and superior capability of penetrating skin tissue, in a non-invasive way, without risking infection, deems them capable as excellent candidates for MN drug delivery (Servatan, Zarrintaj et al. 2020). The microporous aluminosilicate structure of zeolites was used to develop various shapes of MN (tapered, hollow and cylindrical shapes). Zeolite MNs (ZMNs) were characterised by sufficient mechanical strength and safety by assessment of zeolite MN geometry to its axial force achieving a safety factor of 3.2-4.3. This was owed to the sharp edge of crystals on the tip. From *in vivo* (mouse model) TDD applications of influenza vaccine the zeolite MNs indicated successful vaccination (Poon 2013).
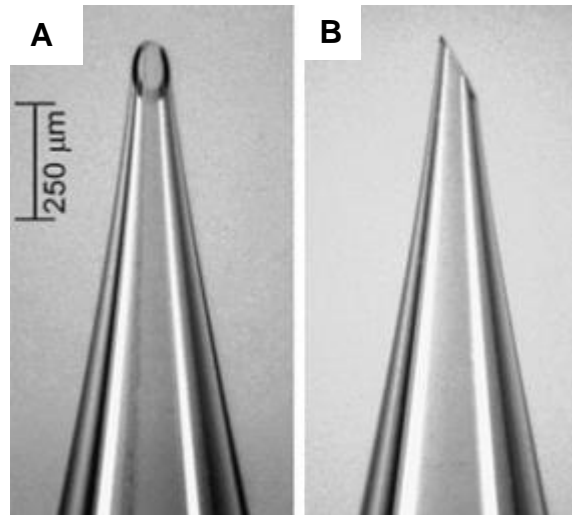
Figure 9 (A) Front and (B) side views of a hollow, glass microneedle (Larrañeta, Lutton et al. 2016).

2.4.3 Fabrication of MNs

2.4.3.1 Micromolding

The most common fabrication method for MNs is based on micro-molding processes (Ruggiero, Vecchione et al. 2018). This usually involves photolithography and molding techniques to produce the polydimethysiloxane (PDMS) micromold (usually made in one step by drilling on the surfaces of 2mm thick PDMS sheets with a laser beam which is then filled with the material such as ceramics, polymeric formulation (sugars, natural and synthetic polymers). This method has high scalability but is limited by its number of processing steps, preparation of master template and not all drugs can be used (thermo liable) (Wang, Qi Lei, Zhu et al. 2016).

2.4.3.2 Lithography, wet and dry etching

Lithography and wet etching has been a popular method for the fabrication of silicon and glass MNs. The drawbacks of such methods include the need for specialist equipment (clean rooms) and the production of toxic waste, which is expensive, complicated, inconvenient, and not environmentally friendly (Wang, Renxin, Wang et al. 2016).

Advantages of using additive processes such as drawing lithography for the fabrication of MNs allows for the manipulation of the size and shape of MNs to improve mechanical stability, release kinetics, release profile (Lee, JiYong, Park et al. 2015). However, using photocurable polymers can also be problematic as there is potential for the drug to be inactivated by UV radiation and toxic photo-initiator residue in the final MN. This technique has been advanced with the use of an in-situ lens based lithographic approach to alter the tapered cone produced into bevelled, chisel tip MNs using microelectromechanical masking and etching (Indermun, Luttge et al. 2014).

Additive processes including 3D printing, electro-drawing, thermal drawing can produce 3D polymer MN structures from 2D surfaces or droplets (Chen, Z., Ren et al. 2018).

2.4.3.3 Electro drawing

The electro-drawing technique is a non-contact, reduced temperature, UV-free method for the fabrication of PLGA MNs. This technique produced MN arrays with optimised shape and dimension. This method involves a pyroelectric field and micrometric elements which allow temperature control on a microscale and a pyroelectric crystal controlling the EHDA action once voltage is applied to the circuit (Ruggiero, Vecchione et al. 2018). 3D printing is a flexible process allowing for personalisation and customisation, but the resolution is limited and so the length of the resultant MNs is on a millimetre scale with tip diameters of 100 µm.

Droplet-born air blowing includes better fabrication conditions without the need for heat or UV irradiation and has good productivity and has been commercialised (Chen, Z., Ren et al. 2018).

2.4.3.4 Thermal drawing

Thermal drawing involves a heating a polymer which is vertically drawn by a metal pillar structure at a controlled speed. This is followed by cooling then the neck is fractured by fast drawing forming the MN structure. However, issues regarding the fracturing stage which ultimately leads to a flat or elongated apex hence limiting insertion ability as well as the tip. Although it is a relatively simple technique optimisation has been problematic thus different fabrications have been investigated in recent years (Choi, C. K., Lee et al. 2013).

2.4.3.5 Magnetorheological drawing lithography

Most recently magnetorheological drawing lithography (MRDL) has been investigated as a novel method for efficient fabrication of MNs, bio-inspired MNs and MN arrays. This additive technique rapidly draws a 3D MN structure from a droplet of curable magnetorheological fluid (CMRF) which is drawn directly from any substrate to form a 3D MN under a magnetic field. This technique amalgamates the advantages of thermal drawing (without the need for a mask and UV irradiation) and does not require adjustments to the drawing temperature. These MNs were able to prove the flexibility and feasibility of the MRDL technique (Chen, Z., Ren et al. 2018).

In addition to potential drug delivery applications there has been a rise in demand for smart medical devices capable of bio sensing. Earlier MN designs were usually based on micromachining and photolithographic methods. The preparation of polymeric MN arrays has led to the innovation of more advanced sensor designs. The typical approach to MN sensor design includes the

deposition of metallic layers through sputtering or evaporation onto polymer structures. Advanced designs emerging in this remit include sensors with conductive/catalytic particles.   With the use of carbon Nps within an inert/biocompatible polymer could increase the possibility of developing electroanalytical sensors (Hegarty, McConville et al. 2019).

2.4.3.6 Droplet air born blowing

The droplet air born (DAB) blowing process was investigated by Kim et al and it was found that it provides gentle (4-25 °C) and rapid (less than 10 minutes) MN fabrication whilst minimising drug loss. Drug loading can be controlled by pressure and time of the droplet dispenser as well as the air blowing shapes the droplet to the MN providing enough force sufficient to penetrate skin. DAB- based insulin DMNs have shown potential in providing complete drug delivery without any drug wastage (Kim, Jung Dong, Kim et al. 2013). This method has been combined with centrifugal lithography (two droplet DAB) to fabricate DMNs and assess activity of encapsulated drugs. It was reported that the manufacturing process for DMNs by centrifugal lithography exerted less stress on the drug loaded DMNs minimising activity loss over time thus confirming centrifugal lithography efficient for DMN fabrication (Huh, Kim et al. 2018). Kim et al's research into allergen (*Dermatophagoides farinae* (*D. farinae*) extract (*DfE*)) loaded MNs (fabricated using DAB) for allergen specific immunotherapy (SIT) and atopic dermatitis (AD) showed stable allergenicity evoking immunogenic responses all without side effects compared to subcutaneous injection. This method of fabrication was achieved within 10 minutes at less extreme conditions (not needing heat/UV irradiation) (Table 2) (Kim, Ji Hye, Shin et al. 2018).

Table 1 Summary of materials used for microneedle-based therapeutics

Type of Material	Example	Application	Engineering Method	Limitations/Toxicity	Future perspectives	Ref.
Metals	Ti	Ocular drug delivery.	Lithographic patterning and deep reactive ion etching.	For sustained drug delivery, a nano or micro-particle carrier is essential. The loading efficiency of these MNs can be improved by increasing thickness but could lead to increased insertion force and trauma.	Further studies are necessary to determine the most suitable formulations and conditions for higher molecular weight drugs and/or the different formulation challenges.	(Khandan, Kahook et al. 2016)
	Pd	Transdermal Electroanalysis	Three-step needle casting process.	Currently the working electrode is made up of MNs. However, a separated counter and reference system can be fabricated which can be positioned with the current MN providing a more refined MN sensor system.	Further adaptations can be made to the metallic-powder-polymer mixture with more control over particle size can advance the performance of the metallic conductor.	(McConville, Davis 2016)
	Au	Gene delivery	Template synthesis method	The integration of recombinant DNA into the host genome was not stable.	This system shows promising approach for gene delivery to microalgae but can be applied to other plants.	(Mukaibo, Johnson et al. 2015)
	Ti	Electrochemical biosensing	Micro machining	Insufficient deposition parameter data reduced MN sensing ability	Further investigation is required for the use of N-UNCD MN electrodes with	(Skoog, Miller et al.

Polymers	Application	Method	Results	Future work	Reference
PLA	Insulin	Insulin loaded onto PLA RSMN using micro-molding.	Elasticity of skin made it problematic for RSMNs to be inserted. The longer length RSMNs can achieve complete insertion but could be painful and cause bleeding.	Need to optimise the RSMN structure (length) for complete insertion but no pain	(Zhu, Chen et al. 2017)
PVA:PVP (9:1)	Management of Arthritis	Micromolding	Upon storage for three months, a significant change in needle axial fraction force was detected due to moisture absorption.	Higher animal experiments with locally applied patches could confirm the scope of drug deposition.	(Amodwala, Kumar et al. 2017)
PVP and methacrylic acid	Tranexamic acid	Micromolding using lithography method	PVP MNs (36-needles) were fully dissolved in Albino rat skin after 7 h. However, conical microneedles (12-needle) disappeared in 6 h.	Future studies may investigate the use of polymer MNs loaded with TXA in melasma animal models; further research may attempt to fabricate a tranexamic acid polymer microneedle with flexible base for easier use.	(Machekposhti, Soltani et al.)
Gantrez ®640 AN-139, PEG	Paediatric drug delivery.	Laser engineering using molds.	This system was not applied or used for humans.	For clinical uses, these MNs will have to demonstrate efficacy and safety, usability in human volunteers.	(Caffarel-Salvador, Tuan-Mahmood 2015)

immobilised biomolecules (e.g. antibodies and enzymes) for selective electrochemical detection of biomolecules.

PEGDA	Electrochemical biosensor	Photolithography	The molecular weight of PEGDA determined the MNs mechanical properties (indentation, hardness and so diffusion of analytes and penetration of MNs in skin). This could limit the amount of PEGDA in the polymeric solution.	A more complex signal processing based on chronoamperometric signal could result in a faster response of the device (order of second dozens).	...et al. 2015) (Caliò, Dardano et al. 2016)
TA, TD, maltose sucrose, xylitol and mannitol	Sugar glass MNs for drug delivery	Low temperature vacuum-forming methodology.	The hygroscopic nature of sugars, processing, handling and storage of them is problematic.	The incorporation of the relevant therapeutic molecules as it can affect drug loading and stability of the sugar glass substrates and properties of the materials to be delivered. Hygroscopicity of sugars need to be considered for packaging and storage.	(Zhu, Wang et al. 2016)
Parylene-based MNEA (P-MNEA) with Si MNs	EEG monitoring	Etching and lithographic patterning	The ratio of the height to the interval of needles is a bit small (about 0.4), which means the density of needle is limited.	Further investigation is required as only preliminary testing was carried out.	(Wang, Renxin, Jiang et al. 2017)

	Name	Application	Fabrication method	Findings	Future work	Reference
	Hyaluronic acid	Tuberculosis	Micromolding	There was not a significant increase in total IgG with the BCG-MN group.	Further study needed to determine whether there was absorbance or binding to BCG vaccine	(Chen, F., Yan et al. 2017)
Inorganic	Bioceramic Composite Gel/Hap MNs	Insulin	Template method.	At higher temperatures biological activity of insulin reduced from 95% (at 37 °C for 12 h) to ~25% due to insulin denaturation at higher temperatures.	Improve the mixing process and MN fabrication method to protect proteins activity.	(Yu, Jiang, Liu, Li, Tong et al. 2017)
	Hollow Borosilicate GMNs	Precise microinjection into skin	Drawn glass micropipette techniques and rotary drilling method.	Skin deformation was limited by the drilling insertion method and pressing the base of the device into skin.	Other materials and other fabrication processes should be investigated as rotary drilling made it difficult to insert multi-needle arrays into skin.	(Wang, Ping M., Cornwell et al. 2006)
	LB-MSN-OVA	Antigen delivery	MSNs were synthesised and loaded with OVA and coated with (LB-MSN-OVA)	The deposition in the skin may alter the bio-distribution and clearance of MSNs after MN insertion.	Further, systematic bio-distribution studies need to carry out to thoroughly assess toxicity and safety of this system in humans and animals.	(Tu, Du et al. 2017)
	Zeolite	Influenza vaccination	Template synthesis method.	Sharper tip needles have improved safety with lower insertion force but zeolites cannot stick to sharper areas, as	Optimisation of the fabrication process to produce more efficient needles with better geometry. Extending the study for 4 weeks with a range of doses for the TDD	(Poon 2013)

| ECS modified Silk fibroin | Drug delivery | Micro-moulding | Pure SF microneedles are unsuitable for long-term release of loaded drugs as they are soluble and have burst release. | they are susceptible to cracking. | application of the influenza vaccination, prime, boost can ensure ZMN influenza TDD of influenza efficiency. | (Yin, Kuang et al. 2018) |

Ti: Titanium; MNs: microneedles; PVP: polyvinylpyrrolidone; Pd: Palladium; Au: Gold; N-UNCD: Nitrogen incorporated ultrananocrystalline diamond; PLA: Polylactic acid; RSMN: Rapidly separating microneedle; PVA: Polyvinyl acetate; PEG: Polyethylene glycol; HFMN: hydrogel forming microneedle; PEGDA: Polyethylene (glycol) Diacrylate; GMNs: Glass Microneedles; Gel-Hap: gelatin-hydroxyapetite; LB-MSN-OVA: lipid bilayer-coated, antigen-loaded mesoporous silica nanoparticles; ZMNs : zeolite microneedles, ECS; 2-ethoxyethanol

Table 2 The various functional microneedles fabricated out of different materials

MN composition	Engineering	Application	Minimum dimensions	Material applications	Processing conditions	References
Biocompatible resin	3D printing	MN shaping – inkjet printing for coating MNs with insulin solution	15x15x1 pyramid and cone 48 MNs each	Polymers	SLA using photopolymerization of light sensitive polymers using CAD. High resolution printer	(Pere, Economidou et al. 2018)
PLGA	Micro-molding and electro-drawing.	MN shaping	Pillars of 500 μm and 300 μm curvature radii below 20 μm	Polymers	Pyroelectric field, micro-heaters operating at constant power.	(Ruggiero, Vecchione et al. 2018)
CMRF Epoxy novolac resin and magnetic (iron) particles	Magnetorheological drawing lithography	Bio-signal monitoring, EII, ECG, EMG, EEG tests	Curved MAE H: 600 μm and the average tip radius is 12 μm.	Metals	Magnetic field, Elasto-capillary self-thinning and magneto-capillary self-shrinking, which greatly affect the microneedle height and tip radius.	(Ren, Jiang et al. 2017, Chen, Z., Ren et al. 2018)
PVP sumatriptan solution	Mold technique	Delivery of sumatriptan	600 needles consistent pitch (350 μm), NH (500 μm) NW (300 μm)	Polymers	Formulations are syringed into moulds. Pressure, temperature.	(Ronnander, Simon et al. 2018, Ripolin, Quinn et al. 2017)
The polymer in MN fabrication epoxy based SU-8 and the microneedle	Photolithographic technique	EEG monitoring, MN shaping	Cone-shaped H 500 μm a Base 100 μm in diameter and a tip smaller than 30 μm	Biocompatible metal	SU-8 and the MNA is formed on a glass carrier. A single, "back-side" photolithographic exposure is applied for the formation of sharp and appropriately-sloped.	(Stavrinidis, Michelakis et al. 2016, Baek, Han et al. 2011)

Material	Fabrication	Application	Dimensions	Materials	Description	Reference
Flexible P-MNEA	KOH-dicing-KOH process	EEG monitoring	P-MNEA H: 190 μm Si MN) and 10 μm-thick parylene substrate Rigid MNEA H: 190 μm-high Si MN and 200 μm-thick Si substrate	P-MNEA shows its potential in the long-term monitoring of EEG.	Parylene-based MNEA is demonstrated, which consists of individual silicon microneedles and is enclosed with flexible biocompatible materials	(Wang, Renxin, Jiang et al. 2017)
Coated steel MNs	Wire electrical discharge machining, electro-polishing	Hydrophobic peptides/antigens for skin delivery via CMNs	Solid MNs H:450 μm W: × 200 μm	Metals	Choice of excipient, intrinsic hydrophobic properties of the chosen peptide, surface morphology and roughness of the MNs, coating thickness. Can identify CA of the formulation coating and delivery to produce reproducible coating of MNs.	(Zhao, X., Birchall et al. 2016, Zhao, X., Coulman et al. 2017)
Stainless steel	Micromolding, lithography	On and off switch for first time thermopneumatically actuated microneedle array	Base diameter 230 μm, tip OD 130 μm, TID 100 μm and height 400 μm)	Polymers, metals	Thermopneumatic force, microheater, temperature sensor.	(Jung, M., An et al. 2016)
PLGA, PVP, PLA, PVA cyclodextrin, chitosan, Alg-APBA/HA	Micro-molding	Levonegestral, BCG, thermos-pneumatically actuated microneedle		Polymers, metals	Laser power/speed- for engraving patterns. Computer aided design, micromilling, master mold, PDMS mold, PDMS monomer and curing agent mixture.	(Márquez-Graña, Bryan et al. 2017, Wang, Qi Lei, Zhu et al. 2016, Chen, F., Yan et al. 2017, Yin, Kuang et al. 2018, Yao, Quan et al. 2017, Yu, Jiang, Zhang et al. 2017)

43

Material	Method	Application	Specifications		Notes	Reference
PLGA MN master Silk Fibroin	Thermally drawn micromolds	Controlled drug delivery and MN shaping	Slender, normal, bullet. 177, 84.5, and 190 µm. 3x3 arrays.	Polymers	Temperatures, drawing speeds, drawing heights, or parallelism in the drawing setup. Only applicable to thermoplastic materials, natural biomaterials are incompatible with this method of thermal drawing to fabricate master molds with high aspect ratios and replicate the shape by micromolding..	(Lee, JiYong, Park et al. 2015)
HA, PVA	Molding and casting process	TDD by encapsulating drug into HA layer as a shell when inserted into skin. The drug dissolves once the HA layer separates. (LMNs)	5 by 5 arrays	Polymers	PVA layer as core shell, HA layer to encapsulate drug.	(Q. L. Wang, Zhang et al. 2018)
Sodium hyaluronate	Droplet-born air blowing (DAB) method	Allergen-specific immunotherapy e.g. atopic dermatitis including other allergic diseases, such as allergic rhinitis, asthma, and food allergies.	76-microneedle array (needle pitch, 1.4 mm; needle length, 0.25 mm).	Allergen loaded MNs proven to be safe and show stable allergenicity.	DAB fabrication conditions are less extreme. Gamma radiation, concentration of allergen,	(Kim, Ji Hye, Shin et al. 2018)

MNs: microneedles; PVP: polyvinylpyrrolidone; LMN: Layered microneedle; PVA: Polyvinyl acetate; HFMN: hydrogel forming microneedle; PEGDA: Polyethylene (glycol) Diacrylate; GMNs: Glass Microneedles; CMRF: Curable magnetorheological fluid; HA: hyaluronic acid; PLGA: poly-lactic glycolic acid; H: height; NH: needle height; PMNEA: Parylene-based microneedle electrode array (P-MNEA)

2.5 Electrohydrodynamic Atomisation

2.5.1 Introduction

EHDA is a versatile one step fabrication technique with major potential within the pharmaceutical and cosmetic industry. The process involves using electrical forces as a driving force for liquid atomisation resulting in the fabrication of various micrometre or nanometre structures for drug delivery. This technology can also greatly assist with the ongoing advancements within nanotechnology (tissue engineering, regenerative medicine and drug delivery). The major benefits of nanotechnology include enhanced drug delivery with nano sized drug delivery systems as there is the ability for complex release kinetics, multi-functional properties hence why it has become popularised within the pharmaceutical remit in particular drug delivery. EHDA can operate at ambient temperatures and be optimised to produce Nps for various pharmaceutical applications (Mehta et al., 2017).

2.5.1.1 The EHDA Process

The EHDA process involves the utilisation of electric forces for the atomisation of liquids. A schematic of the EHDA process is shown in Figure 10. A charge accumulates at the exit of a liquid jet which, when overcome, leads to the deposition of particles or fibres (Grace and Marijnissen, 1994). The atomised structures deposit on a ground electrode which is positioner under the nozzle. The process parameters include flow rate, deposition distance, applied voltage, liquid properties, surface tension, electrical conductivity (EC) and viscosity (Kim and Kim, 2011). EHDA occurs either as Es (production of particles) or Esp (production of fibres), with high surface area to volume ratio, robust complex architectures with complex release profiles. It's the electric current as well as

solution properties which dictates which spraying mode will occur. (Moreira, Lawson et al. 2020).
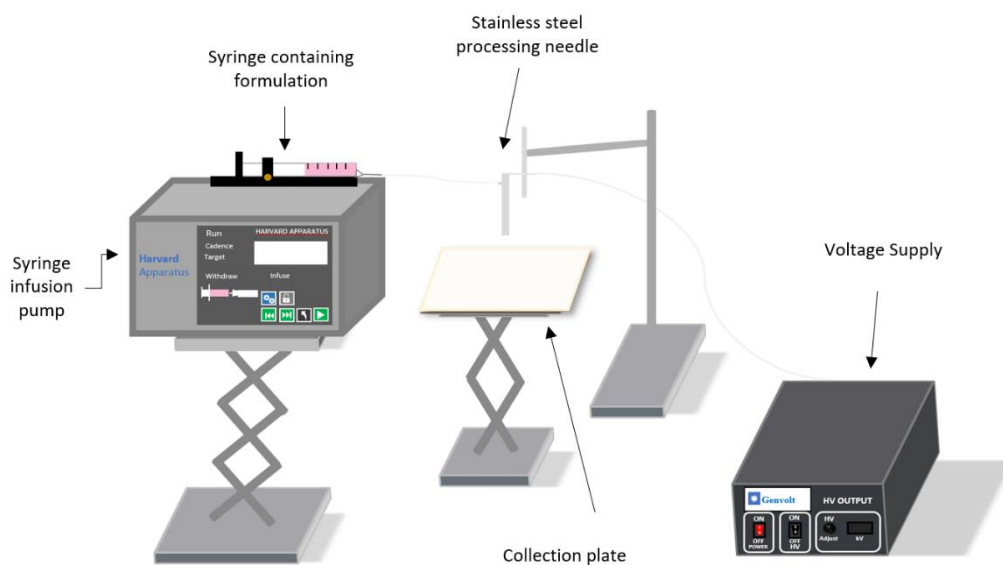
Figure 10 Schematic of EHDA setup

2.5.1.2 Characterising the Electrohydrodynamic jet

In recent years the EHDA process has been used to generate particles with diameters that range from micron to nano scales with a narrow size distribution. EHDA can produce monodispersed droplets with controlled size with the right formulation characteristics. The popularity of the Taylor cone jet (stable Es jetting mode) is owed to its ability to produce monodisperse structures in the nano-micro size range with a small size distribution which can be greatly beneficial for a wide range of applications. As there has been a surge in the demand for nanomedicine (Wang, Qisi, Wang et al. 2021).

2.5.1.3 Modes of EHDA

Zeleny first reported in 1914 the process of EHDA (Xie, Jiang et al. 2015). With it being an atomisation technique whereby a liquid jet breaks up into droplets due to electrical and mechanical forces. The atomiser nozzle is usually a metal capillary in which a formulation (liquid/suspension) is fed through silicon tubing which is pumped. With the application of a high voltage between the nozzle and electrode, shear stress is generated on the liquid surface causing the jet to elongate and disintegrate into droplets. The droplets formed are usually within the nano size range with a narrow size distribution, but it is dependent on the processing conditions which include the electric field, flow rate, geometry of the nozzle dimension and rheology of the formulation used. There are a range of jetting modes that can be achieved including dripping, micro-dripping, spindle, multi-spindle, cone-jet and multi-jet (Wang, D., Rocks et al. 2012).

The cone jet is amongst the most common spraying modes. A stable cone jet (also referred to as a Taylor cone) can occur within a certain range of electric potential and flow rate. The electrified meniscus appears successively convex, linear sides and concave with an increase in electric potential.

2.5.1.4 Criteria for EHDA

The rheology of solutions is important as the formulation needs to possess certain physical characteristics for it to be utilised in the EHDA process. Therefore, physical characterisation of solutions needs to take place this includes electrical conductivity (EC), surface tension (ST), viscosity and density measurements. Generally, more viscous solutions tend to result in Es (particles) and less viscous solutions result in Esp (fibres) (Ghorani, Tucker 2015). When the electrical stress overcomes the surface tension of a liquid it can be atomized/EHDA occurs. EC plays a crucial role in EHDA. Thus, organic solvents are more favourable in EHDA as they usually have low ST so the electrical stress can overcome it. The identification of a suitable solvent is critical as it needs to ensure the polymer can

dissolve as the surface morphology of the particles generated depends on the solvent's physiochemical properties. Generally, Es a polymeric solution with a solvent with low vapour pressure and a high boiling temperature (N, N-dimethylformamide (DMF)) leads to particles with a smaller size and smoother surface morphology. It may also yield a bimodal size distribution due to weaker polymer chain entanglement. In contrast solvents with high vapour pressure, low boiling temperature and faster evaporation and in turn rapid evaporation rate (e.g., DCM) may lead to the formation of textured and/or highly porous surfaces and even hollow structures. Rapid solvent evaporation reduces the time that polymer chains need to re-arrange within the droplet during rapid solidification (Xie, Jiang et al. 2015).

2.5.1.5 Electrospraying

In 1600, William Gilbert first observed and recorded the EHDA phenomenon, which was referred to simply as Es. In 1750 a French physicist (Jean-Antoine (Abbe) Nollet)) reported the earliest observation on Es, two centuries prior to the terminology being generated, demonstrating the flow of water from a container would aerolise if the container was electrified and put close to electrical ground. A century later Lord Kelvin invented a setup which consisted of two liquid nozzles that were bridged to collection reservoirs opposite to each other. This demonstrated minor differences in charging between the water dripping from the nozzles instantly caused by differences in kilovolt scale and ES from the nozzles.

In 1960 Taylor developed a mathematical model of the EHDA process, simulating the conical shape of the liquid phase in the presence of electrical field which later became known as Taylor Cone. In the 1980s, Fenn and his co-workers carried out studies that in turn made it possible to introduce dissolved analytes into the gas phase for mass analysis in Es. It was in 2002 John Bennett Fenn won the Nobel Prize in chemistry for his contribution to Es ionisation for analysing biological macromolecules (Mehta, Prina, Haj-Ahmad et al. 2017).

Rayleigh first researched the Es phenomena over a century ago in 1982. This began with the analysis of the instability following the evaporation of highly charged droplets. The maximum limit of surface charge density (Rayleigh limit) is a result of the charged nature of droplets (Zhao, Y., Yao 2017). Once surface tension at the surface of the droplet is overcome by the electrostatic force this leads to Coulomb fission of the liquid droplets into smaller droplets. This rupture phenomena were identified by Gomez and tang Charge and fission of droplets in electrostatic sprays (Mehta, Prina, Haj-Ahmad et al. 2017). An electric field (Coulombic forces on ions or charges inside the fluid) can alter dynamics of fluids. With the presence of more ions the more powerful the Coulombic forces will be. A number of opposite forces prevent the ions from moving freely (Naderi, Shams et al. 2019)

EHDA is a well-known technique to generate very fine droplets with mono dispersed size from a liquid under the influence of electrical forces. The applications of EHDA is not limited to the pharmaceutical industry as there has been many other applications reported including the food industry, raindrops in thunderclouds, combustion, crop spraying and electrospray ionisation mass spectroscopy. This technique has gained favourable attention since the 1990s for the production and processing of micro-nanoparticulate materials in a rich variety of applications (Xie, Jiang et al. 2015).

In recent years the technique has made significant developments with the ability to engineer complex active nano/micro structures through optimisation of process parameters, material attributes and selection, nozzle, needle design, collection method (distance and substrate).

2.5.1.6 Electrospinning

Esp typically leads to the production of fibres with the application of an electrostatic field on the liquid formulation (polymeric solutions are commonly used). A solution with higher viscosity and higher polymer concentration tends to be used for the intention of producing fibres. As this solution will form a charged jet which undergoes bending instability until a whipping motion occurs forming fibres. This approach has gained much attraction due to ability to fabricate large quantities of fibres in a single step process making it more feasible and promising for use in tissue engineering, wound dressings, biosensors, bioengineering, anti-cancer therapy. Their high surface area, small pore size and potential of forming three dimensional structures for advanced therapeutics and technologies render them great candidates in many industries (Husain, Lau et al. 2016).

Esp results in the production of nano (less than 100 nm) to micron sized nanofibres by an electrostatically driven jet of polymeric solution. The alignment of electrospun nanofibres can lead to highly functional complex three-dimensional structures (nanowires, nanotubes) (Thakkar, Misra 2017).

2.5.2 Process parameters of electrospraying and electrospinning

For Es or Esp to occur several EHDA process parameters and ambient conditions need to be considered. These all heavily impact the spraying pattern and depends on the physical properties of the solution. This includes polymer molecular weight, concentration of polymer, surface tension and viscosity and electrical conductivity. EHDA process parameters include the flow rate, applied voltage and capillary tip to collector plate distance. The ambient conditions include temperature and humidity (Ghorani, Tucker 2015)**.** All of these factors impact morphology of the resultant fibrous structures. Therefore, the manipulation of the various parameters can lead to the production of structures with desirable characteristics (size, morphology) (Husain, Lau et al. 2016)

2.5.2.1 Electrical conductivity

The physical properties of solutions are of paramount importance in EHDA. It is these factors that determine the characteristics of resultant structures (morphology, size). The electric field is the driving force for EHDA. Once applied a charge accumulates at the jet. The coulombic repulsion forces are higher with higher EC which in turn competes with the visco-elastic forces of the solution allowing the polymeric network to break up and the dispersion of smaller droplets. Solutions with high EC values can make the Es process unstable as competition arises between EC and surface tension. This can lead to elongation of the cone jets resulting in elongated particles or potentially fibres. Lower EC values are generally favoured (Bock, Dargaville et al. 2012, Faraji, Sadri et al. 2017).

The general trend observed is that with an increase in electrical conductivity there is a decrease in the fibre diameter. With low EC, elongation of the jet occurs leading to unstable non-uniform fibres being formed (Bhardwaj, Kundu 2010).

2.5.2.2 Viscosity

The viscosity of a solution is integral in the production of fibres and dictates the size and morphology. For Esp to occur an optimum viscosity is required. With increasing viscosity this increases the chance of beads to form and enlarge, it also increases the fibre diameter altering the shape of beads to become spindle like (Ghorani, Tucker 2015).

2.5.2.3 Surface tension

Visco-elastic stress resists further changes in morphology during Esp. The surface tension alone doesn't impact the size of beads. However, during the EHDA process it competes with electrical forces which causes tension in the fibres leading to thinning (Husain, Lau et al. 2016). Solutions with higher surface tension tend to hinder the esp process due to the instability of the jet and so solutions with lower surface tension are preferred (Bhardwaj, Kundu 2010).

2.5.2.4 Flow rate

The flow rate can influence size and morphology of particles. The selection of a suitable flow rate is required to ensure that the solvent has completely evaporated which isn't possible with a high flow rate. If there hasn't been complete solvent evaporation prior to the deposition of particles it could result in deformities in the particle morphology. For monodispersed spherical particles to be formed a low flow rate is required to allow for adequate polymer chain entanglements to occur (Bock, Dargaville et al. 2012).

The flow rate heavily influences the jet velocity and transfer rate of materials. Lower flow rates are more favourable as there is more time for the solvent in the solution to evaporate from the jet before reaching the collector. Studies show that the morphology of fibre and pore diameter increases with increased flow rate for polystyrene fibres. Higher flow rates typically lead to the formation of beaded fibres due to insufficient drying time of solvent before reaching the collector (Bhardwaj, Kundu 2010).

2.5.2.5 Applied voltage

Smaller particle sizes have been found when the applied voltage was increased. This is due to elongation of the jet and stretching thus affecting the particle morphology, by going from a spherical shape to being elongated and potentially form beaded fibres if the polymer concentration was high (Bock, Dargaville et al. 2012)

Fibres can only be formed once the threshold voltage has been achieved. By manipulating the applied voltage, the jet can be altered to produce the desired structures. It has been cited that the increase in applied voltage can lead to stretching of the solution as a result of coulombic forces in the jet decreasing the fibre diameter. Hussain et al, 2016 demonstrated that with higher applied voltage along with lower working distances resulted in smoother beaded fibres. There was no change in average diameter size (Husain, Lau et al. 2016)

2.5.2.6 Capillary tip to collector distance

The deposition distance has a large impact of surface morphology of particles. If the distance between capillary tip to collector distance is too small, then there will not be enough time for the solvent to evaporate potentially leading to collapsed particles being deposited on the collector plate or agglomeration of particles resulting in larger size distributions. The larger distance increases the transit time for droplets and more evaporation of solvent, thus producing more spherical particles as the polymer chains can effectively diffuse in the droplet prior to deposition (Rezvanpour, Krantz et al. 2012).

With larger deposition distances fibres are able to dry appropriately as they deposit avoiding the possibility of forming beaded fibres (Husain, Lau et al. 2016).

2.5.2.7 Temperature

During the Es process temperature affects the evaporation of solvent. At a fixed temperature and high relative humidity, the evaporate rate decreases. At a higher temperature the drying and solidification of particles increases which in turn decreases particle size (Zehtabiyan-Rezaie, Saffar-Avval et al. 2020, Boda, Li et al. 2018).

Fibre diameter has been found to increase as the ambient temperature increased. This could be due to a decrease in viscosity in polymer solution at higher temperatures. (Bhardwaj, Kundu 2010). At higher temperatures these nanofibres are generally more uniform (Thakkar, Misra 2017)

2.5.2.8 Humidity

Bodnar and Rosell-Liompart, (2013) assessed electrosprayed ethyl cellulose particles in butanone and DCM solvent at varying humidity levels. They reported a range of morphologies of resultant particles which were flatter, conjugated, and pancake-shaped or dimpled from a primary droplet. Therefore, increased humidity would result in more deformed structures with unfavourable morphologies (Ikeuchi, Tane et al. 2012, Xie, Jiang et al. 2015).

With low humidity electrospun fibres dried at a faster rate due to the rapid evaporation of solvent. With a high evaporation rate of solvent at the needle tip the Esp process would only occur for a limited period of time before being clogged. A volatile solvent is usually selected as there is appropriate solvent evaporation between the capillary tip and the collector plate ensuring the formation of fibres (Bhardwaj, Kundu 2010). With increased humidity circular pores can form on the nanofibres (Thakkar, Misra 2017).

2.5.2.9 Solution concentration

Fibres can only form with a minimum solution concentration. With low solution concentrations beaded fibres are usually produced. By increasing the solution concentration, the shape of beads become more spherical then spindle like then finally smooth uniform fibres with higher diameters due to the increase in viscosity. However, if the concentration is too high it becomes difficult to form continuous fibres due to the failure of maintaining the flow of solution thus resulting in larger diameter fibres. The concentration has the biggest impact on viscosity and surface tension (Bhardwaj, Kundu 2010).

2.5.2.10 Molecular weight

The molecular weight of polymers has a major impact on the rheological (viscosity) and electrical (EC) properties of the solution. LMW polymeric solutions will result in beaded fibres and fibres with bigger average diameters with a higher molecular weight polymer. The molecular weight directly impacts the entanglement of polymer chains which has a large effect on Esp. A higher molecular weight polymer isn't always necessary if there are enough intermolecular interactions instead of chain entanglements (Bhardwaj, Kundu 2010).

2.5.2.11 Polymer choice

Selecting the right polymer is integral in the EHDA process as it will heavily influence the size, morphology and functionality of the resultant nano-micron sized particular/fibrous structure. A suitable solvent is also selected to dissolve the polymer prior to Es/Esp. A fume chamber is usually recommended due to the toxicity of polymers (Bhardwaj, Kundu 2010). Literature suggests that with higher polymer concentrations increases the EC and surface tension which can result in an unstable jet and so larger particle diameter (Pawar, Thakkar et al. 2018). For

Esp to occur the polymer concentration and viscosity must be optimal. Lower polymer concentration solutions result in Es. In the case of Es a lower concentration of polymer generally leads to smooth particles with smaller sizes and polydispersity index (PDI) (Thakkar, Misra 2017).

2.5.2.12 Solvent choice

The selection of a suitable solvent for chosen polymer in the EHDA process is vital as it will impact the morphology of the resultant structures. Ribbon like fibres can form if the solvent is not volatile due to solvent retention. A solvent with an extremely high volatility can lead to increased particle size and adversely impact surface morphology as well as porosity as the evaporation rate will have increased. Highly volatile solvent can also clog the capillary which will directly impact the jet stability (Awasthi, Kulkarni et al. 2012, Pawar, Thakkar et al. 2018).

2.5.3 Applications of Electrosraying and Electrospinning

The simplest ES method comprises of single nozzle spraying. There has been many applications of single nozzle has been demonstrated using a range of active biomaterials and encapsulation of genes and anti-cancer and other bioactive agents (Mehta, Prina, Haj-Ahmad et al. 2017).

There has been considerable attention on electrospun nanofibers as they have a high surface area to volume ratio, high porosity and being capable of manipulating fibres into achieving desirable attributes, through changing solution and process parameters. Therefore, electrospun fibres are increasingly being used in a wide variety of applications (Bhardwaj, Kundu 2010)

2.5.3.1 Protein Delivery

Proteins and peptides are considered the most multifunctional biomolecules in the body, behaving as catalysts in biochemical reactions, accelerating the inflammatory responses and regulation cell proliferation and differentiation as well as metabolic and signalling pathways. Endogenous protein function can give rise to various pathological conditions including, genetic, metabolic, inflammatory and oncological diseases. In 1982 recombinant insulin was the first FDA approved recombinant protein-based drug. More than 60 FDA-approved protein drugs have been commercially available with a great number currently being reviewed for preclinical and clinical trials. Gomez et al (1998) utilised EHDA for the fabrication of nano sized (110 nm) biologically active insulin particles by Es insulin in a range of solvents. The findings demonstrated that smaller sized particles can be achieved at lower flow rates using lower concentration of insulin in solution (Gomez, Bingham et al. 1998).

The clinical application of protein and peptide based therapeutic agents have been greatly hindered by the formulation challenges as well and route of administration. The oral route presents potential high compliance and ease of administration but issues with premature gastrointestinal degradation. Proteins possess HMWs thus presenting many ionisable groups, bypassing biological membranes like intestinal epithelium or the blood brain barrier could prove difficult. Thus, the majority of peptide and protein-based therapies being delivered via the parenteral route. Once they enter the bloodstream, they have short half-lives making them susceptible to clearance by immune cells or elimination by the liver, kidneys depending on their physiochemical and structural characteristics propose several drawbacks (Moreira, Lawson et al. 2020)

Esp is capable of fabricating fibres with favourable properties including controlled release profile and complex architectures. This method allows for proteins to be encapsulated within a polymeric shell during Esp. (Moreira, Lawson et al. 2020).

2.5.3.2 Antibiotic therapy

A range of antibiotics have been available for the treatment of bacterial infections but maintaining continuous activity requires repeated administration. If this is not achieved, then the minimum inhibition concentration (MIC) is not reached or exceeded which can result in antibiotic resistance. Therefore, if the drug concentration above MIC is sustained then antibiotic resistance will be prevented and the intended therapeutic effect will be provided.

Curcumin has many properties including being an antioxidant, anti-inflammatory, analgesic anti-cancer and antimicrobial. Earlier studies addressed the solubility issues with curcumin by utilising the spray drying process (Guo, Li et al. 2020). Wang et al 2009 demonstrated improved curcumin solubility with the spray drying process by encapsulation in gelatin with great antimicrobial activity against more gram positive than gram negative bacteria as well as fungi.(Wang, Yu, Lu et al. 2009) Gomez-Estaca et al successfully encapsulated curcumin in gelatin via EHDA. The composite electrosprayed gelatin particles had 100% encapsulation efficiency with 10% (w/w) loading of curcumin which showed broad spectrum antibacterial activity for *L. monocytogenes*, *S. enterica*, *S. aureus*, and *E. coli*, respectively (Gómez-Estaca, Balaguer et al. 2017)

PLGA was utilised for the encapsulation of antiobiotic metronidiazole with the use of trifluroethanol. The electrosprayed particles measured 1774± 167 nm respectively with a controlled release profile. Biocompatibility of the PLGA microparticle system was ensured by cell proliferation assay using mesenchymal stem cells (Prabhakaran, Zamani et al. 2015).

Mai et al, 2017 effectively encapsulated curcumin into PLA microcapsules via Esp using EHDA which exhibited excellent antibacterial activity against *Escherichia coli, S aureus* with good biocompatibility and low cytotoxicity. This system also showed a sustained drug release profile (Mai, Chen et al. 2017).

2.5.3.3 Gene Therapy

Gene therapy involves incorporation of foreign genes into living cells. Previous gene delivery methods have been limited to a few bacterial species due to the low efficiency of transformation, complex operation protocols, damage to cells as well as costly devices. Es process has shown great promise in delivering DNA materials into plasmid allowing the plasmid to penetrate the cell membrane and so delivered the required genes into cells. This process eliminates the need to prepare competent cells which is a vital time-consuming step in traditional DNA transformational methods. Gold Nps have also been reported as potential carriers for gene delivery as they are readily conjugated with biomolecules. These particles can greatly enhance plasmid transformation efficiency by optimising Np size, having a suitable buffer solution and adequate cell growth conditions. Manipulation of the applied voltage during Es can further optimise Np delivery (Lee, Yi-Hsuan, Wu et al. 2011).

2.5.3.4 Cancer treatment

Cancer is responsible for millions of deaths globally. Although there has been extensive research in this area issues remain with efficacious targeted therapy. There are many challenges which need to be overcome. Thus, oncological research is more focussed on finding new efficient therapies. The most common and accessible oncology treatment includes orally or intravenously administered drugs which are limited by their physical properties (drug solubility, poor pharmacodynamics and physiological conditions (pH 7.4) amount to ineffective therapeutic concentration at the target site. Nano medicine has been a promising approach with the use of polymers in commercially available approved treatment for various types of cancers including breast, ovarian and retinoblastoma.

EHDA has been successfully used for loading chalcone (KAZ-3) into mesoporous formulations. Chalcone has anti-inflammatory, antipyretic, analgesic and

antioxidant activities which has gained attention for cancer treatment (Sayed, Karavasili et al. 2018). Co-axial EHDA has been utilised for the treatment of cancer with the used of electrosprayed doublewalled microparticles for local delivery (Davoodi, Feng et al. 2015).

Reardon et al, 2017 research involved loading PLGA Nps with cisplatin using EHDA. The system provided controlled release of cisplatin a usually toxic chemotherapy drug. There was effective internalisation within the endolysosomal compartment of cancer cells as well as improved cytotoxic effects (Reardon, Parhizkar et al. 2017).

Electrosprayed poly(epsilon-caprolactone) microparticles containing embelin demonstrated better drug loading, encapsulation efficiency, morphology and in-vitro release compared to fabrication via emulsion- solvent evaporation method. There was initial burst release followed by controlled release size (3.14 +/- 0.05 μm). This system shows great potential for lung cancer treatment (Cortez Tornello, Feresin et al. 2018)

Electrospun PCL scaffolds have been used to accommodate breast cancer cells. This shows great scope for Esp scaffolds for cell culture applications which would greatly benefit cancer research (Rabionet, Puig et al. 2020). Esp has also been utilised in the fabrication of biomedicated nanofibres for local chemotherapy and preventing wound infections. Here electrospun curcumin has been used as a non-toxic chemotherapic agent which showed excellent antibacterial and anticancer properties. These nanofibres also exhibited a sustained drug release profile (Sedghi, Shaabani et al. 2017).

2.5.3.5 Bioengineering

Tissue engineering involves the maintenance, improvement and restoration of tissues which includes, dermal, bone, heart, blood, vessels and nerve. Generating scaffolds for the reparation of damaged bone tissues by the production of porous topographic substrates by mimicking the extra cellular matrix is difficult. It is essential for scaffolds to possess the appropriate pore size, surface chemistry, biodegradability, excellent mechanical strength and geometry. There has been an increase in the use of Nps for bone tissue engineering. Esp has been a simpler economic process compared to other fibre fabrication method with better control over pore size, morphology and geometry (Jayaraman, Gandhimathi et al. 2015, Behtaj, Karamali et al. 2020). More recently dual scale scaffolds have been fabricated via 3D printing and Esp producing 3d anisotropic scaffolds with aligned nano scale fibres layer by layer. These dual scale scaffolds exhibited enhanced osteogenic marker expressions (Huang, Aslan et al. 2020).

Nanofibre based wound dressings have been investigated as potential drug delivery systems to enhance and accelerate the healing process whilst avoiding skin infections. Rosa Sequiera et al demonstrated the potential of Esp PVA and lysine membranes with ibuprofen and lavender oil (anti-bacterial agent). This system provided an initial burst following a sustained release profile as the wound healed. There was strong antibacterial action against *S.aureus* and *P.aeruginosa* without impairing human fibroblast viability (Sequeira, Miguel et al. 2019).

Yang et al, 2015, developed a 3D biomedical hybrid scaffold using PCL and collagen which possessed tunable pore structure and high mechanical strength via Esp. These nano-fibrous scaffolds demonstrated superior in-vitro cellular activities with cell viability being two-fold and calcium deposition being seven-fold (Yang, G., Kim et al. 2015).

2.5 Complex EHDA Systems

Monoaxial and coaxial Es processes are similar despite the differences in the experimental setup. Monoaxial Es involves a polymer solution being injected into a capillary nozzle whilst being subjected to a strong external electric field which is created between the nozzle and a grounded collector by a high electric potential generator. Thus, the need for the liquid to be electrically conductive for it to be atomised into fine jet. The jet then breaks up into charged droplets that settle on the grounded collector. Some setups have made use of a closed chamber with continuous air or nitrogen flow that reduces the evaporation rate of solvent and enables smoother and smaller particles to form. With a more viscous liquid or if it solidifies at the onset of jetting then fibres are produced. Monoaxial Es polymeric particles have shown the potential to incorporate and release protein drugs in a sustained manner. However, the release profile is poorly controlled (Mehta, Prina, Haj-Ahmad et al. 2017)

Coaxial Es could evade the technical limitations of monoaxial Es by its core shell design, allowing protein drugs to be dissolved in aqueous solution for encapsulation. More recent work has shown protein drugs can be loaded into polymeric core shell structured particles by Es technique providing high encapsulation efficiency, favourable release profile and remain bioactive. For co-axial Es (two needles concentrically arranged) with differing gauge sizes are situated coaxially to dispense two solutions simultaneously. The two formulations can either mix or phase separate at the needle tip but this is dependent on the solvent. Microbubble production can occur via EHDA by replacing the core solution with a gas stream. A polymeric shell forms a barrier around a gas core (Davoodi, Feng et al. 2015).

Further advancements in EHDA have resulted in the development of multi-nozzle systems able to generate particles and fibres in larger amounts with greater complexity. This involves several nozzles and syringes in the process which enable the production of fibrous mats. These multi-nozzles can be further modified by being configured in a range of geometries which include circular,

triangular or hexagonal (Yang, Y., Jia et al. 2010). A triaxial (three nozzle) Es setup has been used to fabricate multi-layered nanofibers measuring 25 μm PCL was used as an intermediate layer and gelatine as the core were Esp (Mehta, Prina, Haj-Ahmad et al. 2017)

2.6 Quality by design

The pharmaceutical industry has seen a shift from good manufacturing practice (GMP) towards Quality by Design (QBD). GMP has been important in the pharmaceutical industry for many years. However, agencies have recognised the need for a change in the current approach. This is due to the need to carry out numerous tests. This shift in attitude has led the focus towards a more strategic approach whereby quality is built into the product.

The Food and Drug Administration (FDA) has introduced a more modernised version incorporating more process risk factors including risk mitigation, risk control, process risk determination to ensure that the process is efficient. This approach has been further modified by the European Medicines Agency (EMA) as well as other groups and formed the "Quality by Design" approach. The application of QBD allows for risk focussed cooperation between competent agencies and manufacturers offering higher robustness and efficiencies. Product quality need not be proven by means of analytics and end product testing. This approach focusses more so on building quality into the product therefore the manufacturing process being the focal point.

Quality by Design (QBD) is a promising alternative to GMP (Javed, Alam et al. 2019). It involves a more focussed approach with regards to the product quality and looking at the process parameters and optimising those (Amasya, Aksu et al. 2019).

2.6.1 Quality by design principles

2.6.1.1 Quality target product profile

The initial phase of the QBD approach is to form the Quality Target Product Profile (QTPP) (shown in Figure 11) which is the first stage in product development cycle in order to ensure that the required quality characteristics are achieved. This includes assigning well defined attributes to a given drug product. In the QTPP critical quality attributes (CQA's) define some of the critical parameters involved in product development. The variation in raw materials and processes are likely to influence the critical parameters. Therefore, this needs to be observed and evaluated throughout product development to ensure the product remains within safe and efficacious levels. CQAs are vital as they can affect the drug product (Soni, Kale et al. 2020). This approach is more concerned with building the required quality into a product (QTPP) would include critical material attributes (CMA) which is necessary in identifying and optimising the selected materials (Jhawat, Gulia et al. 2020).

Identify QTPPs → Idenitfy CQAs, CMAs and CPPs → Set up DoE → Define design space → Identify and control sources of variability → Continuous monitoring of manufacturing process

Figure 11: Summary of the Quality by Design Approach

2.6.1.2 Risk Assessment

Risk assessment forms the base of the QBD framework. It focusses primarily on the identification, analysis and evaluation of risks detected for a formulation. These risks are evaluated by the Ishikawa diagram. The screening design factors in these parameters and attributes and produces a design of experiments (Kovács, Berkó et al. 2017).

Carrying out a risk assessment enables the user to ensure that all factors are considered, and the control strategy has been implemented by ensuring all risk assessment parameters are considered by setting up the design space.

To ensure that the control strategy has been implemented correctly this is achieved by setting up a design space and completion of all risk assessment parameters. The risk assessment can be carried out effectively by using the Ishikawa Fishbone diagram. The Ishikawa diagram is drawn up so there can be a better understanding of cause and effect of a process that will be useful in tracing down the reason of any failures or variations (Soni, Kale et al. 2020). It is relatively straightforward making it easy to understand and suitable as an initial risk assessment during the early development phase (Uhlenbrock, Sixt et al. 2017).

These parameters that affect the performance of the process includes the CMAs, CPPs and CQAs. The risk assessment is used to identify the risk parameters establish a DoE to associate the CMAs and CPPs to CQAs to produce a design space for the process outlining optimal working conditions with the desired QTPP. This is via use of a risk control strategy to identify causes of variability, continuous monitoring and improving the manufacturing process.

This involves identify potential issues, the likelihood of it occurring and the consequences. Following this the risk control and review must be applied. According to ICH Q9 risk control is related to the procedures that should be implemented for risk reduction. During the risk assessment analysis of variance

(ANOVA) and multiple linear regression are used to evaluate the experimental data. ANOVA assesses the significance of each factor and their interactions while multiple linear regression is applied to produce variables equation (Cunha, Costa et al. 2020).

An extensive risk assessment is the basis for subsequent process characterisation. A common method able to characterise risk in terms of impact, occurrence and detectability at a higher degree of detail is known as "failure mode and effects analysis" (FMEA) which can give further information which is helpful during product characterisation (Uhlenbrock, Sixt et al. 2017).

2.6.1.3 Critical Quality Attributes

QBD involves the identification of the different materials which affect the process called CQAs Identification of these can control the product life cycle (Soni, Kale et al. 2020). Their identification is usually derived from the QTPP.

The raw materials being used play a crucial role in the process. They have a direct impact on the process and the drug attributes CQAs usually refer to selecting the right quantity of excipients and drug (Cunha, Costa et al. 2020).

2.6.1.4 Critical Material Attributes

CMAs define the limits whereby materials should fit to assure a guarantee of good quality of excipients, drugs and any other materials used in the process (Cunha, Costa et al. 2020).

2.6.1.5 Process Analytical Technique

PAT arose when manufacturers needed to identify a new process to direct quality control towards a science-based approach allowing real-time control of the manufacturing process thus reducing safety risks in the final product and therein patients. PAT is referred in ICH9 as a means of rapid assessment of material characteristics which provides efficient process optimization and ensures the final product has the desired quality standards. Thus, PAT can control the CPPs, CMAs and CQAs. ICH Q8 advises for the use of PAT to maintain the process in the established design space. PAT involves data collection, multivariate data analysis, process control, continuous process improvement and prior scientific knowledge. Depending on whether a sample is present or absent, PAT is divided into either in-line, on-line or at-line (Cunha, Costa et al. 2020).

2.6.1.6 Design of Experiments

The first design of experiments (DOE) includes the initial examination of product and process quality and characterisation of product and process quality as well as process parameters. The therapeutic and quality requirements and performance parameters together are defined as different components of QBD. This includes the quality target product profile (QTPP), critical material attributes (CMAs), critical quality attributes (CQAs) and critical process parameters (CPPs) to improve the quality of product via efficient control on the quality of raw materials and process variables (Jhawat, Gulia et al. 2020).

Even with prior scientific knowledge and selection of the known factors produces a large set of CPPs, screening designs may need to be carried out to see if they have any negative effects on the CMAs (Dispas, Avohou et al. 2018). A DoE utilises computer aided processes and process stimulations to produce mathematical models. There are a range of models including screening design, factorial design, Box-Behnken, Plackett-Burman and Taguchi design (Waghule, Dabholkar et al. 2021).

2.6.1.7 Design Space

The DS is linked closely with the QBD approach. It is a multidimensional combination of the interactions between the input variables. The design space creates an area in which you can operate where the CMAs are within the acceptance limits. It is also referred to as the control/knowledge space. The DS correlates with a variety of operating conditions whereby CMAs operate within the acceptance limits. With a larger DS the method can be considered robust due to changes of operating conditions within the DS will not compromise the quality of results (Dispas, Avohou et al. 2018).

2.6.1.8 JMP

JMP Pro software was used to generate all experimental designs. It can be used to create the screening design which incorporates all the factors (CQAs and CMAs) and produces a table with a randomised set of experiments. This mathematical model then statistically analyses the data and visually illustrates the findings. The predictive analytical tools aim to enhance and build a model to predict the behaviour of new processes and new risks.

2.7 Conclusion

This chapter evaluates the use of MNs for TDD. This includes the materials used, fabrication method as well as clinical application. An extensive review of EHDA was carried out to gain further understanding of the process itself as well as the parameters affecting it. Understanding the fundamental principles of QBD has also provided an insight to the potential of it yielding optimal results. From this I was able to move forward applying QBD to the EHDA process to coat MNs for efficacious TDD.

2.8 References

ABDO, J.M., SOPKO, N.A. and MILNER, S.M., 2020. The applied anatomy of human skin: A model for regeneration. *Wound Medicine,* 28, pp. 100179.

AHMED SAEED AL-JAPAIRAI, K., MAHMOOD, S., HAMED ALMURISI, S., REDDY VENUGOPAL, J., REBHI HILLES, A., AZMANA, M. and RAMAN, S., 2020. Current trends in polymer microneedle for transdermal drug delivery. *International journal of pharmaceutics,* 587, pp. 119673.

ALEXANDER, A., DWIVEDI, S., AJAZUDDIN, GIRI, T.K., SARAF, S., SARAF, S. and TRIPATHI, D.K., 2012. Approaches for breaking the barriers of drug permeation through transdermal drug delivery. *Journal of Controlled Release,* 164(1), pp. 26-40.

AMASYA, G., AKSU, B., BADILLI, U., ONAY-BESIKCI, A. and TARIMCI, N., 2019. QbD guided early pharmaceutical development study: Production of lipid nanoparticles by high pressure homogenization for skin cancer treatment. *International Journal of Pharmaceutics,* 563, pp. 110-121.

AMODWALA, S., KUMAR, P. and THAKKAR, H.P., 2017. Statistically optimized fast dissolving microneedle transdermal patch of meloxicam: A patient friendly approach to manage arthritis. *European Journal of Pharmaceutical Sciences,* 104, pp. 114-123.

ANIRUDHAN, T.S. and NAIR, S.S., 2019. Development of voltage gated transdermal drug delivery platform to impose synergistic enhancement in skin permeation using electroporation and gold nanoparticle. *Materials Science and Engineering: C,* 102, pp. 437-446.

AWASTHI, R., KULKARNI, G.T., PAWAR, V.K. and GARG, G., 2012. Optimization Studies on Gastroretentive Floating System Using Response Surface Methodology. *Aaps Pharmscitech,* 13(1), pp. 85-93.

BALÁZS, B., VIZSERÁLEK, G., BERKÓ, S., BUDAI-SZŰCS, M., KELEMEN, A., SINKÓ, B., TAKÁCS-NOVÁK, K., SZABÓ-RÉVÉSZ, P. and CSÁNYI, E., 2016. Investigation of the Efficacy of Transdermal Penetration Enhancers Through the Use of Human Skin and a Skin Mimic Artificial Membrane. *Journal of Pharmaceutical Sciences,* 105(3), pp. 1134-1140.

BARBERO, A.M. and FRASCH, H.F., 2017. Effect of stratum corneum heterogeneity, anisotropy, asymmetry and follicular pathway on transdermal penetration. *Journal of Controlled Release,* 260, pp. 234-246.

BARONI, A., BUOMMINO, E., DE GREGORIO, V., RUOCCO, E., RUOCCO, V. and WOLF, R., 2012. Structure and function of the epidermis related to barrier properties. *Clinics in dermatology,* 30(3), pp. 257-262.

BEHTAJ, S., KARAMALI, F., MASAELI, E., G. ANISSIMOV, Y. and RYBACHUK, M., 2020. Electrospun PGS/PCL, PLLA/PCL, PLGA/PCL and pure PCL scaffolds for retinal progenitor cell cultivation. *Biochemical engineering journal,* , pp. 107846.

BELOKHVOSTOVA, D., BERZANSKYTE, I., CUJBA, A., JOWETT, G., MARSHALL, L., PRUELLER, J. and WATT, F., 2018. Homeostasis, regeneration and tumour formation in the mammalian epidermis. *The International journal of developmental biology,* 62(6-7-8), pp. 571-582.

BENSON, H., GRICE, J., MOHAMMED, Y., NAMJOSHI, S. and ROBERTS, M., 2019. Topical and Transdermal Drug Delivery: From Simple Potions to Smart Technologies. *Current drug therapy,* 16(5), pp. 444-460.

BHARDWAJ, N. and KUNDU, S.C., 2010. Electrospinning: A fascinating fiber fabrication technique. *Biotechnology Advances,* 28(3), pp. 325-347.

BOCK, N., DARGAVILLE, T.R. and WOODRUFF, M.A., 2012. Electrospraying of polymers with therapeutic molecules: State of the art. *Progress in Polymer Science,* 37(11), pp. 1510-1551.

BODA, S.K., LI, X. and XIE, J., 2018. Electrospraying an enabling technology for pharmaceutical and biomedical applications: A review. *Journal of Aerosol Science,* 125, pp. 164-181.

BOURAS, N., MADJOUBI, M.A., KOLLI, M., BENTERKI, S. and HAMIDOUCHE, M., 2009. Thermal and mechanical characterization of borosilicate glass. *Physics Procedia,* 2(3), pp. 1135-1140.

CAFFAREL-SALVADOR, E., TUAN-MAHMOOD, T., MCELNAY, J.C., MCCARTHY, H.O., MOONEY, K., WOOLFSON, A.D. and DONNELLY, R.F., 2015. Potential of hydrogel-forming and dissolving microneedles for use in paediatric populations. *International journal of pharmaceutics,* 489(1-2), pp. 158-169.

CALIÒ, A., DARDANO, P., DI PALMA, V., BEVILACQUA, M.F., DI MATTEO, A., IUELE, H. and DE STEFANO, L., 2016. Polymeric microneedles based enzymatic electrodes for electrochemical biosensing of glucose and lactic acid. *Sensors and Actuators B: Chemical,* 236, pp. 343-349.

CÁRCAMO-MARTÍNEZ, Á, MALLON, B., DOMÍNGUEZ-ROBLES, J., VORA, L.K., ANJANI, Q.K. and DONNELLY, R.F., 2021. Hollow microneedles: A perspective in biomedical applications. *International journal of pharmaceutics,* 599, pp. 120455.

CEVC, G. and VIERL, U., 2010. Nanotechnology and the transdermal route: A state of the art review and critical appraisal. *Journal of Controlled Release,* 141(3), pp. 277-299.

CHEN, B., WEI, J. and ILIESCU, C., 2010. Sonophoretic enhanced microneedles array (SEMA)—Improving the efficiency of transdermal drug delivery. *Sensors and Actuators B: Chemical,* 145(1), pp. 54-60.

CHEN, F., YAN, Q., YU, Y. and WU, M.X., 2017. BCG vaccine powder-laden and dissolvable microneedle arrays for lesion-free vaccination. *Journal of Controlled Release,* 255, pp. 36-44.

CHEN, M., LIN, Z. and LING, M.-., 2016. Near-Infrared Light-Activatable Microneedle System for Treating Superficial Tumors by Combination of Chemotherapy and Photothermal Therapy. *Acs Nano,* 10(1), pp. 93-101.

CHEN, Y., CHEN, B.Z., WANG, Q.L., JIN, X. and GUO, X.D., 2017. Fabrication of coated polymer microneedles for transdermal drug delivery. *Journal of Controlled Release,* 265, pp. 14-21.

CHEN, Y., QUAN, P., LIU, X., WANG, M. and FANG, L., 2014. Novel chemical permeation enhancers for transdermal drug delivery. *Asian Journal of Pharmaceutical Sciences,* 9(2), pp. 51-64.

CHEN, Y., WANG, M. and FANG, L., 2013. Biomaterials as novel penetration enhancers for transdermal and dermal drug delivery systems. 20(5), pp. 199-209.

CHEN, Z., REN, L., LI, J., YAO, L., CHEN, Y., LIU, B. and JIANG, L., 2018. Rapid fabrication of microneedles using magnetorheological drawing lithography. *Acta Biomaterialia,* 65, pp. 283-291.

CHOI, C.K., LEE, K.J., YOUN, Y.N., JANG, E.H., KIM, W., MIN, B. and RYU, W., 2013. Spatially discrete thermal drawing of biodegradable microneedles for vascular drug delivery. *European Journal of Pharmaceutics and Biopharmaceutics,* 83(2), pp. 224-233.

CHOI, S., KIM, Y.C., PARK, J., HUTCHESON, J., GILL, H.S., YOON, Y., PRAUSNITZ, M.R. and ALLEN, M.G., 2010. An electrically active microneedle array for electroporation. *Biomedical Microdevices,* 12(2), pp. 263-273.

CHOU, S. and WOODROW, K.A., 2017. Relationships between mechanical properties and drug release from electrospun fibers of PCL and PLGA blends. *Journal of the Mechanical Behavior of Biomedical Materials,* 65, pp. 724-733.

CORTEZ TORNELLO, P.R., FERESIN, G.E., TAPIA, A., DZIECIUCH, M., CUADRADO, T.R. and ABRAHAM, G.A., 2018. Effect of processing techniques on new poly(epsilon-caprolactone)-embelin microparticles of biomedical interest. *Advances in Polymer Technology,* 37(6), pp. 1570-1580.

CUNHA, S., COSTA, C.P., MOREIRA, J.N., SOUSA LOBO, J.M. and SILVA, A.C., 2020. Using the quality by design (QbD) approach to optimize formulations

of lipid nanoparticles and nanoemulsions: A review. *Nanomedicine: Nanotechnology, Biology and Medicine,* 28, pp. 102206.

DANGOL, M., YANG, H., LI, C.G., LAHIJI, S.F., KIM, S., MA, Y. and JUNG, H., 2016. Innovative polymeric system (IPS) for solvent-free lipophilic drug transdermal delivery via dissolving microneedles. *Journal of Controlled Release,* 223, pp. 118-125.

DAVIDSON, A., AL-QALLAF, B. and DAS, D.B., 2008. Transdermal drug delivery by coated microneedles: Geometry effects on effective skin thickness and drug permeability. *Chemical Engineering Research and Design,* 86(11), pp. 1196-1206.

DAVOODI, P., FENG, F., XU, Q., YAN, W., TONG, Y.W., SRINIVASAN, M.P., SHARMA, V.K. and WANG, C., 2015. Coaxial electrohydrodynamic atomization: Microparticles for drug delivery applications. *Journal of Controlled Release,* 205, pp. 70-82.

DISPAS, A., AVOHOU, H.T., LEBRUN, P., HUBERT, P. and HUBERT, C., 2018. 'Quality by Design' approach for the analysis of impurities in pharmaceutical drug products and drug substances. *TrAC Trends in Analytical Chemistry,* 101, pp. 24-33.

DONNELLY, R.F., MORROW, D.I.J., SINGH, T.R.R., MIGALSKA, K., MCCARRON, P.A., O'MAHONY, C. and WOOLFSON, A.D., 2009. Processing difficulties and instability of carbohydrate microneedle arrays. *Drug development and industrial pharmacy,* 35(10), pp. 1242-1254.

DONNELLY, R.F., SINGH, T.R.R., GARLAND, M.J., MIGALSKA, K., MAJITHIYA, R., MCCRUDDEN, C.M., KOLE, P.L., MAHMOOD, T.M.T., MCCARTHY, H.O. and WOOLFSON, A.D., 2012. Hydrogel-Forming Microneedle Arrays for Enhanced Transdermal Drug Delivery. *Advanced Functional Materials,* 22(23), pp. 4879-4890.

DONNELLY, R. and DOUROUMIS, D., 2015. Microneedles for drug and vaccine delivery and patient monitoring. *Drug Delivery and Translational Research,* 5(4), pp. 311-312.

ELTAYIB, E., BRADY, A.J., CAFFAREL-SALVADOR, E., GONZALEZ-VAZQUEZ, P., ZAID ALKILANI, A., MCCARTHY, H.O., MCELNAY, J.C. and DONNELLY, R.F., 2016. Hydrogel-forming microneedle arrays: Potential for use in minimally-invasive lithium monitoring. *European Journal of Pharmaceutics and Biopharmaceutics,* 102, pp. 123-131.

FARAJI, S., SADRI, B., VAJDI HOKMABAD, B., JADIDOLESLAM, N. and ESMAEILZADEH, E., 2017. Experimental study on the role of electrical conductivity in pulsating modes of electrospraying. *Experimental Thermal and Fluid Science,* 81, pp. 327-335.

FERNANDO, G.J.P., ZHANG, J., NG, H., HAIGH, O.L., YUKIKO, S.R. and KENDALL, M.A.F., 2016. Influenza nucleoprotein DNA vaccination by a skin targeted, dry coated, densely packed microprojection array (Nanopatch) induces potent antibody and CD8+ T cell responses. *Journal of Controlled Release,* 237, pp. 35-41.

GHORANI, B. and TUCKER, N., 2015. Fundamentals of electrospinning as a novel delivery vehicle for bioactive compounds in food nanotechnology. *Food Hydrocolloids,* 51, pp. 227-240.

GILL, H.S., DENSON, D.D., BURRIS, B.A. and PRAUSNITZ, M.R., 2008. Effect of microneedle design on pain in human volunteers. *Clinical Journal of Pain,* 24(7), pp. 585-594.

GOMEZ, A., BINGHAM, D., JUAN, L.D. and TANG, K., 1998. Production of protein nanoparticles by electrospray drying. *Journal of Aerosol Science,* 29(5), pp. 561-574.

GÓMEZ-ESTACA, J., BALAGUER, M.P., LÓPEZ-CARBALLO, G., GAVARA, R. and HERNÁNDEZ-MUÑOZ, P., 2017. Improving antioxidant and antimicrobial properties of curcumin by means of encapsulation in gelatin through electrohydrodynamic atomization. *Food Hydrocolloids,* 70, pp. 313-320.

GUO, J., LI, P., KONG, L. and XU, B., 2020. Microencapsulation of curcumin by spray drying and freeze drying. *LWT,* 132, pp. 109892.

HAJ-AHMAD, R., KHAN, H., ARSHAD, M., RASEKH, M., HUSSAIN, A., WALSH, S., LI, X., CHANG, M. and AHMAD, Z., 2015. Microneedle Coating Techniques for Transdermal Drug Delivery. *Pharmaceutics,* 7(4), pp. 486-502.

HAPGOOD, K., LITSTER, J.D. and WANG, C., 2015. Pharmaceutical particles. *Chemical Engineering Science,* 125, pp. 1-3.

HEGARTY, C., MCCONVILLE, A., MCGLYNN, R.J., MARIOTTI, D. and DAVIS, J., 2019. Design of composite microneedle sensor systems for the measurement of transdermal pH. *Materials Chemistry and Physics,* 227, pp. 340-346.

HONG, X., WU, Z., CHEN, L., WU, F., WEI, L. and YUAN, W., 2014. Hydrogel Microneedle Arrays for Transdermal Drug Delivery. *Nano-Micro Letters,* 6(3), pp. 191-199.

HUANG, B., ASLAN, E., JIANG, Z., DASKALAKIS, E., JIAO, M., ALDALBAHI, A., VYAS, C. and BÁRTOLO, P., 2020. Engineered dual-scale poly (ε-caprolactone) scaffolds using 3D printing and rotational electrospinning for bone tissue regeneration. *Additive Manufacturing,* 36, pp. 101452.

HUH, I., KIM, S., YANG, H., JANG, M., KANG, G. and JUNG, H., 2018. Effects of two droplet-based dissolving microneedle manufacturing methods on the

activity of encapsulated epidermal growth factor and ascorbic acid. *European Journal of Pharmaceutical Sciences,* 114, pp. 285-292.

HUSAIN, O., LAU, W., EDIRISINGHE, M. and PARHIZKAR, M., 2016. Investigating the particle to fibre transition threshold during electrohydrodynamic atomization of a polymer solution. *Materials Science and Engineering: C,* 65, pp. 240-250.

IKEUCHI, M., TANE, R. and IKUTA, K., 2012. Electrospray deposition and direct patterning of polylactic acid nanofibrous microcapsules for tissue engineering. *Biomedical Microdevices,* 14(1), pp. 35-43.

INDERMUN, S., CHOONARA, Y.E., KUMAR, P., DU TOIT, L.C., MODI, G., LUTTGE, R., GOVENDER, M. and PILLAY, V., 2017. In Vitro and In Vivo Evaluation of a Hydrogel-Based Microneedle Device for Transdermal Electro-Modulated Analgesia. *Journal of pharmaceutical sciences,* 106(4), pp. 1111-1116.

INDERMUN, S., LUTTGE, R., CHOONARA, Y.E., KUMAR, P., DU TOIT, L.C., MODI, G. and PILLAY, V., 2014. Current advances in the fabrication of microneedles for transdermal delivery. *Journal of Controlled Release,* 185, pp. 130-138.

INGROLE, R. and GILL, H., S., 2019. Microneedle Coating Methods: A Review with a Perspective. *the Journal of Pharmacology and Experimental Therapeutics,* 370(3), pp. 555-569.

ITA, K., 2015. Transdermal delivery of drugs with microneedles: Strategies and outcomes. *Journal of Drug Delivery Science and Technology,* 29, pp. 16-23.

JAVED, M.N., ALAM, M.S., WAZIRI, A., POTTOO, F.H., YADAV, A.K., HASNAIN, M.S. and ALMALKI, F.A., 2019. Chapter 12 - QbD Applications for the Development of Nanopharmaceutical Products. , pp. 229-253.

JAYARAMAN, P., GANDHIMATHI, C., VENUGOPAL, J.R., BECKER, D.L., RAMAKRISHNA, S. and SRINIVASAN, D.K., 2015. Controlled release of drugs in electrosprayed nanoparticles for bone tissue engineering. *Advanced Drug Delivery Reviews,* 94, pp. 77-95.

JHAWAT, V., GULIA, M., GUPTA, S., MADDIBOYINA, B. and DUTT, R., 2020. Integration of pharmacogenomics and theranostics with nanotechnology as quality by design (QbD) approach for formulation development of novel dosage forms for effective drug therapy. *Journal of Controlled Release,* 327, pp. 500-511.

JUNG, J.H., CHIANG, B., GROSSNIKLAUS, H.E. and PRAUSNITZ, M.R., 2018. Ocular drug delivery targeted by iontophoresis in the suprachoroidal space using a microneedle. *Journal of Controlled Release,* 277, pp. 14-22.

KAMBLE, P., SADARANI, B., MAJUMDAR, A. and BHULLAR, S., 2017. Nanofiber based drug delivery systems for skin: A promising therapeutic approach. *Journal of Drug Delivery Science and Technology,* 41, pp. 124-133.

KHAN, H., MEHTA, P., MSALLAM, H., ARMITAGE, D. and AHMAD, Z., 2014. Smart microneedle coatings for controlled delivery and biomedical analysis. *Journal of drug targeting,* 22(9), pp. 790-795.

KHANDAN, O., KAHOOK, M.Y. and RAO, M.P., 2016. Fenestrated microneedles for ocular drug delivery. *Sensors and Actuators B-Chemical,* 223, pp. 15-23.

KIM, J.H., SHIN, J.U., KIM, S.H., NOH, J.Y., KIM, H.R., LEE, J., CHU, H., JEONG, K.Y., PARK, K.H., KIM, J.D., KIM, H.K., JEONG, D.H., YONG, T., PARK, J. and LEE, K.H., 2018. Successful transdermal allergen delivery and allergen-specific immunotherapy using biodegradable microneedle patches. *Biomaterials,* 150, pp. 38-48.

KIM, J.D., KIM, M., YANG, H., LEE, K. and JUNG, H., 2013. Droplet-born air blowing: Novel dissolving microneedle fabrication. *Journal of Controlled Release,* 170(3), pp. 430-436.

KIM, Y., PARK, J. and PRAUSNITZ, M.R., 2012. Microneedles for drug and vaccine delivery. *Advanced Drug Delivery Reviews,* 64(14), pp. 1547-1568.

KOUTSONANOS, D.G., DEL PILAR MARTIN, M., ZARNITSYN, V.G., SULLIVAN, S.P., COMPANS, R.W., PRAUSNITZ, M.R. and SKOUNTZOU, I., 2009. Transdermal influenza immunization with vaccine-coated microneedle arrays. *PloS one,* 4(3), pp. e4773.

KOVÁCS, A., BERKÓ, S., CSÁNYI, E. and CSÓKA, I., 2017. Development of nanostructured lipid carriers containing salicyclic acid for dermal use based on the Quality by Design method. *European Journal of Pharmaceutical Sciences,* 99, pp. 246-257.

LARRAÑETA, E., LUTTON, R.E.M., WOOLFSON, A.D. and DONNELLY, R.F., 2016. Microneedle arrays as transdermal and intradermal drug delivery systems: Materials science, manufacture and commercial development. *Materials Science and Engineering: R: Reports,* 104, pp. 1-32.

LEE, H.J., SON, Y., KIM, D., KIM, Y.K., CHOI, N., YOON, E. and CHO, I., 2015. A new thin silicon microneedle with an embedded microchannel for deep brain drug infusion. *Sensors and Actuators B-Chemical,* 209, pp. 413-422.

LEE, J.W., PARK, J. and PRAUSNITZ, M.R., 2008. Dissolving microneedles for transdermal drug delivery. *Biomaterials,* 29(13), pp. 2113-2124.

LEE, J.W., GADIRAJU, P., PARK, J., ALLEN, M.G. and PRAUSNITZ, M.R., 2011. Microsecond thermal ablation of skin for transdermal drug delivery. *Journal of Controlled Release,* 154(1), pp. 58-68.

LEE, J., PARK, S.H., SEO, I.H., LEE, K.J. and RYU, W., 2015. Rapid and repeatable fabrication of high A/R silk fibroin microneedles using thermally-drawn micromolds. *European Journal of Pharmaceutics and Biopharmaceutics,* 94, pp. 11-19.

LEE, S., JEONG, W. and BEEBE, D., 2003. Microfluidic valve with cored glass microneedle for microinjection. *Lab on a Chip,* 3(3), pp. 164-167.

LEE, Y., WU, B., ZHUANG, W., CHEN, D. and TANG, Y.J., 2011. Nanoparticles facilitate gene delivery to microorganisms via an electrospray process. *Journal of microbiological methods,* 84(2), pp. 228-233.

LHERNOULD, M.S., DELEERS, M. and DELCHAMBRE, A., 2015. Hollow polymer microneedles array resistance and insertion tests. *International Journal of Pharmaceutics,* 480(1), pp. 152-157.

LIU, K., SUNG, K.C., AL-SUWAYEH, S.A., KU, M., CHU, C., WANG, J. and FANG, J., 2011. Enhancement of transdermal apomorphine delivery with a diester prodrug strategy. *European Journal of Pharmaceutics and Biopharmaceutics,* 78(3), pp. 422-431.

LOIZIDOU, E.Z., INOUE, N.T., ASHTON-BARNETT, J., BARROW, D.A. and ALLENDER, C.J., 2016. Evaluation of geometrical effects of microneedles on skin penetration by CT scan and finite element analysis. *European Journal of Pharmaceutics and Biopharmaceutics,* 107, pp. 1-6.

LUANGVEERA, W., JIRUEDEE, S., MAMA, W., CHIARANAIRUNGROJ, M., PIMPIN, A., PALAGA, T. and SRITURAVANICH, W., 2015. Fabrication and characterization of novel microneedles made of a polystyrene solution. *Journal of the Mechanical Behavior of Biomedical Materials,* 50, pp. 77-81.

MA, G. and WU, C., 2017. Microneedle, bio-microneedle and bio-inspired microneedle: A review. *Journal of Controlled Release,* 251, pp. 11-23.

MACHEKPOSHTI, S.A., SOLTANI, M., NAJAFIZADEH, P., EBRAHIMI, S.A. and CHEN, P., 2017. Biocompatible polymer microneedle for transdermal delivery of tranexamic acid. *Journal of Controlled Release,* 10(261), pp. 87-97.

MAHONY, D., CAVALLARO, A.S., STAHR, F., MAHONY, T.J., QIAO, S.Z. and MITTER, N., 2013. Mesoporous Silica Nanoparticles Act as a Self-Adjuvant for Ovalbumin Model Antigen in Mice. *Small,* 9(18), pp. 3138-3146.

MAI, Z., CHEN, J., HE, T., HU, Y., DONG, X., ZHANG, H., HUANG, W., KO, F. and ZHOU, W., 2017. Electrospray biodegradable microcapsules loaded with

curcumin for drug delivery systems with high bioactivity. *Rsc Advances,* 7(3), pp. 1724-1734.

MALINOVSKAJA-GOMEZ, K., ESPUELAS, S., GARRIDO, M.J., HIRVONEN, J. and LAAKSONEN, T., 2017. Comparison of liposomal drug formulations for transdermal iontophoretic drug delivery. *European Journal of Pharmaceutical Sciences,* 106, pp. 294-301.

MALINOVSKAJA-GOMEZ, K., LABOUTA, H.I., SCHNEIDER, M., HIRVONEN, J. and LAAKSONEN, T., 2016. Transdermal iontophoresis of flufenamic acid loaded PLGA nanoparticles. *European Journal of Pharmaceutical Sciences,* 89, pp. 154-162.

MARTANTO, W., MOORE, J.S., COUSE, T. and PRAUSNITZ, M.R., 2006. Mechanism of fluid infusion during microneedle insertion and retraction. *Journal of Controlled Release,* 112(3), pp. 357-361.

MATRIANO, J.A., CORMIER, M., JOHNSON, J., YOUNG, W.A., BUTTERY, M., NYAM, K. and DADDONA, P.E., 2002. Macroflux Microprojection Array Patch Technology: A New and Efficient Approach for Intracutaneous Immunization. *Pharmaceutical Research,* 19, pp. 63-70.

MCCONVILLE, A. and DAVIS, J., 2016. Transdermal microneedle sensor arrays based on palladium: Polymer composites. *Electrochemistry Communications,* 72, pp. 162-165.

MCGRATH, M.G., VRDOLJAK, A., O'MAHONY, C., OLIVEIRA, J.C., MOORE, A.C. and CREAN, A.M., 2011. Determination of parameters for successful spray coating of silicon microneedle arrays. *International Journal of Pharmaceutics,* 415(1), pp. 140-149.

MCGRATH, M.G., VUCEN, S., VRDOLJAK, A., KELLY, A., O'MAHONY, C., CREAN, A.M. and MOORE, A., 2014. Production of dissolvable microneedles using an atomised spray process: Effect of microneedle composition on skin penetration. *European Journal of Pharmaceutics and Biopharmaceutics,* 86(2), pp. 200-211.

MEHTA, P., HAJ-AHMAD, R., RASEKH, M., ARSHAD, M.S., SMITH, A., VAN DER MERWE, S.M., LI, X., CHANG, M. and AHMAD, Z., 2017. Pharmaceutical and biomaterial engineering via electrohydrodynamic atomization technologies. *Drug Discovery Today,* 22(1), pp. 157-165.

MIGDADI, E.M., COURTENAY, A.J., TEKKO, I.A., MCCRUDDEN, M.T.C., KEARNEY, M., MCALISTER, E., MCCARTHY, H.O. and DONNELLY, R.F., 2018. Hydrogel-forming microneedles enhance transdermal delivery of metformin hydrochloride. *Journal of Controlled Release,* 285, pp. 142-151.

MILLER, M.A., YU, F., KIM, K. and KASTING, G.B., 2017. Uptake and desorption of hydrophilic compounds from human stratum corneum. *Journal of Controlled Release,* 10(261), pp. 307-317.

MONKARE, J., NEJADNIK, M.R., BACCOUCHE, K., ROMEIJN, S., JISKOOT, W. and BOUWSTRA, J.A., 2015. IgG-loaded hyaluronan-based dissolving microneedles for intradermal protein delivery. *Journal of Controlled Release,* 218, pp. 53-62.

MOREIRA, A., LAWSON, D., ONYEKURU, L., DZIEMIDOWICZ, K., ANGKAWINITWONG, U., COSTA, P.F., RADACSI, N. and WILLIAMS, G.R., 2020. Protein encapsulation by electrospinning and electrospraying. *Journal of Controlled Release,* 329(10), pp. 1172-1197.

MUKAIBO, H., JOHNSON, E.A., MIRA, F., ANDRION, K., OSTEIKOETXEA, X., PALMA, R. and MARTIN, C.R., 2015. Template-synthesized gold microneedle arrays for gene delivery to the Chlamydomonas reinhardtii chloroplast. *Materials Letters,* 141, pp. 76-78.

NADERI, P., SHAMS, M. and GHASSEMI, H., 2019. Investigation on the onset voltage and stability island of electrospray in the cone-jet mode using curved counter electrode. *Journal of Electrostatics,* 98, pp. 1-10.

NARAYAN, R., NAYAK, U.Y., RAICHUR, A.M. and GARG, S., 2018. Mesoporous Silica Nanoparticles: A Comprehensive Review on Synthesis and Recent Advances. *Pharmaceutics,* 10(3), pp. 118.

NURUNNABI, M., REVURI, V., HUH, K.M. and LEE, Y., 2017. Chapter 14 - Polysaccharide based nano/microformulation: an effective and versatile oral drug delivery system. *Nanostructures for Oral Medicine.* Amsterdam, Netherlands: Elsevier, pp. 409-433.

O'MAHONY, C., HILLIARD, L., KOSCH, T., BOCCHINO, A., SULAS, E., KENTHAO, A., O'CALLAGHAN, S., CLOVER, A.J.P., DEMARCHI, D. and BARED, G., 2017. Accuracy and feasibility of piezoelectric inkjet coating technology for applications in microneedle-based transdermal delivery. *Microelectronic Engineering,* 172, pp. 19-25.

OUYANG, Q., FENG, X., KUANG, S., PANWAR, N., SONG, P., YANG, C., YANG, G., HEMU, X., ZHANG, G., YOON, H.S., TAM, J.P., LIEDBERG, B., ZHU, G., YONG, K. and WANG, Z.L., 2019. Self-powered, on-demand transdermal drug delivery system driven by triboelectric nanogenerator. *Nano Energy,* 62, pp. 610-619.

OVSIANIKOV, A., CHICHKOV, B., MENTE, P., MONTEIRO-RIVIERE, N.A., DORAISWAMY, A. and NARAYAN, R.J., 2007. Two photon polymerization of polymer-ceramic hybrid materials for transdermal drug delivery. *International Journal of Applied Ceramic Technology,* 4(1), pp. 22-29.

PARK, J. and PRAUSNITZ, M.R., 2010. Analysis of the Mechanical Failure of Polymer Microneedles by Axial Force. *Journal of the Korean Physical Society,* 56(4), pp. 1223-1227.

PASTORE, M., N., KALIA, Y., N, HORSTMANN, M. and ROBERTS, M., S., 2015. Transdermal patches: history, development and pharmacology. *British journal of pharmacology,* 172(9), pp. 2179-2209.

PAWAR, A., THAKKAR, S. and MISRA, M., 2018. A bird's eye view of nanoparticles prepared by electrospraying: advancements in drug delivery field. *Journal of Controlled Release,* 286, pp. 179-200.

PLANZ, V., LEHR, C. and WINDBERGS, M., 2016. In vitro models for evaluating safety and efficacy of novel technologies for skin drug delivery. *Journal of Controlled Release,* 242, pp. 89-104.

POON, T.H.Y., 2013. *Zeolite microneedles: fabrication, mechanics and transdermal drug delivery.* M.Phil edn. Honk Kong: The Honk Kong University of Science and Technology.

PRABHAKARAN, M.P., ZAMANI, M., FELICE, B. and RAMAKRISHNA, S., 2015. Electrospraying technique for the fabrication of metronidazole contained PLGA particles and their release profile. *Materials Science and Engineering: C,* 56, pp. 66-73.

PRAUSNITZ, M.R., 2004. Microneedles for transdermal drug delivery. *Advanced Drug Delivery Reviews,* 56(5), pp. 581-587.

PYO, S.M. and MAIBACH, H.I., 2019. Skin Metabolism: Relevance of Skin Enzymes for Rational Drug Design. Skin Pharmacology and Physiology. *Skin pharmacology and physiology,* 32, pp. 283-294.

QINDEEL, M., ULLAH, M.H., FAKHAR-UD-DIN, AHMED, N. and REHMAN, A.U., 2020. Recent trends, challenges and future outlook of transdermal drug delivery systems for rheumatoid arthritis therapy. *Journal of Controlled Release,* 327, pp. 595-615.

RABIONET, M., PUIG, T. and CIURANA, J., 2020. Manufacture of PCL scaffolds through electrospinning technology to accommodate Triple Negative Breast Cancer cells culture. *Procedia CIRP,* 89, pp. 98-103.

RAI, P., GAUTAM, N. and CHANDRA, H., 2017. An Experimental Approach of Generation of Micro/Nano Scale Liquid Droplets by Electrohydrodynamic Atomization (EHDA) Process. *Materials Today: Proceedings,* 4(2, Part A), pp. 611-620.

REARDON, P.J.T., PARHIZKAR, M., HARKER, A.H., BROWNING, R.J., VASSILEVA, V., STRIDE, E., PEDLEY, R.B., EDIRISINGHE, M. and KNOWLES,

J.C., 2017. Electrohydrodynamic fabrication of core-shell PLGA nanoparticles with controlled release of cisplatin for enhanced cancer treatment. *International Journal of Nanomedicine,* 12, pp. 3913-3926.

REZVANPOUR, A., KRANTZ, W.B. and WANG, C., 2012. Scaling analysis of the electrohydrodynamic atomization (EHDA) process for pharmaceutical particle fabrication. *Chemical Engineering Science,* 80, pp. 81-90.

ROSS, S., SCOUTARIS, N., LAMPROU, D., MALLINSON, D. and DOUROUMIS, D., 2015. Inkjet printing of insulin microneedles for transdermal delivery. *Drug Delivery and Translational Research,* 5(4), pp. 451-461.

ROXHED, N., GRISS, P. and STEMME, G., 2008. Membrane-sealed hollow microneedles and related administration schemes for transdermal drug delivery. *Biomedical Microdevices,* 10(2), pp. 271-279.

RUGGIERO, F., VECCHIONE, R., BHOWMICK, S., COPPOLA, G., COPPOLA, S., ESPOSITO, E., LETTERA, V., FERRARO, P. and NETTI, P.A., 2018. Electro-drawn polymer microneedle arrays with controlled shape and dimension. *Sensors and Actuators B: Chemical,* 255, pp. 1553-1560.

RZHEVSKIY, A.S., SINGH, T.R.R., DONNELLY, R.F. and ANISSIMOV, Y.G., 2018. Microneedles as the technique of drug delivery enhancement in diverse organs and tissues. *Journal of Controlled Release,* 270, pp. 184-202.

SAYED, E., KARAVASILI, C., RUPARELIA, K., HAJ-AHMAD, R., CHARALAMBOPOULOU, G., STERIOTIS, T., GIASAFAKI, D., COX, P., SINGH, N., GIASSAFAKI, L.N., MPENEKOU, A., MARKOPOULOU, C.K., VIZIRIANAKIS, I.S., CHANG, M., FATOUROS, D.G. and AHMAD, Z., 2018. Electrosprayed mesoporous particles for improved aqueous solubility of a poorly water soluble anticancer agent: in vitro and ex vivo evaluation. *Journal of Controlled Release,* 278, pp. 142-155.

SEBASTIA-SAEZ, D., BURBIDGE, A., ENGMANN, J. and RAMAIOLI, M., 2020. New trends in mechanistic transdermal drug delivery modelling: Towards an accurate geometric description of the skin microstructure. *Computers & Chemical Engineering,* 141, pp. 106976.

SEDGHI, R., SHAABANI, A., MOHAMMADI, Z., SAMADI, F.Y. and ISAEI, E., 2017. Biocompatible electrospinning chitosan nanofibers: A novel delivery system with superior local cancer therapy. *Carbohydrate Polymers,* 159, pp. 1-10.

SEQUEIRA, R.S., MIGUEL, S.P., CABRAL, C.S.D., MOREIRA, A.F., FERREIRA, P. and CORREIA, I.J., 2019. Development of a poly(vinyl alcohol)/lysine electrospun membrane-based drug delivery system for improved skin regeneration. *International journal of pharmaceutics,* 570, pp. 118640.

SERGI, P.N., JENSEN, W. and YOSHIDA, K., 2016. Interactions among biotic and abiotic factors affect the reliability of tungsten microneedles puncturing in vitro and in vivo peripheral nerves: A hybrid computational approach. *Materials Science and Engineering: C,* 59, pp. 1089-1099.

SERVATAN, M., ZARRINTAJ, P., MAHMODI, G., KIM, S., GANJALI, M.R., SAEB, M.R. and MOZAFARI, M., 2020. Zeolites in drug delivery: Progress, challenges and opportunities. *Drug discovery today,* 25(4), pp. 642-656.

SHAHZAD, Y., LOUW, R., GERBER, M. and DU PLESSIS, J., 2015. Breaching the skin barrier through temperature modulations. *Journal of Controlled Release,* 202, pp. 1-13.

SHUKLA, T., UPMANYU, N., AGRAWAL, M., SARAF, S., SARAF, S. and ALEXANDER, A., 2018. Biomedical applications of microemulsion through dermal and transdermal route. *Biomedicine & Pharmacotherapy,* 108, pp. 1477-1494.

SKOOG, S.A., MILLER, P.R., BOEHM, R.D., SUMANT, A.V., POLSKY, R. and NARAYAN, R.J., 2015. Nitrogen-incorporated ultrananocrystalline diamond microneedle arrays for electrochemical biosensing. *Diamond and Related Materials,* 54, pp. 39-46.

SONI, G., KALE, K., SHETTY, S., GUPTA, M.K. and YADAV, K.S., 2020. Quality by design (QbD) approach in processing polymeric nanoparticles loading anticancer drugs by high pressure homogenizer. *Heliyon,* 6(4), pp. e03846.

TAKEUCHI, I., SHIMAMURA, Y., KAKAMI, Y., KAMEDA, T., HATTORI, K., MIURA, S., SHIRAI, H., OKUMURA, M., INAGI, T., TERADA, H. and MAKINO, K., 2019. Transdermal delivery of 40-nm silk fibroin nanoparticles. *Colloids and Surfaces B: Biointerfaces,* 175, pp. 564-568.

TER HORST, B., CHOUHAN, G., MOIEMEN, N.S. and GROVER, L.M., 2018. Advances in keratinocyte delivery in burn wound care. *Advanced Drug Delivery Reviews,* 123, pp. 18-32.

THAKKAR, S. and MISRA, M., 2017. Electrospun polymeric nanofibers: New horizons in drug delivery. *European Journal of Pharmaceutical Sciences,* 107, pp. 148-167.

THAKUR, R.R.S., FALLOWS, S.J., MCMILLAN, H.L., DONNELLY, R.F. and JONES, D.S., 2014. Microneedle- mediated intrascleral delivery of in situ forming thermoresponsive implants for sustained ocular drug delivery. *Journal of Pharmacy and Pharmacology,* 66(4), pp. 584-595.

TSUCHIYA, K., JINNIN, S., YAMAMOTO, H., UETSUJI, Y. and NAKAMACHI, E., 2010. Design and development of a biocompatible painless microneedle by the ion sputtering deposition method. *Precision Engineering-Journal of the*

International Societies for Precision Engineering and Nanotechnology, 34(3), pp. 461-466.

TU, J., DU, G., REZA NEJADNIK, M., MÖNKÄRE, J., VAN DER MAADEN, K., BOMANS, P., SOMMERDIJK, N., SLÜTTER, B., JISKOOT, W., BOUWSTRA, J. and KROS, A., 2017. Mesoporous Silica Nanoparticle-Coated Microneedle Arrays for Intradermal Antigen Delivery. *Pharamceutical Research,* 34(8), pp. 1693-1706.

UDDIN, M.J., SCOUTARIS, N., KLEPETSANIS, P., CHOWDHRY, B., PRAUSNITZ, M.R. and DOUROUMIS, D., 2015. *Inkjet printing of transdermal microneedles for the delivery of anticancer agents.*

UHLENBROCK, L., SIXT, M. and STRUBE, J., 2017. Quality-by-Design (QbD) process evaluation for phytopharmaceuticals on the example of 10-deacetylbaccatin III from yew. *Resource-Efficient Technologies,* 3(2), pp. 137-143.

VAN DER MAADEN, K., JISKOOT, W. and BOUWSTRA, J., 2012. Microneedle technologies for (trans)dermal drug and vaccine delivery. *Journal of Controlled Release,* 161(2), pp. 645-655.

VINAYAKUMAR, K.B., HEGDE, G.M., NAYAK, M.M., DINESH, N.S. and RAJANNA, K., 2014. Fabrication and characterization of gold coated hollow silicon microneedle array for drug delivery. *Microelectronic Engineering,* 128, pp. 12-18.

VRDOLJAK, A., MCGRATH, M., CAREY, J., DRAPER, S., HILL, A., O'MAHONY, C., CREAN, A. and MOORE, A., 2012. Coated microneedle arrays for transcutaneous delivery of live virus vaccines. *Journal of Control Release,* 159(10), pp. 34-42.

WAGHULE, T., DABHOLKAR, N., GORANTLA, S., RAPALLI, V.K., SAHA, R.N. and SINGHVI, G., 2021. Quality by design (QbD) in the formulation and optimization of liquid crystalline nanoparticles (LCNPs): A risk based industrial approach. *Biomedicine & Pharmacotherapy,* 141, pp. 111940.

WAGHULE, T., SINGHVI, G., DUBEY, S.K., PANDEY, M.M., GUPTA, G., SINGH, M. and DUA, K., 2019. Microneedles: A smart approach and increasing potential for transdermal drug delivery system. *Biomedicine & Pharmacotherapy,* 109, pp. 1249-1258.

WANG, D., ROCKS, S.A. and DOREY, R.A., 2012. Electrohydrodynamic atomization deposition of PZT sol–gel slurry and sol infiltration on the films. *Journal of the European Ceramic Society,* 32(8), pp. 1651-1658.

WANG, P.M., CORNWELL, M., HILL, J. and PRAUSNITZ, M.R., 2006. Precise microinjection into skin using hollow microneedles. *Journal of Investigative Dermatology,* 126(5), pp. 1080-1087.

WANG, Q.L., ZHU, D.D., CHEN, Y. and GUO, X.D., 2016. A fabrication method of microneedle molds with controlled microstructures. *Materials Science and Engineering: C,* 65, pp. 135-142.

WANG, Q., WANG, Z., YANG, S., LI, B., XU, H., YU, K. and WANG, J., 2021. Experimental study on electrohydrodynamic atomization (EHDA) in stable cone-jet with middle viscous and low conductive liquid. *Experimental Thermal and Fluid Science,* 121, pp. 110260.

WANG, R., WANG, W. and LI, Z., 2016. An Improved Manufacturing Approach for Discrete Silicon Microneedle Arrays with Tunable Height-Pitch Ratio. *Sensors,* 16(10), pp. 1628.

WANG, Y., LU, Z., LV, F. and BIE, X., 2009. Study on microencapsulation of curcumin pigments by spray drying. *European Food Research and Technology,* 229(3), pp. 391-396.

XIE, J., JIANG, J., DAVOODI, P., SRINIVASAN, M.P. and WANG, C., 2015. Electrohydrodynamic atomization: A two-decade effort to produce and process micro-/nanoparticulate materials. *Chemical Engineering Science,* 125, pp. 32-57.

YANG, Y., JIA, Z., LI, Q., HOU, L., LIU, J., WANG, L., GUAN, Z. and ZAHN, M., 2010. A shield ring enhanced equilateral hexagon distributed multi-needle electrospinning spinneret. *IEEE Transactions on Dielectrics and Electrical Insulation,* 17.5, pp. 1592-1601.

YANG, G., KIM, M. and KIM, G., 2015. A hybrid PCL/collagen scaffold consisting of solid freeform-fabricated struts and EHD-direct-jet-processed fibrous threads for tissue regeneration. *Journal of colloid and interface science,* 450, pp. 159-167.

YANG, J., LIU, X., FU, Y. and SONG, Y., 2019. Recent advances of microneedles for biomedical applications: drug delivery and beyond. *Acta Pharmaceutica Sinica B,* 9(3), pp. 469-483.

YIN, Z., KUANG, D., WANG, S., ZHENG, Z., YADAVALLI, V.K. and LU, S., 2018. Swellable silk fibroin microneedles for transdermal drug delivery. *International Journal of Biological Macromolecules,* 106, pp. 48-56.

YOUSEF, H., ALHAJJ, M. and SHARMA, S., 2019-last update, Anatomy, Skin (Integument), Epidermis. Available: https://europepmc.org/article/nbk/nbk470464.

YU, W., JIANG, G., LIU, D., LI, L., CHEN, H., LIU, Y., HUANG, Q., TONG, Z., YAO, J. and KONG, X., 2017. Fabrication of biodegradable composite microneedles based on calcium sulfate and gelatin for transdermal delivery of insulin. *Materials Science and Engineering: C,* 71, pp. 725-734.

YU, W., JIANG, G., LIU, D., LI, L., TONG, Z., YAO, J. and KONG, X., 2017. Transdermal delivery of insulin with bioceramic composite microneedles fabricated by gelatin and hydroxyapatite. *Materials Science and Engineering: C,* 73, pp. 425-428.

YU, W., JIANG, G., ZHANG, Y., LIU, D., XU, B. and ZHOU, J., 2017. Polymer microneedles fabricated from alginate and hyaluronate for transdermal delivery of insulin. *Materials Science and Engineering: C,* 80, pp. 187-196.

ZAKREWSKY, M., KUMAR, S. and MITRAGOTRI, S., 2015. Nucleic acid delivery into skin for the treatment of skin disease: Proofs-of-concept, potential impact, and remaining challenges. *Journal of Controlled Release,* 219, pp. 445-456.

ZEHTABIYAN-REZAIE, N., SAFFAR-AVVAL, M. and ADAMIAK, K., 2020. On the evaporation enhancement from saline water due to corona discharge generated EHD flow: A numerical and experimental study. *International Communications in Heat and Mass Transfer,* 119, pp. 104988.

ZHAO, X., COULMAN, S.A., HANNA, S.J., WONG, F.S., DAYAN, C.M. and BIRCHALL, J.C., 2017. Formulation of hydrophobic peptides for skin delivery via coated microneedles. *Journal of Controlled Release,* 265, pp. 2-13.

ZHAO, Y. and YAO, J., 2017. Electrostatic characterization of electrohydrodynamic atomization process for particle fabrication. *Powder Technology,* 314, pp. 589-598.

ZHU, D.D., CHEN, B.Z., HE, M.C. and GUO, X.D., 2017. Structural optimization of rapidly separating microneedles for efficient drug delivery. *Journal of Industrial and Engineering Chemistry,* 51, pp. 178-184.

ZHU, D.D., WANG, Q.L., LIU, X.B. and GUO, X.D., 2016. Rapidly separating microneedles for transdermal drug delivery. *Acta Biomaterialia,* 41, pp. 312-319.

Chapter 3 Materials and Methods

This chapter includes all the materials and methods used during this research project. It includes the source of materials along with detailed descriptions of the methodology and characterisation techniques that were used.

3.1 Materials

3.1.1 Polyvinylpyrrolidone

Polyvinylpyrrolidone (PVP) (Figure 12) is a synthetic biocompatible non-ionic water-soluble polymer commonly used in the pharmaceutical industry as an excipient in tablets acting as a binder or filler. The hydroxyl group on the PVP backbone enables breakdown via hydrogen bonding. Due to its hydrophilic nature, it is able to form complexes with hydrophilic and hydrophobic materials thus enabling controlled release profiles. It has many desirable properties including excellent biocompatibility, good solubility, in polar and organic solvents (PranavKumar Shadamarshan, Balaji et al. 2018). PVP was purchased from Ashland (Worcestershire,UK) and was used at two molecular weights $4x10^4$ g/mol and $1.3x10^6$ g/mol.
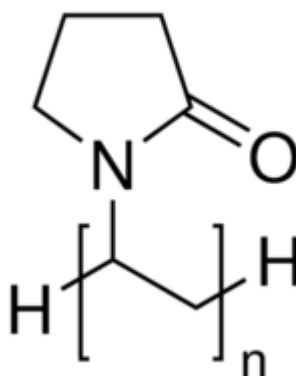

Figure 12: Structure of Polyvinylpyrrolidone

3.1.2 Polycaprolactone

Polycaprolactone (PCL) (Figure 13) is a biodegradable synthetic polyester. Under physiological conditions this hydrophobic polymer undergoes hydrolytic degradation. These elements combined with its excellent biocompatibility has led to its vast use in wound healing, bone implants, tissue scaffolds, tissue engineering of bone and cartilage (PranavKumar Shadamarshan, Balaji et al. 2018). Due to its hydrophobic nature, it has shown a longer degradation profile and therefore has been utilised more heavily in drug delivery in recent years. PCL is a family member of biodegradable aliphatic polyesters which are utilised in biomaterials in prosthetics and drug delivery systems. Due to excellent characteristics such as non-toxicity, biocompatible, approval by the FDA for use in humans and good fabrication properties (Azimi, Nourpanah et al. 2014). PCL is gaining popularity in the field of targeted drug delivery. It has been most frequently used in tissue engineering applications due to its low cost, being easy to process and ability to maintain its structure. The backbone including carboxyl groups and the unsubstituted polyester backbone terminated with carboxylic acids limits its application in terms of unmediated cell attachment whilst being robust, adaptable and very flexible using different physiochemical steps (Behtaj, Karamali et al. 2020). PCL was purchased from Sigma Aldrich (Dorset,UK) and was used at 2 molecular weights (1.3×10^4 g/mol and 8×10^4 g/mol).
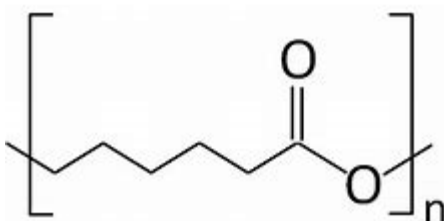
Figure 13: Structure of Polycaprolactone

3.1.3 Fluorescein

Fluorescein (FL) (Figure 14) is an organic xanthene dye. It is used as a fluorescent tracer and has acted as a model dye in biological and medical applications. Even in minute quantities it can be detected, it's highly absorptive and extremely water soluble. It has been used in forensics in serology to detect latent blood stains and in pharmaceutics as a tracer and in the medical field during angiograms to show muscle profile. FL has high molar extinction coefficient at the wavelength near 490 nm and large quantum yield with an emission wavelength near 480-600 nm (which results in excellent brightness with high sensitivity and better labelling), whilst proteins neither absorb nor emit light in these regions (Jityuti, Kuno et al. 2020). Fluorescein was purchased from Sigma Aldrich, Dorset, UK and was of analytical grade.
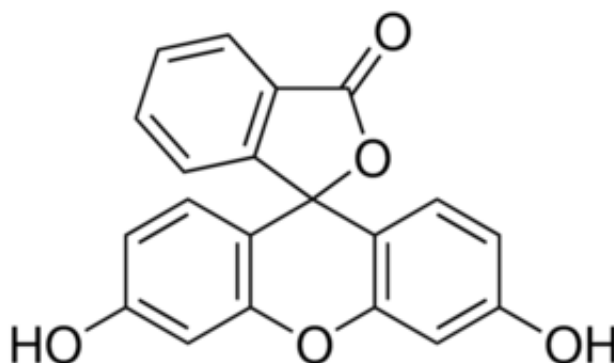
Figure 14: Structure of Fluorescein

3.1.4 Rhodamine B

Rhodamine B (RhB) (figure 15) is a chemical dye used in tracing applications most commonly in water as it is highly soluble and able to detect the rate and direction of transport of molecules. It has been used to stain acid fast organisms such as mycobacterium. RhB has also been used extensively in biotechnology such as fluorescence microscopy, flow cytometry, fluorescence correlation and can be easily detected by ELISA (Guan, Yang et al. 2020). Rhodamine B was purchased from Sigma Aldrich, Dorset, UK and was of analytical grade.
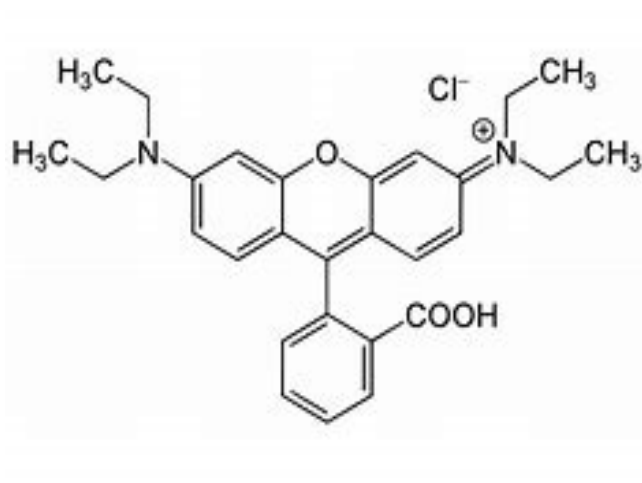
Figure 15: Structure of Rhodamine B

3.1.5 Ethanol

Ethanol (Figure 16) is a widely used solvent in medical and non-medical preparations. It is commonly used in pharmaceutics as well as cosmetics. It's been used as an antiseptic and astringent. The main functional group in ethanol is the hydroxyl group. As oxygen is more electronegative compared to the hydrogen and carbon atom the main form of bonding with other molecules is via hydrogen bonding.

Thus, ethanol is deemed to have good solvent properties and is able to provide an alternative liquid medium for compounds that do not readily dissolve in water or other organic solvents. PVP is known to dissolve in ethanol rapidly; therefore, this indicates that these two components are compatible with one another (Li, F., Men et al. 2018).

Fluorescein as mentioned previously is slightly soluble in ethanol; so it is imperative that they are mixed well. Ethanol is also an ideal solvent to use in EHDA because it known to aid in the formation of a stable cone-jet and its properties such as surface tension, viscosity and electrical conductivity are key parameters that aid in being able to achieve this. Ethanol has a relatively low surface tension which is important in the EHDA process as it prevents sparking from occurring which is often seen with solvents that have a high surface tension such as water (Grace, Marijnissen 1994). Ethanol was purchased from Sigma Aldrich, Dorset, UK and was of analytical grade.
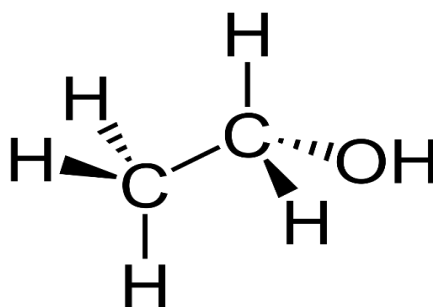
Figure 16: Structure of Ethanol

3.1.6 Dichloromethane

Dichloromethane (Figure 17) is a colourless volatile solvent which is immiscible in water, highly polar and miscible with many organic solvents. It has been used extensively in industry including paint, pharma, degreasing and metal cleaning agents. DCM is classed as an irritant and considered harmful in terms of inhalation and so it is handled carefully. Dichloromethane was purchased from Sigma Aldrich, Dorset, UK and was of analytical grade.
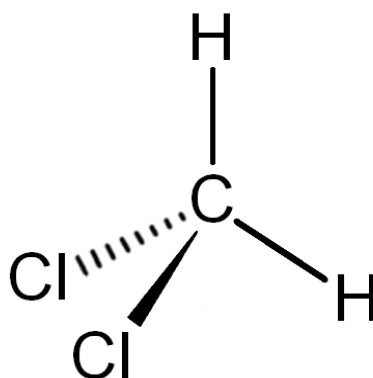
Figure 17: Structure of dichloromethane

3.1.7 Strat-M®

Due to the recurrent lack of availability of biological skin, for testing variation between samples and ethical issues there has been an increasing demand for an inexpensive reproducible in vitro membrane model which stimulates the skin barrier performance in terms of release and permeation. The utilisation of artificial skin membranes can potentially replace the need for animal or human skin. The criteria include the synthetic membrane being fit for purpose by being inert, providing high permeability and not to occlude drug permeation. The FDA has suggested the use of polymeric membranes for in vitro drug permeation studies (Simon, Amaro et al. 2016).

Strat-M® is a synthetic non-animal-based skin model used primarily for diffusion testing which is predictive of human skin without much variability, safety and storage limitations. Strat-M® is highly comparable to human skin engineered to mimic the different layers and lipid chemistry in skin. The shiny side is usually used for diffusion testing (Figure 18A). Strat-M® has a thickness of 300 µm which is made up of an upper layer of polyolefin (non-woven fabric support) supported by 2 layers of polyether sulfone (PES) as shown in Figure 18B. The membrane layers are more porous and thicker to mimic the different layers in human skin (Haq, Goodyear et al. 2018).
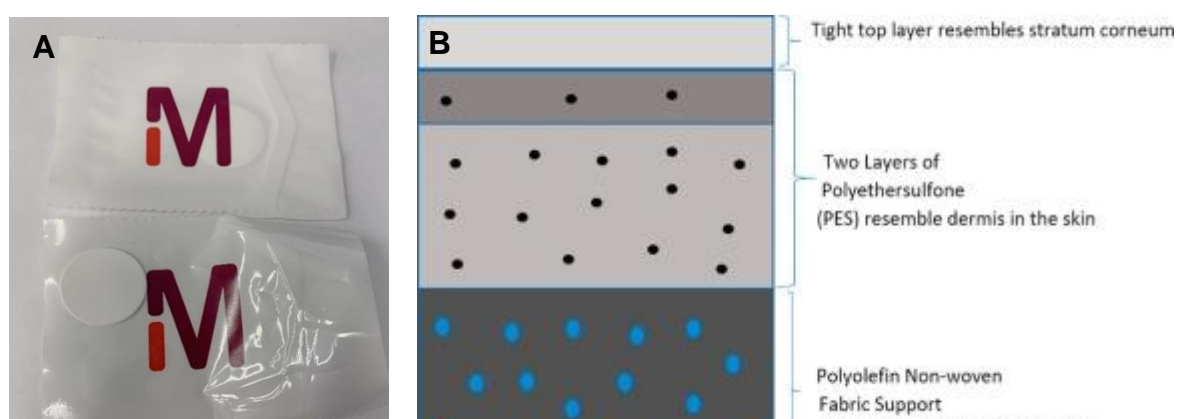
Figure 18: Strat-M® membrane (A) digital image of Strat-M® (B) Strat-M® membrane layers (Haq, Goodyear et al. 2018)

3.2 Methods

3.2.1 Solution characterisation

3.2.1.1 Viscosity

Viscosity measurements were recorded at ambient temperature (20.6 $^{\circ}$C) using a SV-10 Sine-wave Vibro viscometer (A&D, Japan) (Figure 19). Solutions were poured into a plastic holder and the metal vibrators were clamped down when they had reached the surface of the solution. A reading for viscosity (mPa.s) was then recorded and the metal vibrators were cleaned using purified water between each new sample solution reading.
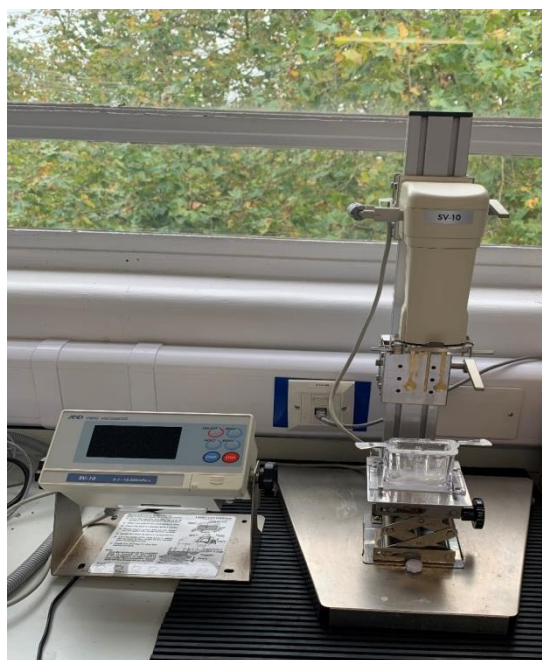
Figure 19: Digital image of an A&D SV-10 sine-wave vibra viscometer

3.2.1.2 Surface Tension

The surface tension of formulations was measured using the Du Nouy ring method. The force required to withdraw a platinum ring from one phase (surface of a liquid) into another phase (gas/air) is measures (Rai, Gautam et al. 2019). The ring is lowered onto the surface of a liquid and with application of an external force the ring is lifted away from the liquid surface (Rezvanpour, Krantz et al. 2012). Surface tension was measured using a torsion balance (White Electrical Instrument, Worcestershire, UK) which is shown in Figure 20.

(Eq.1)

$$\sigma = \frac{F}{L.\cos\theta}$$

Where:

σ = surface tension (N/m)

F = force (N)

L = wetting length of the ring (m)

θ = contact angle between the liquid and the ring
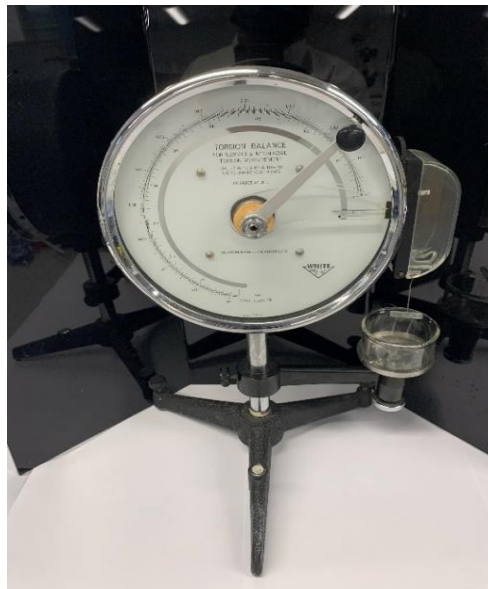
Figure 20: Digital image of a while Elec Ltd Torsion balance

3.2.1.3 Electro-conductivity

The electrical current transmitted from a solution is analysed using a conductivity meter. The EC meter has a probe which has 4 electrodes (probe shown in figure 21). Once the probe is inserted into the sample an alternating current is initiated and is passed between the four electrodes. A Seven Compact S230 conductivity meter (Mettler-Toledo, Switzerland) was used to measure the electrical conductivity of solutions, where prior to each measurement the probe was calibrated using two standards of 1413 S/cm and 12880 S/cm solutions.
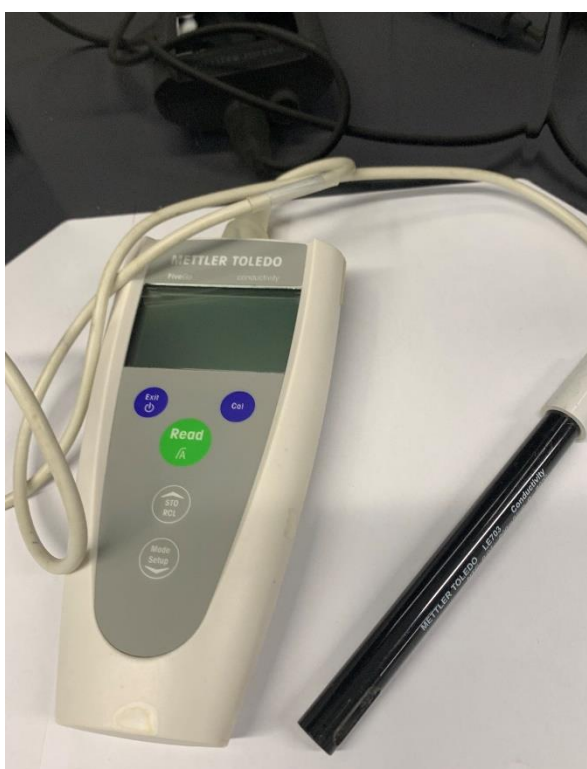
Figure 21: Digital image of a Mettler Toledo Electrical Conductivity Meter

3.2.1.4 Density

Density was obtained using standard 50 mL pyncnometers (VWR, UK). Each pyncnometer (shown in figure 22) was weighed on an analytical balance, filled to full capacity with the solution and then re-weighed. The difference in weight represented the mass (g) of the solution, which was then divided by the volume (50 mL) to get a density value. The following formula is then used to calculate density (Equation 2).

$$Density = \frac{Weight\ of\ bottle\ and\ formulation - Weight\ of\ empty\ bottle}{Volume\ (50\ mL)} \quad \text{(E.q 2)}$$
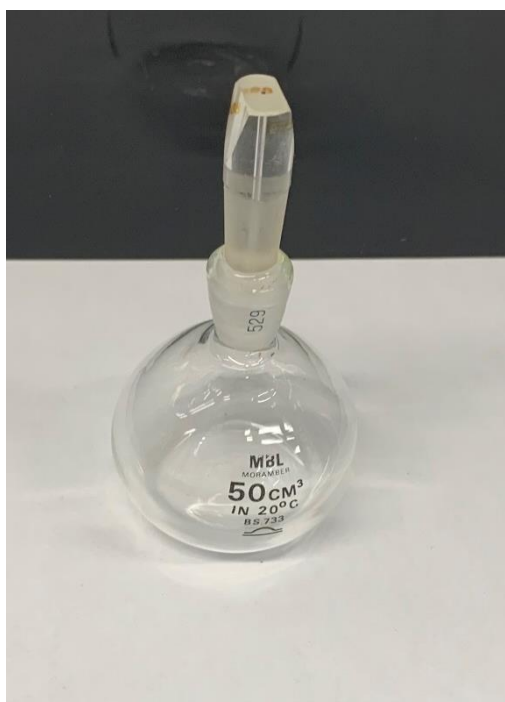
Figure 22: Digital image of a 50 ml pyncnometer

3.2.2 Electrohydrodynamic Atomisation

EHDA is an example of an applied engineering process that can be used to coat the microneedles. The basic principle behind this technique is that it is based on being able to utilize an electrical force which in turn causes the liquid to atomize (Mehta et al., 2017). Once atomised the liquid is electrically imposed out of a nozzle in the form of a jet (Mehta et al., 2017.) As the liquid is being forced out of the nozzle by means of a high electric field; due to this high electrical potential the liquid becomes dispersed into fine droplets (Jaworek and Sobczyk, 2008). The advantage of using EHDA is that uniform nanoparticles are produced in a single step process (Anu Bhushani,J. 2014).

A syringe containing 5 mL of formulation was secured to a syringe infusion pump (Harvard apparatus, pump 11-Elite, USA) which controlled the flow rate of polymer-drug solution. The solution then passed through silicon tubing which was connected to a stainless-steel coaxial needle device (single needle was used in this study) at various flow rates (between 1-100 µL/min). This device was attached to a high-power voltage supply (Glassman High Voltage Supply, UK) (Nguyen, Clasen and Van den Mooter, 2016). Figure 23 shows a typical display of the EHDA setup with a Samsung NX2000 camera. The Es/Esp process carried out under ambient temperature.
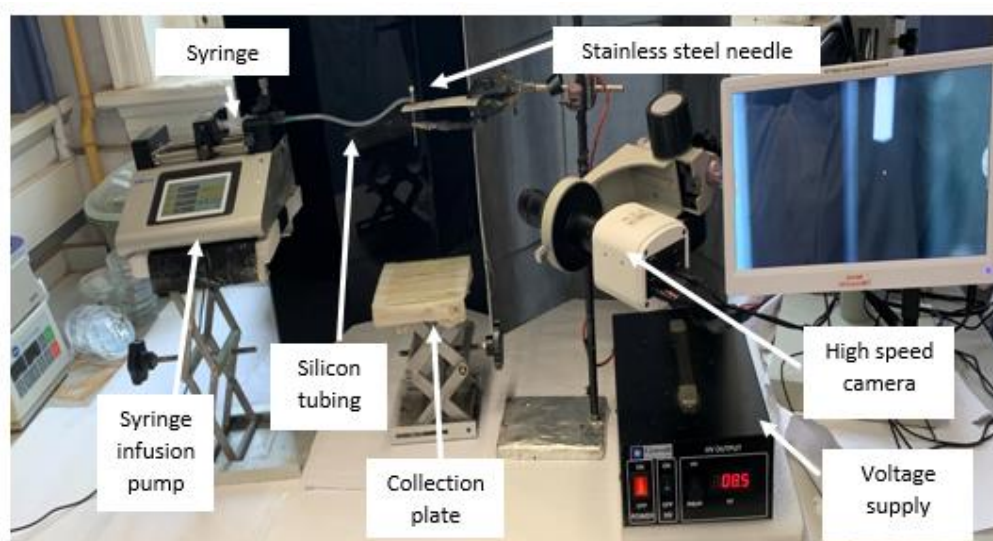
Figure 23: Digital image of the EHDA setup with a Samsung NX2000 camera

3.2.3 Scanning Electron Microscopy

Scanning electron microscopy (SEM) is an example of imaging analysis that is widely used throughout the pharmaceutical industry (shown in Figure 24). It is an analytical tool that can be used to study and provide information on samples morphology. It can also be used as an identification tool; this is because each type of material has a unique and different crystal structure which therefore displays different optical characteristics hence can aid in identifying a sample.

Samples were gold coated prior to analysis (S150B, Edwards, Crawley, West Sussex, UK) this was carried out under vacuum using using a Zeiss Evo HD-15 (using an accelerating voltage of 5 kV) to produce micrographs. Flow rates between 1-100 uL/min with applied voltages 5 to 20 kV with magnifications of x5 k and x40 k; termed as low and high magnifications using Leica DME Optical Microscope using XL1 Camera Software.

Figure 24: Digital image of a Zeiss Evo HD-15 Scanning Electron Microscope

3.2.4 Differential Scanning Calorimetry

Differential Scanning Calorimetry (DSC) is a thermal analytical technique (Figure 25). The fundamental principle of DSC is that it monitors and records the heat flow between a sample and an inert reference sample during a specified temperature range. Following the application of heat the sample may undergo chemical (hydrolysis) or physical (melting) changes which may emit (exothermic energy) or requiring energy to take place (endothermic). The changes in energy is analysed and measured which allows thermal transitions such as melting point and re-crystallisation processes to be recorded.

Figure 25: Digital image of Jade Differential Scanning Calorimeter

3.2.5 Goniometry

Goniometry involves the observation of a liquid droplet when it comes into contact with a solid surface (Figure 26). Contact angle is the quantitative analysis of this wetting of a solid. A precision syringe is used to produce a droplet of water onto the sample on a microscope slide. Contact angle measurements were carried out using ThetaLite T100 contact angle goniometer; using OneAttension software to analyse data. 10 µL of distilled water droplets were used. Each sample was carried out and assessed in sessile drop mode in triplicate and an average was obtained.

Figure 26: Digital image of a Thetalite TL100 goniometer

3.2.6 Fourier Transform Infared Spectroscopy

Infared spectroscopy studies the interactions between light and matter. Fourier Transform Infared (FTIR) Spectroscopy (Figure 27) is a commonly used analytical technique used for the identification of a sample. The spectrum produced corresponds to the sample's functional groups and bonds in terms of position of the peaks. Each functional group/bond has a specific wavenumber. By identifying the functional groups, the structure can be determined.
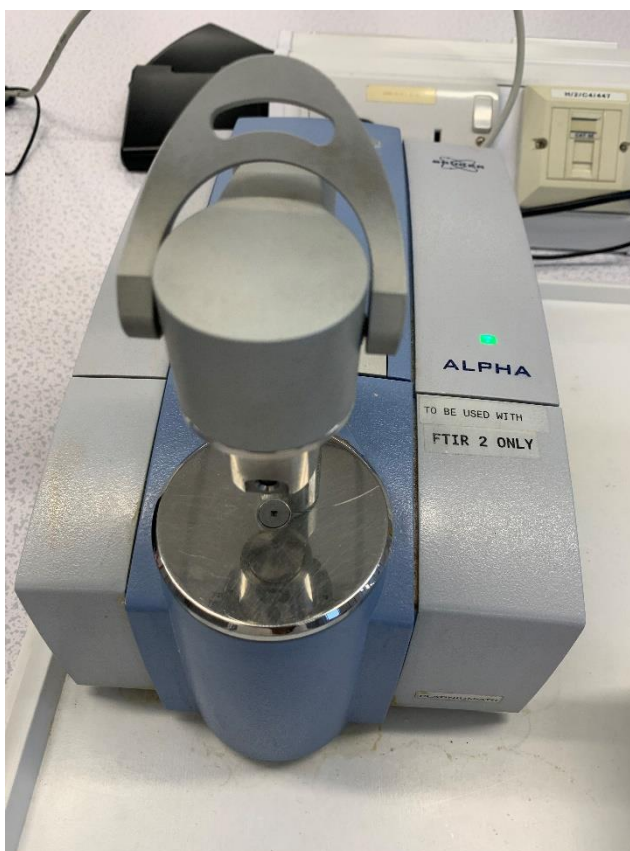
Figure 27: Digital image of ATR-FTIR spectrophotometer fitted with Bruker Alpha Opus 27 FTIR

3.2.7 Ultra-Violet Spectroscopy

UV spectroscopy is an analytical technique (shown in Figure 28) used to determine and quantify the amount of drug in a solution. The majority of drugs absorb light in the UV wavelengths thus using the UV spectrum of the drug and selecting an analytical wavelength which tends to be the maximum absorption of the drug amount. This allows for the quantification of the amount of drug in a particular solution. A beam of light excited the species from ground state to an excited state (electronic transition).

Figure 28: Digital image of a UV-Vis Spectrophotometer

3.2.8 Release Kinetic Modelling

Mathematical modelling of drug release can provide better understanding of drug release profiles and to predict in-vivo performance. Table 3 displays various mathematical models which can be used to determine drug release kinetics of different formulations. Amongst the models the most commonly used include zero order, first order, Higuchi and Korsmeyer-Peppas model.

Table 3: Commonly used kinetic models in pharmaceutics (Lu, ten Hagen 2020)

Release kinetic model	Mathematical equation
Zero order	$Q = Q_0 + k * t$
First order	$Q / Q_0 = 1 - e^{(-k * t)}$
Higuchi	$Q = k * t^{1/2}$
Korsmeyer-Peppas	$Q / Q_0 = k * t^n$

Q represents the amount of drug released at time t;
Q_0 is the initial amount of drug
k is the release constant.

3.2.9 Drug Release and Permeability

Drug permeation through a biological membrane is vital to understand the impact as this is key in the absorption and distribution of the released drug. Vertical Franz diffusion cells (shown in Figure 29) is the most common method used for ex vivo permeation studies. The donor and receptor compartment are separated by StratM® membrane is amongst the most separated by synthetic skin model Strat-M as opposed to SC in human skin. Samples are removed from the sampling port and cumulative amounts of API (dye) is measured over time. The results allow for the permeability coefficient (P_{app}) to be calculated and compared to known values in literature. P_{app} (flux) is the rate of drug permeated/ accumulated in the receptor compartment per surface area of the tissue membrane used in the study. The experiment was carried out at 37°C.

Figure 29: Vertical Franz Diffusion Testing

3.2.10 Confocal laser scanning microscope imaging studies

Confocal laser scanning microscopy (CLSM) is an optical technique which requires a fluorescence response from a sample by rastering a laser over a scan area with a spatial pinhole used in the detection channel to eliminate out of focus light. This method of imaging has been widely used and greatly advanced biomedical research in particular as well as materials science (Hackley, Jubb et al. 2020). Z stack images were acquired with a 63× oil-immersion lens under a Zeiss LSM 780 CLSM (Carl Zeiss Microscopy GmbH, Berlin, Germany) with the appropriate filters. Images were obtained with ZEN 2011 software.

3.2.11 Quality by design

Quality by design (QBD) takes a systematic approach to the development of a drug delivery system. It begins with pre-defined objectives and there is much emphasis on the product and the process itself. It eliminates the need for end product testing as quality is built into the product. This is ensured by focussing on the manufacturing process.

QBD requires a lot of attention with regards to the manufacturing process as highlighted in the literature review. This begins with a QTPP profile being tabulated followed by risk assessments (Ishikawa diagram). The QTPP allows for the correct input variables to be entered into JMP pro software generating randomised experiments which ultimately leads to further robust full factorial designs and in turn a design (control) space which outlines the optimal working regions.

3.3 References

AZIMI, B., NOURPANAH, P., RABIEE, M. and ARBAB, S., 2014. Poly (epsilon-caprolactone) Fiber: An Overview. *Journal of Engineered Fibers and Fabrics,* 9(3), pp. 74-90.

BEHTAJ, S., KARAMALI, F., MASAELI, E., G. ANISSIMOV, Y. and RYBACHUK, M., 2020. Electrospun PGS/PCL, PLLA/PCL, PLGA/PCL and pure PCL scaffolds for retinal progenitor cell cultivation. *Biochemical engineering journal,* pp. 107846.

GRACE, J.M. and MARIJNISSEN, J.C.M., 1994. A review of liquid atomization by electrical means. *Journal of Aerosol Science,* 25(6), pp. 1005-1019.

GUAN, J., YANG, J., ZHANG, Y., ZHANG, X., DENG, H., XU, J., WANG, J. and YUAN, M., 2020. Employing a fluorescent and colorimetric picolyl-functionalized rhodamine for the detection of glyphosate pesticide. *Talanta,* , pp. 121834.

HACKLEY, P.C., JUBB, A.M., BURRUSS, R.C. and BEAVEN, A.E., 2020. Fluorescence spectroscopy of ancient sedimentary organic matter via confocal laser scanning microscopy (CLSM). *International Journal of Coal Geology,* 223, pp. 103445.

HAQ, A., GOODYEAR, B., AMEEN, D., JOSHI, V. and MICHNIAK-KOHN, B., 2018. Strat-M® synthetic membrane: Permeability comparison to human cadaver skin. *International Journal of Pharmaceutics,* 547(1), pp. 432-437.

JITYUTI, B., KUNO, M., LIWPORNCHAROENVONG, T. and BURANAPRAPUK, A., 2020. Selective protein photocleavage by fluorescein derivatives. *Journal of Photochemistry and Photobiology B: Biology,* 212, pp. 112027.

LI, F., MEN, Z., LI, S., WANG, S., LI, Z. and SUN, C., 2018. Study of hydrogen bonding in ethanol-water binary solutions by Raman spectroscopy. *Spectrochimica Acta Part A: Molecular and Biomolecular Spectroscopy,* 189, pp. 621-624.

PRANAVKUMAR SHADAMARSHAN, R., BALAJI, H., RAO, H.S., BALAGANGADHARAN, K., VIJI CHANDRAN, S. and SELVAMURUGAN, N., 2018. Fabrication of PCL/PVP Electrospun Fibers loaded with Trans-anethole for Bone Regeneration in vitro. *Colloids and Surfaces B: Biointerfaces,* 171, pp. 698-706.

RAI, P., GAUTAM, N., CHANDRA, H. and KUMAR, V., 2019. Generation of Micro/Nano Scale Particles and Capsules by Electro hydrodynamic Atomization (EHDA) Process. *Materials Today: Proceedings,* 18, pp. 4374-4383.

REZVANPOUR, A., KRANTZ, W.B. and WANG, C., 2012. Scaling analysis of the electrohydrodynamic atomization (EHDA) process for pharmaceutical particle fabrication. *Chemical Engineering Science,* 80, pp. 81-90.

SIMON, A., AMARO, M.I., HEALY, A.M., CABRAL, L.M. and DE SOUSA, V.P., 2016. Comparative evaluation of rivastigmine permeation from a transdermal system in the Franz cell using synthetic membranes and pig ear skin with in vivo-in vitro correlation. *International Journal of Pharmaceutics,* 512(1), pp. 234-241.

Chapter 4 Pre-formulation

4.1. Introduction

This chapter assesses formulations and their use within EHDA. This chapter of pre-formulation looks at the production of particles and fibres.

4.2. Background

The most conventional forms of drug delivery include oral and parenteral however although these routes remain popular with the ease of administration and the most common amongst dosage forms, they are not without their limitations. Hepatic degradation is a major flaw associated with the oral route as well as patient compliance with the parenteral route and limited to what drug compounds can be used.

The skin measures approximately 2 m^2 and has posed a great challenge in transdermal drug delivery with the skins most formidable barrier SC being difficult to penetrate and being the primary obstacle for drug delivery through the skin (Ahmed Saeed AL-Japairai, Mahmood et al. 2020). There have been many approaches for drug delivery through the skin which include sonophoresis (Ahmed Saeed AL-Japairai, Mahmood et al. 2020), iontophoresis (Malinovskaja-Gomez, Espuelas et al. 2017, Ouyang, Feng et al. 2019), chemical permeation enhancers (Chen, Y., Quan et al. 2014), thermal ablation (Lee, Jeong Woo, Gadiraju et al. 2011). Literature has reported limited success via these approaches and so the investigation of MN systems has been increasing (Zhao, X., Coulman et al. 2017). MNs provide a safe relatively painless and effective solution for overcoming this barrier and safely being able to administer drug (Skoog, Miller et al. 2015). There are many fabrication methods for MNs as well as the drug formulation. The API can either be incorporated during fabrication of the MN or within a coating formulation for MNs (Ma, Wu 2017).

Nano medicine has been the focus in recent years. Polymers have been the primary focus with their vast potential with a large range of applications (Davoodi, Feng et al. 2015). Es and Esp via EHDA has been utilised for many applications most of which consist of nano scale drug delivery systems (Sedghi, Shaabani et al. 2017).

The aim of this chapter is to explore various polymeric solutions and their applicability for EHDA and whether Es or Esp occurs and ultimately characterising the resultant structures.

4.3 Materials and Methods

4.3.1 Materials

PVP (4×10^4 g/mol and 1.3×10^6 g/mol) were sourced from Ashland, UK. PCL (1.4×10^4 and 8.0×10^4), Ethanol, DCM were all purchased from Sigma Aldrich, Dorset, UK. All reagents were of analytical grade.

4.3.2 Methods

4.3.2.1 Solution Preparation

Solutions of 1 % w/v and 5% w/v LMW (4×10^4 g/mol) and HMW PVP (1.3×10^6 g/mol) were prepared by dissolving the polymer in ethanol (50 mL). Solutions of 1 % w/v and 5% w/v LMW PCL (1.4×10^4 g/mol) and HMW PCL (8.0×10^4 g/mol) were prepared by dissolving the polymer in DCM. Table 4 summarises the eight formulations used in this study and their composition.

Table 4: Composition of polymeric solutions

Formulation	Polymer	Polymer Molecular Weight (g/mol)	Concentration (% w/v)
F1	PVP	4.0×10^4	1%
F2	PVP	4.0×10^4	5%
F3	PVP	1.3×10^6	1%
F4	PVP	1.3×10^6	5%
F5	PCL	1.4×10^4	1%
F6	PCL	1.4×10^4	5%
F7	PCL	8.0×10^4	1%
F8	PCL	8.0×10^4	5%

4.3.2.2 Physical characterisation of polymeric solutions

Physical properties (viscosity, surface tension, electrical conductivity and density) of the solutions were examined. Each parameter was tested in triplicate and an average with standard deviation was then calculated. These methods were carried out as outlined in section 3.2.1.1, 3.2.1.2, 3.2.1.3 and 3.2.1.4.

4.3.2.3 EHDA Set-up

Figure 23 shows the EHDA setup, and the method was carried out as outlined in 3.2.2.

4.3.2.4 EHDA Spraying modes and jetting maps

To assess the various spraying modes, a 5 mL syringe containing solution was electrosprayed or electrospun at varying voltages (5-15 kV) and flow rates (1-100 µL/min) digital images were then taken when different jet formations was observed using a Samsung NX2000 camera (Setup shown in figure 23). At each flow rate the voltage that produced a stable jet, unstable jet, and dripping mode were observed and recorded. These values were used to construct jetting maps enabling the identification of the optimum flow rate and voltage range to be identified for each formulation.

4.3.2.5 Imaging

Solutions containing different concentrations and molecular weights of polymer were atomised at varying flow rates and voltages to assess the morphology and characteristics of the resultant structures. SEM micrographs were taken for these. This was carried according to the method listed in section 3.2.3.

4.4 Results and Discussion

4.4.1 Solution Characterisation

4.4.1.1 Viscosity

It has been well documented that the formation of a stable cone jet is dependent upon the balance of various factors including ST, liquid pressure, EC, density and viscosity. The viscosity heavily dictates whether Es or Esp will occur. With higher viscosity readings the structures produced in EHDA will be larger. High viscosity of a LMW polymer solution in which particles are expected can actually result in larger structures or potentially fibres being formed as the Taylor cone jet transforms into multi-jet. Liquid flow rate affects the ability to form a stable cone jet with low viscosity liquids (Wang, Zhentao, Wang et al. 2020).

As the viscosity of the solution increases, the surface tension decreases as represented in Figure 30 A and B which shown the Esp of PCL (Faraji, Sadri et al. 2017) and further confirmed by Abel 2019 (Bongiovanni Abel, Liverani et al. 2019). A similar trend can be seen with PVP. DCM has shown compatibility with PCL carriers in studies conducted by Xie et al. in 2015 (Xie, Jiang et al. 2015). DCM has a low viscosity of 0.44 µS/cm and low density of 0.166 g/mL (Figure 30 B) and hence has a very insignificant impact on the overall viscosity of the solution.

The formation of fibres is often seen because when the molecular weight of the polymer increased so did the viscosity (Husain, Lau et al. 2016). This is also to be expected as molecular weight reflects the entanglement of the polymer chains and a higher molecular weight meaning the chains are more rigid and held more tightly together so the viscosity will be much higher compared to lower molecular weight polymers (Ghorani, Tucker 2015). Therefore fibres can be expected with F3,F4,F7 and F8.
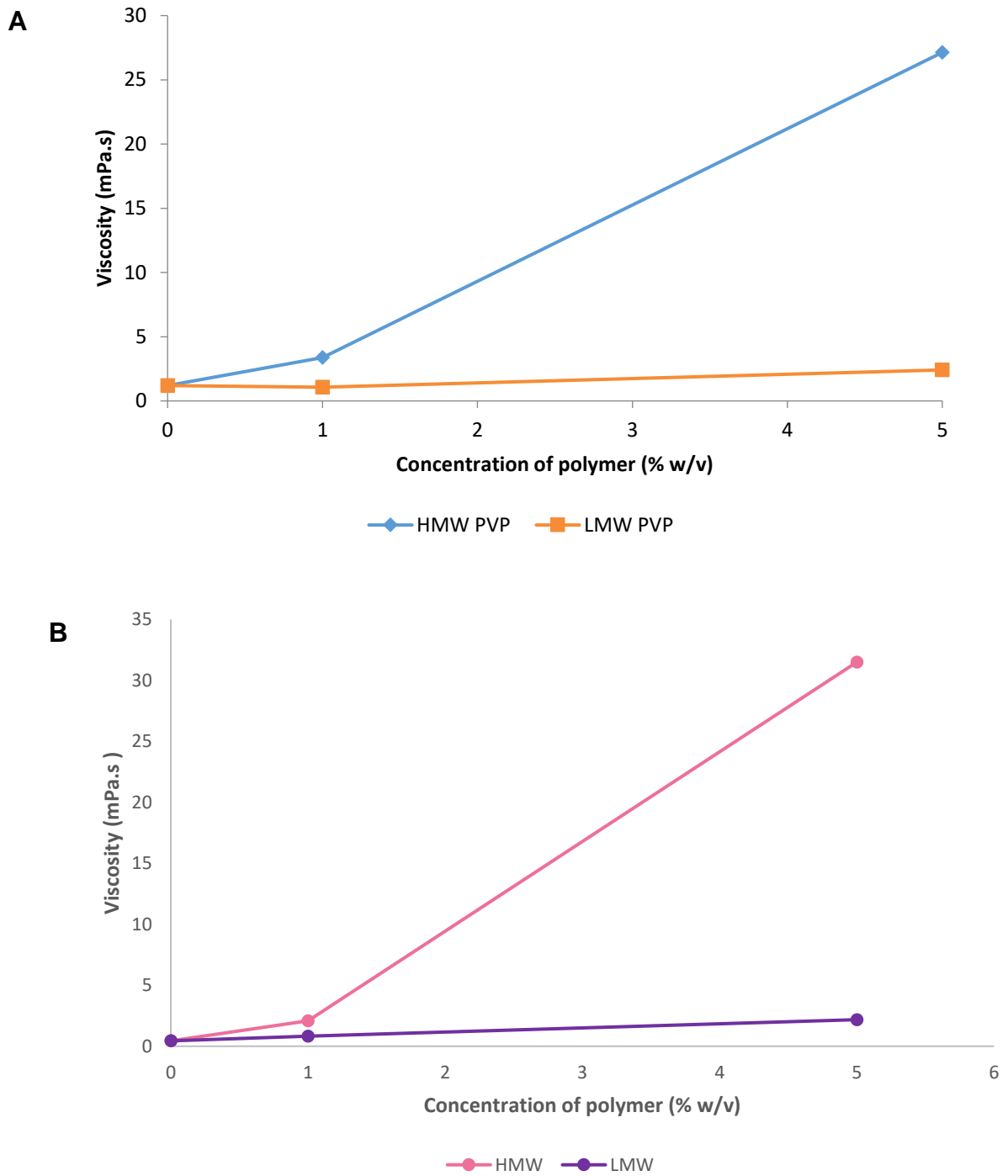
Figure 30: Average viscosity of (A) F1-F4 (PVP), (B) F5-F8 (PCL)

4.4.1.2 Surface Tension

.

Surface tension of a polymeric solution is also another important factor that influences the EHDA process. EHDA is only able to occur when the electric stress is able to overcome the surface tension to form a stable cone jet (Xie, Jiang et al. 2015). This charge repulsion is the rationale for the particle breakdown into nano-sized particles, as the liquid is ejected from the capillary needle and accumulated on the collection plate (Husain, Lau et al. 2016). The surface tension must be lower than 50 mN/m for a liquid to be atomised under the influence of electrical field. The electrical stress must overcome the surface tension to achieve a stable cone-jet (Wang, Zhentao, Wang et al. 2020). As the surface tension was below this value for all PVP formulations (displayed in figure 31A with F2) which shows the highest surface tension reading at 0.015 N/m. Therefore, ethanol is deemed a good solvent and these results show that it is suitable for EHDA. These findings are supported by Khan et al whereby similar results for PVP and ethanol were found (Khan, Mehta et al. 2014).

However, with the PCL formulations with DCM as the solvent F5, F6 and F8 (shown in figure 31B) exhibited lower surface tension values however F7 had a surface tension value of 0.057 N/m. It can be assumed that F7 (the higher molecular weight PCL solution at 1%) will be problematic during the spraying process and form beads. Low surface tension values are preferred for stable Es and Esp as this parameter can compete with electrical conductivity. DCM is considered more volatile, rapid solvent evaporation rate which means there is less time for the polymer chains to rearrange themselves so this could also explain any potential deformities (Bock, Dargaville et al. 2012).
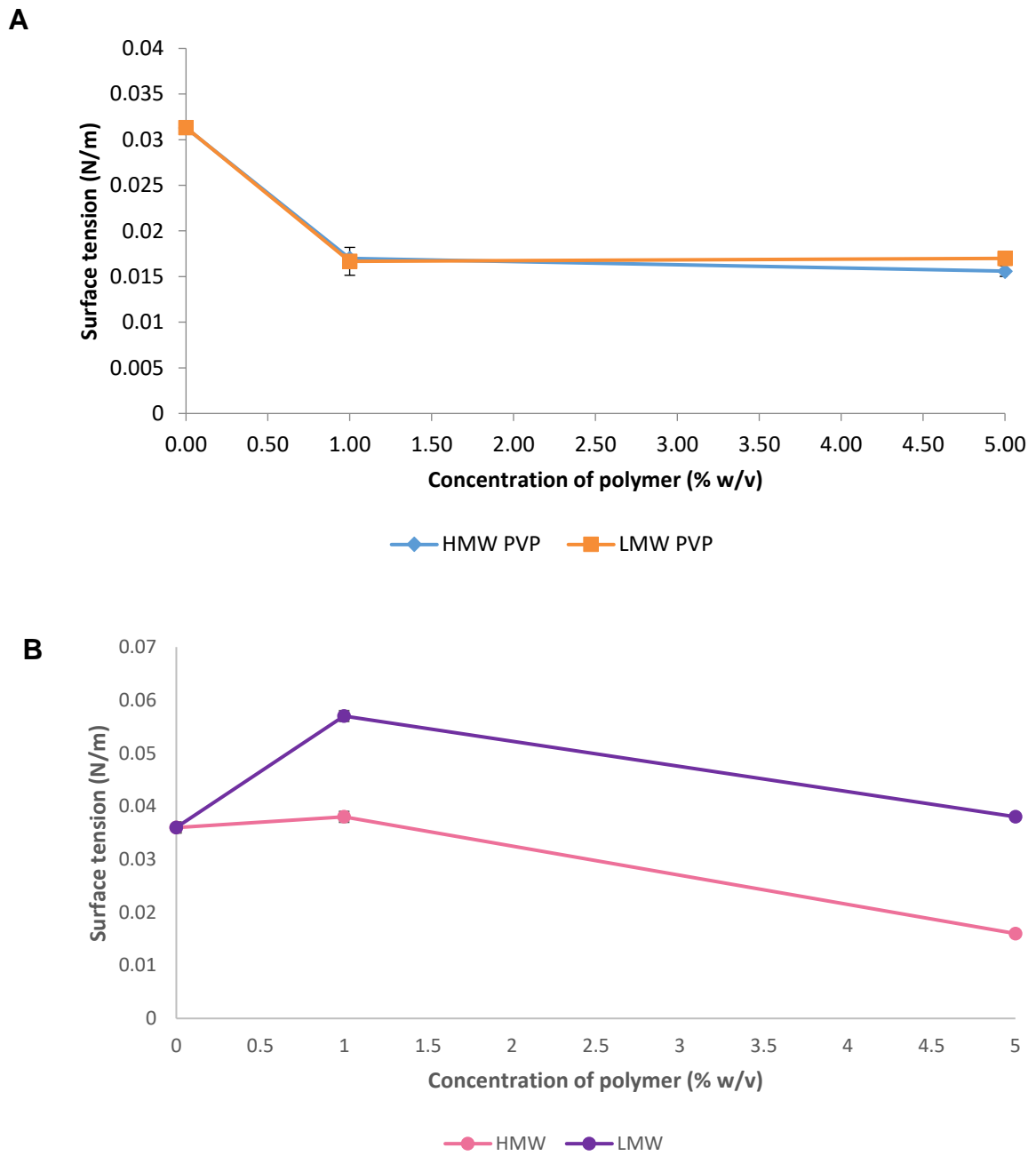
A

B

Figure 31: Average surface tension (A) F1-F4 (PVP), (B) F5-F8 (PCL)

4.4.1.3 Electro-conductivity

As can be seen in Figure 32A, the general trend for both high and low molecular weight PVP is that as the concentration of the polymer increases so does the recorded electrical conductivity. The results for electrical conductivity HMW PVP at both 1% and 5% w/v were all very similar and fell into a very narrow range. For example, for the 1% w/v (solution the recorded electrical conductivity was at 3.01 µs/cm respectively. Similarly, a narrow-recorded range was also seen for the 5% w/v solution at 2.94 µS/cm.

Faraji et als study, found that the overall stability of the Es process is dependent on the electrical conductivity of a sample to a certain extent (Faraji, Sadri et al. 2017). It is also believed that an increase in conductivity leads to smaller droplet sizes which occur because during the process there is more of a charge in the liquid solution. Figure 32B shows that 1% w/v 1.4×10^3 g/mol- PCL acquires the highest conductivity value at 7.85 µS/cm and 5% w/v 8×10^3 g/mol-PCL with the lowest conductivity value at 6.69 µS/cm. It is believed that with an increase in EC would reduce fibre diameter. Alternatively, low EC values elongate the jet leading to non-uniform fibres (Bhardwaj, Kundu 2010).

Similarly, to the electrical conductivity results although error bars were added to the graph they do not show because the standard deviation was far too low. For example it was at ±0.0058 and ±0.0153 for 1% w/v of LMW and HMW PVP respectively.

A
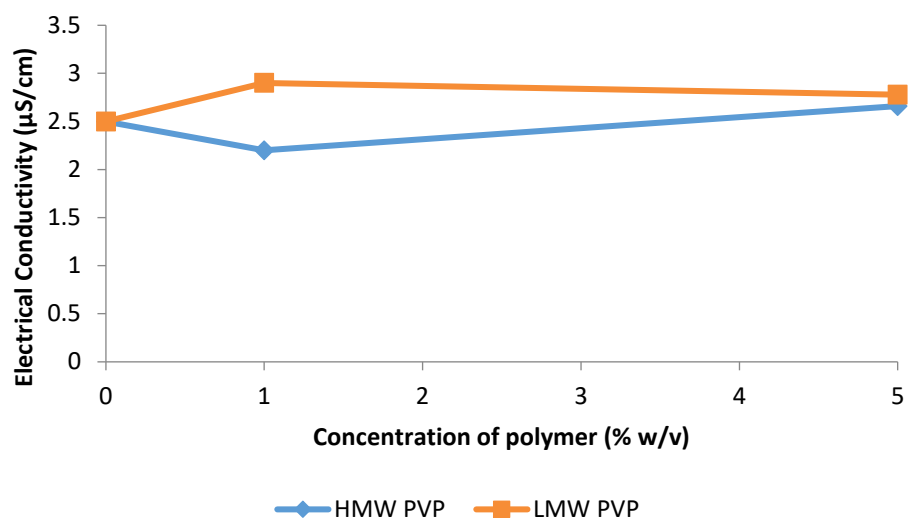
B
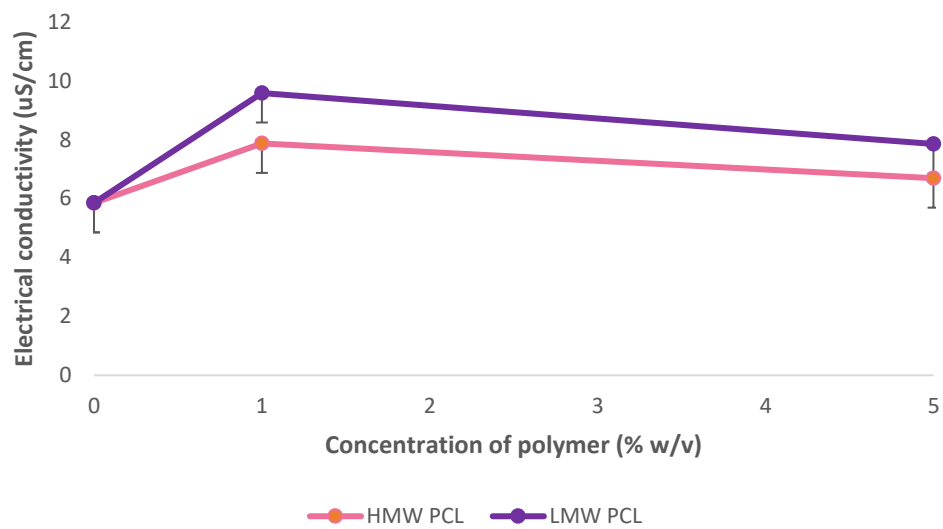
Figure 32: Average Electrical conductivity (A) F1-F4 (PVP) (B) F5-F8 (PCL)

4.4.1.4 Density

Similarly, to the trend observed in the Figure 33A and B as the concentration of both the high and low molecular weight polymers increased so did the density. For HMW PVP at 1% w/v a reading of 0.789 g/ml was found compared to 0.797 g/ml for HMW PVP at 5% w/v. This was seen with both polymers which is confirmed by the data from PCL whereby HMW PCL at 1% w/v 1.270 g/ml and at 5% w/v the value was 1.66 g/ml.

The density of polymer solutions is another important factor that can influence the EHDA process as it dictates whether particles or fibres are going to be produced (Bock, Dargaville et al. 2012). The critical polymer concentration (C_{ov}) has been heavily researched and been found that it can influence the formation of particles. The critical concentration of each polymeric solution can be found; this is when the polymer chain begins to overlap and entangle. In order to produce particles, a low entanglement density is required (Xie, Jiang et al. 2015). Density has been considered to have a limited effect, on the formation of a cone jet in most Es cases. It can however heavily influence the way in which the jet breaks up. This can have a major impact in with the transitioning from varicose to kink instability in cone jet mode (Wang, Qisi, Wang et al. 2021).

A

B
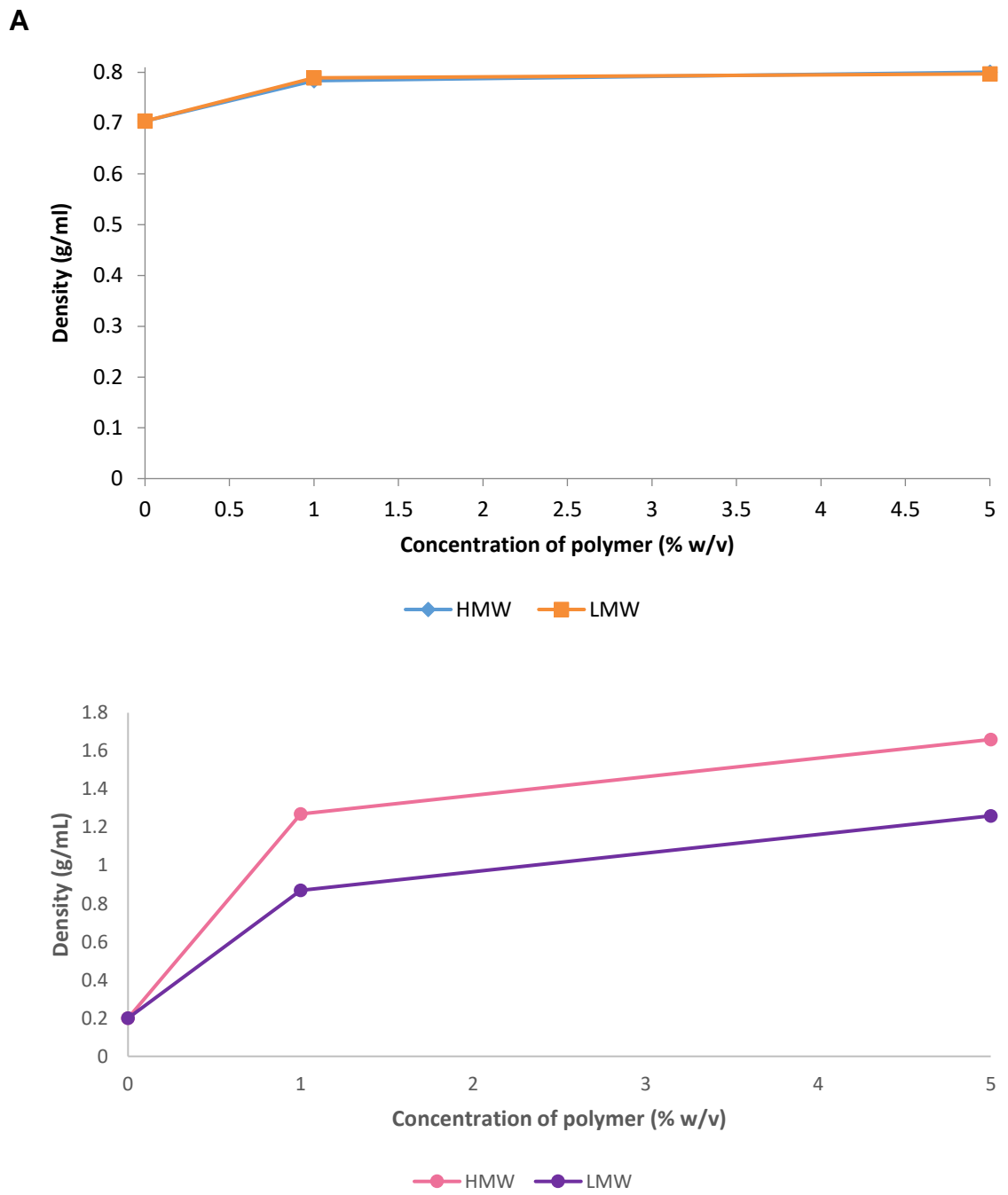
Figure 33: Average Density (A) F1-F4 (PVP) (B) F5-F8 (PCL)

4.5 Optimising the EHDA process

4.5.1 Jetting modes

The emission of a liquid formulation as it exits a stainless-steel needle is described as a jet in EHDA. The way in which the liquid breaks up will determine the EHD spraying mode (Wang, D., Rocks et al. 2012). Initially all liquid droplets eject from the capillary tip which is also referred to as dripping mode, here the liquid breaks up into smaller droplets which leads to poly-dispersed atomised structures (Wang, Zhentao, Li et al. 2019). Upon exposure to an externally applied electric field, the electrostatic forces allow the liquid to stabilise as it infuses through the needle. This revolutionary work was first investigated by Zeleny in 1914. There are various spraying modes identified including dripping, micro-dripping, spindle, cone-jet-multi jet which are displayed in Figure 34. These modes are observed according to the geometrical forms of liquid emitted from the capillary nozzle and the jetting behaviour in its disintegration into drops (Bock, Dargaville et al. 2012, Faraji, Sadri et al. 2017).

Rayleigh first documented the stability of an electrically charged drop. Further work investigated the correlation between the electric stress and surface tension of the liquid (Zhao, Y., Yao 2017). The electro-spraying phenomena is a complex engineering system highly influenced by various process parameters such as the physical properties of the liquid formulation, electrode, nozzle configurations, pressure and the surrounding media (Mehta, Prina, Haj-Ahmad et al. 2017).

Table 5: Summary of the various jetting modes

	Dripping		Jet
Dripping	Regular large droplets.	**Cone jet**	A smooth and stable cone jet breaks up into finer uniform droplets.
Micro-dripping	Production of fine droplets with a narrow size distribution and low frequency, generally occurs at low liquid flow rates.	**Precession**	The liquid jet rotates around the capillary axis
Spindle	Elongated spindles occur at high flow rates with increased electrical forces.	**Oscillating**	Liquid jet oscillates in its own plane with a lashing motion.
Multi-spindle	Occurs at higher flow rates and high voltages which produces multiple spindles	**Multi-jet**	A few fine jets form on the circumference of the capillary exit.

Research suggests the most typical spraying modes include dripping, spindle, cone-jet, multi-jet modes depending on the geometrical form of the liquid drop formed at the meniscus/jet at the outlet of the capillary (Naderi, Shams et al. 2019). Other modes of spraying recorded are summarised Table 5 which include micro-dripping, multi-spindle, ramified meniscus, oscillating jet and precession have been observed similarly with a single capillary but dependent upon the liquid and process parameters.

Amongst the aforementioned spraying modes, the Taylor cone-jet mode (shown in Figure 34F) has been the most interesting and heavily investigated and widely used spraying mode in industrial applications including surface coating and E-jet 3D printing (Wang, Wang et al. 2021). The ability to produce monodisperse particles in the nano size range has gained considerable attention. The potential application of such structures in the pharma industry is massive in particular drug delivery.
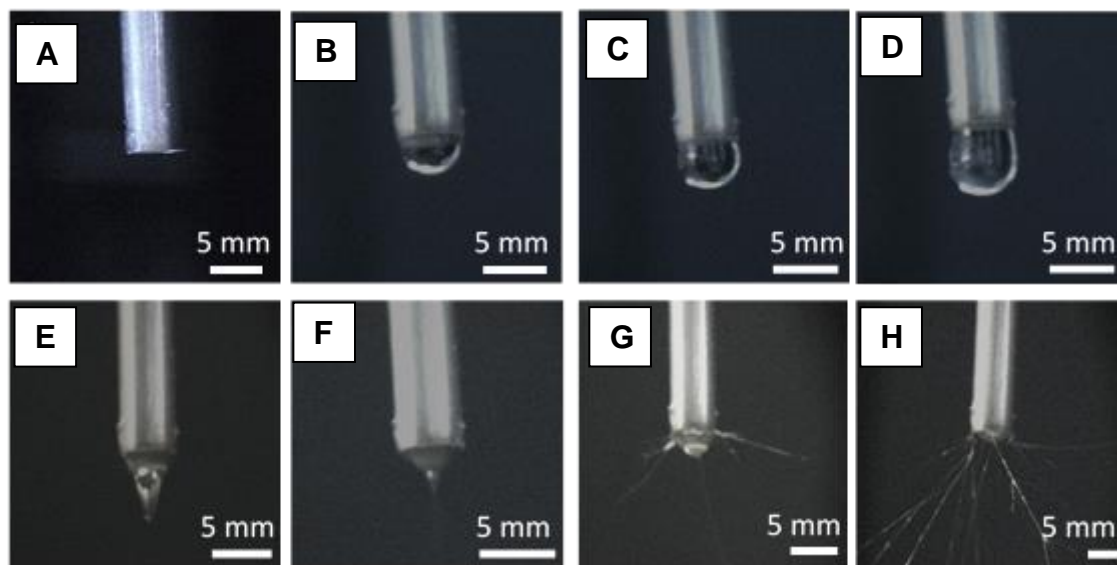
Figure 34: Jetting images using a high-resolution camera and single needle for different jetting modes (A) No flow, (B) Dripping mode, (C) Micro-dripping, (D) Rapid Dripping, (E) Unstable Cone Jet, (F) Stable Cone jet, (G) Unstable Multi-Jet and (H) Multi Jet

4.5.2 Jetting maps

The jetting maps produced in figure 35 display the range of flow rates with the corresponding applied voltage required for various jetting modes. When the flow rate is too slow/fast and the voltage is extremely low/high (depending on the formulation) in most cases dripping mode occurs. This is due to insufficient electrical force being applied which can't overcome the surface tension of liquid so it cannot break up and form a stable cone jet. Almost all jetting maps showed a wide range whereby a stable jet could form. F1 and F2 being the lower molecular weight PVP showed a significant difference with regards to the

unstable jetting regions. F1 consisted of a lower concentration so Es occurred and its visible there is a much higher unstable region compared to F2 (5%). This trend is very similar to that found with the lower molecular weight PCL samples F5 and F6 whereby F5 exhibited a larger unstable region to F6. This is owed to difficulty in obtaining a stable taylor cone jet. These finding are supported by literature whereby increased flow rate and high voltages tend to result in an unstable jet. This is due to the solvent not having enough time to evaporate when the flow rate is too high. This could also lead to the morphology of particles produced being more deformed (Xie, Jiang et al. 2015).

The higher molecular weight PVP jetting maps shown in figure 35 F3 and F4 showed slightly smaller stable jetting regions as with fibre formation it tends to produce better fibres at a lower flow rate and less applied voltage (Bhardwaj, Kundu 2010). At 10 µl/min with an applied voltage of 15 kV all 8 formulations could form a stable cone jet/multi-jet. The working distance for all these formulations were kept the same (15 cm) to avoid any bias and a further variable impacting the study. These maps provide a valuable operating window and guide for Es and Esp such formulations and could prove useful for further applications and optimising the process. The final flow rates and applied voltages selected for F1, F2, F3 and F4 were 10 µl/min and 10 kV, for F5, F6, F7 and F8 it was 50 µl/min and 15 kV. The deposition distance for all samples was kept at 15 cm.

F1

F2

F3

F4

124

F5

Applied voltage (kV)

SAFETY THRESHOLD

stable jetting

unstable jetting

dripping mode

Flow Rate (µl/min)

F6

Applied voltage (kV)

SAFETY THRESHOLD

Stable jetting

Unstable jetting

Dripping mode

Flow Rate (µl/min)
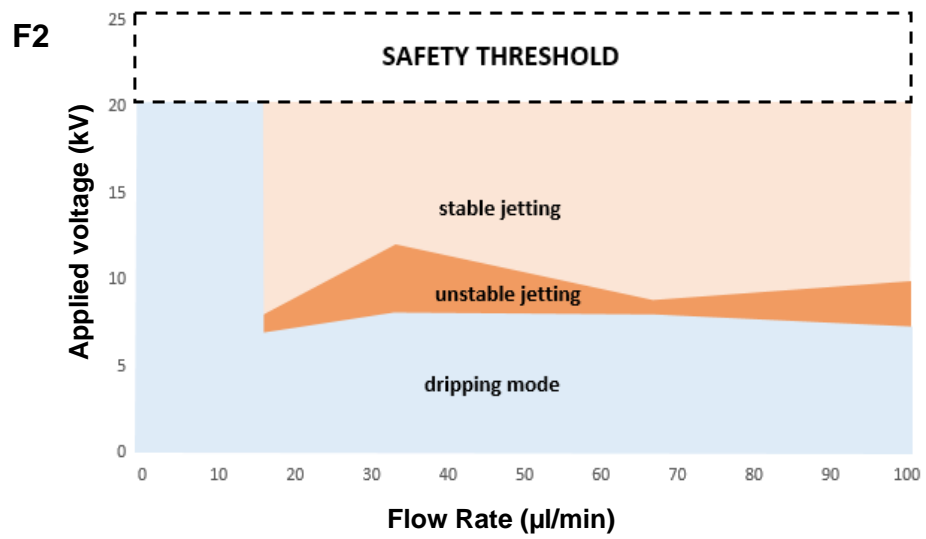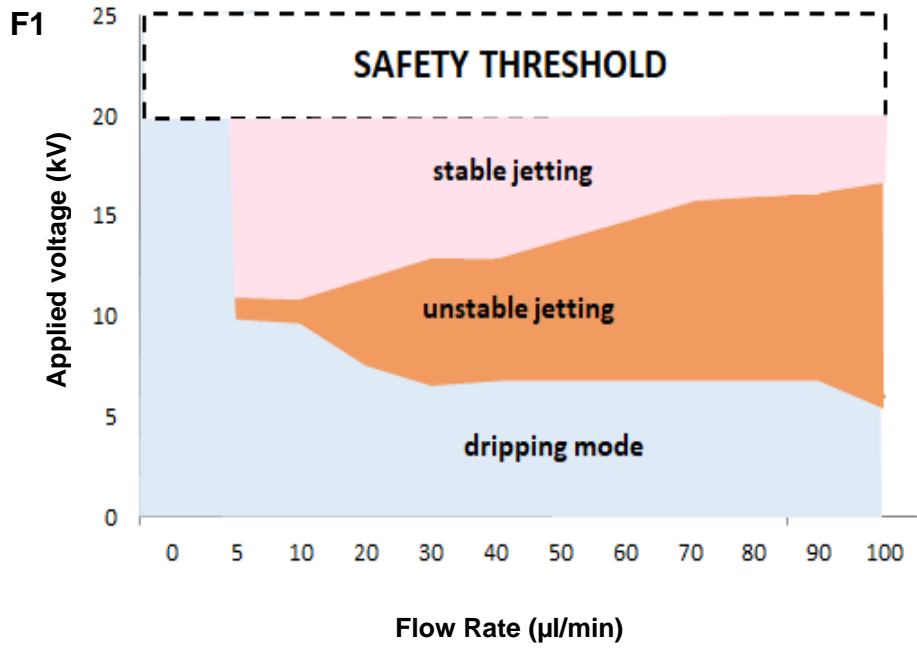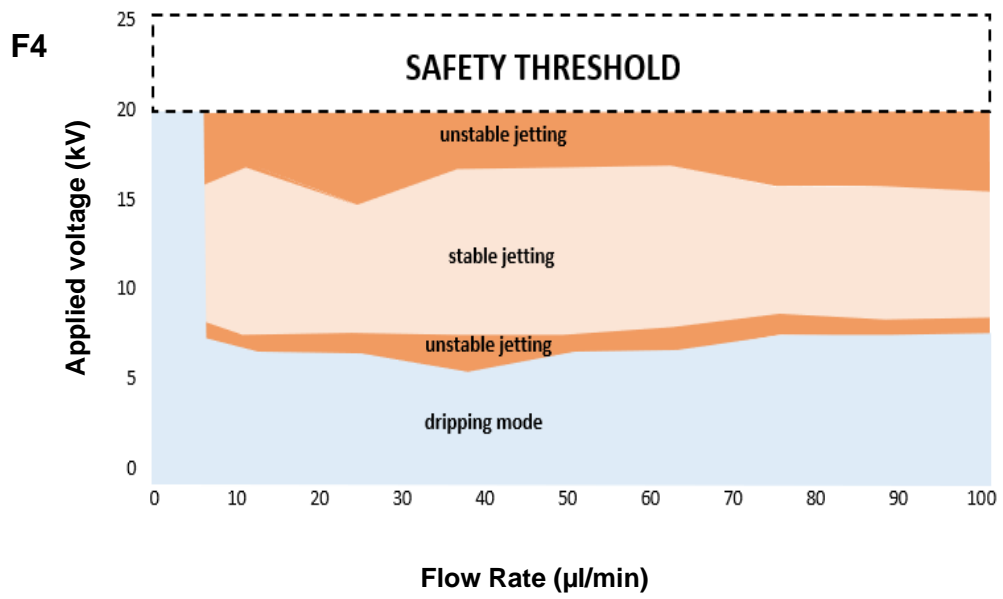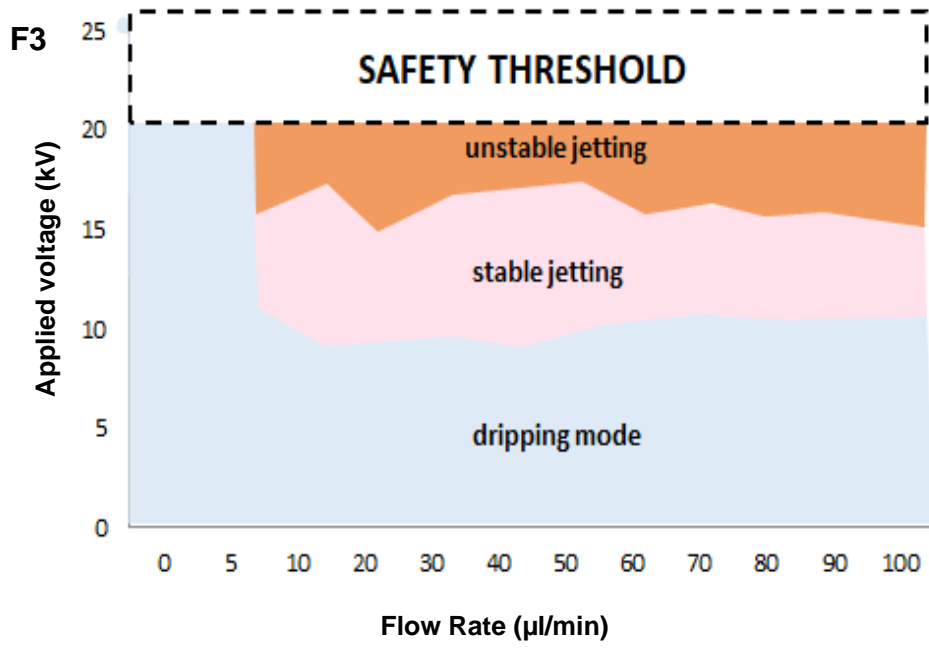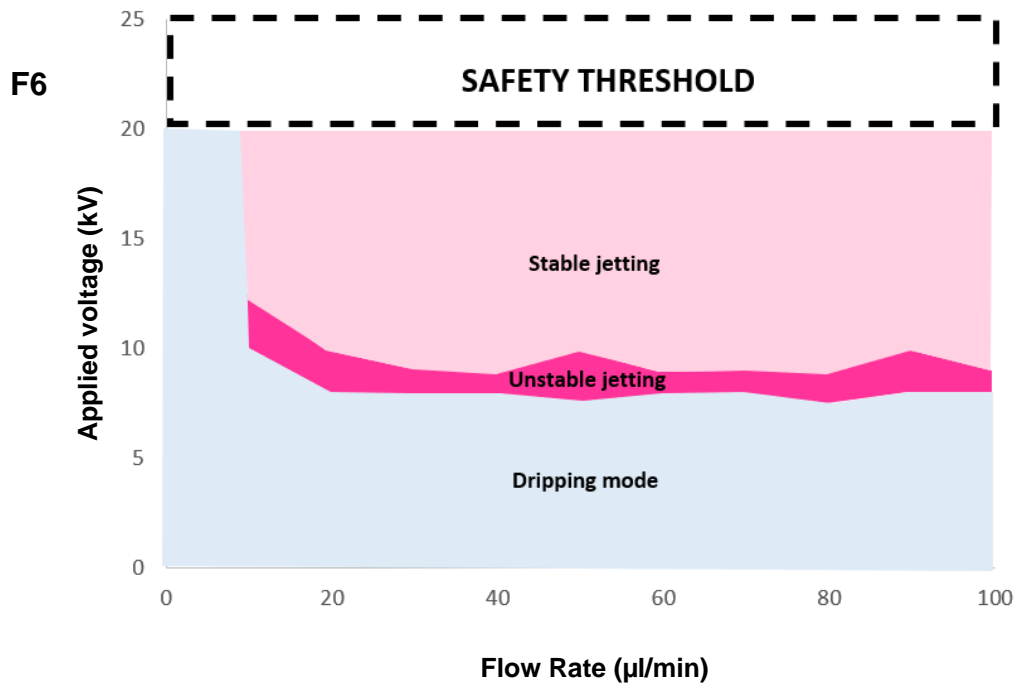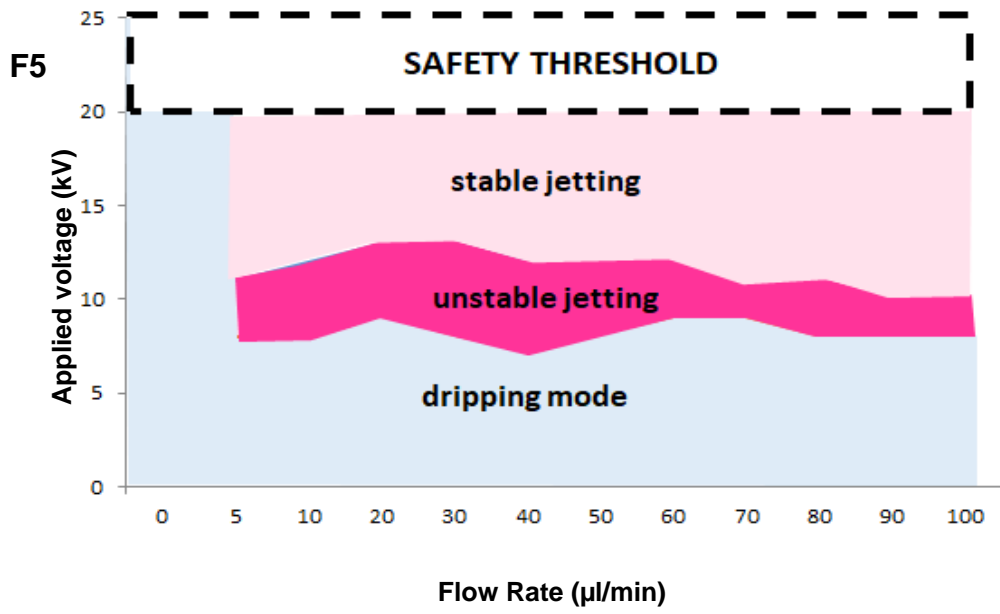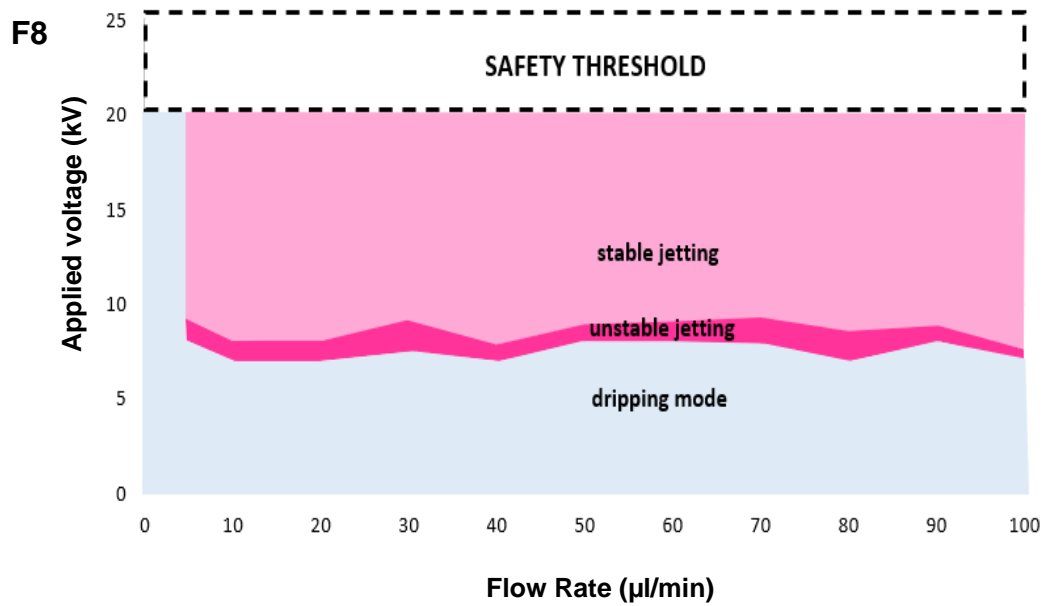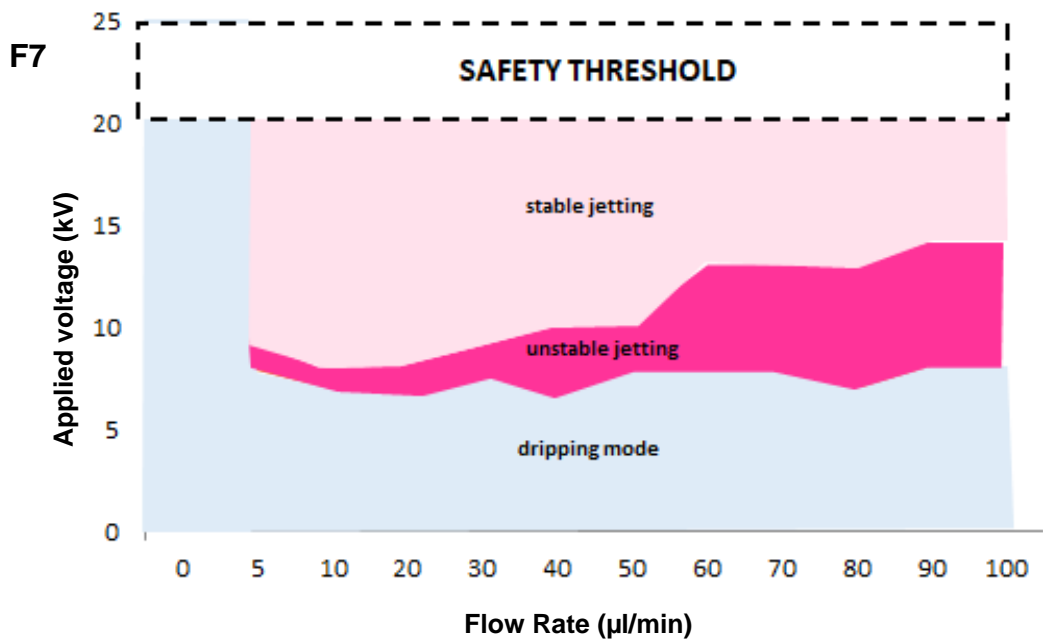
Figure 35: Jetting maps to determine the relationship between flow rate and voltage for formulations F1-F8

4.5.3 Coating characterisation

4.5.3.1 Imaging

SEM micrographs show that for F1 and F2 (Figure 36A and B) at high and low concentrations but at a LMW of PVP show that there are small spherical PVP particles within the nano range at a concentration. F5 and F6 micrographs (Figure 36E and F) show particles also at a lower molecular weight. These particles appear mostly spherical with some tails and some agglomeration. This deformity could be due to rapid solvent evaporation of dichloromethane (highly volatile) which reduces the time polymers have to re-arrange within the droplet as it solidifies (Xie, Jiang et al. 2015, Pawar, Thakkar et al. 2018).

The fibres depicted in figure 36D and H are the higher molecular weight and higher concentrations of PVP and PCL which exhibit larger uniform fibres as literature suggests due to the increase in viscosity. The higher molecular weight also has a large impact on chain entanglement (Bhardwaj, Kundu 2010).
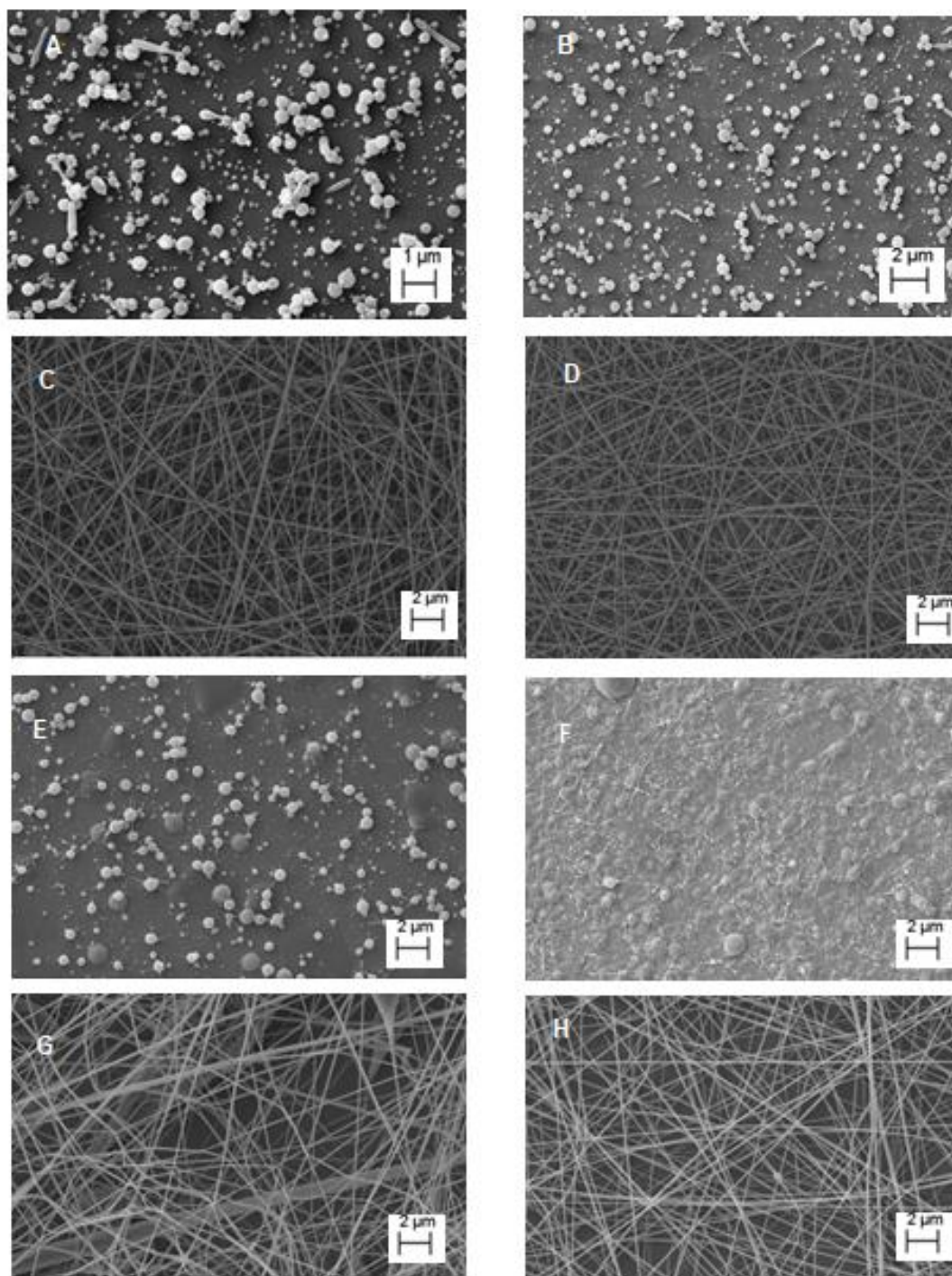
Figure 36: SEM micrographs of formulations (A-H) (F1-F8)

4.5.3.2 Size and size distribution

The demand for nano and micron scaled particles and fibres have increased greatly in pharmaceutics. The ability to manipulate and optimise such structures has gained significant interest. Nano sized particles have received much attention due to their small size, increased loading ability as carriers due to the high surface area to volume ratio leading to enhanced drug delivery. SmartTiff software along with SEM was used to collate particle and fibre size distribution. Figure 37A and B displays the size distribution of all 8 solutions. The data shows again that the particles are negatively skewed with more than 57% of particles being under 500 nm with a similar trend showed with fibres with the majority of fibres in the micron size range with more than 42% being under 0.5 µm.

The average diameter for the particles F1,F2,F5,F6 were 0.69± 0.0321, 0.63 ± 0.0251, 0.52 ± 0.0231, 0.59 ± 0.0152 µm respectively. There was a larger amount of PCL particles which some seemed to have agglomerated. This could be due to rapid solvent evaporation and insufficient evaporation time. In comparison the PVP particles appear more spherical and there was a higher proportion under 500 nm.

The average diameter for the fibres F3,F4,F7,F8 were 7.58 ± 0.0624, 5.17 ± 0.0557, 9.87 ± 0.0251, 6.13 ± 0.0208 µm respectively. Similarly, to the trend observed with particles PCL fibres exhibited more beading than the PVP fibres which could explain the slightly larger sizes and the differences in size distribution. F7 is a lower concentration of the higher molecular weight polymer showing more irregular fibres with more beading which can be due to unstable multi-jet being formed during the Esp process. F8 which had a higher concentration of polymer and so smaller sizes and more smooth fibres.

A
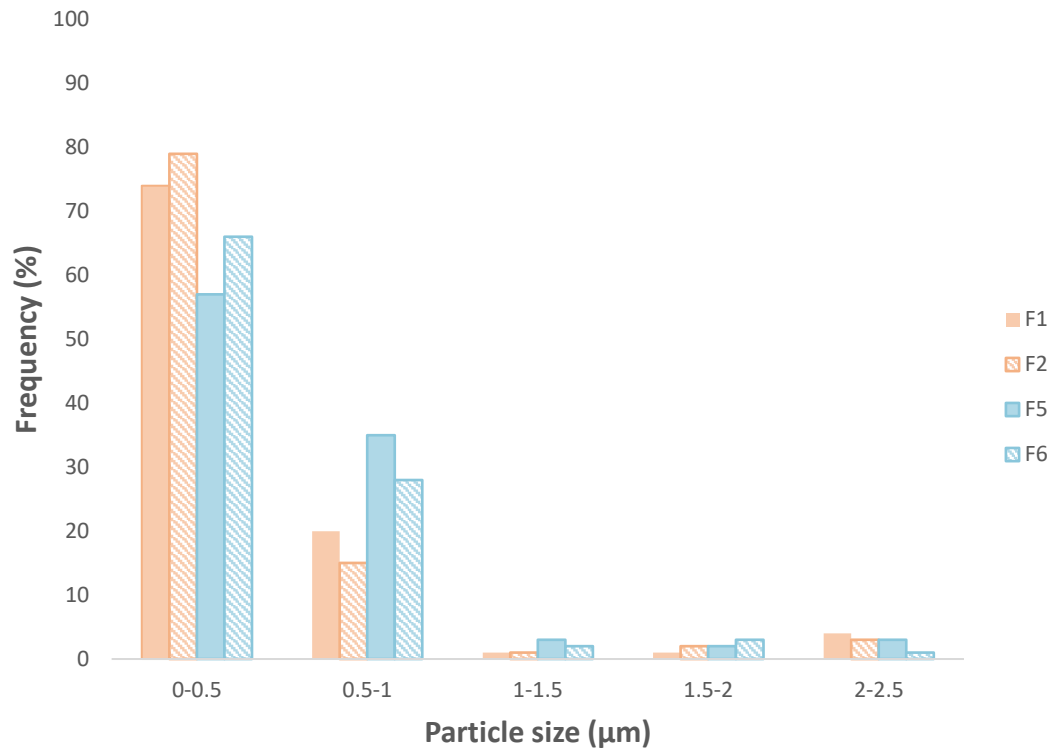
B
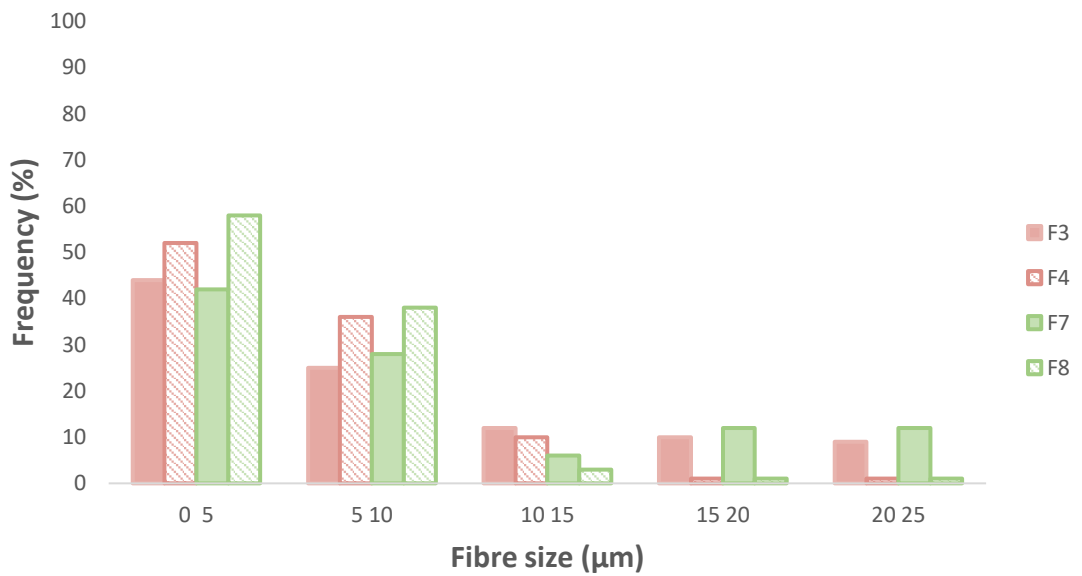
Figure 37 Size distribution (A) particles (F1,F2,F5,F6), (B) fibres (F3,F4,F7,F8)

4.6 Conclusion

This study investigated the effects of different solution properties on the EHDA process. The solutions were physically characterised and assessed to examine their suitability for EHDA. The results suggested that lower concentrations of LMW polymeric formulations would result in Es and higher concentration HMW polymeric formulations would result in Esp which was confirmed with SEM. From the results EC, ST and viscosity play a major role in cone jet stability during Es and so smaller size particles potentially being formed. The various jetting modes of EHDA were also established these included digital images which provided a better insight into the Es and Esp process. It also helped to identify the most suitable spraying mode and determining what jet was stable resulting in structures with better morphology. This also allowed for the construction of jetting maps. These maps distinguish various regions of which stable jetting should be achieved.

The resultant electrosprayed or electrospun particular and fibrous structures were assessed and characterised. Morphological studies exhibited primarily smooth PVP fibres (F3 and F4) with some beaded fibres with the PCL (F7 and F8) formulation and spherical particles with the PVP formulations (F1 and F2 compared to F5 and F6).

Although the solutions were adequately characterised, and jetting maps provided a good indicator with regards to which flow rate to use there were still issues with the structures produced (evident in SEM pictures) which shows that further optimisation is needed. The application of QBD can add significant value via optimisation of formulations with regards to the EHDA process and ensuring that the resultant structures are of the desired size and morphology. Thermal analysis and spectroscopic techniques can also provide valuable information.

4.7 References

AHMED SAEED AL-JAPAIRAI, K., MAHMOOD, S., HAMED ALMURISI, S., REDDY VENUGOPAL, J., REBHI HILLES, A., AZMANA, M. and RAMAN, S., 2020. Current trends in polymer microneedle for transdermal drug delivery. *International journal of pharmaceutics,* 587, pp. 119673.

BHARDWAJ, N. and KUNDU, S.C., 2010. Electrospinning: A fascinating fiber fabrication technique. *Biotechnology Advances,* 28(3), pp. 325-347.

BOCK, N., DARGAVILLE, T.R. and WOODRUFF, M.A., 2012. Electrospraying of polymers with therapeutic molecules: State of the art. *Progress in Polymer Science,* 37(11), pp. 1510-1551.

BONGIOVANNI ABEL, S., LIVERANI, L., BOCCACCINI, A.R. and ABRAHAM, G.A., 2019. Effect of benign solvents composition on poly(ε-caprolactone) electrospun fiber properties. *Materials Letters,* 245, pp. 86-89.

CHEN, Y., QUAN, P., LIU, X., WANG, M. and FANG, L., 2014. Novel chemical permeation enhancers for transdermal drug delivery. *Asian Journal of Pharmaceutical Sciences,* 9(2), pp. 51-64.

DAVOODI, P., FENG, F., XU, Q., YAN, W., TONG, Y.W., SRINIVASAN, M.P., SHARMA, V.K. and WANG, C., 2015. Coaxial electrohydrodynamic atomization: Microparticles for drug delivery applications. *Journal of Controlled Release,* 205, pp. 70-82.

FARAJI, S., SADRI, B., VAJDI HOKMABAD, B., JADIDOLESLAM, N. and ESMAEILZADEH, E., 2017. Experimental study on the role of electrical conductivity in pulsating modes of electrospraying. *Experimental Thermal and Fluid Science,* 81, pp. 327-335.

GHORANI, B. and TUCKER, N., 2015. Fundamentals of electrospinning as a novel delivery vehicle for bioactive compounds in food nanotechnology. *Food Hydrocolloids,* 51, pp. 227-240.

HUSAIN, O., LAU, W., EDIRISINGHE, M. and PARHIZKAR, M., 2016. Investigating the particle to fibre transition threshold during electrohydrodynamic atomization of a polymer solution. *Materials Science and Engineering: C,* 65, pp. 240-250.

KHAN, H., MEHTA, P., MSALLAM, H., ARMITAGE, D. and AHMAD, Z., 2014. Smart microneedle coatings for controlled delivery and biomedical analysis. *Journal of drug targeting,* 22(9), pp. 790-795.

LEE, J.W., GADIRAJU, P., PARK, J., ALLEN, M.G. and PRAUSNITZ, M.R., 2011. Microsecond thermal ablation of skin for transdermal drug delivery. *Journal of Controlled Release,* 154(1), pp. 58-68.

MA, G. and WU, C., 2017. Microneedle, bio-microneedle and bio-inspired microneedle: A review. *Journal of Controlled Release,* 251, pp. 11-23.

MALINOVSKAJA-GOMEZ, K., ESPUELAS, S., GARRIDO, M.J., HIRVONEN, J. and LAAKSONEN, T., 2017. Comparison of liposomal drug formulations for transdermal iontophoretic drug delivery. *European Journal of Pharmaceutical Sciences,* 106, pp. 294-301.

MEHTA, P., HAJ-AHMAD, R., RASEKH, M., ARSHAD, M.S., SMITH, A., VAN DER MERWE, S.M., LI, X., CHANG, M. and AHMAD, Z., 2017. Pharmaceutical and biomaterial engineering via electrohydrodynamic atomization technologies. *Drug Discovery Today,* 22(1), pp. 157-165.

NADERI, P., SHAMS, M. and GHASSEMI, H., 2019. Investigation on the onset voltage and stability island of electrospray in the cone-jet mode using curved counter electrode. *Journal of Electrostatics,* 98, pp. 1-10.

OUYANG, Q., FENG, X., KUANG, S., PANWAR, N., SONG, P., YANG, C., YANG, G., HEMU, X., ZHANG, G., YOON, H.S., TAM, J.P., LIEDBERG, B., ZHU, G., YONG, K. and WANG, Z.L., 2019. Self-powered, on-demand transdermal drug delivery system driven by triboelectric nanogenerator. *Nano Energy,* 62, pp. 610-619.

PAWAR, A., THAKKAR, S. and MISRA, M., 2018. A bird's eye view of nanoparticles prepared by electrospraying: advancements in drug delivery field. *Journal of Controlled Release,* 286, pp. 179-200.

SEDGHI, R., SHAABANI, A., MOHAMMADI, Z., SAMADI, F.Y. and ISAEI, E., 2017. Biocompatible electrospinning chitosan nanofibers: A novel delivery system with superior local cancer therapy. *Carbohydrate Polymers,* 159, pp. 1-10.

SKOOG, S.A., MILLER, P.R., BOEHM, R.D., SUMANT, A.V., POLSKY, R. and NARAYAN, R.J., 2015. Nitrogen-incorporated ultrananocrystalline diamond microneedle arrays for electrochemical biosensing. *Diamond and Related Materials,* 54, pp. 39-46.

WANG, D., ROCKS, S.A. and DOREY, R.A., 2012. Electrohydrodynamic atomization deposition of PZT sol–gel slurry and sol infiltration on the films. *Journal of the European Ceramic Society,* 32(8), pp. 1651-1658.

WANG, Q., WANG, Z., YANG, S., LI, B., XU, H., YU, K. and WANG, J., 2021. Experimental study on electrohydrodynamic atomization (EHDA) in stable cone-

jet with middle viscous and low conductive liquid. *Experimental Thermal and Fluid Science,* 121, pp. 110260.

WANG, Z., LI, R., TIAN, L., XIA, L., ZHAN, S., WANG, J. and TU, J., 2019. Visualization of periodic emission of drops with micro-dripping mode in electrohydrodynamic (EHD) atomization. *Experimental Thermal and Fluid Science,* 105, pp. 307-315.

WANG, Z., WANG, Q., LI, B., ZHANG, Y., WANG, J. and TU, J., 2020. An experimental investigation on cone-jet mode in electrohydrodynamic (EHD) atomization. *Experimental Thermal and Fluid Science,* 114, pp. 110054.

XIE, J., JIANG, J., DAVOODI, P., SRINIVASAN, M.P. and WANG, C., 2015. Electrohydrodynamic atomization: A two-decade effort to produce and process micro-/nanoparticulate materials. *Chemical Engineering Science,* 125, pp. 32-57.

ZHAO, X., COULMAN, S.A., HANNA, S.J., WONG, F.S., DAYAN, C.M. and BIRCHALL, J.C., 2017. Formulation of hydrophobic peptides for skin delivery via coated microneedles. *Journal of Controlled Release,* 265, pp. 2-13.

ZHAO, Y. and YAO, J., 2017. Electrostatic characterization of electrohydrodynamic atomization process for particle fabrication. *Powder Technology,* 314, pp. 589-598.

Chapter 5 Development and optimisation of electrically atomised particular and fibrous coatings using QBD

5.1. Introduction

This chapter incorporates a systemic approach known as QBD to optimise the EHDA process and in turn generate particles and fibres within a desired range which can be used for potentially coating MNs.

5.2. Background

QBD provides an alternative approach to conventional pharmaceutical development strategies (Javed, Alam et al. 2019). It involves taking a "systematic approach to development with pre-defined objectives" focussing more on the product and processes based on science and risk management (Amasya, Aksu et al. 2019). This approach begins with the construction of a QTPP which includes and defines all requirements that the final product is expected to meet and satisfy. The information necessary for a QTPP often include the dosage form, strength, purity limits etc. QbD takes a systematic approach in pharmaceutical development by identifying the CQAs of a product and their potential interaction and impact during the manufacturing process (Ohage, Iverson et al. 2016). The majority of CQAs are often associated with the design of the drug substance and the manufacturing process. Common examples include identity, appearance, colour, content uniformity. It is from identifying the CQAs that a fitting limit/range is assigned to each to make sure that the desired product quality is achieved. With respect to nanoparticles the CQAs would include, appearance, particle size and polydispersity. The CPPs are factors which heavily impact the manufacturing

process and therefore need to be controlled and monitored throughout. The manufacturing process within this research is EHDA.

EHDA utilises an electrical field to atomise liquids for the fabrication of various structures (Rezvanpour, Krantz et al. 2012). The two main forms as researched in Itis a non- conventional solvent-based method, which depending on formulation properties can lead to as ES or ESP (Smeets, Clasen et al. 2017). The findings from chapter 4 demonstrated the occurrence of Es, with LMW weight polymers resulting in particles being formed. With HMW polymers led to Esp which led to fibres. EHDA has many applications including paint, polymers (Hwang, Kim et al. 2016), ceramics (Li, J. L. 2006), food industry (Echegoyen, Fabra et al. 2017), cosmetics (Mehta, P., Picken et al. 2019) and emerging in drug delivery.

Within the TDD remit MNs have gained much attention due to the ability to overcome the skins formidable barrier SC. Many designs exist however coated MNs have been of interest in this research. Many materials have been considered, PVP and PCL are both FDA approved synthetic biodegradable water-soluble polymers (PranavKumar Shadamarshan, Balaji et al. 2018) which have been recognised as potential matrices for drugs and successfully used encapsulating agents. Reksammunadar et al, demonstrated successful encapsulation of β-carotene (1 wt.% w/v) within a PVP (10 wt.% w/v) matrix through ESP. Antioxidant activity was exerted by the composite nanifibres (Reksamunandar, Edikresnha et al. 2017). Successful encapsulation of sumatriptan succinate in PVP DMNs was demonstrate by Ronnander et al. These MNs exhibited rapid drug release (Ronnander, Simon et al. 2018). Whilst drugs encapsulated within a PVP matrix demonstrate rapid release, MNs loaded with PCL and a drug showed a more sustained release profile. This is supported by Anderson et al whose research showed that the *in vitro* release of PCL MNs loaded with furosemide was within 18 hours at 37 °C (Andersen, Andersen et al. 2018).

This study focusses on utilising the application of QBD principles to the EHDA process for the fabrication of optimised particle and fibre structures within a

desired set range. This involved evaluation of polymeric coatings with the including of a dye acting as model drug. These formulations were atomised using a step fabrication method (EHDA) which was optimised by QBD. This also involves assessing the polymeric formulations and the resultant particular and fibrous structures followed by thermal, spectroscopic analysis, to show the interaction of the polymers and dye.

5.3 Materials and Methods

5.3.1 Materials

PVP (4 x10^4 g/mol and 1.3x10^6 g/mol) were sourced from Ashland, UK. PCL (1.4x10^4 and 8.0x10^4), Ethanol, DCM, FL and RhB dye were all purchased from Sigma Aldrich, Dorset, UK. All reagents were of analytical grade.

5.3.2 Methods

5.3.2.1 Implementation of QBD

5.3.2.1.1 Identification of quality target product profile and selection of critical quality attributes

The protocol for QbD was applied in this study and examined for dye-loaded MN coatings. In line with implementing QbD to the EHDA process a risk assessment was carried out identifying the factors that can affect the process and the chosen CQAs the foundation of QbD is based on having knowledge to exert control and better understanding of the relationship between CQAs and CPPs which are essential for QTPP. There are many types of risk assessments that can be performed within a QbD framework; examples of such assessments include cause and effect (fishbone) diagrams, PHA and FMEA. According to ICH Q8, QbD implementation begins with identifying the QTPP which outlines the quality, safety and efficacy of the product.

Table 6: QTPP for PVP-FL nanoparticles

Quality Attribute	Target	Critical (Yes/No)
Route of admistration	Transdermal	No
Dosage form	Nanoparticles to be sprayed onto staibless steel microneedles	No
Active	Positive for API (fluoroscein)	Yes
Polymeric carrier	PVP	No
Solvent	Ethanol	No
Appearance	Spherical particles	Yes
Release profile	>75% released in 4 hours	Yes
Encapsulation efficiency	>80%	Yes
Particle size	< 500 nm	Yes
Polydispersity	<0.3	Yes

Table 7: QTPP for PVP-FL nano/micro fibres

Quality Attribute	Target	Critical (Yes/No)
Route of admistration	Transdermal	No
Dosage form	Nano/micro fibres to be spun onto stainless steel microneedles	No
Active	Positive for API (fluoroscein)	Yes
Polymeric carrier	PVP	No
Solvent	Ethanol	No
Appearance	Smooth fibres	Yes
Release profile	TBD	Yes
Encapsulation efficiency	>80%	Yes
Fibre size	< 2um	Yes
Polydispersity	<0.8	Yes
Coating method	EHDA	No

139

Table 8: QTPP for PCL-RhB nanoparticles

Product Attribute	Target	Criticale (Yes/No)
Route of administration	Transdermal	No
Dosage Form	Dye loaded nanoparticles sprayed onto stainless steel MN	No
Active	Rhodamine-B dye (model drug)	Yes
Polymeric Carrier	PCL	No
Solvent	DCM	No
Appearance	Spherical particles	Yes
Release Profile	Sustained release over a minimum of 7 days	Yes
Encapsulation efficiency	> 80 %	Yes
Particle Size	1 - 500 nm	Yes
Poly-Dispersity Index	<0.3	Yes
Coating Method	EHDA process	No

Table 9: QTPP for PCL- RhB nano/micro fibres

Product Attribute	Target	Critical (Yes/No)
Route of administration	Transdermal	No
Dosage Form	Dye loaded nano/micro fibres spun onto stainless steel MN	No
Active	Rhodamine-B dye (model drug)	Yes
Polymeric Carrier	PCL	No
Solvent	DCM	No
Appearance	Smooth fibers	Yes
Release Profile	Sustained release over a minimum of 7 days	Yes
Encapsulation efficiency	> 80 %	Yes
Fibre Size	< 2um	Yes
Poly-Dispersity Index	<0.8	Yes
Coating Method	EHDA process	No

The QTPP for the four dye-loaded formulations are shown in tables 6-9. This was generated by research and literature findings. CQAs are defined as a physical, chemical, biological or microbiological property or characteristic that should be within an acceptable limit, range, or distribution to confer the desired product quality. Variability of CPPs has an impact on the CQAs thus the management and control of them are essential. Preliminary studies of solutions enable fixed concentrations being established for the solutions used in the study. EHDA has three main process parameters: the flow rate and the driving force (electric current/voltage) and deposition distance. Here, the flow rate, applied voltage and deposition distance were the parameters being investigated. The shape of particles and fibres were characterised according to Table 10 and 11 These tables were generated with literature findings (Wang, Baolin, Chen et al. 2019, Pawar, Thakkar et al. 2018, Rai, Gautam et al. 2017, Cortez Tornello, Feresin et al. 2018, Xie, Jiang et al. 2015, Khan, Mehta et al. 2014).

Using JMP software, the DOE was created for each of the polymers (PVP and PCL) to produce structures with desirable shape, size and polydispersity. This was achieved by optimising the EHDA process i.e. altering various process parameters (voltage, deposition distance and flow rate). A full factorial design was carried out which was able to generate and verify the response surface plots. These plots encompass the interactions between the formulation variables and process parameters to assure quality in the product. Working within the limits of these in theory ensures quality. With a more comprehensive design space/response surface plot, there is ample flexibility within the process parameters.

Table 10: Shape scoring table for particles

Score	Description
0	Full agglomeration, no visible particles
1	Fibres, no visible particles
2	Irregular particles with major agglomeration
3	Irregular particles with minor agglomeration
4	Irregular particles with no agglomeration
5	Spherical particles with cranes and major agglomeration
6	Spherical particles with cranes and minor agglomeration
7	Spherical particles with cranes and no agglomeration
8	Spherical particles with major agglomeration
9	Spherical particles with minor agglomeration
10	Spherical particles with no agglomeration

Table 11 Shape scoring table for fibres

Score	Description
0	Elongated particles with tails
1	Multi-layered spindle fibres
2	Spindle fibres
3	Irregular fibres with rough, uneven surfaces
4	Irregular fibres with uneven surfaces
5	Rough fibres with major beading
6	Rough fibres with minor beading
7	Rough fibres with no beading
8	Smooth fibres with major beading
9	Smooth fibres with minor beading
10	Smooth uniform fibres

Risk involves identifying and determining the probability of some form of harm occurring and establishing the potential impact of such harm. When carrying out a risk assessment (RA) potential CPP's are established, and it creates a link between the CQA's and CPP's. The risk assessments that exist within QBD include the cause and effect (fishbone diagram), preliminary hazard assessments (PHA) and failure modes and effects analysis (FMEA). The most common amongst these RA is the ishikawa diagram (Figure 38) which consists of a central problem statement which forms the backbone and main branch of the diagram and there are smaller branches derived from the central statement which identify all possible factors affecting said statement.
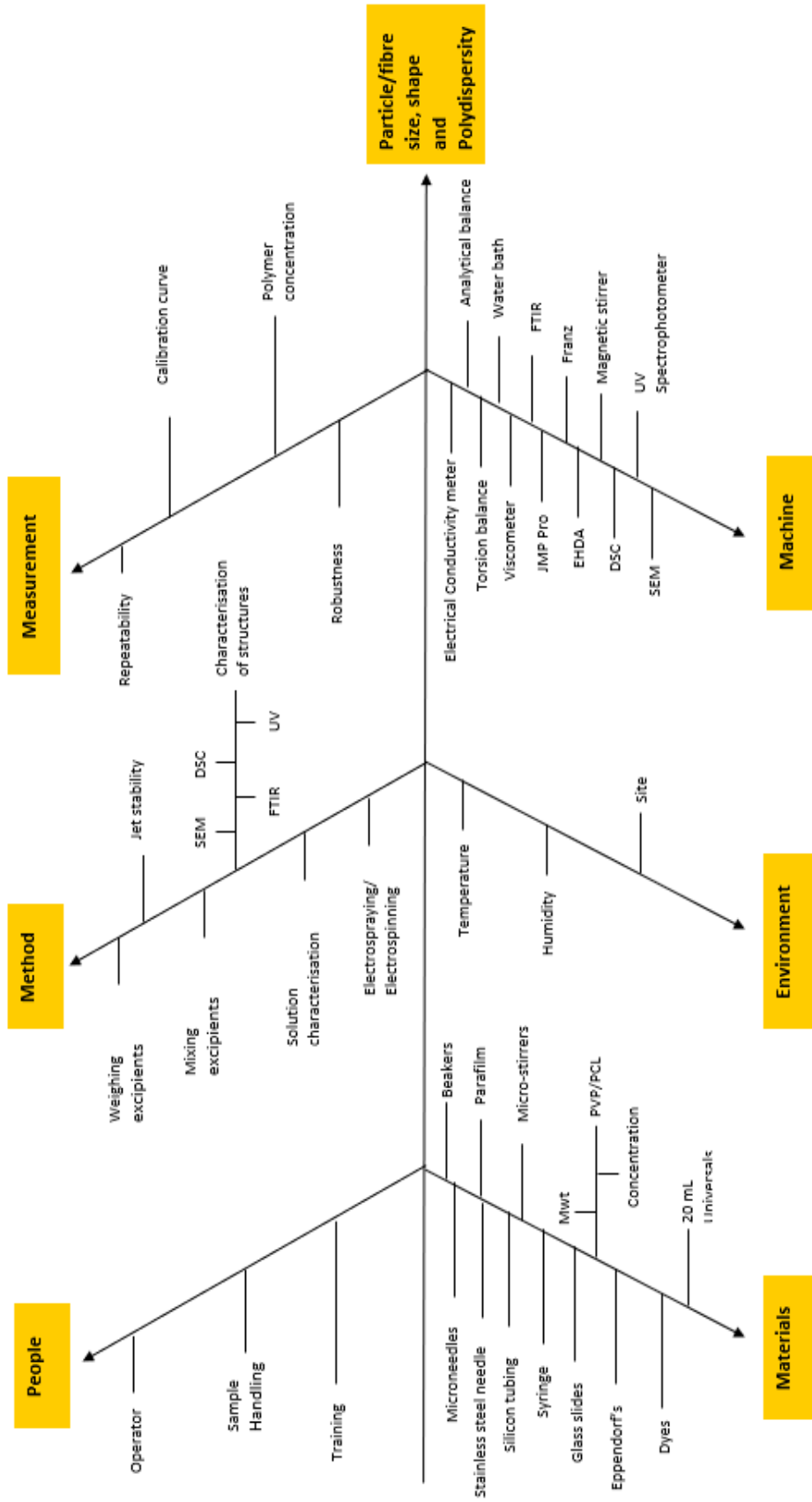
Figure 38: Ishikawa diagram for the EHDA process

144

Table 12: Preliminary traffic light assessment for EHDA process

CQA	CPPs				
	Deposition distance	Flow rate	Applied Voltage	Molecular Weight of Polymer	Drying time
Particle Size	🟥	🟥	🟥	🟥	🟧
Appearance	🟥	🟥	🟥	🟥	🟧
Polydispersity	🟧	🟩	🟧	🟩	🟩
Encapsulation efficiency	🟧	🟩	🟧	🟥	🟩

KEY:

🟩 Low risk

🟧 Medium risk

🟥 High risk

It is common practice to also perform a Preliminary Hazard Assessment (PHA) which is also known as a "traffic light" assessment (Table 12). This form of assessment is a simplistic way of being able to determine which unit operations may negatively affect the chosen CQA's. It does this by listing all the unit operations in a manufacturing process and categorising the risk as either being low or high in relation to the identified quality attributes. Table 12 represents an example of a traffic light assessment associated with the EHDA process which impacts all formulations.

The fishbone diagram and traffic light assessment summarise the effects of critical factors that may affect the final product quality. The CPPs include flow rate, applied voltage and deposition distance and molecular weight of polymer. This is also confirmed in literature and research where these parameters have been identified as critical (Wang, Baolin, Chen et al. 2019).

Following completion of risk assessments, the next stage involves the DoE approach. DoE is a large constituent of QBD. It can be described as the multi-dimensional combination and interaction of input variables. (e.g., material attributes) and process parameters that have been demonstrated to provide quality assurance. The statistical software and experimental tool allow for the optimal working conditions to be achieved. The parameters can then be manipulated and varied to establish if there is a relationship and/or effect on the process (Shekhawat, Pokharkar 2019).

5.3.2.1.3 JMP Pro Software

Prior to atomisation experiments, JMP software was used to generate the screening design DOE. As the appropriate molecular weight and concentration was selected it was no longer a factor being investigated within JMP software. A full factorial design was then carried out and the responses and factors were input into the system to optimise the process Thus, the next set of experiments were generated, carried out and the results fed back into JMP. JMP then analysed all results to statistically explore the data and to visually illustrate the findings. The predictive analytical tools (predictive profilers and response surface plot) which aid to build, enhance and develop a model to predict what will happen with new processes or new risks.

5.3.2.2 Solution Preparation

Preliminary experiments utilised solutions as described in 4.3.2.1. For the following experiments 5% w/v solutions were prepared and for dye loaded formulations a duplicate solution was made with addition of fluorescein dye at 0.05% w/w of PVP concentration. For the PCL formulations RhB dyes at 0.05% w/w of PCL concentration were made. Table 13 summarises the eight formulations used in this study and their composition.

Table 13: Formulation composition (F1-F8)

Formulation	Polymer	Polymer Molecular Weight (g/mol)	Dye
F1	PVP	4.0×10^4	--
F2	PVP	4.0×10^4	Fluorescein
F3	PVP	1.3×10^6	--
F4	PVP	1.3×10^6	Fluorescein
F5	PCL	1.4×10^4	--
F6	PCL	1.4×10^4	Rhodamine B
F7	PCL	8.0×10^4	--
F8	PCL	8.0×10^4	Rhodamine B

5.3.2.3 Physical characterisation of polymeric solutions

Physical properties (viscosity, surface tension, electrical conductivity, and density) of the solutions were examined and carried out as outlined in chapter 4.4.1. Each parameter was tested in triplicate

5.3.2.4 EHDA Set-up

A syringe containing 5 mL of formulation was secured to a syringe infusion pump (Harvard apparatus, pump 11-Elite, USA) which controlled the flow rate of polymer-drug solution. The solution then passed through silicon tubing which was connected to a stainless-steel needle device (single needle was used in this study) at various flow rates (ranging from 15-50 µL/min). This device was attached to a high-power voltage supply (Glassman High Voltage Supply, UK). The Es or Esp process carried out under ambient temperature of 23 °C.

5.3.2.5 EHDA Jetting maps

The jetting behaviour of each formulation was assessed at various voltages and flow rates as outlined in 4.3.2.5 with the addition of dyes (FL in PVP formulations and RhB in PCL formulations).

To assess the various spraying modes, a 5 mL syringe containing solution was Es or Esp at varying voltages (5-20 kV) and flow rates (1-100 µL/min) digital images were then taken when different jet formations was observed using a Samsung NX2000 camera. At each flow rate the voltage that produced a stable jet, unstable jet, and dripping mode were observed and recorded. These values were used to construct jetting maps enabling the identification of the optimum flow rate and voltage range to be identified for each formulation.

5.3.2.6 EHDA Coating application

Prior to spraying on MNs, glass microscope slides were utilised for preliminary analysis with characterisation carried out on these slides. Deposition distance, flow rate and voltage were determined by QBD and set for each polymeric formulation.

5.3.2.7 Coating characterisation

5.3.2.7.1 Imaging and Size Distribution

Prior to coating the MNs, solutions containing different concentrations and molecular weights of polymer were atomised at varying flow rates, deposition distances and voltages to assess the morphology and characteristics of the resultant structures. This was according to the QBD (DOE generated using JMP). This allowed the most optimal process parameters to be selected for each formulation. SEM micrographs was taken for these samples including the coated MNs. SEM was carried out according to 4.3.2.5

5.3.2.7.2 DSC

All 8 formulations as well as the dyes and raw polymers were analysed by Jade DSC (PerkinElmer precisely, Shelton, USA) and Pyris Jade DSC software, to analyse thermal transitions. The temperature scale of the DSC machine calorimeter was calibrated using Indium with a known melting point of T_m, of 156.6 °C. The sample was placed into an aluminium pan and then covered with a lid with holes, followed by crimping. The sample was loaded into the machine and scanned from 20 °C – 300 °C with a heating and cooling rate of 20 °C/min under a flow of nitrogen gas.

FTIR was used to analyse all 8 formulations as well as the dyes and raw polymers. Prior to any measurement, FTIR (IRPrestige-21, Japan) background was scanned 10 times and a range of 400-4000 cm^{-1} was determined. The samples were then clamped into place above a dense crystal and scanned ten times. The peaks' wavenumbers were identified and labelled using the Bruker Opus 7.0 FTIR software.

5.4 Results and Discussion

5.4.1 Solution Characterisation

Table 14: Physical characterisation of polymeric solutions

PHYSICAL PROPERTY	PVP 4.0x10³ g/mol	PVP 1.3x10⁶ g/mol	PCL 1.4x10³ g/mol	PCL 8.0x10³ g/mol
Electrical Conductivity (μS/cm)	3.01 ± 0.035	2.65 ± 0.015	7.82± 0.035	6.35 ± 0.53
Density (g/mL)	0.79 ± 0.029	0.80 ± 0.043	1.26 ± 0	1.66 ±0.00058
Surface Tension (N/m)	0.018 ± 0.00082	0.038 ± 0	0.037 ± 0.001	0.016 ± 0
Viscosity (mPa.s)	2.43 ± 0.0058	3.12 ± 0.058	2.18 ± 0.1	31.5 ± 0.1

5.4.1.1 Viscosity

As the molecular weight increases so does the viscosity (Table 14). This trend can be seen with PVP 2.43, 3.12 *mPa.s* and PCL with values 2.18 and 31.5 *mPa.s* respectively. Literature suggests the formation of fibres with higher molecular weight and concentrations of polymers (Xie, Jiang et al. 2015).

5.4.1.2 Surface Tension

The surface tension also has a large effect on the EHDA process as it usually competes with EC. In terms of Es EHDA is only able to occur when the electric stress is able to overcome surface tension to form a stable jet (Xie, Jiang et al. 2015). The surface tension must be lower than 50 mN/m for a liquid to be atomised under the influence of electrical field. The electrical stress must overcome the surface tension to achieve a stable cone-jet. As the surface tension was below this value for all solutions it can be assumed that either molecular weight of polymer and concentration (if based solely on surface tension alone) can be used for the EHDA process (Xie, Jiang et al. 2015, Husain, Lau et al. 2016).

5.4.1.3 Electro-conductivity

As can be seen in Table 14, the general trend for high and LMW PVP is that the EC is very similar and falls into a very small range (3.01 µs/cm and 2.65µs/cm respectively). This is desirable as high EC can result in

5.4.1.4 Density

As shown in Table 14 the density values obtained with high and low molecular weights of PVP were very small 0.79 g/mL, 0.80 g/mL respectively. PCL showed slightly higher density at a higher molecular weight 1.66 g/mL compared to lower molecular weight PCL with a density value of 1.26 g/mL respectively. Lower density values can be seen with the lower molecular weight PVP and PCL which is required for the production of particles (Wang, Jiamian, Jansen et al. 2019).
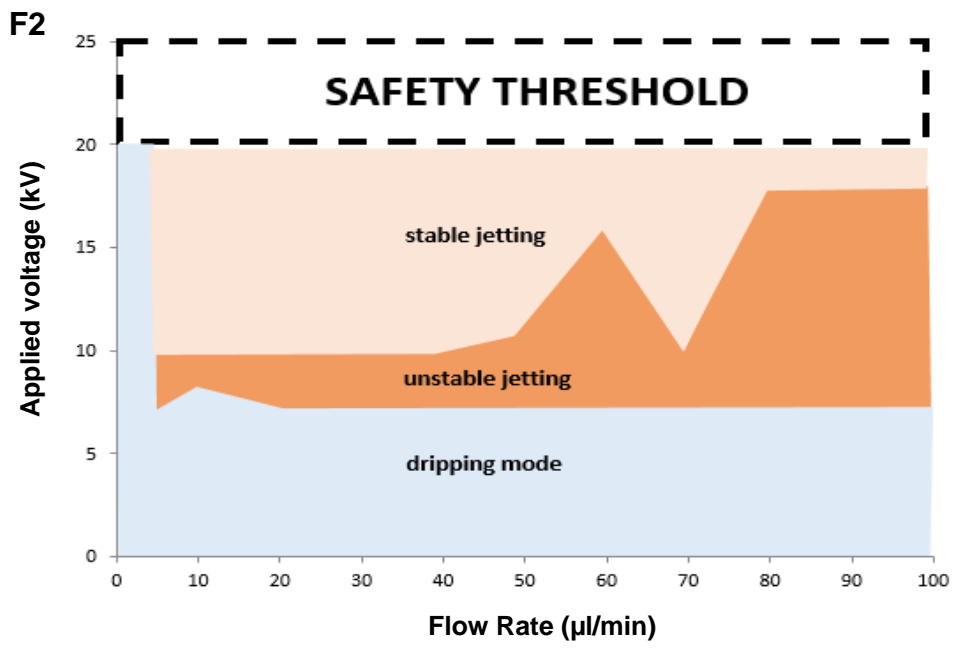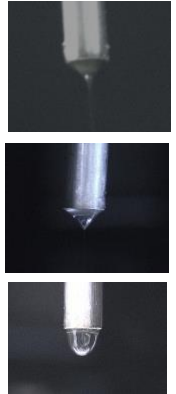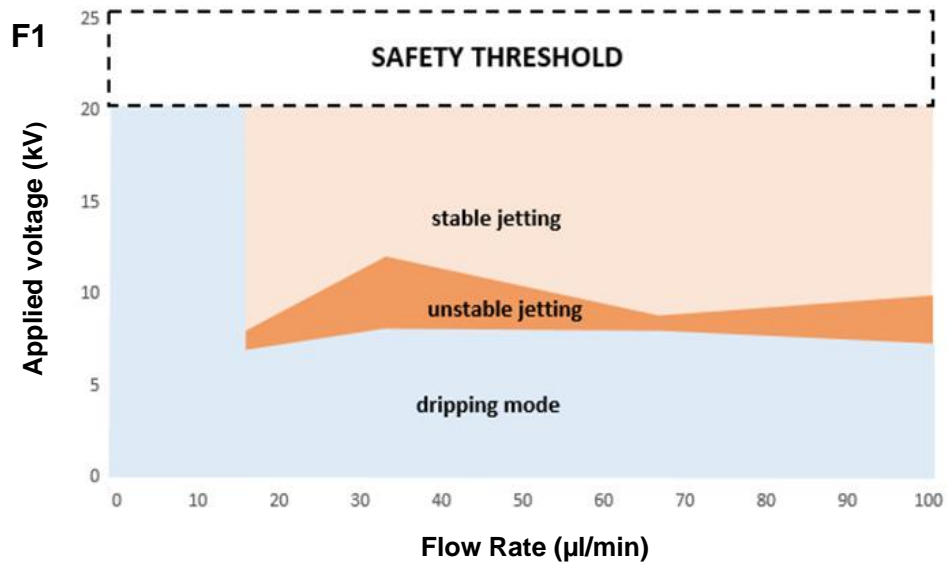
5.4.2 Optimising the EHDA process

The fundamental principle of EHDA involves a liquid emerging from the nozzle under the action of surface tension being subjected to an acceleration force in the form of an electric field. The polydispersity index (mean particle size and uniformity of particle size in the distribution depends on the spraying mode. The es droplet can vary from few hundred nanometres to micrometres. Therefore, the physical properties of the solution and experimental design is paramount in the determination of the spraying mode. The EHDA set up was done so with the attachment of a high-speed camera to capture real time live footage of Es and Esp in action. Stable cone jets were observed with Figure 39 F1, F2, F5 and F6 insets. The modes were observed from micro-dripping to Taylor cone, as the voltage increases. The map highlights the various regions which includes the different spraying modes and the stable jetting regions. It is in the stable jetting region where a stable cone jet is formed, and the resultant spray will lead to the deposition of atomised nanoparticles. The lower viscosity solutions (low polymer weight and lower concentration) yielded smaller droplets and lower polydispersity (Le, Myrick et al. 2018). The opposing characteristics were found with higher molecular weight and higher concentration polymeric solution, which led to electrospinning with the system (Yu, M., Ahn et al. 2016).

The dripping mode occurs when no voltage is applied. Regular, large droplets detach from the capillary to form drops as the electrical force and the weight of the drop overcomes the capillary forces. With a voltage increase, the meniscus elongates, and the drop becomes smaller. The most efficient mode of attaining a narrow particle size distribution is the 'cone-jet' mode, also known as the stable Taylor cone. The liquid forms a cone with a thin jet at its apex where the liquid elongates into a long, fine jet and then fragments into droplets under the influence of electrostatic forces. Figure 39 F3, F4, F7 and F8 insets illustrate a 'multi-jet' mode where the meniscus flattens with small cones at separate points at the circumference of the capillary, whereby fine jets of liquid are ejected. The 'precession' mode occurs when the liquid escapes the capillary in the form of a skewed cone and changes into a thin jet at its apex. This mode differs from

'cone-jet' as the jet in the 'precession' mode rotates around the capillary axis (Rosell-Llompart, Grifoll et al. 2018).

As seen in Figure 39, the formulations containing dye as opposed to polymer alone had distinctive differences. Almost all formulations show one stable jetting region. There was better stability below 15 kV. However, in Figure 39 F4 the higher molecular weight polymer with fluorescein dye has a very different jetting map compared to Figure 39 F3. With F4 the jetting map showing 2 unstable regions making it more problematic to spray fibres.

For the PCL formulations, similar behaviour was shown whereby Figure 39 F5, F6 and F7 have one unstable region. There is also a larger stable jetting region. Whereas Figure 39 F8 has a large unstable jetting region compared to Figure 39 F7 where there is only a small unstable jetting area for PCL alone. In summary a flow rate between 15-25uL/min was sufficient for F2 and F4 and 15-80 µL/min for F6 and F8 samples with a voltage ranging between 10-20kV.

F1

F2

F3

Applied voltage (kV) vs Flow Rate (µl/min)

SAFETY THRESHOLD

stable jetting

unstable jetting

dripping mode

F4

Applied voltage (kV) vs Flow Rate (µl/min)

SAFETY THRESHOLD

unstable jetting

stable jetting

unstable jetting

dripping mode
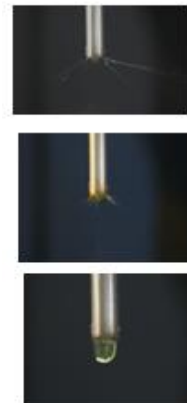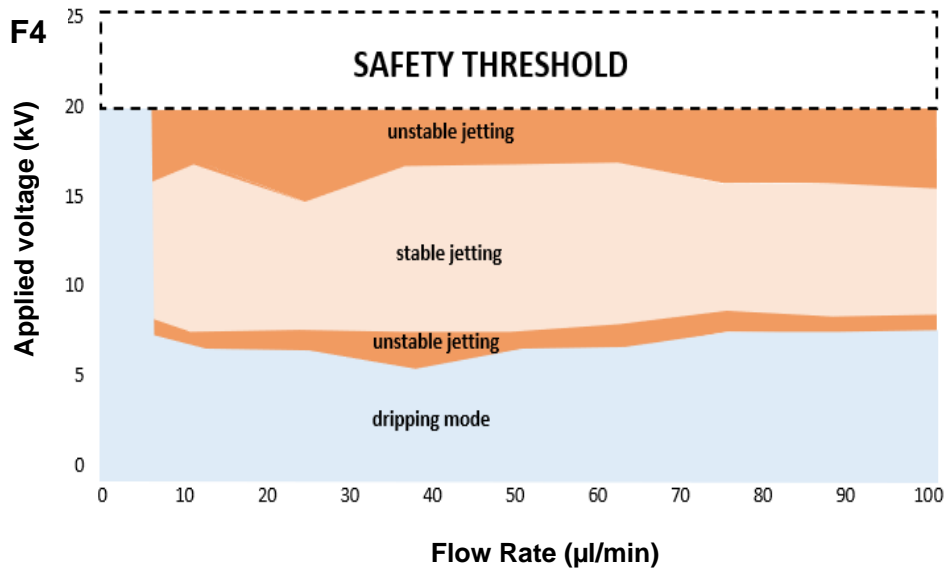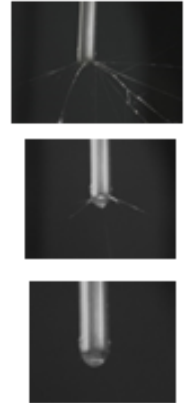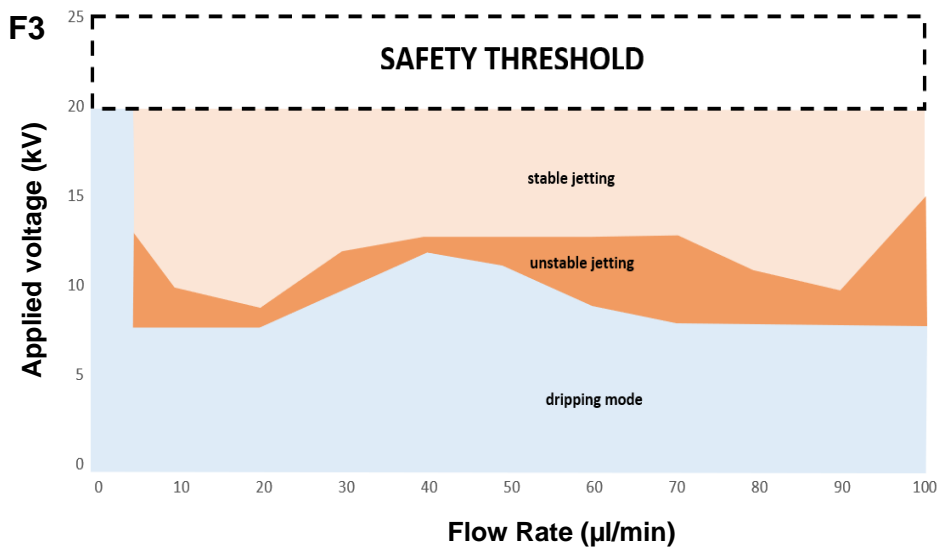
F5
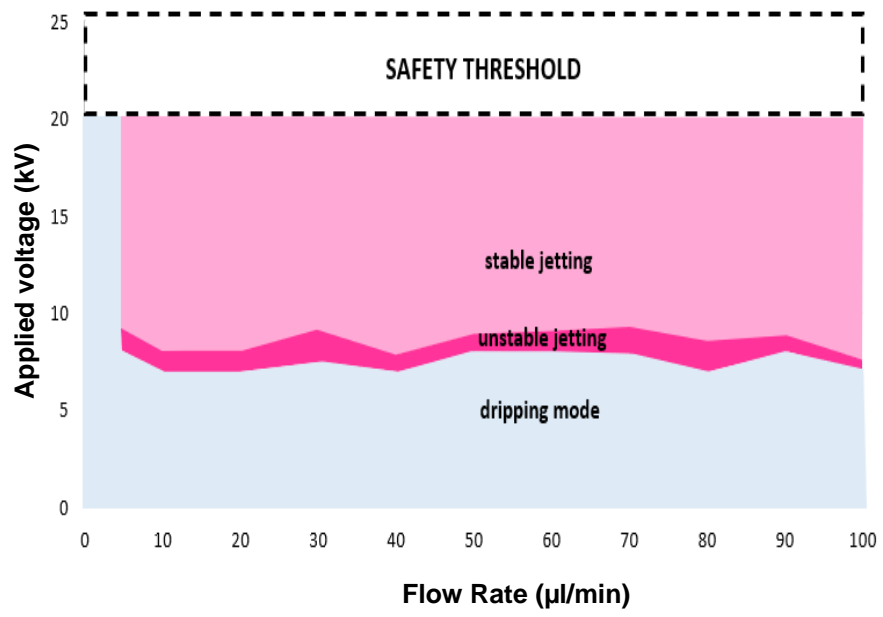
F6
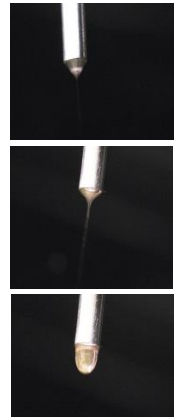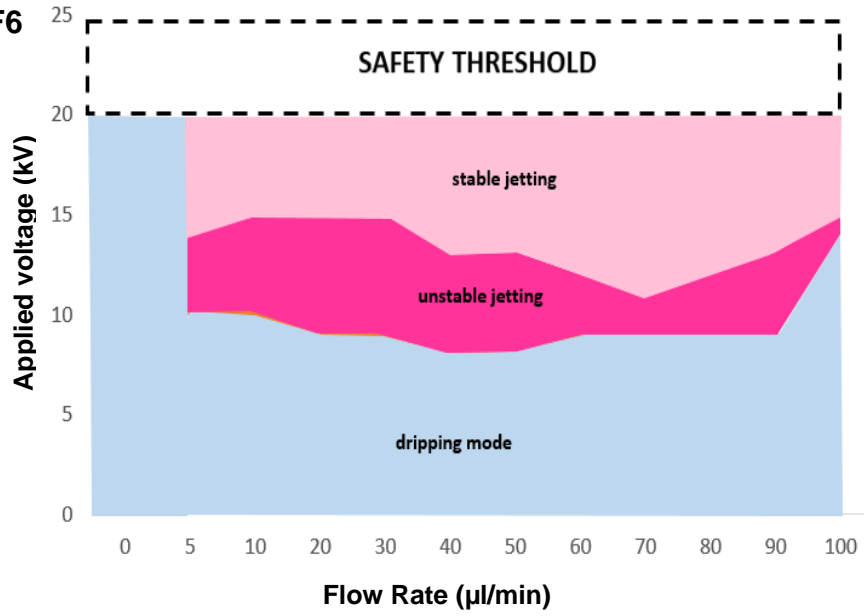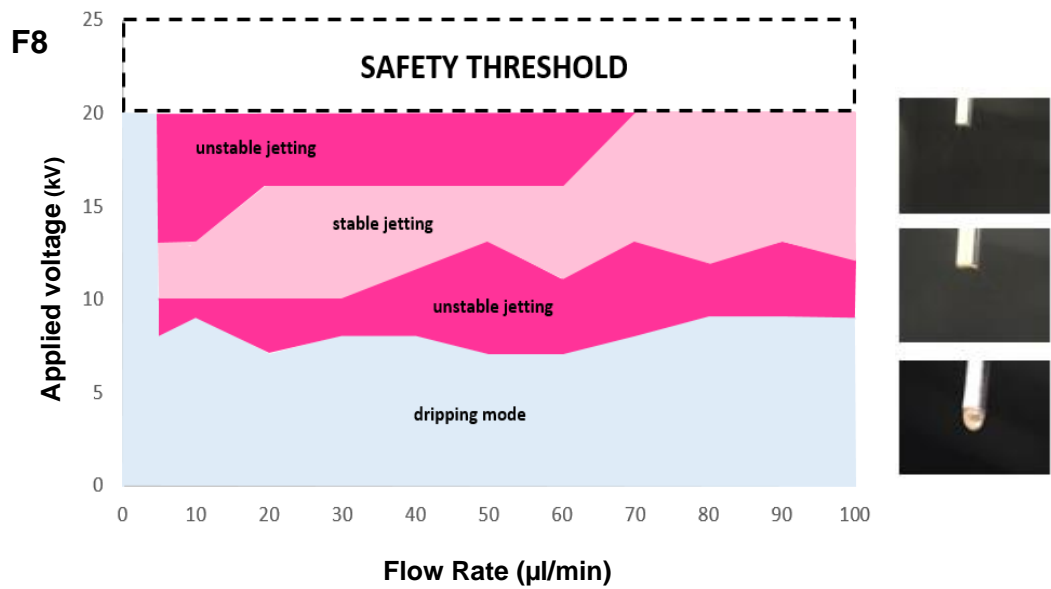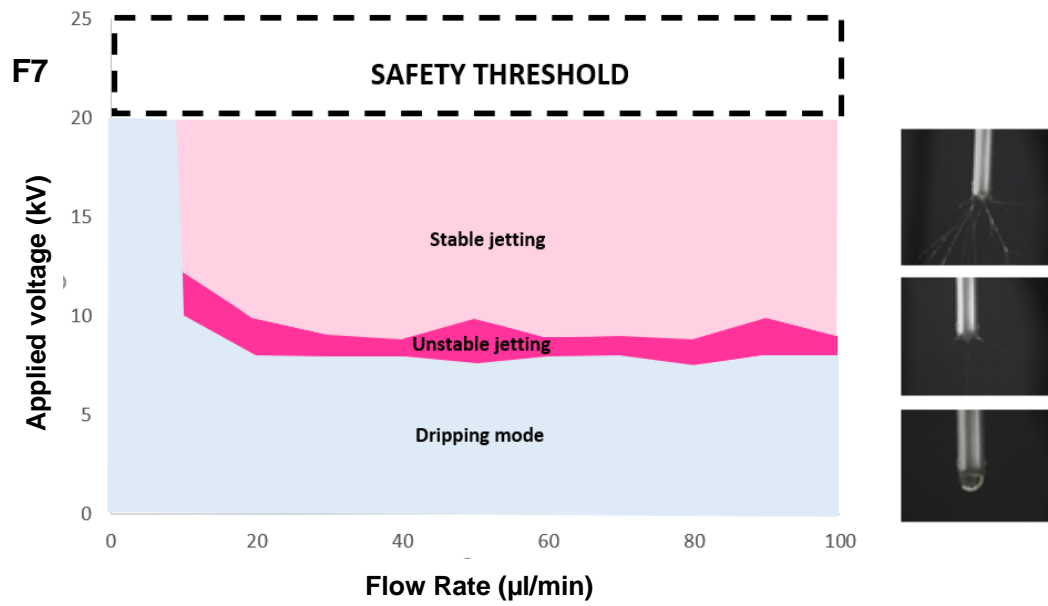
Figure 39: Jetting maps to determine the relationship between flow rate and voltage for formulations F1-F8 with insets for corresponding jetting mode

5.4.3 Evaluation of EHDA process using QBD

Initially the CQA's were identified (particle size, appearance and PD) of the product were chosen as the responses being looked at and the CPPs relating to the EHDA process (flow rate, applied voltage and deposition distance) were also identified as the factors. Molecular weight and concentration of the polymer were also factors being investigated. These factors were selected as they are believed to have a direct effect and impact on said responses. The responses selected were then given high and low limits and the desirability of these limits were also set. Thus, generating a DoE. An example is shown for PVP (Figure 40).

Figure 40: DoE dialogue for PVP

The purpose of the first set of experiments was to ascertain which of the two concentrations and molecular weight of polymer should be selected to produce particles and fibres for each polymer using EHDA. The solutions that were prepared as described in Table 4 were formulated again and each experiment was Es or Esp. The factors and responses were put into JMP Pro software, and the software generated a table of runs. The rationale for these experiments was to produce a full factorial design, whereby parameters that show no desirable responses are eliminated from the remaining DOE providing the next set of experiments.

Once the screening design (Figure 40) had been performed and the results analysed, a further study was performed. The factors being investigated, and their subsequent ranges were defined further. Following the screening designs, four separate verification/robustness full factorial designs were carried out to ensure the most optimal particles/fibres would be produced using the two different polymers. Two designs were for PVP/PCL particles and two more for PVP/PCL fibres. These formulations were prepared as described in Table 13. As the deposition distance was shown to have an impact during the screening design this was taken into consideration and this was set at 10, 12.5 and 15cm; and 15, 20 and 25 µL/min were the flow rates being looked at for PVP particles and for PCL it was 12.5, 15 and 20 cm; and 20, 40 and 60 µL/min. As can be seen from the initial results, the mean particle size for most of the runs were below 500nm as well as the PD results also being low for both particles and for fibres it was within the micron range.

Once the parameters for the particles and fibres were obtained the second set of experiments for PVP and PCL were carried out. The resultant particles/fibres deposited were then assessed using imaging as well as thermal and spectroscopic techniques. The prediction profilers in Figure 41 C-F predict the optimal workspace regions for the three dependent variables. The response surface plots for particle shape and PD can be seen in figure 42. The implementation and analysis of a response surface fractional factorial DOE with a reduced number of runs helped to identify the effects of the selected

independent variables and identify those settings for particles and fibres of optimized quality.

In order to establish a design space the contour profile must have at least two active factors. As can be seen from Figure 41 the prediction profiler flow rate was shown as being an active facor. Therefore in order to obtain a design space for verification studies deposition distance was added to the profile as an active factor.The design space is the white region in the figure and when a process is carried out in this area then producing a product whereby quality is assured.

Flow rate is the only factor that is being shown as influencing PD. The p-value is also less than 0.05 indicating that it is important and that an interaction is taking place between PD and the responses being investigated. The response surface plots shown in figure 42 provide an operating window of whereby to operate. It outlines the areas within which you should work to achieve the optimal size, shape and PD.

A

	Pattern	Mwt of polymer	Conc of polymer	Deposition distance	Flow rate	Particle size	Partical shape	Polydispersity
1	1111	44000	5	15	20	3804	1	0.53
2	1112	44000	5	10	20	•	6	•
3	1113	13000000	1	20	100	900.05	1	0.2
4	1121	13000000	5	10	20	•	6	•
5	1122	13000000	1	10	60	534.1	5	0.56
6	1123	44000	5	20	100	327.74	2	0.53
7	1131	13000000	1	20	60	1243.37	5	0.4
8	1132	13000000	5	15	60	•	6	•
9	1133	13000000	5	20	20	•	6	•
10	1211	44000	5	10	60	322.75	3	0.47
11	1212	13000000	5	20	100	•	6	•
12	1213	44000	5	15	100	494.05	5	0.38
13	1221	13000000	1	15	20	7.58	5	0.51
14	1222	44000	1	10	20	814.73	2	0.15
15	1223	44000	5	10	100	636.33	2	0.51
16	1231	13000000	5	15	100	•	6	•
17	1232	44000	5	20	20	513.83	1	0.51
18	1233	44000	1	15	60	467.89	2	0.75

B

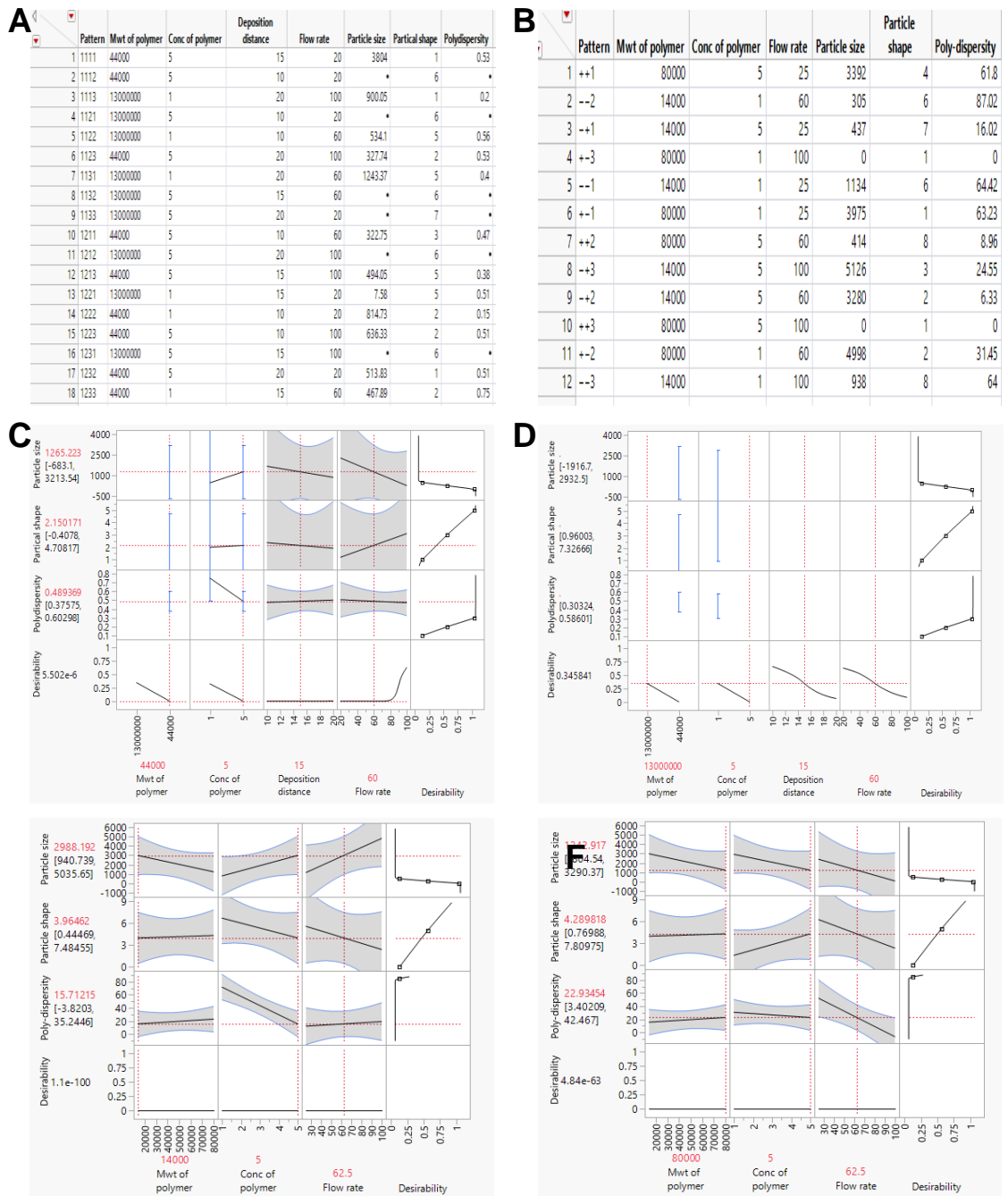|	Pattern	Mwt of polymer	Conc of polymer	Flow rate	Particle size	Particle shape	Poly-dispersity
1	++1	80000	5	25	3392	4	61.8
2	--2	14000	1	60	305	6	87.02
3	-+1	14000	5	25	437	7	16.02
4	+-3	80000	1	100	0	1	0
5	--1	14000	1	25	1134	6	64.42
6	+-1	80000	1	25	3975	1	63.23
7	++2	80000	5	60	414	8	8.96
8	-+3	14000	5	100	5126	3	24.55
9	-+2	14000	5	60	3280	2	6.33
10	++3	80000	5	100	0	1	0
11	+-2	80000	1	60	4998	2	31.45
12	--3	14000	1	100	938	8	64

Figure 41: Screening design of A) PVP and B) PCL. Prediction profile for C) F2, D) F4, E) F6 and F) F8Prediction profile for (A) F2 (B) F4 (C) F6 (D) F8
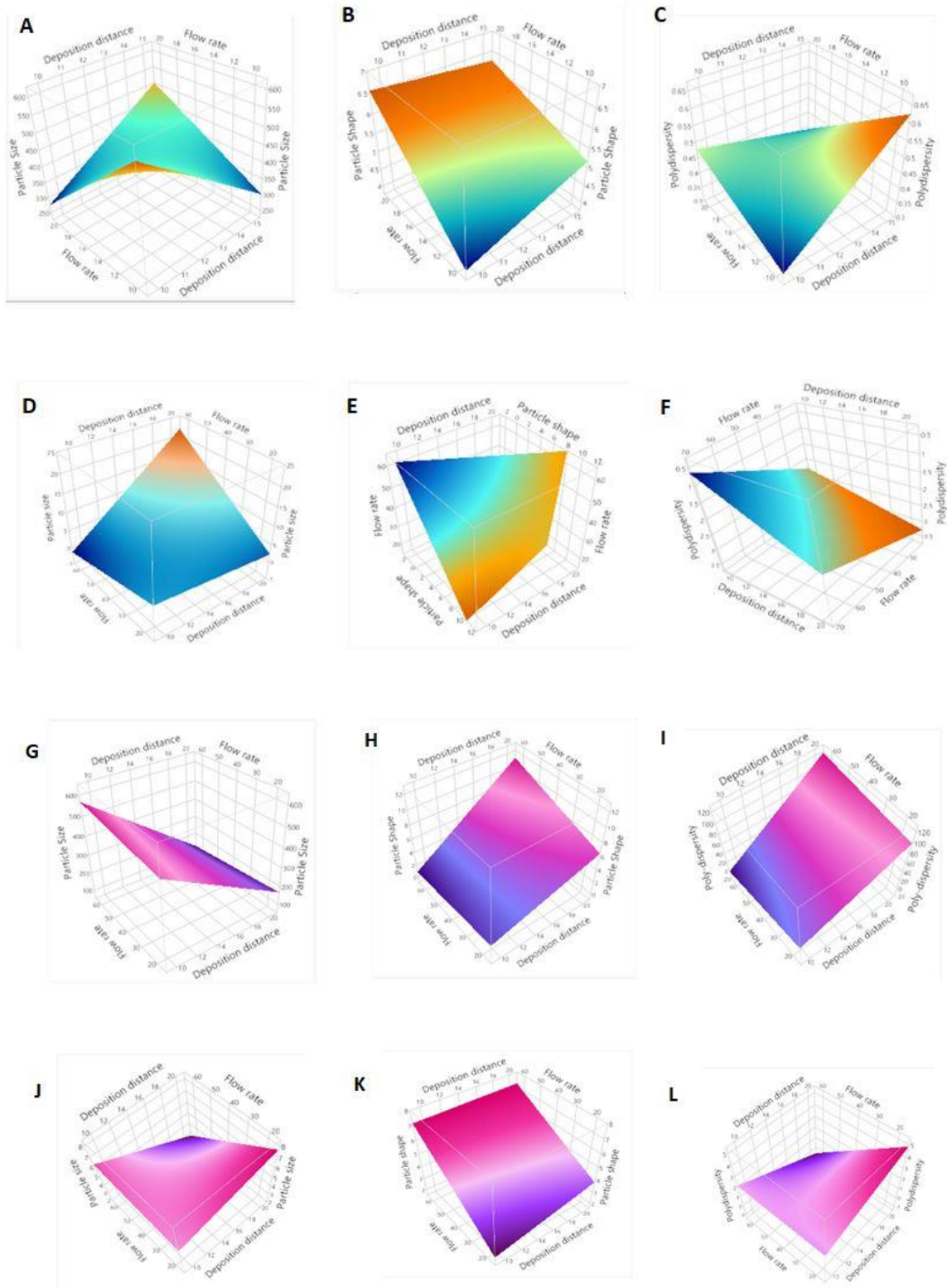
162

Figure 42: Response surface plots for (A-C) F2 (D-F) F4 (G-H) F6 (J-L) F8

5.4.4 Coating characterisation and morphology

Optical images were taken of the finalised formulations which can be seen in Figure 41 A-H. The final optimised particles (PVP particles Figure 41 I and 41 J, PCL particles Figure 41 M and 41 N) and fibres (PVP fibres Figure 41 K and 41 L, PCL fibres Figure 41 O and 41 P). According to the ICH Q8 guidelines a design space can be defined as "the multidimensional combination and interaction of input variables (e.g. Material attributes) and process parameters that have been demonstrated to provide assurance of quality". When working within the designated design space, any change here is not considered by the regulatory authorities as a change in the process therefore this can lead to more flexibility. However, movement out of the design space is considered to be a change and would normally require regulatory approval. Working within the design space guarantees product quality which therefore in turn makes sure that the manufacturing process is robust as well as generating additional financial benefits as there is a reduction in cost as there are less batch failures. Table 15 contains the process parameters selected for the atomised structures shown in Figure 43. These parameters were selected from QBD analysis.

Table 15 Process parameters for optimised structures

Formulation	Flow rate (µL/min)	Applied voltage (k/V)	Deposition distance (cm)
F1	15	14	15
F2	15	14	15
F3	20	12	10
F4	20	12	10
F5	15	15	15
F6	15	15	15
F7	50	13	10
F8	50	13	10

The appearance of the resulting structures from QBD was consistent with all experimental runs producing spherical particles (Figure 43A,B,E and F) Optical microscopy results show small spherical near uniform particles for both F1 and F2 as shown in Figure 43A and B. Whereas in the optical images for the higher molecular weight formulations Figure 43C has smoother fibres and the PVP-FL fibres shown in Figure 43D has smooth looking fibres with some beading. This could be due to formulation instability as well as some instability experience during the electrospinning process. This was further confirmed with SEM.

HMW PVP shows larger sized structures all within the micrometre range (Figure 43K, L). The PD was also higher with this polymer. The mean particle size was selected as being less than 500nm; because the aim is to produce nanoparticles any particles produced that are either at this value or lower will meet the criteria that is set in the QTPP. It has also been stated that nanocarriers that fall into the range of 50-500nm are generally acceptable; it has also been shown that polymeric particles that are <500nm in diameter have a general higher intracellular uptake rate (Lombardo, Kiselev et al. 2019)

At a low flow rate, an array of fibres was produced with varying fibre diameter due to the higher viscosity of the solution. As the flow rate increases, the formation of fibres reduces at the same time as the development of agglomerated material begins to intensify; particularly in Figure 43G. This is due to the short drying time causing non-evaporation of the solvent and low stretching of the solution in the flight between the capillary tip and collector.

With the optical images obtained for PCL the particles sprayed and shown in Figure 43E the particles are slightly less spherical with some particles agglomerating. Figure 43F shows a larger distribution of particles with some near spherical again with some agglomeration. This can be due to the rapid solvent evaporation as DCM is a very volatile solvent. In Figure 43G there are many beaded fibres with the PCL formulation with more unstable fibres electrospun and shown in Figure 43 H.

5.4.4.2 Morphology

Characterising the morphology of nanostructures and more significantly controlling the nanomaterial morphology is a critical factor for pharmaceutical technologies since many drug delivery routes present a criterion whereby the engineered particles must fit in order to achieve therapeutic effect. Figure 43I-P displays the optimised particular and fibrous structures following QBD implementation and DOE analysis. Figure 43I show uniform, spherical PVP particles and this is similar with the dye loaded PVP-FL particles. Figure 43J was produced at a flow rate of 15 µL/min flow rate and a deposition distance of 15cm were chosen as the optimum conditions to spray which is what the JMP data suggested. Similarly, smooth PVP fibres can be seen in both Figure 43K and 43L with the size of fibres measuring very similar. The optimised fibres were produced at a flow rate of 20 µL/min at a deposition distance of 10 cm and the mean fibre size measuring 4.5 µm. The PCL samples however were quite problematic to spray initially due to issues with solvent evaporation and agglomeration however, following DOE analysis 1.4×10^3 g/mol-PCL at 5% w/v, a flow rate of 15 µL/min and a deposition distance of 15 cm produced Nps at a mean size of 209 nm. The PCL fibres produced in Figure 43O and 43P appear smooth with even distribution compared to that found in the optical images, as these were more stable and produced at optimal conditions at a deposition distance of 10 cm and flow rate of 50 µL/min.
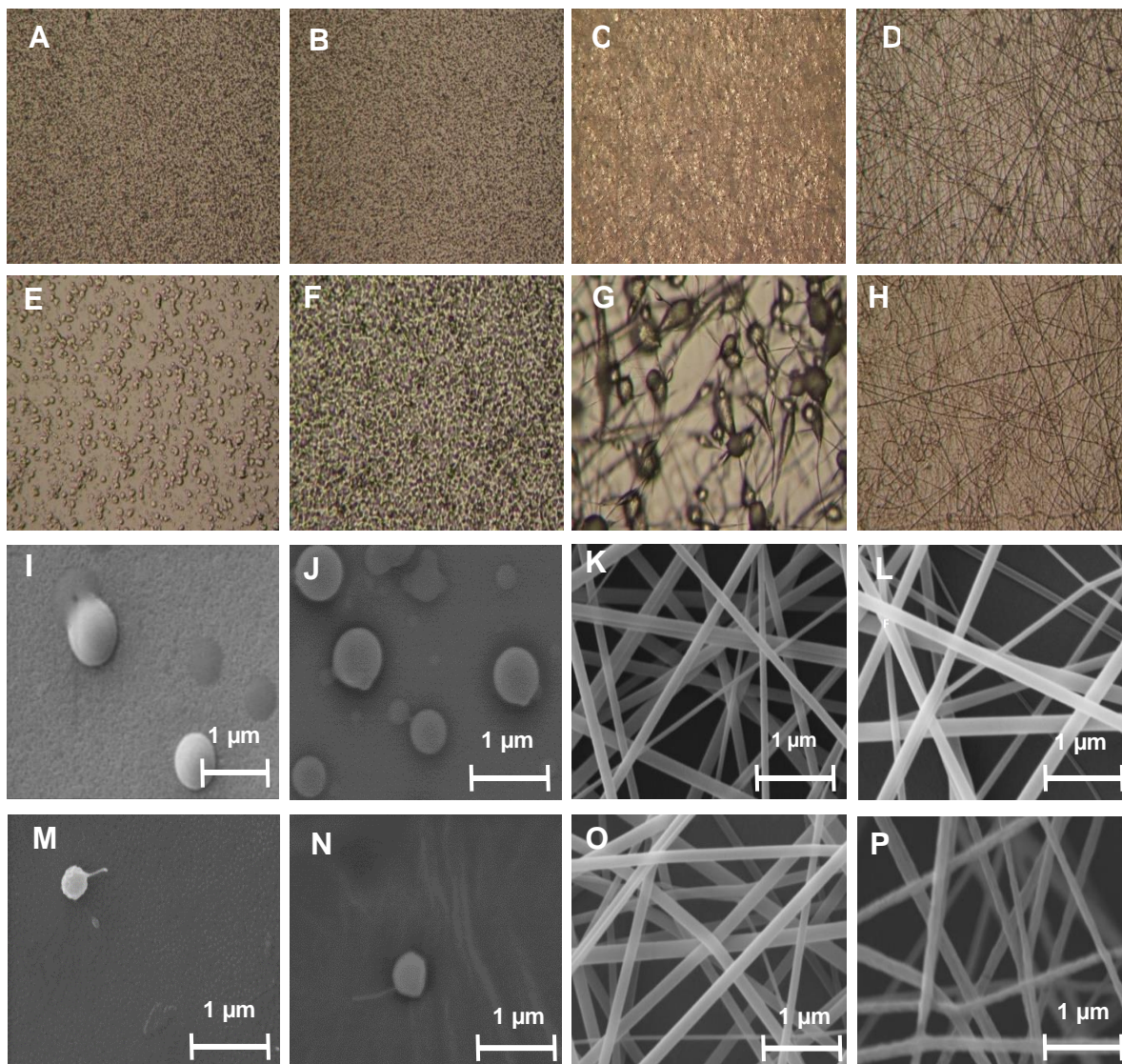
Figure 43: Optical images of A) F1, B) F2. C) F3, D) F4, E) F5, F) F6, G) F7 and H) F8. SEM images of optimised I) F1, J) F2, K) F3, L) F4, M) F5, N) F6, O) F7 and P) F8

5.5 Differential Scanning Calorimetry

Figure 44A displays the DSC thermogram for pure PVP. As can be seen from the thermogram there is a distinctive peak at 120 °C which represents the melting temperature of the sample. In many sources of literature, it is stated that the melting point of pure PVP should fall in the range of 150 °C-180 °C; however, the melting point recorded does not show this and appears to be out by 30 °C. The sample for pure PVP was analysed again to make sure that the recorded melting point was not an anomalous result; but after repeating this particular run a further two times the melting temperature of 120 °C was still recorded.

This slightly lower melting point value may have been recorded and explained by the fact that the PVP being tested had a molecular weight of 4×10^4 g/mol and it has been noted that the molecular weight of a polymer can affect the melting point. This is because an increase or decrease in molecular weight can influence the overall flexibility and/or rigidity of a polymer which can therefore in turn have an effect on the polymers melting point.

The melting point for fluorescein is quoted as being above 300 °C (Sabnis, 2008); and a clear endothermic peak is visible at 340 °C for FL. It can be seen from the thermogram there is also only one single peak representing the melting point; this observation can be to a certain extent be linked to the purity of the sample as there are no other peaks or interactions being shown (Florence and Siepmann, 2009). Making sure that the starting materials themselves at the start of a process are pure and therefore of the desired quality is very important when implementing a QbD approach as in order to make sure that the end product is of exceptional quality each aspect and unit operation of the manufacturing process must also conform to a robust and high-quality procedure.

For the optimised nanoparticles the thermogram a single endothermic peak is visible at approximately 120 ºC. This melting point is the same as is seen on the raw PVP thermogram; therefore, it can be assumed that the PVP and fluorescein dye have fully encapsulated and have formed a single entity. In an article by Chadra *et al.,* they similarly used PVP 4×10^4 g/mol as their polymer drug carrier

but had chosen Domperidone as their drug. When using DSC to characterise the drug product they to only found a single endothermic peak thus indicating the formation of a total inclusion complex (2011).

DSC provides thermal information about the materials used to facilitate in the identification and verification of excipients. DSC results, presented in Figure 44 B, show a single melting peak with a maximum melting temperature (T_m) of unprocessed PCL of 62°C and is confirmed by Bock et al in 2011 where the T_m = 61.2°C. The T_m of unprocessed RhB is 208°C and can be seen on the thermogram Q

However, a second broad peak is observed at 265°C. The phenomenon of double melting peaks is due to the impartial melting and recrystallisation of the crystallite at that specific moment of thermal scanning. The T_m and second peaks are associated with the melting of imperfect and perfect crystallite, respectively (Chen, H., Su et al. 2018). The T_m of F6 and F8 spectra is shown to be slightly decreased (53 °C), implying that smaller crystallites are formed during Es and Esp thus successful encapsulation of RhB within PCL.
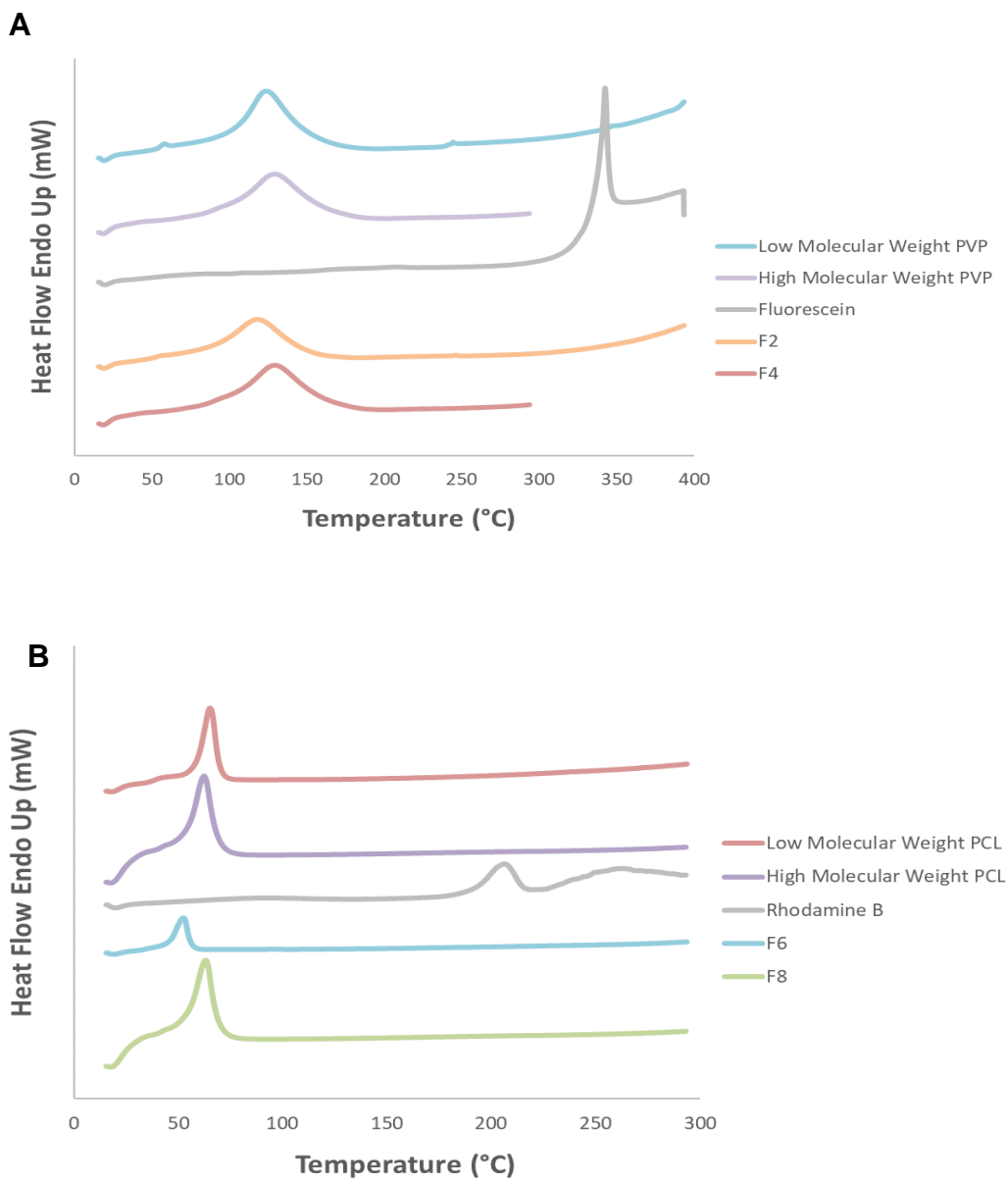
Figure 44: DSC spectra (A) PVP, FL, F2 and F4. (B) RhB, pure PCL, F6 and F8.

5.6 Fourier Transform Infared Spectroscopy Analysis

In recent years EHDA has been more prominent and used more heavily since the process conditions do not appear to affect the structure of the materials being used. FTIR is a spectroscopic technique that allows the user to identify the presence of functional groups of materials. The resultant structures produced using EHDA can be assessed using FTIR analysis to ensure that the integrity of the structures and additives have not being damaged in any way. In this work the raw materials (polymers, dyes in powder form) as well as the atomised structures (particles and fibres). The fingerprint of PVP and FL and PCL and RhB can be seen in the spectra.

The FTIR spectrum shown in Figure 45A is that of the pure PVP. Peaks at 3418.88 cm^{-1} (O-H stretch), 2955 cm^{-1} (C-H asymmetric stretch), 1644.36 cm^{-1} (C=O stretch), 1421.22 (CH_2) and 1285.69 cm^{-1} (C-N vibration) are identified which correspond to the structure of PVP.

Figure 45A also displays the spectrum obtained for pure fluorescein and the following peaks identified in the spectrum confirm that the sample being analysed is that of FL. 1636 cm^{-1} (C=O symmetric stretch), 1588.4 cm^{-1} (COO^- asymmetric stretch), 1457.23 cm^{-1} (C-C stretch), 1366.47 cm^{-1} (C-C stretch) and 1108.08 cm^{-1} (C-H aromatic in plane bend). These peaks and bonds were also identified in an article by Wang *et al.,* when they too were analysing raw FL (Wang, Lili, Roitberg et al. 2001).

The optimised nanoparticles significant peaks include; 3416.14 cm^{-1} (OH stretch), 2953.05 cm^{-1} (CH asymmetric stretch), 1651.33 cm^{-1} (C=O stretch), 1460.96 cm^{-1} (C-C stretch) and 1422.26 cm^{-1} (CH_2 bend). When comparing the spectrum for pure PVP and the optimised nanoparticles they appear to be very similar and the majority of the peaks that were seen in the spectrum for PVP are also visible in the spectrum for the optimised nanoparticles. The peak at 1460.96 cm^{-1} corresponding to the C-C bond is also present in the fluorescein spectrum which can therefore lead to the assumption that FL and PVP have encapsulated together. The peaks also appear much broader and well defined which is often

seen in a spectrum when two or more components are believed to be mixed (Chokki, Darracq et al. 2019).

In Figure 45B, the characteristic absorption peak at 1730 cm^{-1} is the major transmission peak of PCL and arises due to the carbonyl stretching of the C=O. The bands at 2943, 1293, 1238, 1164, 1107 and 1045 cm^{-1} which correspond to asymmetric CH2 stretching, C-O and C-C stretching in the crystalline phase, asymmetric COC stretching, OC-O stretching, symmetric COC stretching and C-O and C-C stretching in the amorphous phase, respectively. The major peaks are confirmed by Gurlek et al. in 2017 (Gurlek, Sevinc et al. 2017). In Figure 45B, the weak intensity band at 3085 cm^{-1} denotes to aromatic C-H bonds, which also arises at 1335 cm^{-1} (plane bending), 815 cm^{-1} (out of plane bending) and at 681 cm^{-1} (wagging vibrations). The peaks at 1691 cm^{-1} and 1644 cm^{-1} are associated with the vibrational stretching of C=N and C=O, respectively. The strong band at 1583 cm^{-1} is due to the asymmetric stretching of the COO- group which is further confirmed by the band at 1469 cm^{-1}, ascribed to symmetric stretching of the group. The aromatic C-C stretch is observed at 1335 cm^{-1} and the C-O results from the 1245 cm^{-1} peak. The major peaks are confirmed by Dukali et al. in 2014 (Dukali, Radovic et al. 2014).
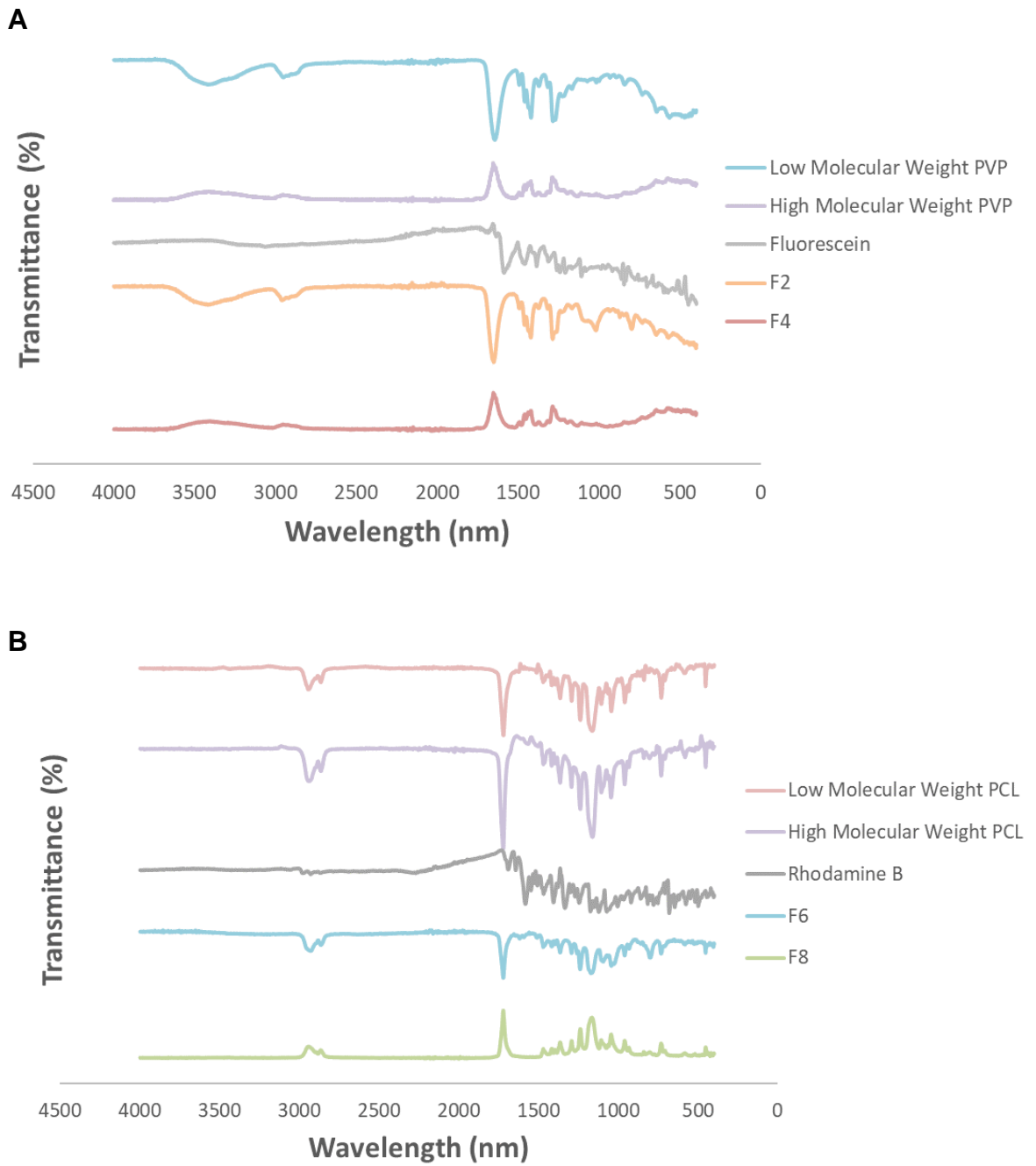
Figure 45: FTIR analysis of (A) High and low molecular weight PVP, Fluorescein, PVP-dye composites and (B) High and low molecular weight PCL, Rhodamine B, PCL-dye composites.

5.7 Conclusion

This study demonstrated the use of QBD and how the application of the QBD principles led to the optimisation of the EHDA process which resulted in the fabrication of optimised structures. This study utilised polymer and dye. The resultant electrsprayed/electrospun particular and fibrous structures were assessed and characterised. Morphological studies exhibited primarily smooth PVP fibres with some beaded fibres with the PCL formulation and spherical particles. PVP showed spherical particles with most being under 500nm which satisfied the QTPP profile set for it. The PVP fibres that were produced were in the nano-micron range. They were smooth and more uniform with no beading again satisfying the QTPP.

Thermal analysis conferred the stability of nanoparticles and nano/micro fibres with DSC also showing the dye was molecular distributed in a state throughout the polymeric matrix with all 4 formulations. Spectroscopic studies also confirmed these findings. These results show great promise for the polymers to act as a matrix for model drug. The application of QBD added significant value via optimisation of formulations with polymer and dye/model drug system. The operating window that QBD provided was paramount to the success of this study. It eliminated the need to run countless experiments and it ensured that the finalised structures met the criteria that was initially set. This shows great scope for QBD and these formulations can now be carried forward to be atomised onto stainless steel MNs. Therefore, the formulations being carried forward will be with a polymer concentration of 5% w/v and dyes.

5.8 References

AMASYA, G., AKSU, B., BADILLI, U., ONAY-BESIKCI, A. and TARIMCI, N., 2019. QbD guided early pharmaceutical development study: Production of lipid nanoparticles by high pressure homogenization for skin cancer treatment. *International Journal of Pharmaceutics,* 563, pp. 110-121.

ANDERSEN, T.E., ANDERSEN, A.J., PETERSEN, R.S., NIELSEN, L.H. and KELLER, S.S., 2018. Drug loaded biodegradable polymer microneedles fabricated by hot embossing. *Microelectronic Engineering,* 195, pp. 57-61.

CHEN, H., SU, C., SHI, G., LIU, G. and WANG, D., 2018. Nature of the double melting peaks of regioregular poly(3-dodecylthiophene). *European Polymer Journal,* 99, pp. 284-288.

CHOKKI, J., DARRACQ, G., POELT, P., BARON, J., GALLARD, H., JOYEUX, M. and TEYCHENÉ, B., 2019. Investigation of Poly(ethersulfone)/Polyvinylpyrrolidone ultrafiltration membrane degradation by contact with sodium hypochlorite through FTIR mapping and two-dimensional correlation spectroscopy. *Polymer Degradation and Stability,* 161, pp. 131-138.

DILLON, C., HUGHES, H., O'REILLY, N.J., ALLENDER, C.J., BARROW, D.A. and MCLOUGHLIN, P., 2019. Dissolving microneedle based transdermal delivery of therapeutic peptide analogues. *International Journal of Pharmaceutics,* 565, pp. 9-19.

DUKALI, R.M., RADOVIC, I.M., STOJANOVIC, D.B., SEVIC, D.M., RADOJEVIC, V.J., JOCIC, D.M. and ALEKSIC, R.R., 2014. Electrospinning of the laser dye rhodamine B-doped poly(methyl methacrylate) nanofibers. *Journal of the Serbian Chemical Society,* 79(7), pp. 867-880.

ECHEGOYEN, Y., FABRA, M.J., CASTRO-MAYORGA, J.L., CHERPINSKI, A. and LAGARON, J.M., 2017. High throughput electro-hydrodynamic processing in food encapsulation and food packaging applications: Viewpoint. *Trends in Food Science & Technology,* 60, pp. 71-79.

FARAJI, S., SADRI, B., VAJDI HOKMABAD, B., JADIDOLESLAM, N. and ESMAEILZADEH, E., 2017. Experimental study on the role of electrical conductivity in pulsating modes of electrospraying. *Experimental Thermal and Fluid Science,* 81, pp. 327-335.

GURLEK, A.C., SEVINC, B., BAYRAK, E. and ERISKEN, C., 2017. Synthesis and characterization of polycaprolactone for anterior cruciate ligament regeneration. *Materials Science and Engineering: C,* 71, pp. 820-826.

HUSAIN, O., LAU, W., EDIRISINGHE, M. and PARHIZKAR, M., 2016. Investigating the particle to fibre transition threshold during electrohydrodynamic

atomization of a polymer solution. *Materials Science and Engineering: C,* 65, pp. 240-250.

HWANG, T.H., KIM, Y.J., CHUNG, H. and RYU, W., 2016. Motionless Electrohydrodynamic (EHD) Printing of Biodegradable Polymer Micro Patterns. *Microelectronic Engineering,* 161, pp. 43-51.

JAVED, M.N., ALAM, M.S., WAZIRI, A., POTTOO, F.H., YADAV, A.K., HASNAIN, M.S. and ALMALKI, F.A., 2019. Chapter 12 - QbD Applications for the Development of Nanopharmaceutical Products. , pp. 229-253.

LE, N., MYRICK, J.M., SEIGLE, T., HUYNH, P.T. and KRISHNAN, S., 2018. Mapping electrospray modes and droplet size distributions for chitosan solutions in unentangled and entangled concentration regimes. *Advanced Powder Technology,* 29(12), pp. 3007-3021.

LI, J.L., 2006. On the meniscus deformation when the pulsed voltage is applied. *Journal of Electrostatics,* 64(1), pp. 44-52.

LOMBARDO, D., KISELEV, M.A. and CACCAMO, M.T., 2019. Smart Nanoparticles for Drug Delivery Application: Development of Versatile Nanocarrier Platforms in Biotechnology and Nanomedicine. *Journal of Nanomaterials,* , pp. 3702518.

MEHTA, P., PICKEN, H., WHITE, C., HOWARTH, K., LANGRIDGE, K., NAZARI, K., TAYLOR, P., QUTACHI, O., CHANG, M.-. and AHMAD, Z., 2019. Engineering optimisation of commercial facemask formulations capable of improving skin moisturisation. *International Journal of Cosmetic Science,* 41(5), pp. 462-471.

OHAGE, E., IVERSON, R., KRUMMEN, L., TATICEK, R. and VEGA, M., 2016. QbD implementation and Post Approval Lifecycle Management (PALM). *Biologicals,* 44(5), pp. 332-340.

PRANAVKUMAR SHADAMARSHAN, R., BALAJI, H., RAO, H.S., BALAGANGADHARAN, K., VIJI CHANDRAN, S. and SELVAMURUGAN, N., 2018. Fabrication of PCL/PVP Electrospun Fibers loaded with Trans-anethole for Bone Regeneration in vitro. *Colloids and Surfaces B: Biointerfaces,* 171, pp. 698-706.

REKSAMUNANDAR, R.P., EDIKRESNHA, D., MUNIR, M.M., DAMAYANTI, S. and KHAIRURRIJAL, 2017. Encapsulation of β-carotene in poly(vinylpyrrolidone) (PVP) by Electrospinning Technique. *Procedia Engineering,* 170, pp. 19-23.

REZVANPOUR, A., KRANTZ, W.B. and WANG, C., 2012. Scaling analysis of the electrohydrodynamic atomization (EHDA) process for pharmaceutical particle fabrication. *Chemical Engineering Science,* 80, pp. 81-90.

RONNANDER, P., SIMON, L., SPILGIES, H. and KOCH, A., 2018. Modelling the in-vitro dissolution and release of sumatriptan succinate from polyvinylpyrrolidone-based microneedles. *European Journal of Pharmaceutical Sciences,* 125, pp. 54-63.

ROSELL-LLOMPART, J., GRIFOLL, J. and LOSCERTALES, I.G., 2018. Electrosprays in the cone-jet mode: From Taylor cone formation to spray development. *Journal of Aerosol Science,* 125, pp. 2-31.

SHARMA, S., HATWARE, K., BHADANE, P., SINDHIKAR, S. and MISHRA, D.K., 2019. Recent advances in microneedle composites for biomedical applications: Advanced drug delivery technologies. *Materials Science and Engineering: C,* 103, pp. 109717.

SHEKHAWAT, P. and POKHARKAR, V., 2019. Risk assessment and QbD based optimization of an Eprosartan mesylate nanosuspension: In-vitro characterization, PAMPA and in-vivo assessment. *International Journal of Pharmaceutics,* 567, pp. 118415.

SMEETS, A., CLASEN, C. and VAN DEN MOOTER, G., 2017. Electrospraying of polymer solutions: Study of formulation and process parameters. *European Journal of Pharmaceutics and Biopharmaceutics,* 119, pp. 114-124.

WANG, B., CHEN, X., AHMAD, Z., HUANG, J. and CHANG, M., 2019. 3D electrohydrodynamic printing of highly aligned dual-core graphene composite matrices. *Carbon,* 153, pp. 285-297.

WANG, J., JANSEN, J.A. and YANG, F., 2019. Electrospraying: Possibilities and Challenges of Engineering Carriers for Biomedical Applications-A Mini Review. *Frontiers in Chemistry,* 7, pp. 258.

WANG, L., ROITBERG, A., MEUSE, C. and GAIGALAS, A.K., 2001. Raman and FTIR spectroscopies of fluorescein in solutions. *Spectrochimica Acta Part A: Molecular and Biomolecular Spectroscopy,* 57(9), pp. 1781-1791.

XIE, J., JIANG, J., DAVOODI, P., SRINIVASAN, M.P. and WANG, C., 2015. Electrohydrodynamic atomization: A two-decade effort to produce and process micro-/nanoparticulate materials. *Chemical Engineering Science,* 125, pp. 32-57.

YU, M., AHN, K.H. and LEE, S.J., 2016. Design optimization of ink in electrohydrodynamic jet printing: Effect of viscoelasticity on the formation of Taylor cone jet. *Materials & Design,* 89, pp. 109-115.

Chapter 6 Characterisation, *in vitro* and *ex vivo* assessment of coated Microneedles

6.1. Introduction

This chapter involves utilising the selected formulations identified in chapter 4 set at the optimised conditions as outlined by QBD and the following characterisation data. The results shown in this chapter of work demonstrate the *in vitro* and *ex vivo* effect of coating microneedles with these formulations. The resultant electrically atomised coatings were analysed with respect to size, shape and stability, the release of dyes from the coatings and the permeation of dye through human and synthetic skin.

The rationale for the use of dyes was due to their ability to act as model drug. Their ability to fluoresce was another favourable factor. In chapter 5 the results suggested that the HMW polymer solutions yielded fibres and the LMW polymers produced nano-micro sized particles at a concentration of 5% w/v.

6.2. Background

As the skin is considered the largest organ, it possesses many protective mechanisms. This includes the SC, which is known to be the formidable barrier. It is very difficult to penetrate and considered the main obstacle for DD through skin (Davidson, Al-Qallaf et al. 2008, Sebastia-Saez, Burbidge et al. 2020). Many passive enhancement (chemical permeation enhancers (Chen, Y., Quan et al. 2014) and physical enhancement (Donnelly, Ryan, Douroumis 2015)) have been investigated as methods to overcome the SC. Microneedles however provided a safe relatively painless and effective solution for overcoming this barrier and safely being able to administer drug (Ma, Wu 2017).

MNs have gained significant interest as transdermal drug delivery systems with the ability to overcome the SC (Zhao, X., Coulman et al. 2017) and deliver a range of complex macromolecules (Yin, Kuang et al. 2018), peptides (Zhao, X., Coulman et al. 2017), proteins (Yin, Kuang et al. 2018), vaccines (Chen, F., Yan et al. 2017), oligonucleotides, insulin (Larrañeta, Lutton et al. 2016, Donnelly, Ryan F., Singh et al. 2012), ovalbumin, (Ma, Wu 2017) plasmid DNA (Fernando, Zhang et al. 2016), siRNA (Tu, Du et al. 2017), human growth hormone (Yu, W., Jiang, Liu, Li, Chen et al. 2017).

MNs, have the ability to overcome many of the limitations of conventional approaches to TDD. They minimise the production of sharp waste, prevent needle-pricking injuries, are self-administrative, improve patient compliance, have more efficient storage conditions and are more cost effective (Arya, Prausnitz 2016, O'Mahony, Hilliard et al. 2017). However, there are some drawbacks of this application such as potential polymer discharge into the skin upon insertion making it unfavourable with polymeric MNs. Recently, biodegradable polymers such as PLGA, have been incorporated into MNs: following insertion into the skin, these devices can degrade safely. Depending on material choice, it is also possible to alter and modify the release profile of the active ingredient. For example, PVP has been used to provide a rapid release (Lee, I-Chi, Wu et al. 2017, Machekposhti, Soltani et al. 2017). Whilst PLGA and PCL have been shown to provide more sustained release of tenofovir (TFV) a small hydrophilic drug. Various blend ratios of polymers (PCL and PLGA) were investigated to assess the release of TFV (PCL/PLGA 20/80). This blend resulted in a faster release rate (zero order) due to the polymer-drug interactions (Chou, Woodrow 2017).

Based on these findings, assessing the potential of PVP and PCL with dyes acting as model drug encapsulated within the polymeric matrices electrically atomised onto stainless steel MNs seemed the natural route of progression for this research. EHDA was used as the engineering technique for coatings.

6.3 Materials and Methods

6.3.1 Materials

PVP ($4.x10^4$ g/mol and $1.3x10^6$ g/mol) were sourced from Ashland, UK. PCL ($1.4x10^4$ and $8.0x10^4$), Ethanol, DCM, FL and RhB dye and Strat-M were all purchased from Sigma Aldrich, Dorset, UK. All reagents were of analytical grade. Stainless steel microneedles were purchased from AdminPatch California U.S.A.

6.3.2 Methods

6.3.2.1 Solution Preparation

Solutions were prepared as outlined in 5.3.3.2.

6.3.2.2 EHDA Set-up and Optimisation

The system set-up was as specified in 3.2.3.

6.3.2.3 Coating Engineering

Microneedles obtained from AdminPatch with an array of 900 needles measured 800 µm-tall microneedles located within 1 sq. cm circular area. The entire device is 20 mm in diameter and is made of medical-grade SS316L stainless steel. For the preparation of coated polymer MNs, EHDA was used. The polymeric solution containing the dye was loaded into a syringe fixed to a pump, which allowed the controlled infusion of the solution throughout the system. The syringe was connected to a conducting stainless-steel needle via silicone tubing. The resulting atomised structures were collected on both microscope slides and MNs.

6.3.2.4 Characterisation of Dye Loaded MNs

6.3.2.4.1 Imaging

Following the results from chapter 5 which was according to the QbD DOE experiments MNs were coated with the selected formulations (5% w/v). This allowed the most optimal process parameters to be selected for each formulation. SEM micrographs was taken for these samples including the coated MNs. SEM was carried out according to the method specified in 3.2.3

6.3.2.4.2 Goniometry

Contact angle of all 8 formulations were characterised using a ThetaLite T100 contact angle goniometer; using OneAttension software to analyse data. 10 µL of distilled water droplets were used. Each sample was carried out and assessed in Sessile Drop mode in triplicate and an average was obtained.

6.3.2.4.3 In Vitro Release and Kinetics

Drug release of the optimised nanoparticles was analysed using UV spectroscopy. A phosphate buffered saline (PBS) medium was used to carry it out. Vials containing 10 mL of PBS) and 10 mg of sample (dyes) was constantly stirred at 90 rpm. At predetermined time points, 1 mL of release was retracted and replaced with 1 mL of fresh PBS at physiological conditions (37 °C). Drug release was determined using UV spectroscopy absorbance with a set wavelength of $\lambda = 494$ nm (for FL) or $\lambda = 595$ nm (for RhB). This was carried out in triplicate and an average was taken. The data collected from these *in vitro* studies were plotted in different kinetic models to assess the release kinetics of dyes from the atomised polymeric coatings.

6.3.2.4.4 Ex-Vivo Franz Diffusion Studies

Transdermal diffusion of dyes was assessed using Franz diffusion cells (Copley Scientific, Nottingham, UK) with a diffusion surface area of 1.77cm^2. Strat M membrane (purchased from Sigma Aldrich) was first punctured with the coated MN manually for a minimum of 10 seconds (up to 30 seconds) until all needles had penetrated/breached the membrane, it was then removed, and the membrane was placed between the donor and receptor compartment (which was filled with 12 mL of PBS and a mini stirrer). The Franz cells were maintained at 37 ± 0.5 °C. An aliquot of 1 mL of sample was withdrawn from the receiver chamber at predetermined intervals and replaced with 1 mL fresh PBS. This receiver solution was agitated using a stirrer bar and magnetic stirrer at 400 rpm to ensure homogeneity throughout the experiments. In avoidance of evaporation the donor cells were covered with parafilm. The experiment was carried out in triplicate for each dye loaded MN. The samples were immediately centrifuged following collection at a speed of 14,000 rpm and the supernatant was analysed. UV spectroscopy (λ = of 494 nm (for FL) or λ = 595 nm (for RhB) was used to analyse samples. The cumulative amount of drug permeating through Strat M was plotted as a function of time.

6.3.2.4.5 Confocal Laser Scanning Microscope Imaging Studies

The permeation experiment was carried out for each dye loaded MNs. After 24h, the formulations were removed from the donor compartment and the Strat-M® membranes were removed and wiped gently from the Franz cells. The membranes were placed immediately on a glass slide, covered with a glass slide and examined with laser scanning confocal microscope [43]. Z-stack images were acquired by stepwise scanning of each membrane from its top to the equatorial plane at 1.16 μm steps with a 63× oil-immersion lens under a Zeiss LSM 780 CLSM (Carl Zeiss Microscopy GmbH, Berlin, Germany) with the appropriate filters. Images were obtained with ZEN 2011 software.

Statistical analysis ANOVA (one–way analysis of variance) was carried out. A significance level of $p < 0.05$ was considered for the differences in results between formulations.

6.4 Results and Discussion

6.4.1 Solution Characterisation and EHDA optimisation

High and low molecular weight 5% w/v PVP solutions at 5% and high and low molecular weight 5%w/v PCL solutions were formulated with and without dye (FL and RhB respectively) and characterised in chapter 5.4.2 and 5.4.3.

6.4.2 Coating characterisation

6.4.2.1 Imaging

Figure 46 displays the morphology of coated MNs with all 8 formulations. Figure 46A shows sparsely coated MNs with the majority of the coating concentrated at the tips (F1) this is quite similar to that found in F2. This can also be due to the deposition distance during the spraying process. As Figure 46E and 46F show a more even coating with PCL particles. The dye loaded F6 PCL particles appear more densely coated (Fig 46F). Fig 46C and 46D display the PVP fibre coated MNs (F3 and F4), with the dye loaded MNs appearing as dense as the polymer alone. The fibres appear very dense and smooth on both. Figure 46G has beaded fibres present with the polymer alone however it is more densely coated in Figure 46H with slightly less beading.
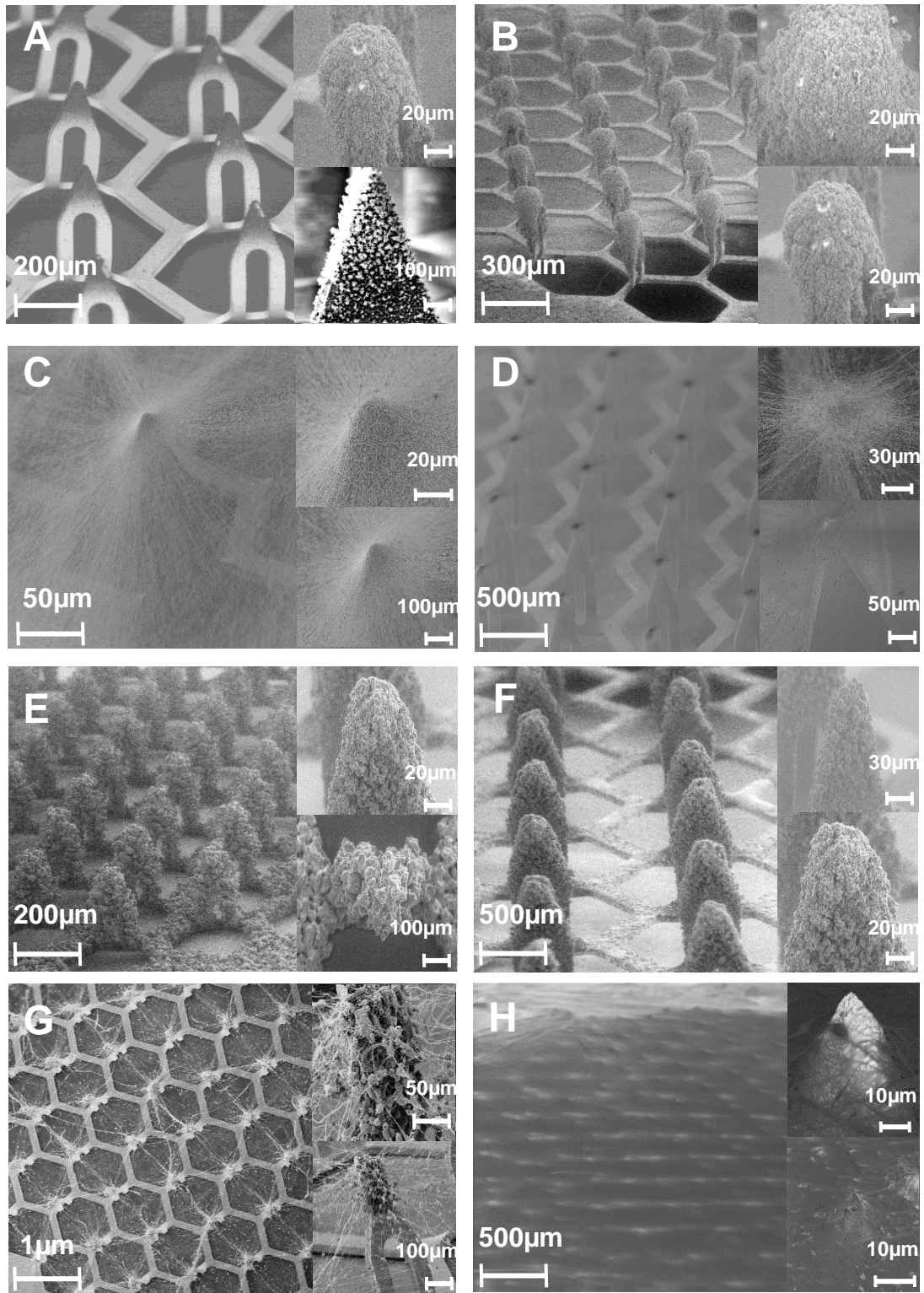
Figure 46: SEM images of coated MNs. A) F1, B) F2. C) F3, D) F4, E) F5, F) F6, G) F7 and H) F8

6.4.2.2 Morphology and Size Distribution

The demand for nano-micro range sized particles has rapidly increased in pharmaceuticals. This revolution has created the need for particles which can be utilised for a range of applications and drug delivery routes. Due to the small sizes and ability to act as carriers when within the nano size range (due to increased surface are to volume ratio) more drug can be delivered. SmartTiff software was used alongside SEM to obtain particle/fibre size distribution. .

The particle size distribution graph for ES PVP and PCL particles shown in Figure 47A are negatively skewed which is desirable. The majority of particles were within the nano size range and this coincides with the PD whereby this value reflects a narrow nanoparticle size distribution with the value closer to 100 nm. This can be seen as important parameters in the QTPP profile and so is a major factor in DOE analysis and the response surface profiles. The average particle size for F1,F2,F5 and F6 were 0.39 ± 0.0791, 0.45 ± 0.0404, 0.57 ± 0.0256 and 0.63 µm ± 0.0435, respectively. There was a significantly larger proportion of PCL particles (F5 and F6) within the larger size ranges which could be due to agglomeration as a result of rapid solvent evaporation experienced with DCM (Xie, Jiang et al. 2015). However, on the whole there was a larger frequency of PVP and PCL particles within the smaller size ranges. This is what was desired and what the criteria listed in Chapter 5. This shows that QBD has been a useful tool in the optimisation of particles. Research supports these findings as particles with small size distributions have a high level of effectiveness in their application

The average fibre diameter for F3,F4,F7 and F8 were 8.80 ± 0.7549, 9.6 ± 0.7937, 11.1 ± 0.4163 and 12.7 ± 0.5033. The fibre diameter graph shows even size distribution within the nano and micro range (Figure 47B) which enables them to mimic the extracellular matrix (Bongiovanni Abel, Liverani et al. 2019). This demonstrates the relevance of QBD and the ability to yield optimised structures by taking a more systematic approach.
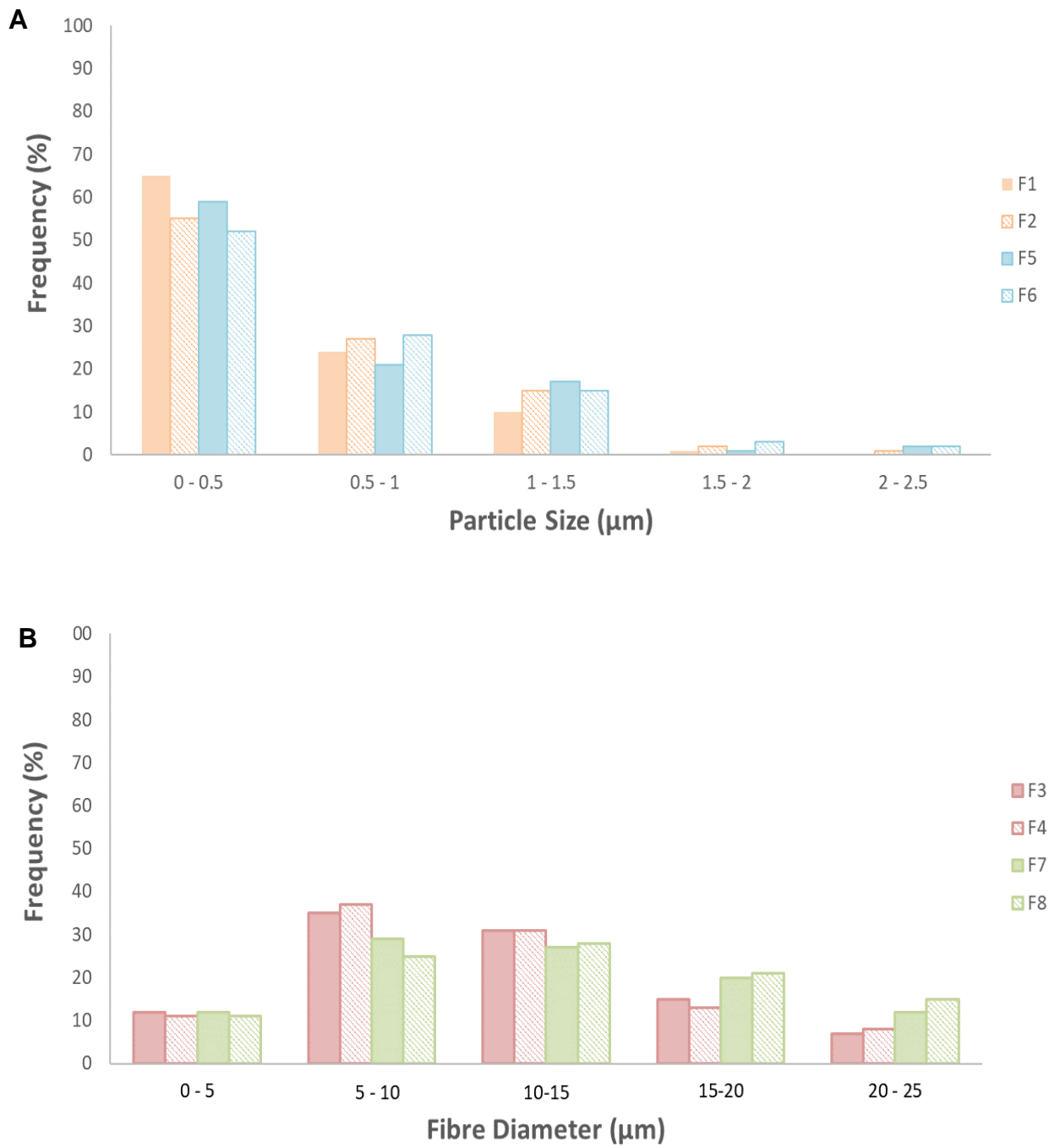
Figure 47: Particle size distribution and B) Fibre diameter distribution
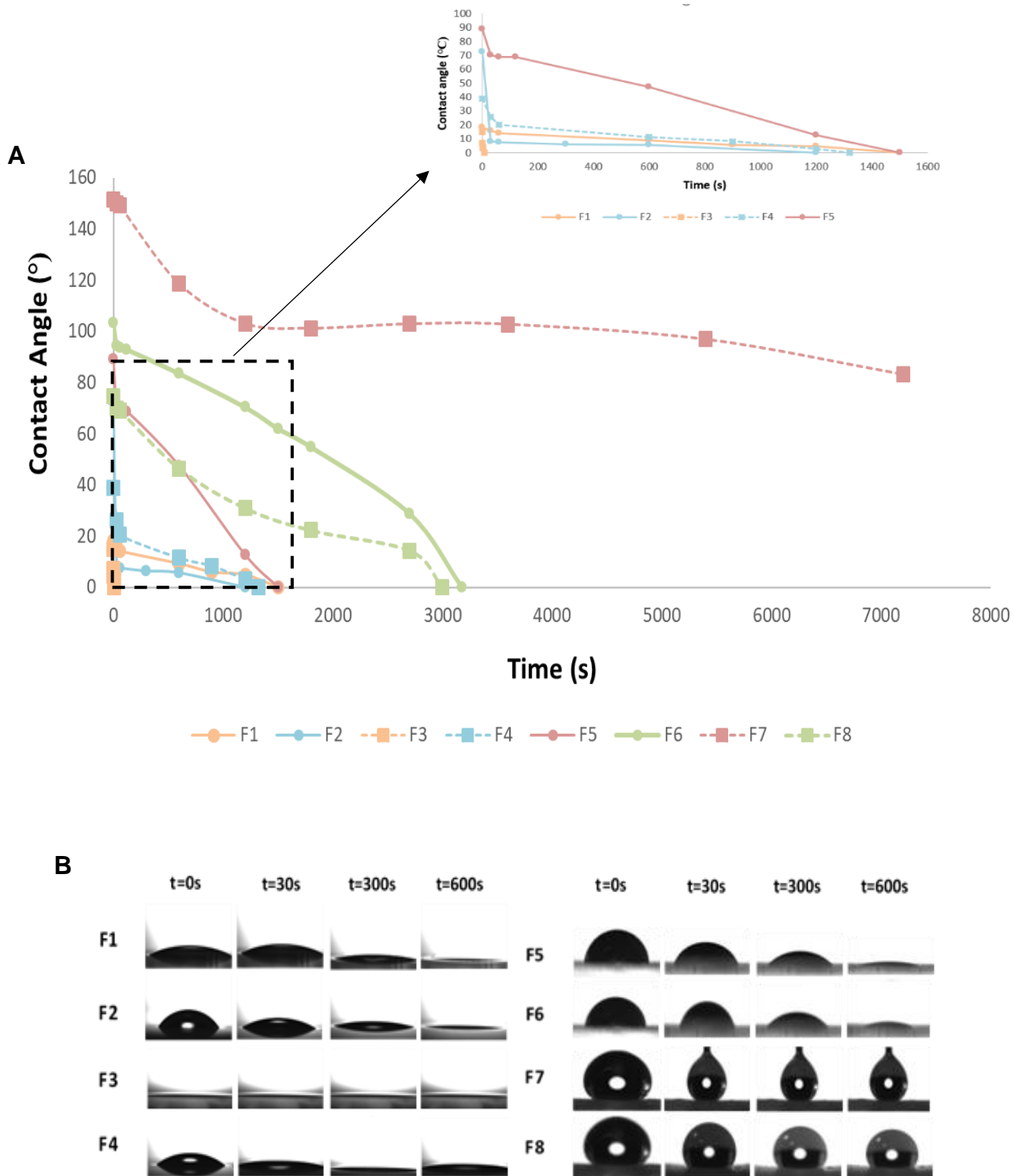
6.4.3 Goniometry

Contact angle (CA) has a major impact on drug release from a device/system and the materials surface is the first point of contact with the biological surroundings. It provides quantitative measurements of the wetting of a solid which is liquid (water is commonly used). Angles lower than 90 ° indicate high wettability whilst angles larger than 90 ° indicate poor wettability. CA was necessary in this study to measure the interaction between the polymeric coatings alone and when included with a dye as these varied in structure (particular/fibrous) they would determine the release and detachment from MNs (Figure 48). The wettability of the surface of the electrically atomised samples were characterised and analysed over time. This included hydrophilic (PVP) and hydrophobic (PCL) particles and fibres making it a potential carrier drug delivery system providing controlled rapid/sustained drug release (Wang, Baolin, Ahmad et al. 2018).

It has been reported that with increasing molecular weight of PVP that the density increases, and the water content decreases (Bensaadi, Arous et al. 2016). This supports the findings in Figure 48 F3 and F4 are the higher molecular weight PVP samples, and the contact angle measurements as seen in Figure 48A is much higher at 0 seconds (14.98 and 39.01° respectively) in comparison to the lower molecular weight PVP F1 and F2. PVP is a more hydrophilic polymer hence the rapid dissipation.

PCL has gained its notoriety being easily accessible, easy to process, good mechanical strength and biodegradation. From the results it is apparent that compared to the PCL polymer alone the dye inclusion further increased the contact angle. This is due to the hydrophobicity of PCL which was improved when modified (Liu, Q., Wang et al. 2019). Its hydrophobicity has a whole host of effects including the adherence of proteins onto a surface thus suggesting optimal contact angle measurements needed for certain applications. Although the surface tension did not vary massively between the PCL formulations, the contact angle for fibres was lower with F8 as their fibre diameter increased more than F7.

F8 is classed as super hydrophobic (Ghobeira, Philips et al. 2019). The higher CA values in comparison to PVP can also be due to PCL stability and resistance to degradation by the deionized water. It's been reported that the test medium, porosity and test medium can all significantly impact CA behaviour (Wang, Baolin, Ahmad et al. 2018).

Figure 48: Contact angle analysis over time for all formulations and B) Digital images taken during contact angle measurements over time for all formulations

6.4.4 In Vitro Release

In vitro release study results are shown in Figure 49. The PVP particle (F2) formulation displayed 100% of FL dye was released within 120 minutes (2 hours) with initial burst release similar to the trend shown with (F4) PVP fibre formulations as FL dye showed 100% release within 300 seconds (5 hours). At 120 minutes, the proportion of drug released was 100%; this satisfies the original QTPP where 75% or more of the drug should have been released before 4 hours. At 30 minutes, approximately 94% of the drug had been released for both F2 and F4; after this point, a plateau had reached as the majority of the drug had already been released. These results are similar to what is reported in literature. Rapid release profiles are associated with PVP with one study reporting up to 100% drug release with PVP coated formulations within 15 minutes (Gumaste, Freire et al. 2017). The slightly longer delay can be attributed to FL. The error bars displayed on the graph above are also narrow suggesting that there was little variation when performing each individual test run and this suggests that the results obtained are both reliable and reproducible.

RhB possesses a distinctive and strong absorption peak, which offers an accurate concentration analysis using UV spectroscopy. The initial burst (1 minute) of shows 44% of RhB being released, which can be observed. An initial burst resulted from the large surface area to volume ratio of the Np, in addition to the surface loading of RhB. From 2 – 10 minutes, the release gradually increases from 44% to 52%. After 10 minutes, the drug released slowly with a total of 75% released after 4 hours. The delayed release was due to the opposing effects of the hydrophobicity of PCL and hydrophilicity of RhB. This hindered the release of RhB thus presenting a sustained release profile. Moreover, the QTPP necessitated a sustained release of RhB over a minimum of 7 days. Approximately, 100% of RhB was released after 7 days, which resonates with the QTPP target for the release profile. The release profile was further confirmed by Cao et al in 2014 where the release profile of RhB from PCL was measured in a study investigating the 'dual drug release from core-shell nanoparticles (Cao,

Wang et al. 2014). The rapid release of PVP formulations in comparison to the sustained release profiles shown with PCL has support from the well documented research of these polymers within the research community.
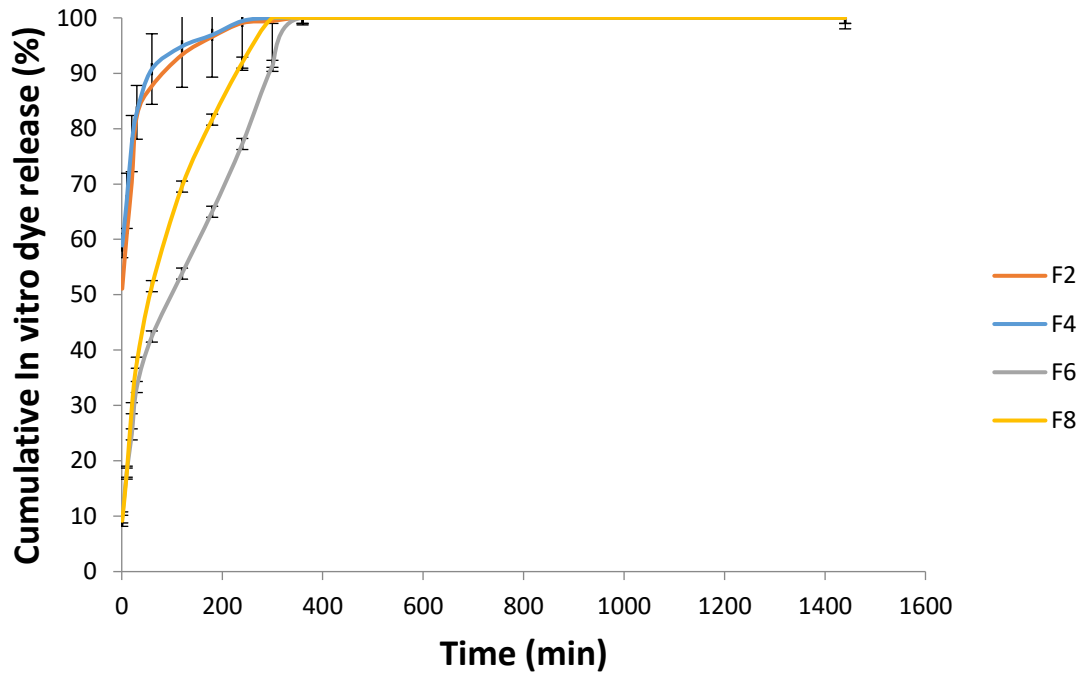

Figure 49: Cumulative In vitro release of dyes from F2, F4, F6 and F8

6.4.5 Release Kinetics

The data from the *in vitro* release of dyes was applied to different kinetic models to determine the most prominent mechanism of dye release from the ES/ESP particles/fibres. The data was fitted to zero-order, first-order, Higuchi and Korsmeyer-Peppas models with the regression values and relevant component values being recorded and the corresponding plots seen in Figure 50A-D.

Drug diffusion must occur in one direction with the initial drug concentration in the polymeric matrix must be higher than the solubility of drug. The swelling capability of the polymeric matrix and dissolution must be negligible, and the drug particles must be smaller than the matrix (Siepmann, Peppas 2011). If perfect sink conditions have been met as well as the set criteria then the Higuchi model can be applied (Paul 2011).

The Korsmeyer-Peppas model is most useful when there are multiple release mechanisms involved (Ritger, Peppas 1987). A release exponent, n, determines the mechanism of drug release. There can be various n values and each depict specific release mechanisms; $n \leq 0.45$ corresponds to quasi-Fickian drug transport, $n = 0.5$ shows Fickian diffusion (molecular diffusion of drug due to a chemical potential gradient), $0.45 < n < 0.89$ relates a Non-Fickian diffusion mechanism, $n = 0.89$ relates to the case II transport with $n > 0.89$ corresponds to the super case II transport (Korsmeyer, Gurny et al. 1983).
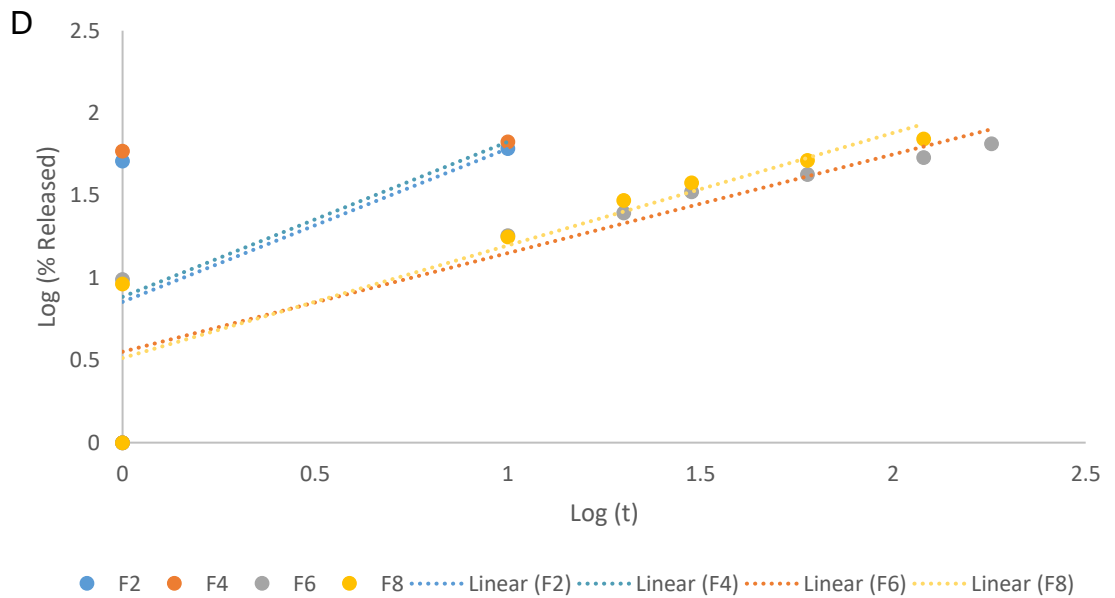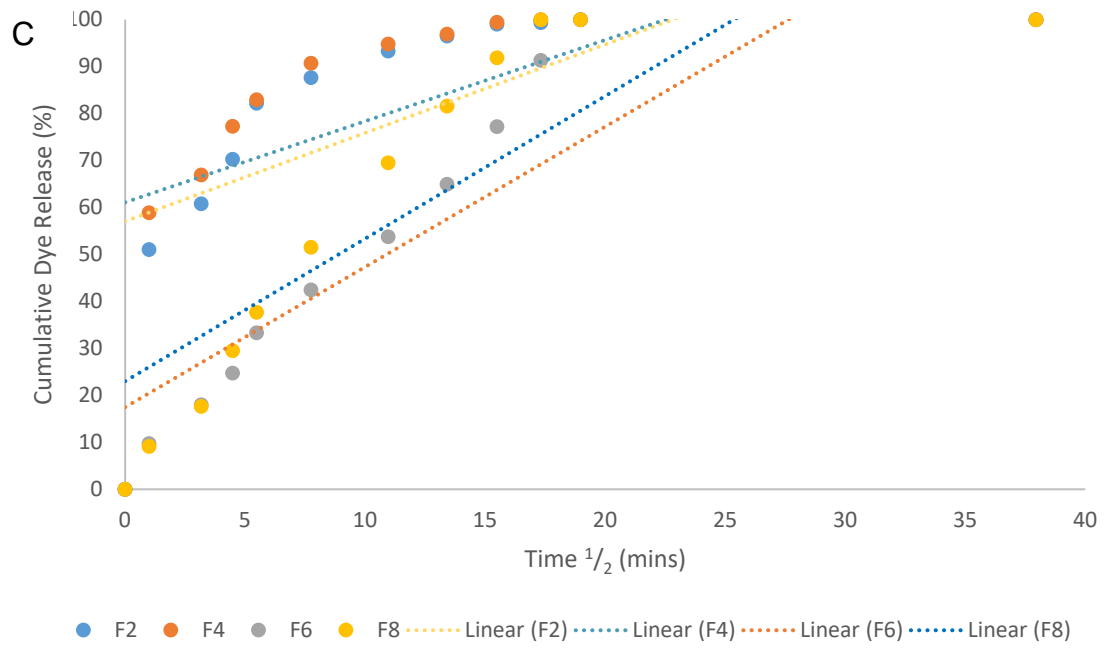
A

B
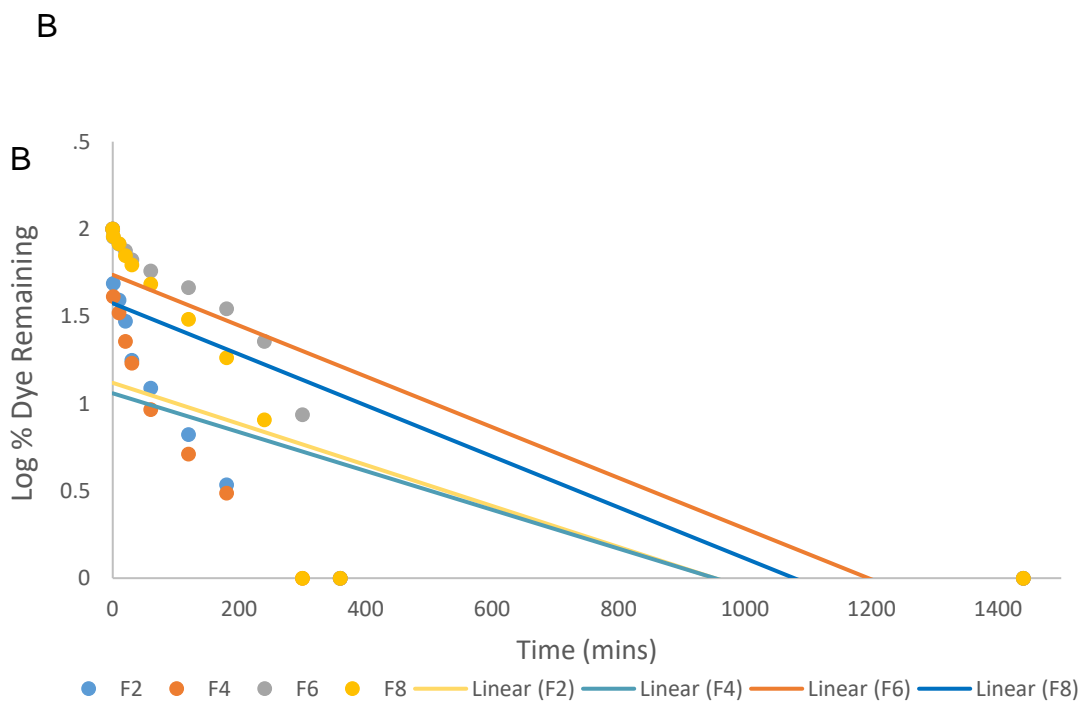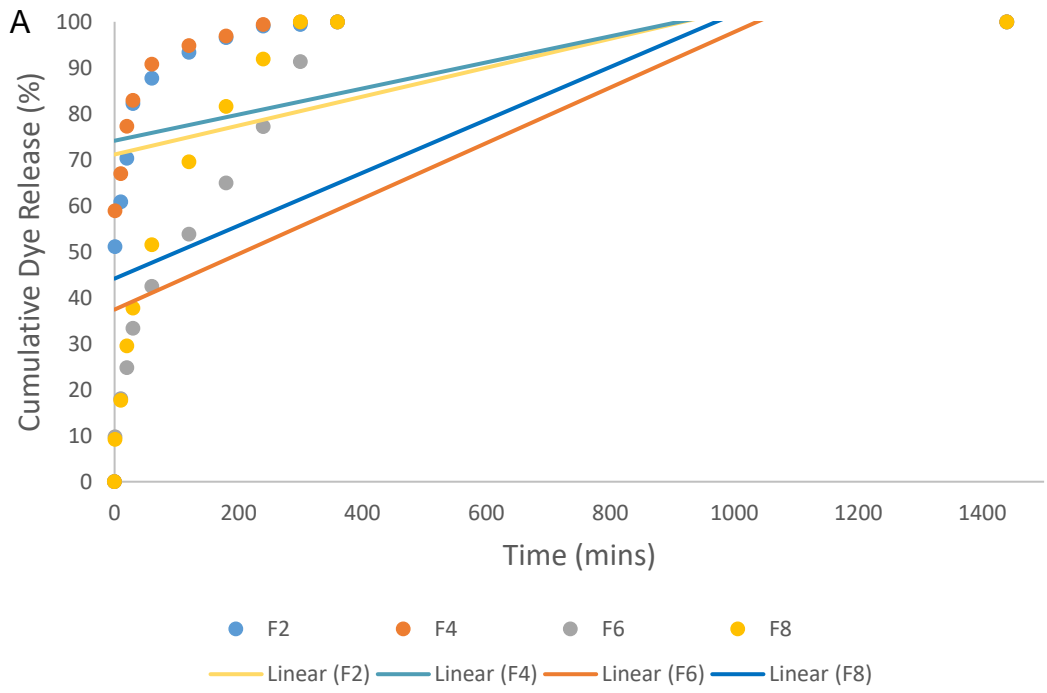
Figure 50: Model fitting (A) Zero order, (B) First order, (C) Higuchi, (D) Korsmeyer-Peppas model

195

Table 16: Release kinetics for dye loaded formulations

Formulation	Zero Order	First Order	Higuchi	Korsmeyer-Peppas R^2	n
F2	0.1797	0.3646	0.4449	0.2833	0.93
F4	0.1543	0.3481	0.3951	0.2736	0.9408
F6	0.3707	0.6559	0.7898	0.7786	0.5591
F8	0.4671	0.5232	0.7132	0.7953	0.6206

The low R^2 values (Table 16) obtained from zero-order and first order models suggest a poor fit for this type of release kinetics. This suggests that the drug concentration had no effect on the release of dye from the coating. These were relatively higher (close to 1) R^2 values for all 4 formulations from Higuchi model analysis which suggests the dyes were released via Fickian diffusion: more specifically quasi-Fickian diffusion. From applying the release data to Korsmeyer-Peppas model the n values for F6 and F8 fall between the 0.5-0.89 ranges and so indicates anomalous case II transport kinetics. The n values for F2 and F4 is >0.89 so it is considered as super case II non- Fickian diffusion (Jain, Jain 2016). Richard Korsmeyer supports the findings for F2 and F4 which have very high (close to 1) n values with research of release from hydrophilic polymers like PVP and the ratio of tracer/excipient. The role of the dynamic swelling and dissolution of the polymeric matrix on the release mechanism (Korsmeyer, Gurny et al. 1983). PCL fibres also showed non-fickian diffusion which is supported by Baolin Wang et al's research (Wang, Baolin, Ahmad et al. 2018).

6.4.6 SEM analysis of Strat-M® membrane and coated microneedles post insertion

In comparison to human skin, synthetic membranes offer many advantages including-controlled membrane thickness, rapid preparation time, homogeneity, more economic and requiring less storage space (Pontes-López, Moreno et al. 2020). Human SC is usually the rate-limiting step for successful active pharmaceutical ingredient (API) delivery. Strat-M® has been designed to encompass similar structural and chemical characteristics found in the human epidermis. Simon et al demonstrated a similar permeation profile of Rivastigmine using Strat-M® compared with pig ear skin (Simon, Amaro et al. 2016). Takashi et al also reported similar diffusion and partition parameters of chemicals in Strat-m® were similar to that found in excised human and rat skin. Further suggesting its use in permeation studies as an alternative to animal or human skin (Uchida, Kadhum et al. 2015).

Figure 51 displays SEM micrographs of the Strat-M® membranes and the coated MNs that were used for permeation studies. The micrographs show the morphology of the synthetic membrane as well as MNs post insertion. In figure 51A the membrane appears very smooth and from the side the layers are visible. The pierced membranes in figure 51Bi), Ci), Di), Ei) show that cavities have been created as the inset pictures show clear holes created by the microneedles whereby the coating is able to permeate through for permeation and drug delivery. As seen in figure 51Bi) and Di), there was a limited number of particles surrounding the pierced craters that have been formed; showing the coating had not accumulated here.

The MNs post insertion show sparse coating on the majority of MNs. The MN tips show near enough no coating suggesting successful insertion and that the dye was able to permeate through from the formulation which was desired. There are some particles on figure 51Cii and 51Dii below the tip suggesting not all of the formulation was able to penetrate through the film. MNs hosting fibrous coatings

however showed no coating remaining on the MN tips. There is a limited quantity of particulae-fibrous structures remaining, but this supports the phenomena whereby upon insertion, the fibres are dragged through the skin. The integrity of MNs was significantly different with each MN. MNs coated with F6 (figure 1G) shows an agglomeration of PCL particles potentially due to rapid solvent evaporation.
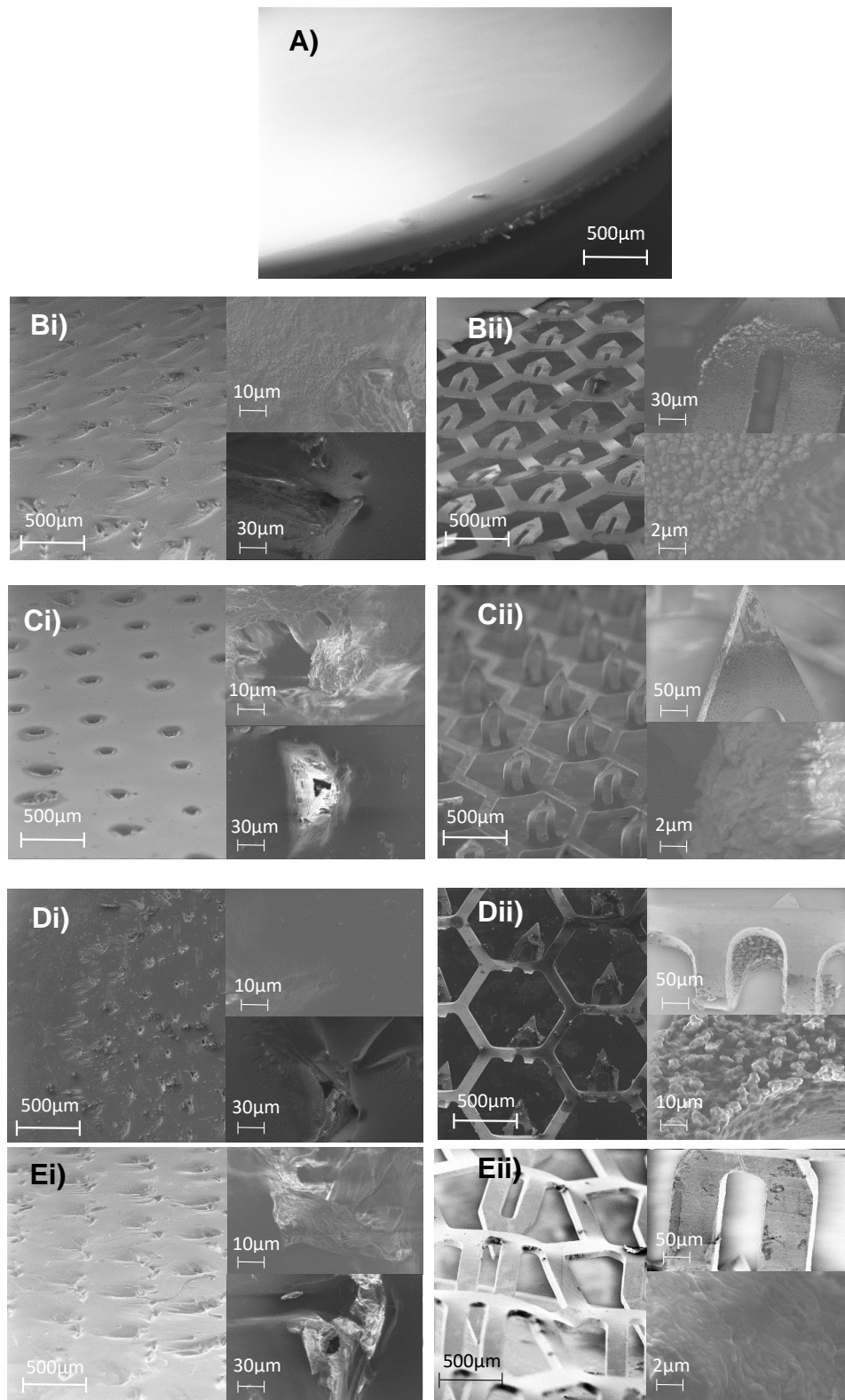
Figure 51:SEM micrograph of (A) unpierced Strat-M®, SEM Micrographs showing i) Strat-M® membrane and ii) coated microneedles post-insertion for (B) F2, (C) F4, (D) F6 &(E) F8

6.4.7 Transdermal Permeation Studies

Permeation studies of dyes across a synthetic skin membrane (Strat-M®) *in-vitro* was carried out using coated stainless-steel microneedles. The conclusion of the experiment led to the production of graphs displaying the cumulative amount of model dye permeating the skin over time (Figure 52). The drug permeation shown in Figure 52 showed that there was significant drug permeation within 6 hours from MN coatings (for F2, F4, F6, F8 was 60, 96, 27 37 $\mu g/cm^2$ respectively). These results show better permeation with fibrous MN coatings.

Table 17: Franz permeation for dye loaded formulations

	F2	*F4*	*F6*	*F8*
Steady state flux ($\mu g/cm^2/h$)	4.9017	5.73729	7.0779	4.5203
Apparent permeability coefficient (cm^2/h)	0.6365	0.8423	0.8925	0.8748

The state flux values (Table 17) for F4 and F8 which are the ESP dye loaded polymer formulations exhibited higher flux values (5.7373 and 4.5203 $\mu g/cm^2/h$ respectively) compared to the ES particle coated MNs F2 and F4 (4.9017and 4.5203 $\mu g/cm^2/h$ respectively). There was a significant difference in the permeation of PVP fibres in comparison to the other formulations and this can be attributed to molecular dispersion of dye within PVP. With the fast swelling of porous nano sized fibres and large surface area allowing the fluorescein dye to leach out. This can also be due to the reduction in the amount of polymer which behaves as a diffusion barrier for the dye hence an increase in dye release (Kamble, R. N., Gaikwad et al. 2016). Ronnader et al's research supports the findings with a similar release profile with higher molecular weight PVP and sumatriptan loaded MNs. It was also reported that there was a twofold increase in cumulative drug release over a 24 hour period by increasing the sumatriptan

succinate concentration by a factor of 2 (Ronnander, Simon, Spilgies, Koch, and Scherr 2018, He, Zhong et al. 2018).

In vitro release is not the only issue that can have an impact on skin permeation of a drug. It is also possible that the interaction of the nanoparticles with the SC is responsible for the greater or smaller increase in drug skin permeation. A good deal of research has been carried out with respect to the behaviour of surfactants and oleic acid as permeation enhancers. Oleic acid has the ability to interact with the ceramide head groups of the SC destroying the hydrogen bonding of the lipid bilayers and in turn enhancing drug skin permeation (da Rocha, Souza et al. 2019, Hathout, Elshafeey 2012).
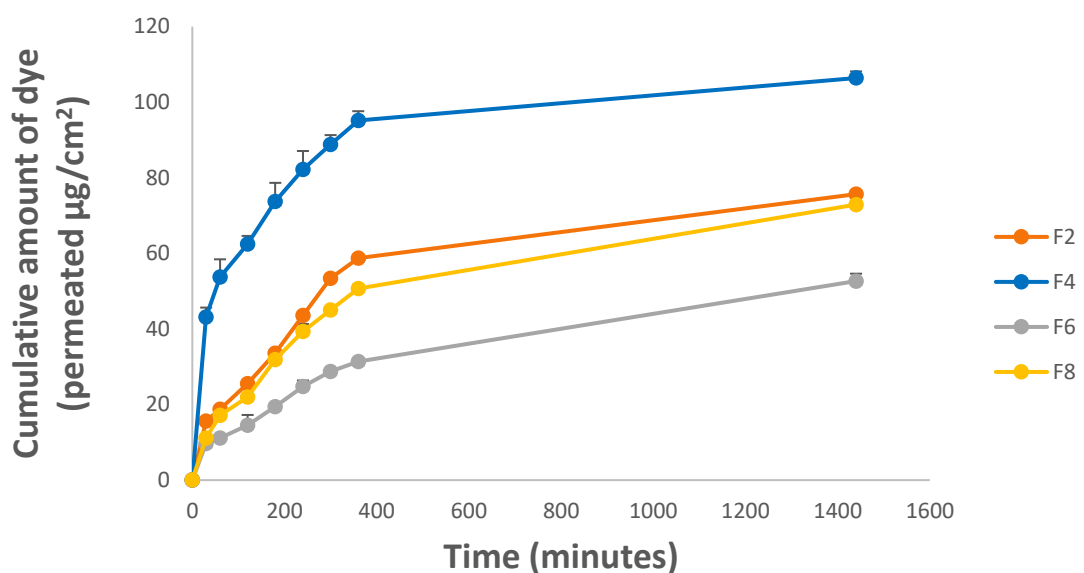

Figure 52: Cumulative drug permeation over time

6.4.8 Confocal Laser Scanning Microscope Imaging

The distribution of FL and RhB in the Strat-M® membrane was visualized confocal laser scanning microscopy (CLSM). The strong green signal is attributed to the fluorescein while the red signal is attributed to RhB. CLSM is often used as an imaging technique for further information about transdermal permeation such as the extend and the penetration route. Figure 53 demonstrates Z stack images of the Strat-M® membranes pierced with (A) F2, (B) F4, (C) F6 & (D) F8 MNs. High fluorescence intensities were maintained across the membrane in all formulations while F8 and F4 seem to have a more intense signal especially in lower depth. CLSM imaging indicates the high potential of the investigated MNs for transdermal delivery. Moreover, Figure 53 reveals the size and shape of the MNs while the tip of the microneedle reaches the lowest depth (z=10).
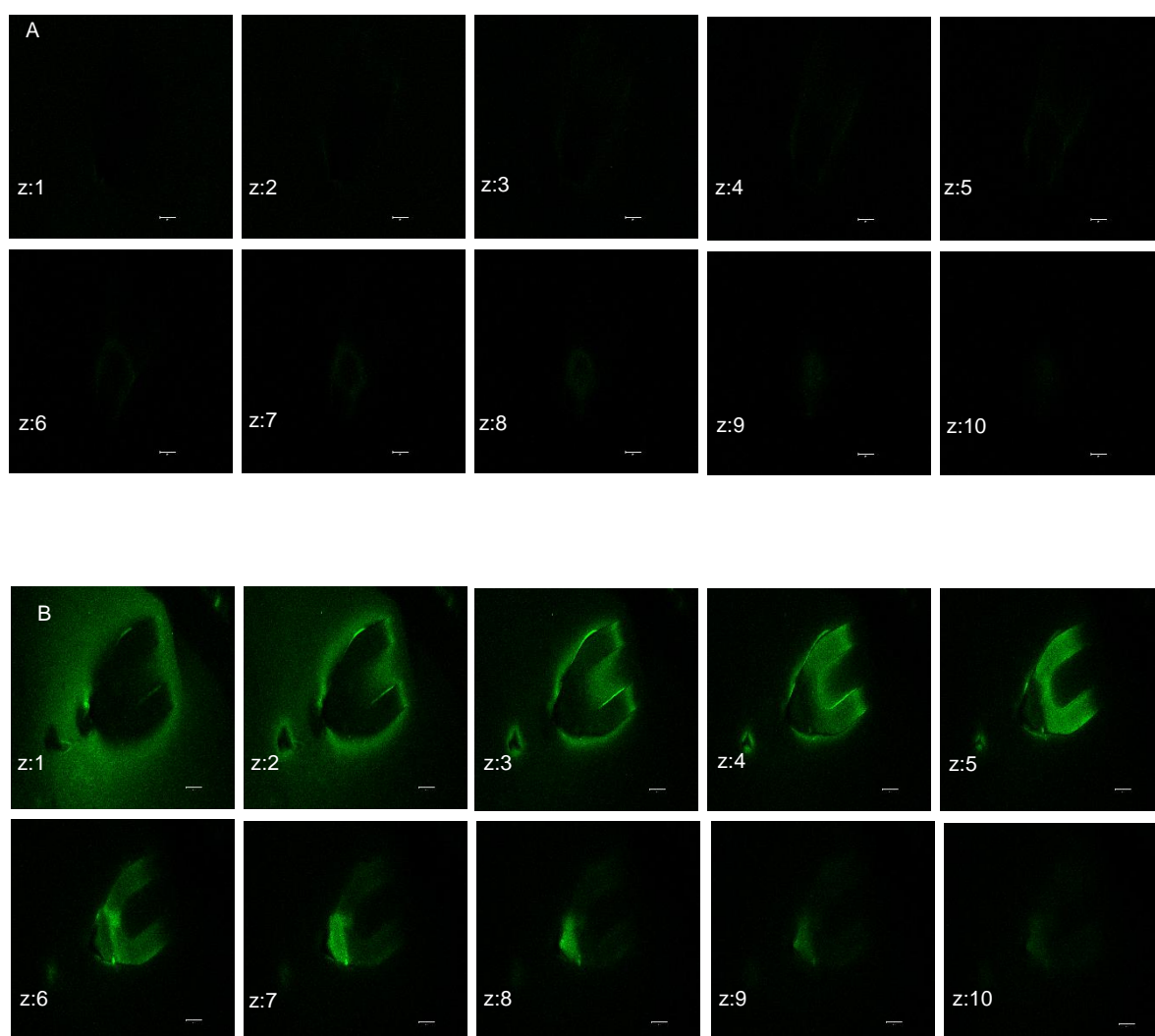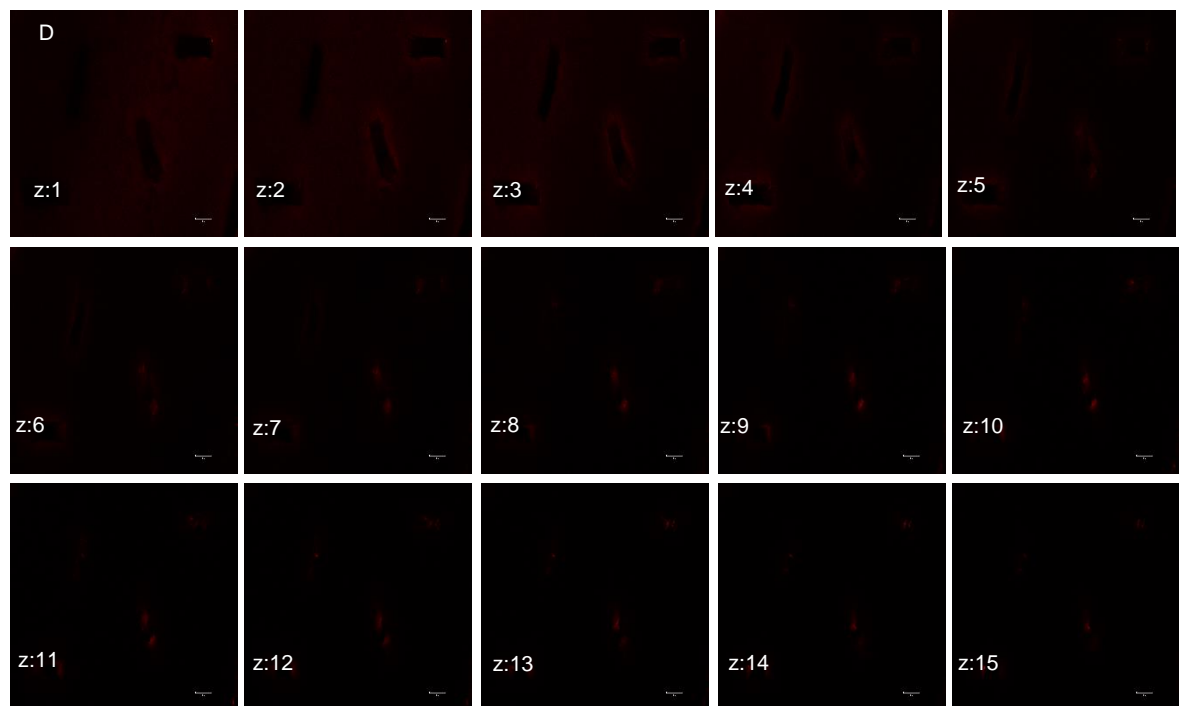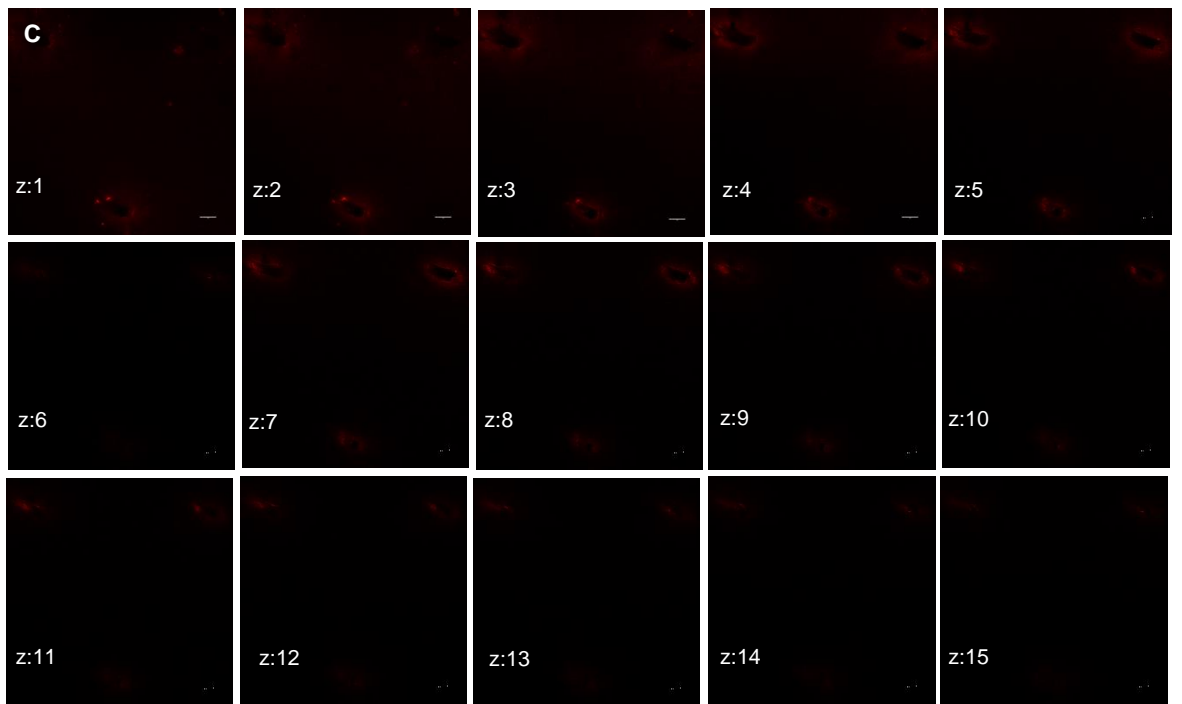
Figure 53 CLSM (63 x objective) Z stack images of the Strat-M® membranes pierced with (A) F2, (B) F4, (C) F6 & (D) F8 MNs scale bar 10 µm

203

6.5 Conclusion

This study demonstrated the effects of different polymeric MN coatings loaded with dye. The results from Chapter 5 aided the findings in this chapter. Due to the characterisation of solutions and the application of QBD principles to make the EHDA process more robust. The flow rate and applied voltage for F2 and F6 was achieved at 15 µl/min, 15 cm and for F4 was 20 µl/min, 10 cm and for F8 it was 50 µl/min and 10 cm. The applied voltage for these formulations was between 10-20 kV. This yielded optimised MN coatings containing dye (model drug) were atomised all within the nano-micron range. MNs were utilised in this study as these systems can successfully bypass the SC thus providing efficacious TDD.

The resultant atomised ES/ESP particular and fibrous structures were assessed and characterised. Morphological studies exhibited primarily smooth fibres with PVP and some beaded fibres with the PCL formulation and spherical particles. However, the size distribution shows that the majority were still in the nano-micron range which was what was identified in the QTPP. The drug skin permeation results showed that the *in-vitro* delivery of dye in the receiver compartment after a few hours was quite high. These results demonstrate that the MN shafts successfully pierced the Strat-M® (synthetic skin) membrane and dissolved thus releasing a high percentage of their drug load. These results show great promise for the polymers to act as a matrix for model drug. This shows that coated stainless steel microneedles can be utilised for a whole host of applications. The fact that the dye was successfully incorporated suggests it could also be used as a tracer alongside a drug which is beneficial for release and permeation studies. As expected, the dye did not adversely affect, the Es and Esp process which was what QBD data suggested. Alternatively, permeation can potentially be improved with the inclusion of a permeation enhancer which can enhance drug skin permeation.

6.6 References

ARYA, J. and PRAUSNITZ, M.R., 2016. Microneedle patches for vaccination in developing countries. *Journal of Controlled Release,* 240, pp. 135-141.

BENSAADI, S., AROUS, O., KERDJOUDJ, H. and AMARA, M., 2016. *Evaluating molecular weight of PVP on characteristics of CTA membrane dialysis.*

BONGIOVANNI ABEL, S., LIVERANI, L., BOCCACCINI, A.R. and ABRAHAM, G.A., 2019. Effect of benign solvents composition on poly(ε-caprolactone) electrospun fiber properties. *Materials Letters,* 245, pp. 86-89.

CAO, Y., WANG, B., WANG, Y. and LOU, D., 2014. *Dual Drug Release from Core–Shell Nanoparticles with Distinct Release Profiles.*

CHEN, F., YAN, Q., YU, Y. and WU, M.X., 2017. BCG vaccine powder-laden and dissolvable microneedle arrays for lesion-free vaccination. *Journal of Controlled Release,* 255, pp. 36-44.

CHEN, Y., QUAN, P., LIU, X., WANG, M. and FANG, L., 2014. Novel chemical permeation enhancers for transdermal drug delivery. *Asian Journal of Pharmaceutical Sciences,* 9(2), pp. 51-64.

CHOU, S. and WOODROW, K.A., 2017. Relationships between mechanical properties and drug release from electrospun fibers of PCL and PLGA blends. *Journal of the Mechanical Behavior of Biomedical Materials,* 65, pp. 724-733.

DA ROCHA, P.B.R., SOUZA, B.D.S., ANDRADE, L.M., DOS ANJOS, J.L.V., MENDANHA, S.A., ALONSO, A., MARRETO, R.N. and TAVEIRA, S.F., 2019. Enhanced asiaticoside skin permeation by Centella asiatica-loaded lipid nanoparticles: Effects of extract type and study of stratum corneum lipid dynamics. *Journal of Drug Delivery Science and Technology,* 50, pp. 305-312.

DAVIDSON, A., AL-QALLAF, B. and DAS, D.B., 2008. Transdermal drug delivery by coated microneedles: Geometry effects on effective skin thickness and drug permeability. *Chemical Engineering Research and Design,* 86(11), pp. 1196-1206.

DAYANA, I., SEMBIRING, T., TETUKO, A.P., SEMBIRING, K., MAULIDA, N., CAHYARANI, Z., SETIADI, E.A., ASRI, N.S., GINTING, M. and SEBAYANG, P., 2019. The effect of tetraethyl orthosilicate (TEOS) additions as silica precursors on the magnetite nano-particles (Fe3O4) properties for the application of ferro-lubricant. *Journal of Molecular Liquids,* 294, pp. 111557.

DONNELLY, R.F., SINGH, T.R.R., GARLAND, M.J., MIGALSKA, K., MAJITHIYA, R., MCCRUDDEN, C.M., KOLE, P.L., MAHMOOD, T.M.T., MCCARTHY, H.O. and WOOLFSON, A.D., 2012. Hydrogel-Forming Microneedle

Arrays for Enhanced Transdermal Drug Delivery. *Advanced Functional Materials,* 22(23), pp. 4879-4890.

DONNELLY, R. and DOUROUMIS, D., 2015. Microneedles for drug and vaccine delivery and patient monitoring. *Drug Delivery and Translational Research,* 5(4), pp. 311-312.

FERNANDO, G.J.P., ZHANG, J., NG, H., HAIGH, O.L., YUKIKO, S.R. and KENDALL, M.A.F., 2016. Influenza nucleoprotein DNA vaccination by a skin targeted, dry coated, densely packed microprojection array (Nanopatch) induces potent antibody and CD8+ T cell responses. *Journal of Controlled Release,* 237, pp. 35-41.

GHOBEIRA, R., PHILIPS, C., LIEFOOGHE, L., VERDONCK, M., ASADIAN, M., COOLS, P., DECLERCQ, H., DE VOS, W.H., DE GEYTER, N. and MORENT, R., 2019. Synergetic effect of electrospun PCL fiber size, orientation and plasma-modified surface chemistry on stem cell behavior. *Applied Surface Science,* 485, pp. 204-221.

GUMASTE, S.G., FREIRE, B.O.S. and SERAJUDDIN, A.T.M., 2017. Development of solid SEDDS, VI: Effect of precoating of Neusilin® US2 with PVP on drug release from adsorbed self-emulsifying lipid-based formulations. *European Journal of Pharmaceutical Sciences,* 110, pp. 124-133.

HATHOUT, R.M. and ELSHAFEEY, A.H., 2012. Development and characterization of colloidal soft nano-carriers for transdermal delivery and bioavailability enhancement of an angiotensin II receptor blocker. *European Journal of Pharmaceutics and Biopharmaceutics,* 82(2), pp. 230-240.

HE, P., ZHONG, Q., GE, Y., GUO, Z., TIAN, J., ZHOU, Y., DING, S., LI, H. and ZHOU, C., 2018. Dual drug loaded coaxial electrospun PLGA/PVP fiber for guided tissue regeneration under control of infection. *Materials Science and Engineering: C,* 90, pp. 549-556.

JAIN, A. and JAIN, S.K., 2016. In vitro release kinetics model fitting of liposomes: An insight. *Chemistry and Physics of Lipids,* 201, pp. 28-40.

KAMBLE, R.N., GAIKWAD, S., MASKE, A. and PATIL, S.S., 2016. Fabrication of electrospun nanofibres of BCS II drug for enhanced dissolution and permeation across skin. *Journal of Advanced Research,* 7(3), pp. 483-489.

KORSMEYER, R.W., GURNY, R., DOELKER, E., BURI, P. and PEPPAS, N.A., 1983. Mechanisms of solute release from porous hydrophilic polymers. *International Journal of Pharmaceutics,* 15(1), pp. 25-35.

LARRAÑETA, E., LUTTON, R.E.M., WOOLFSON, A.D. and DONNELLY, R.F., 2016. Microneedle arrays as transdermal and intradermal drug delivery systems:

Materials science, manufacture and commercial development. *Materials Science and Engineering: R: Reports,* 104, pp. 1-32.

LEE, I., WU, Y., TSAI, S., CHEN, C. and WU, M., 2017. Fabrication of two-layer dissolving polyvinylpyrrolidone microneedles with different molecular weights for in vivo insulin transdermal delivery. *Rsc Advances,* 7(9), pp. 5067-5075.

LIU, Q., WANG, H., CHEN, L., LI, W., ZONG, Y., SUN, Y. and LI, Z., 2019. Enzymatic degradation of fluorinated Poly(ε-caprolactone) (PCL) block copolymer films with improved hydrophobicity. *Polymer Degradation and Stability,* 165, pp. 27-34.

MA, G. and WU, C., 2017. Microneedle, bio-microneedle and bio-inspired microneedle: A review. *Journal of Controlled Release,* 251, pp. 11-23.

MACHEKPOSHTI, S.A., SOLTANI, M., NAJAFIZADEH, P., EBRAHIMI, S.A. and CHEN, P., 2017. Biocompatible polymer microneedle for transdermal delivery of tranexamic acid. *Journal of Controlled Release,* 10(261), pp. 87-97.

O'MAHONY, C., HILLIARD, L., KOSCH, T., BOCCHINO, A., SULAS, E., KENTHAO, A., O'CALLAGHAN, S., CLOVER, A.J.P., DEMARCHI, D. and BARED, G., 2017. Accuracy and feasibility of piezoelectric inkjet coating technology for applications in microneedle-based transdermal delivery. *Microelectronic Engineering,* 172, pp. 19-25.

PAUL, D.R., 2011. Elaborations on the Higuchi model for drug delivery. *International journal of pharmaceutics,* 418(1), pp. 13-17.

PONTES-LÓPEZ, S., MORENO, J., ESTEVE-TURRILLAS, F.A. and ARMENTA, S., 2020. Development of a simulation chamber for the evaluation of dermal absorption of volatile organic compounds. *Atmospheric Pollution Research,* 11(5), pp. 1009-1017.

RITGER, P.L. and PEPPAS, N.A., 1987. A simple equation for description of solute release II. Fickian and anomalous release from swellable devices. *Journal of Controlled Release,* 5(1), pp. 37-42.

RONNANDER, P., SIMON, L., SPILGIES, H., KOCH, A. and SCHERR, S., 2018. Dissolving polyvinylpyrrolidone-based microneedle systems for in-vitro delivery of sumatriptan succinate. *European Journal of Pharmaceutical Sciences,* 114, pp. 84-92.

SEBASTIA-SAEZ, D., BURBIDGE, A., ENGMANN, J. and RAMAIOLI, M., 2020. New trends in mechanistic transdermal drug delivery modelling: Towards an accurate geometric description of the skin microstructure. *Computers & Chemical Engineering,* 141, pp. 106976.

SIEPMANN, J. and PEPPAS, N.A., 2011. Higuchi equation: Derivation, applications, use and misuse. *International Journal of Pharmaceutics,* 418(1), pp. 6-12.

SIMON, A., AMARO, M.I., HEALY, A.M., CABRAL, L.M. and DE SOUSA, V.P., 2016. Comparative evaluation of rivastigmine permeation from a transdermal system in the Franz cell using synthetic membranes and pig ear skin with in vivo-in vitro correlation. *International Journal of Pharmaceutics,* 512(1), pp. 234-241.

TU, J., DU, G., REZA NEJADNIK, M., MÖNKÄRE, J., VAN DER MAADEN, K., BOMANS, P., SOMMERDIJK, N., SLÜTTER, B., JISKOOT, W., BOUWSTRA, J. and KROS, A., 2017. Mesoporous Silica Nanoparticle-Coated Microneedle Arrays for Intradermal Antigen Delivery. *Pharamceutical Research,* 34(8), pp. 1693-1706.

UCHIDA, T., KADHUM, W.R., KANAI, S., TODO, H., OSHIZAKA, T. and SUGIBAYASHI, K., 2015. Prediction of skin permeation by chemical compounds using the artificial membrane, Strat-M™. *European Journal of Pharmaceutical Sciences,* 67, pp. 113-118.

WANG, B., AHMAD, Z., HUANG, J., LI, J. and CHANG, M., 2018. Development of random and ordered composite fiber hybrid technologies for controlled release functions. *Chemical Engineering Journal,* 343, pp. 379-389.

XIE, J., JIANG, J., DAVOODI, P., SRINIVASAN, M.P. and WANG, C., 2015. Electrohydrodynamic atomization: A two-decade effort to produce and process micro-/nanoparticulate materials. *Chemical Engineering Science,* 125, pp. 32-57.

YIN, Z., KUANG, D., WANG, S., ZHENG, Z., YADAVALLI, V.K. and LU, S., 2018. Swellable silk fibroin microneedles for transdermal drug delivery. *International Journal of Biological Macromolecules,* 106, pp. 48-56.

YU, W., JIANG, G., LIU, D., LI, L., CHEN, H., LIU, Y., HUANG, Q., TONG, Z., YAO, J. and KONG, X., 2017. Fabrication of biodegradable composite microneedles based on calcium sulfate and gelatin for transdermal delivery of insulin. *Materials Science and Engineering: C,* 71, pp. 725-734.

ZHAO, X., COULMAN, S.A., HANNA, S.J., WONG, F.S., DAYAN, C.M. and BIRCHALL, J.C., 2017. Formulation of hydrophobic peptides for skin delivery via coated microneedles. *Journal of Controlled Release,* 265, pp. 2-13.

Chapter 7 Conclusions and Future work

7.1 General conclusion

The aim of this research was to demonstrate the potential of EHDA for the engineering of MN coatings. The thesis comprised of three experimental chapters whereby the first involved characterising polymeric solutions for the suitability of EHDA as well as jetting behaviour of Es and Esp (Chapter 4) This was followed by the application of QBD to the EHDA process to make sure it was more reliable and robust ensuring that quality was built into the product (Chapter 5). This was followed by characterisation of the optimised MN coatings (Chapter 6).

Chapter 4 examined the effects of two different polymers at two different concentrations in the EHDA process. This involved PVP and PCL at concentrations of 1 and 5 % w/v at low and high molecular weights. It was determined that the lower molecular weight polymeric solutions led to Es thus production of particles. The higher molecular weight solutions resulted in Esp which produced fibres. Jetting maps showing regions whereby stable jetting can occur was constructed however SEM images showed that the resultant structures were not optimal with distorted morphology (irregular larger sized particles and rough beaded fibres).

This led to the application of QBD to the EHDA process forming Chapter 5. This study carried through the formulations from Chapter 4, but it involved taking a systematic approach. By applying QBD a full factorial design was able to optimise the process parameters of EHDA to ensure that the formulations (polymer and dye) resulted in the fabrication of optimised structures within the nano-micron size range. With majority of particles being under 500 nm and fibres in the nano-micron range. Spectroscopic and thermal analysis conferred successful encapsulation of dye within the polymeric matrix.

Chapter 6 included the formulations and used the data from Chapter 5 to ensure that optimal MN coatings were yielded from applying QBD to the EHDA process.

This chapter involved the characterisation and *in vitro* and *ex vivo* assessment of MN coatings. From the QBD data the flow rate and applied voltage for F2 and F4 was 15 µl/min, 20 µl/min, 10 cm. For F6 and F8 15 µl/min, 15 cm and 50 µl/min and 10 cm. The MN coating morphologies satisfied the QTPP profile.

Contact angle measurements gave an indication as to the wettability of polymers and as expected PVP showed more rapid dissipation due to being hydrophilic whereas PCL was very hydrophobic with much larger contact angle measurements which is owed to its resistance to degradation by deionized water and super hydrophobicity.

In vitro release studies showed 100% release of PVP within two hours (F2) and four hours (F4). PCL showed a more sustained release profile with 75% released in 4 hours for F6 and F8. This all fit with QBD and satisfied the QTPP profile. Release kinetics suggested that F2 and F4 showed supercase II non-fickian diffusion as the n values were over 0.89. This was expected as they are hydrophilic. F6 and F8 had an n value between 0.5 and 0.89 and so anomalous case II transport kinetics is more fitting.

From the permeation data PVP showed the most significant difference in permeation this could be due to the distribution of dye within the polymeric matrix and fast swelling of fibres resulting in FL leaching out. The confocal laser scanning microscopy results show high levels of intensity at lower depths suggested great insertion.

The SEM of Strat-M® post insertion confirms good permeation as there is little to no particles or fibres left on the tips of MNs. In particular fibrous MNs showed no fibres or residue on MN tips supporting the phenomena that fibres are dragged through the skin upon insertion. These results show the reliability of QBD in making sure that the EHDA process was robust, and the structures produced were optimal. This MN system satisfied the QTPP profile and shows great potential for future drug delivery application.

7.2 Future Work

Fabrication of MNs via EHDA using polymers as encapsulation agents and dyes behaving as model drug yielded promising results. This proof of concept shows the potential of EHDA for an array of drug delivery systems. For clinical application however, further research is necessary to validate and complement the data obtained from these coated medical devices.

This study involved the characterisation and assessment of two polymers (PVP and PCL) for MN coatings. However, there is a large array of polymers which may demonstrate more positive results. PLGA has been successfully Es and Esp using EHDA with extremely promising results. This included controlling the size and drug loading with higher encapsulation efficiencies. This polymer can be further modified by altering the ratio of lactic acid and glycolic acid which varies the crystallinity and hydrophobicity of the formulation.

This drug delivery system can be further enhanced with the potential use of permeation enhancers such as oleic acid. These enhancers can be used alongside a drug/API and the effects assessed. A promising penetration enhancer includes super multi-functional nanoparticles like dendrimers which have gained interest in recent years and have great scope. These nano sized starburst molecules can be used within a carrier matrix to provide efficacious drug delivery. Manipulation of the generation of dendrimer can result in increased efficacy depending on the treatment. Used initially as penetration enhancers, current therapies explored using dendrimers include diabetes and cardiovascular therapy. Carrier systems can also be further modified. Mesoporous silica nanoparticles have reported promising results. With their nano sizes and high loading ability, able to provide targeted controlled drug delivery and efficiency make them an attractive approach.

Single needle Es and Esp was utilised in this study however co-axial and multi-axial EHDA could further enhance the drug delivery system. This study had limited in-vivo characterisation which would be beneficial in providing biocompatibility data and toxicity with an MTT assay for example citing

cytotoxicity. This would all provide further validity if proven efficacious and gives great scope for personalised drug delivery. Over the past decade there has been a surge in the commercial availability of MNs and the demand could increase further. In particular with vaccines as a global pandemic is underway. The self-administration ability of MNs could help considerably and the painless aspect would greatly improve compliance.

The application of QBD for future work can be beneficial in terms of optimisation and ensuring the EHDA process is reliable which in turn should led to a product with quality being formed. Thus, it can be applied to a more complex EHDA system (co-axial, multi-nozzle etc.). By taking a systematic approach optimised structures can be fabricated possessing the necessary characteristics and fitting the set criteria. This makes the process more reproducible and reliable. This could also prove useful for commercialisation.